Øystein Krøvel

Design of Large Permanent Magnetized Synchronous Electric Machines

Low Speed, High Torque Machines
- Generator for Direct Driven Wind Turbine
- Motor for Rim Driven Thruster

Thesis for the degree of Philosophiae Doctor

Trondheim, February 2011

Norwegian University of Science and Technology
Faculty of Information Technology, Mathematics and Electrical Engineering
Department of Electric Power Engineering

NTNU – Trondheim
Norwegian University of
Science and Technology

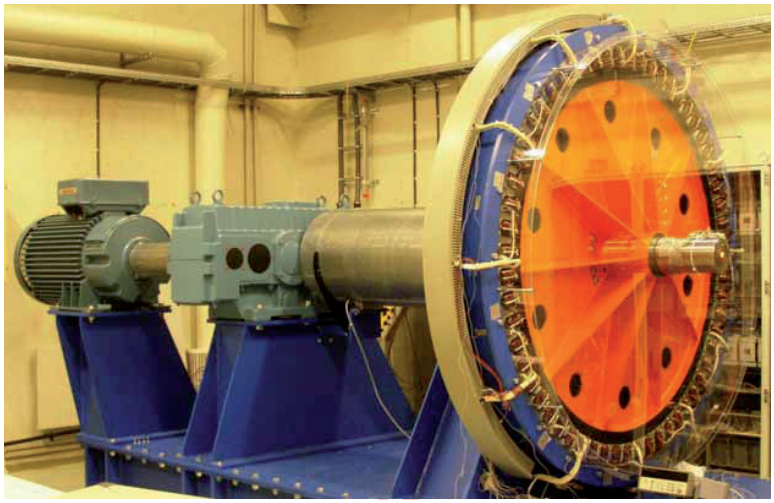

NTNU
Norwegian University of Science and Technology

Thesis for the degree of Philosophiae Doctor

Faculty of Information Technology, Mathematics and Electrical Engineering
Department of Electric Power Engineering

ISBN 978-82-471-2568-7 (printed ver.)
ISBN 978-82-471-2569-4 (electronic ver.)
ISSN 1503-8181

Doctoral theses at NTNU, 2011:25

Printed by NTNU-trykk

Acknowledgments

This work is not a result of only my efforts, but the sum of the efforts from all those who have given me the opportunities, influenced me and helped me since I started this work in 2003. My supervisor, Professor Robert Nilssen, has been a great inspiration. The practical angle would not have been possible without the support from Prof. Nilssen, the inventors behind Norpropeller AS, Normann Sandøy and Reidar Vårdal, and Brunvoll AS. The inventors' ability to simplify problems and Brunvoll's industrial capabilities provided the practical experience needed to get the prototype thruster built.

My colleagues at the department of Electric Power Engineering have been of great inspiration and support. So have also my friends at SmartMotor AS and Brunvoll AS. Thanks are also given to the people at the workshop at the dept. of Electric Power Eng. for help regarding instrumentation, measurements, and mechanical issues. Especially thanks for building my small table model and the larger wind generator.

The funding for the PhD study has come from RSO at NTNU and local resources at the department of electric power engineering. The funding for the prototype thruster came through the TEFT-program for the preliminary work and through local industrial finances for the building of the prototype. The funding for the wind laboratory came through strategic resource from NTNU and the dept. of electric power engineering. The table model was built using resources at the workshop, leftover components, such as copper and stator lamination, and spare parts from other projects.

Thanks to CleanPower AS, my employer, for giving me time and resources to finish my PhD. Without the company's understanding finishing would not have been possible. Also a special thanks to Randi, who I owe the inspiration and energy to finish this work.

Kristiansund 11/1 -2011

Øystein Krøvel

Abstract

This work presents the design of two prototype permanent magnetized electric machines for two different applications where large permanent magnet machines might be used. Existing technology have been used as the fundament for new design and adapted to new applications, contributing, hopefully, to the development of better and more environmental friendly energy conversion.

The first application presented is represented with a prototype made in cooperation with the industry in which a PM-motor is integrated into a propeller unit. Both because of the industrial connection, and the integration between the PM-motor and the propeller, the choices made for the PM-motor are conservative trying to reduce the risk.

The direct rim driven thruster prototype includes a surface mounted radial flux permanent magnet machine (SM RFPM) with fractional slot winding with a q around 1. Other engineering features were introduced to make the integration of propeller and motor feasible, but without the PM-machine the thruster would not have reached the performance demand. An important part of the project was to show that the SM RFPM enables this solution, providing high performance with a large air gap. The prototype has been tested in sea, under harsh conditions, and even though the magnets have been exposed directly to sea water and been visible corroded, the electric motor still performs well within the specifications.

The second application is represented with a prototype PM-generator for wind turbines. This is an example of a new, very low speed high torque machine. The generator is built to test phenomena regarding concentrated coils, and as opposed to the first application, being a pure academic university project, its success is not connected to its performance, but with the prototype's ability to expose the phenomena in question.

The prototype, or laboratory model, of the generator for direct driven wind turbines features SM RFPM with concentrated coils (CC). An opportunity to push the limits for the design was given, and taken, choosing a relative high frequency and open slots to investigate the consequences of large reluctance variations in the air gap and distorted MMF. The main purpose of the PM generator is to explore a very low speed machine with high pole number and concentrated coils with coils wound around every other tooth. The study leading to the design included a discussion of scaling of the prototype from the full size generator, which parameters to keep, which to stress and which to forget. An investigation of the winding layout and winding factors included building a smaller table model for testing of different winding configurations, was also an important part of the work. Though the prototype has its flaws, or experimental setbacks, it successfully enhances the characteristic of the low speed, high pole number and slot geometry focusing on the harmonic content of the MMF and the consequences for the losses and reactance.

Publications

A Study of the Research Activity in the Nordic Countries on Large Permanent Magnet Synchronous Machines [1]

Krøvel, Ø., Nilssen, R., Nysveen, A.
NORPIE 2004

This paper presents an overview of the activity on large Permanent Magnet Synchronous Machines (PMSM) in the Nordic countries. It is found that the Nordic countries are in the leading end of the development of large PMSM. This is much due long traditions of ship building, an important application for large PMSM, and pioneer work in wind conversion. The focus has mainly been on the radial flux permanent magnet machines, but in the later years also attention has been given to axial and transverse flux permanent magnet machines. The industry has started to use large PMSM; e.g. ABB has their compact azipod® with radial flux machine, Siemens has a radial flux submarine motors and Jeumont uses axial flux generator in wind turbines. The impression is that at the time, the large machine manufacturers in Europe have radial flux machines in their assortment and are developing the axial flux technology. While the smaller and more specialized companies have already developed axial flux machines for their applications.

Design of an Integrated 100kW Permanent Magnet Synchronous Machine in a Prototype Thruster for Ship Propulsion [2]

Krøvel, Ø. Nilssen, R. Skaar, S. Løvli, E. Sandøy, N.
ICEM 2004

Traditional electrical motors are mechanically coupled through gear and shaft to their load. This paper presents a direct driven permanent magnet (PM) motor integrated into a ship propeller. It is proven that an integration of PM-motor and propeller is possible. This design has better hydrodynamic properties than standard tunnel and azimuth thrusters. The electric machine is a surface mounted PM-machine with 22 poles and number of slots per pole per phase equal to 1.09.

Thermal Properties of a Prototype Permanent Magnetized Electrical Motor Embedded in a Rim Driven Thruster [3]

Krøvel, Ø. Andresen, K. Sandøy, N.
NORPIE 2006

For machine designs it is usually the thermal limits that set the boundaries for how high the power density of a machine can be. This paper shows calculations of losses and temperatures together with temperature measurements on a 100 kW surface mounted radial flux permanent machine (SM RFPM). The special feature of this machine is that it is totally enclosed in water, which yields very good cooling. The measurements confirm this.

Design and Measurements on a Small Radial Flux Permanent Magnet Generator with Concentrated Coils [4]

Krøvel, Ø. Nilssen, R.
COMSOL Conference 2006

The paper shows calculations of inductance, induced voltage and torque using Comsol Multiphysics (CM) 3.2b and 3.3. Calculated values are compared with measurements. It is found that for the inductance calculations it is not sufficient, with such a short machine, to only consider the active part using 2D calculations. 3D calculation of the inductance gives improved results. The voltage calculations are within what can be expected when considering the uncertainties in material properties and mechanical tolerances. This goes for both the fundamental and its harmonics. Especially is the harmonic content influenced by the mechanical tolerance. Torque calculations were also performed, both for loaded machine with locked rotor and unloaded machine with rotation (cogging). The results from the cogging torque calculations gave a considerable DC-offset, but the curve shape resembled what would be expected.

Slotless, Toroidal Wound, Axially-Magnetized Permanent Magnet Generator for Small Wind Turbine Systems [5]

S.E. Skaar, Ø. Krøvel, R. Nilssen and H. Erstad
AUPEC 2003

A toroidal wound three phase axially-magnetized, disc type, permanent magnet generator is presented in this paper. For a novel wind turbine application the generator must have a low reluctance torque and need to be direct-driven to reduce mechanical losses in the application. For this purpose the stator winding is wound around a slotless ring core. The rotor disc has 18 surface mounted magnet poles. A test of a proto type generator will be presented.

Distribution, coil-span and winding factors for PM machines with concentrated windings [6]

S. E. Skaar, Ø. Krøvel, R. Nilssen
ICEM 2006

Usage of concentrated windings in electrical machines is a well-known topic, yet there has not been presented a direct approach on winding factor calculation. In this paper a method for directly calculating the winding factor, without doing a winding layout first, is proposed. A feasible region for the number of slots per pole per phase for machines with concentrated windings is also presented. The effect the odd and even number of slots have on both the winding space harmonics and the air gap force is discussed.

Table of Content

Chapter 1
Introduction

The PhD-project has been financed by strategic funding (RSO) at NTNU, with a purpose of raising the general knowledge nationally of large permanent magnetized machines. The department of electrical power engineering has organized the project as part of the Energy Efficient All Electric Ship (AE^3S) project. The aim of this work has thus been towards applications within the all-electric ship.

AE^3S consisted of both industrial and academic participants. From NTNU the departments of Electrical Power Engineering and Marine Technology are involved, and the industrial partners are ABB, AkerKvaerner, Brunvoll, MARINTEK, SmartMotor and Norpropeller [7]. The ambition of the project is to investigate the problems, advantages and other consequences designing an all-electric ship, replacing hydraulic motors, pistons and small combustion engines with electric motors with drives, giving a dynamic system, with a distributed power plant.

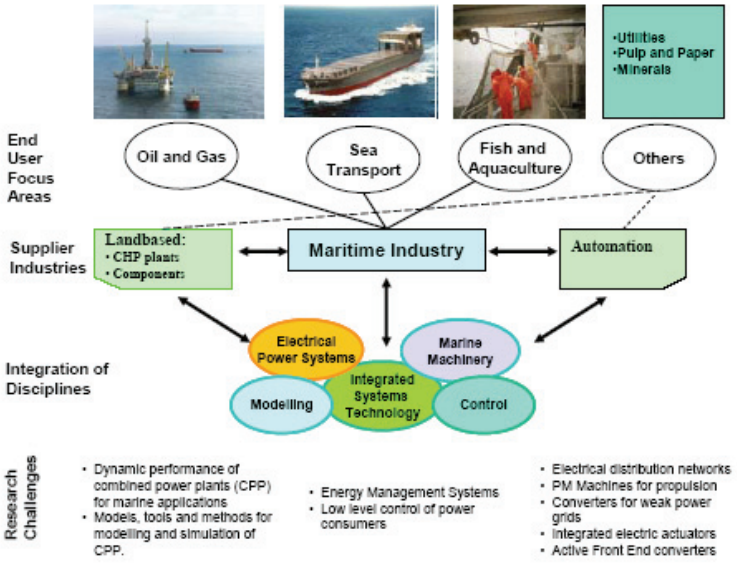

Fig. 1 Overview of the project constellation [7]

RSO together with the department also funded the building of a prototype wind generator. This is an example of a very low speed high torque machine including a range of applications on an all-electric ship. The generator is built using technology developed by SmartMotor AS and was a followed by a larger project funded by the Norwegian Research

Council titled “Utvikling av morgendagens Permanent Magnet maskiner for energiproduksjon” and “Store vindmøllegeneratorer” [8].

The work has mainly been carried out at the dept. of Electric Power Engineering, Energy Conversion group at the Norwegian University of Science and Technology (NTNU), Trondheim, Norway, first as a scientific assistant from august 2002 to October 2003, then as PhD-student until March 2007. The period between October 2004 and July 2005 was spent at WEMPEC, University at Wisconsin, WI, USA, as a guest researcher. From April 2007 the candidate has been employed by CleanPower AS, Kristiansund.

1.1 Scope of work

The object of this work is to do basic research on large electrical permanent magnetized machines and to increase the general know how of PM nationally, a very wide and free assignment. The progress of the work has included a study of the applications of large PM machines, both industrial and academic, a choice of focus, both regarding application and technical angle and design and testing of the prototypes. The work has been characterized with a practical experimental focus spending much time on practical issues such as organizing, follow up of construction and assembly and setting up tests and testing.

Permanent magnet machines have some promising features when it comes to application where direct drive, low speed and high torque are desired or required parameters. The typical applications for such machines, at least in Norway, are generators for wind turbines, motors for ship propulsion, actuators for rudder and thruster applications, crane and winch application. Based on a study of academic publications and publicised industrial products and projects [1] and considering the application of interest for the national industry, it was chosen to look at two applications in this study.

The first application chosen as an example for this work is the direct rim driven propellers, chosen because PM’s is one of the enabling technologies for this applications, and because this is an example of a highly integrated application. It is also an application of interest for national (and regional) industry. The large air gap, high pole number and the fact that the rotor is surrounded by water, eliminates both wound rotor synchronous machines and induction machines as feasible solutions.

The second application is direct driven generators for wind turbines. Electromagnetically this is a very interesting application in which PM’s enables a higher frequency, smaller pole spans and lower diameter at equal speed, compared to wound field synchronous machines. It was also driven by the fact that the awareness of new renewable energy sources within international, national and local funding organisations were high, which gave the possibility to build a laboratory model of direct driven generator for wind turbines.

Both applications for the full size power are considered low speed high torque machines. The first application is fairly specialised towards thrusters and propellers, but the concept is also valid for low head turbines and pumps. The concept is characterized by the tip speed of the propeller which is in the area of 20-30m/s. The second application is an example of a very low speed machine, with a more general design, and can also be utilized in applications for winch and rudder machines or other low speed high torque machines. The concept is characterized by the very low rotating speed, where the tip speed of the very large rotor of the wind turbine limits the rotating speed, resulting in 16-17rpm for 3MW.

Both applications can benefit from radial, axial or transverse flux machines. It was chosen to investigate the radial flux machines for both applications. For the thruster this was a

natural choice since the machine is wrapped around a cylinder with limitations on the inner and outer diameter, and that a conservative design was needed to prove the concept. For the wind generator several topologies were evaluated, but early in the project it was decided that the most interesting focus for the generator would be to investigate the concept and phenomena of high pole number and concentrated coils in a radial flux machine. The concept is based on technology developed locally and has promising features regarding simplicity and compactness among others.

Two hypotheses were put forward to set the ground for further work:

- **Hypotheses one**
  For PM motors in rim driven propulsion system the diameter is given by the propeller and is much larger than would have been natural for the speed and power of the electric motor. This implies a relative high peripheral speed, large diameter to length ratio, with relative long pole pitch or high frequency. It can therefore be assumed that a natural choice is a RFPM with more than three (number of phases) slots per pole, and a relative high frequency.
- **Hypotheses two**
  For PM generators in wind turbines the reduced diameter compared to wound rotor designs results in cost and weight savings. But with classical windings with q>1 the full effect of the short pole pitch is not utilized. Using a winding with concentrated coils (q ~= 1/3) the frequency can be increased, the diameter reduced and the slots made wider, making a more compact machine with less active materials and with high fill factor.

1.2 Large Permanent Magnetized Machines

A large permanent magnet machine is still normally small compared to classical large synchronous electric machine. Large electric machines are typically low speed generators in hydro power plants of several hundred MW or high speed turbo generators in thermal plants up to GW. A way to determine whether a machine is large, medium or small (electrically) is to look at the power per pole of the machine. An example is a typical wind turbine of 3MVA and 17rpm which gives a power per pole of about 14kVA (@30Hz), while a field wound machine for hydro power will have power per pole of maybe 8MVA (14 poles, 112MVA). Using this approach almost all PM-machines can be considered small, electrically. Thus a large permanent magnetized machine refers to a machine that is large within its area of use. Typically a large PM-machine have a power rating higher than 1MW and a diameter larger than 2m.

1.2.1 Brief history of electrical machines

The electric machine has existed since the middle of the 19th century and has grown to become an important part of our modern daily life. From the large synchronous generators to the vast amount of industrial inductions machines and the billions of small DC-machines and single phase machines surrounding us every day at home, in the car or at work, many of them PM-machines. P. Dunsheath's has in his "A History of Electrical Engineering" [9] tried to tell some of the history concerning electric machines. For the history on magnets Overshott gives a good overview in his article "Magnetism: it is permanent" in 1991 [10].

The concept of electricity and magnetism has been known for quite a while. Compasses have been reported as far back as 2637BC in china (chi-nan; chariot pointing south). Lodestones were described around 55BC. Electricity was most likely first observed as lightning. Temple of Juno and Temple of Solomon had metal roof with swords and spears

pointing upwards, and metallic rain pipes, thus preventing damage from lighting. The effect was probably not well understood, but it worked.

The connection between electricity and magnetism was probably first observed by sailors that had seen lightning demagnetize the needle in their compass. Oersted did the first controlled discovery of how electric current could turn a magnetic needle at a lecture winter 1819-20. That is Romagnosi had in 1802 seen that a voltaic cell could slightly change the needles direction. But Romagnosi did not close the circuit. Shortly after Oersted's discovery Ampere started publishing his work on laws and principles on electromagnetism that makes up the base of today's electrical engineering. Arago presented his rotating copper plate that could change the direction of a magnetic needle depending on the rotation direction (Arago's Disc). Faraday was the first to create rotation using current and magnetism. On September 3rd 1821 he conducted a series of experiments where he was able to rotate a conductor around a magnet and a magnet around a conductor (Fig. 2). Later he made his own version of Arago's Disc namely Faradays disc (Fig. 3).

Thus were all the components for the rotating electric machines at hand, and one of the first to utilize it were M. Hypolite Pixii, of Paris. He made a two pole axial flux machine with a vertical shaft, using a soft iron horseshoe magnet (Fig. 4). This could either create sparks or alternating current. The machine was made public in Paris on 3rd September 1831. Since sparks was the ultimate visual result for electricity at the time, this was what he showed.

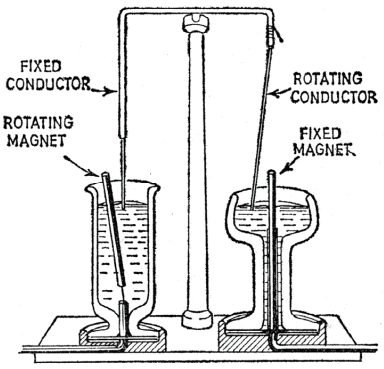

Fig. 2 Faradays rotating conductor and magnet [9]

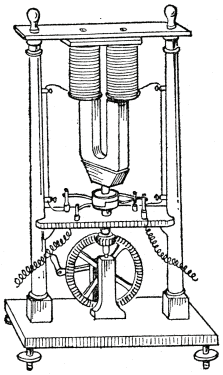

Fig. 4 Pixii's rotating machine [9]

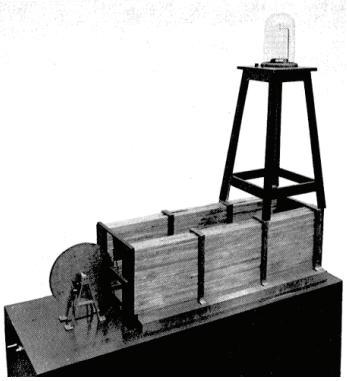

Fig. 3 Faradays Disc [9]

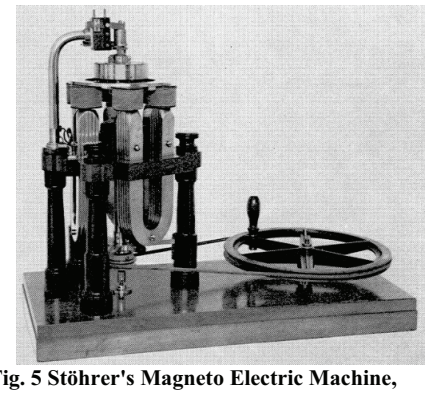

Fig. 5 Stöhrer's Magneto Electric Machine, 1843. Six poles and six coils [9]

Great work has since been done to improve the efficiency and usability of the electric machines; direct current was introduced, permanent magnets were replaced by electromagnets (Abbés Moigno and Raillard, 1836), mercury was replaced by brushes (Sturgeon), multi pole versions were presented (e.g Stöhrer, Fig. 5) and self and separate excitation was introduced (Wilde). Tesla identification of the rotating electric field (1882) and invention of Tesla machine (1889 [11]) made way for the second industrial revolution making possible the efficient generation and long distance distribution of electrical energy using the alternating current transmission system [12]. De Cogan has a short and enlightening article about Tesla's advances in the Eng. Science and education journal [13].

This chapter has barely touched the surface of the history and was mostly meant to point to some interesting early machines as Pixii's and Stöhrer's vertical axial flux machines. For more information Dunsheats book [9] gives a good overview, internet is of course a vast source of information. Some interesting pictures of early machines can be found at [14], and free open sources as wikipedia.org may supply more or less accurate and good information.

1.2.2 The permanent magnet

The PM's consist usually of sintered or bonded materials. They are pressed into whatever shape wanted, but usually into rectangles or parts of arcs. The direction of magnetism is preferably parallel magnetised in any direction.

The MMF, or ampere turns (NI), from magnets is relatively independent of the area, it is mostly depending on the length in the magnetizing direction. It is usually considered being rectangular, since magnets are even rectangular, or have a fixed radial length. There are numerous geometric shapes of magnets, but usually they are rectangular. Other commonly used shapes is the loaf, or bread, shape with parallel sides, flat bottom and circular surface towards the air gap (Fig. 7) and the cylindrical magnet with either parallel or radial sides.

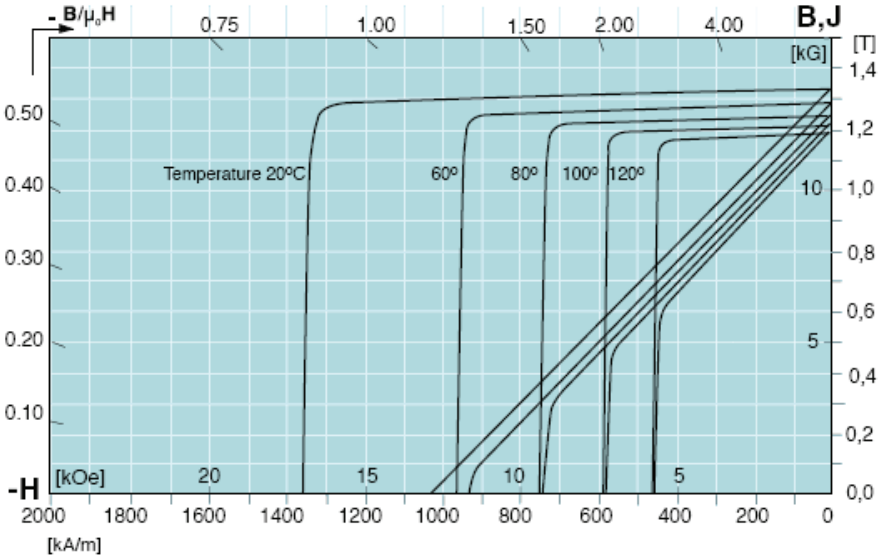

Fig. 6 Example data sheet for a sintered neodymium PM, from Neorem Magnets Oy, [15]

The permanent magnet yields a permanent magnetism in the machine, hence no magnetizing losses. Since there are no losses creating the MMF the length of the air gap doesn't affect the efficiency of the machine, only the investments cost. Actually, a large air

gap in a permanent magnet machine can reduce rotor losses since the tooth reluctance and load dependent flux variation in the rotor are reduced. But at the same time the constant magnetisation can be a challenge during assembly and it is generally assumed that a PM-machine must be connected to the grid via a converter due to the lack of voltage control. The converter also enables smooth speed and torque control.

For the early magnets it was a problem that magnets would demagnetize given high currents, they could even be destroyed if taken out of their magnetic circuit. The quality has now increased to such a level that it is difficult to fully demagnetize a magnet mounted in a machine, the remanent flux density is so high that flux densities up to those in field wound machines can be achieved and the price so low that it can compete with wound field synchronous and induction machines in standard applications.

In Fig. 6 an example of a data sheet for a sintered neodymium magnet is given. It has parameters for remanent flux density, how the flux density changes depending on the magnetic field and how the performance changes with temperature. There are several different grades of magnets with different remanent flux density, coercivity and temperature dependency. The most common magnet as of now is the neodymium magnet (NdFeB) because of its high remanent flux density and low price, while Aluminium Nickel Cobalt magnets (AlNiCo) and Samarium Cobalt (SmCo) magnets have other features such as higher temperatures limits and are less corrosives. Most magnets are sintered, but there are other types too. For example plastic bonded magnets have less conductivity and thus fewer losses than sintered and might have better performance for high frequency machines.

Trout [16] present an interesting overview of the magnets history and the development of the manufacturing of magnets, and he doesn't leave much chance for the western (US) manufactures for the future for mass production of magnets. He means that China, with its access to raw material and cheap labour will dominate the marked. As long as China is stable and interested in selling, it's all good, but being dependent of only one country for raw materials, and also, more or less, only one country manufacturing magnets can become a problem in the future. And a problem will of course affect availability, the price and thus the interest for using PM-machines.

1.2.3 Types of PM-machines

There are generally three types of PM-machines: Radial, Axial and Transversal flux machines. The names arise from the direction of the magnetic flux in the air gap. Also some types of switched reluctance machines (SRM) use PM in their construction, but they will not be further discussed here. The axial and transversal flux machines will not be discussed further since the focus is on radial flux permanent magnet machines.

The different types can then again be divided into number of air gaps, whether rotor or stator is in centre, whether there are stator teeth or not, iron in stator or not, iron in rotor or not etc. The variation of PM-machines are large, but even though the possibilities for variation are present, the most common PM-machine is radial flux machine with iron in both stator and rotor and a slotted stator with more than one slot per pole and phase.

1.2.3.a Radial Flux Permanent Magnet (RFPM) Machine

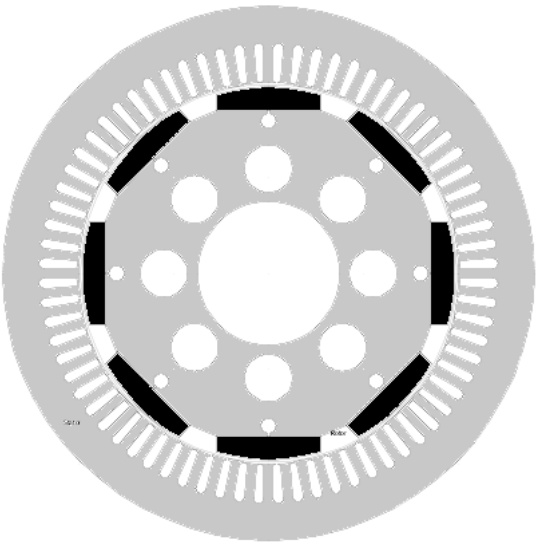

Fig. 7 Example of radial flux PM machine with bread (loaf) shaped poles (magnets)

The radial flux machine is the classical type of electric machine. Close to all commercial induction and wound synchronous machines are radial flux machines. A cylinder rotates inside another, usually supported by bearings in the centre. The magnetic force has a radial and tangential component, were the sum of radial forces around the air gap ideally is zero and the sum of tangential forces yields the output torque. Given constant magnetic and current loading (flux density and current per circumference) the output torque is proportional to the square of the air gap diameter and proportional to the air gap length:

$$T_{gap} = k \cdot D_g^{\,2} \cdot L \tag{1}$$

The advantage of RFPM is the balanced radial forces, easy assembly and that is very similar to already existing machine technology. The limiting factor of the RFPM is that the current and magnetic flux have to go through the same cross sectional area. The current density's upper limit is given by thermal properties of the machine and the magnetic flux is limited by the saturation of iron. Thus for a given rating the current and magnetic flux needs a certain area to flow through.

There are in general two types of RFPM, one with surface mounted magnets (SM) and one with buried or interior magnets (IM). In the SM machine the magnets magnetization is in radial direction. Hallbach array is also an option for SM RFPM, removing the iron yoke. In machines with IM magnets with the magnetizing direction either in radial, tangential or something in between (for example V-shape) is used. Using IM an amplification of the flux in the air gap can be achieved. This is useful when using ferrite magnets, which have a relative low remanent flux density. IM RFPM is also favoured for some servo applications since the buried magnets represent a very distinct difference in d and q axis inductance.

The windings of the RFPM are usually distributed windings with one or two layers. For smaller and simpler machines concentrated coils have been used. Brushless DC machines are also often built with concentrated coils since it is possible to design the machine to give trapezoidal voltage, integration of the square MMF gives a trapezoidal, or triangular shaped voltage. There are also some examples of multi air gap radial flux machines, but they are rare.

1.2.3.b Axial Flux Permanent Magnet (AFPM) Machine

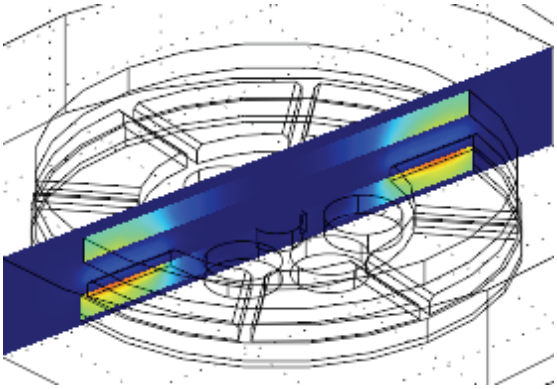

Fig. 8 Example of one sided AFPM without teeth

Axial flux permanent magnet machines were among the first to be built, though they had little knowledge of the magnetic path, poor magnets (soft iron horseshoe magnets) and all over low performance, they could produce alternating current or sparks, which was the ultimate show off for electricity at the time [9]. The AFPM couldn't compete with the radial flux induction and synchronous machines because of the poor quality of the permanent magnets at the time. With the introduction of high quality PM's the use of AFPM have grown and they are used commercially in applications demanding short machines or high power densities.

As for the RFPM, the magnetic flux and current share the same area, thus for a given cross section there will be a limit for the force, or torque, created. Given constant magnetic and current loading the torque is only depending on the diameters. Assuming that the inner diameter has an optimum fixed size relative to the outer diameter a simplified equation for the torque can be found:

$$T_{gap} = k \cdot D^3 \tag{2}$$

Another advantage for the AFPM is that the machine uses more of the volume of the machine than RFPM to create force. Especially for large low speed machines where the active volume in a RFPM is a thin shell along the air gap, the AFPM can fill more of the volume with active materials (Fig. 9). Though it should be said that optimization shows that due to the loss of torque at lower diameters and that there must be room for end turns at the inner diameter, the optimum difference in inner and outer diameter is not that big, maybe 0.7-0.8 [17]. But given the same outer dimensions an AFPM would yield more torque per volume, but it would also have a higher price per torque since more of the active area is creating a force at smaller radii than the RFPM.

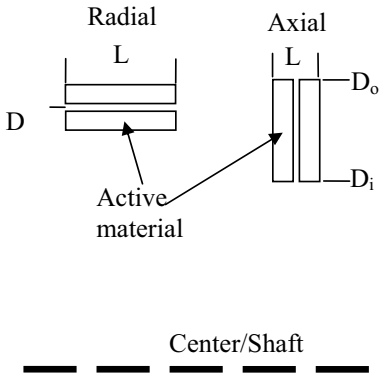

Fig. 9 Comparison of the diameter of active material in radial and axial machines

The RFPM machines are usually depending on iron as flux paths, and it's not so much to gain by using multiple air gaps. For the AFPM machines the use of multiple air gaps is the way to increase the machine length and there are more options when it comes to how to design the machine; rotor or stator in centre, flux going straight through or turning in stator and/or rotor, ironless stators, or specially shaped powder cores to utilize the flux paths etc. In Fig. 10 an overview for dual air gap AFPM machines are shown.

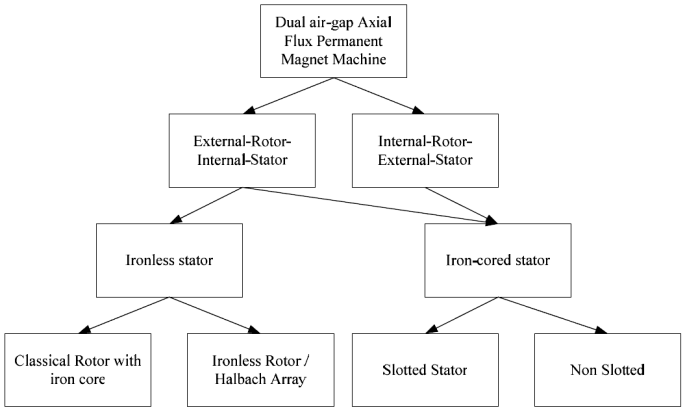

Fig. 10 An overview of different types of dual air gap AFPM machines [18]

1.2.3.c Transversal Flux Permanent Magnet (TFPM) Machine

The credit for developing or inventing the TFPM has gone to Weh and his work on the field in the eighties (e.g. [20]). As opposed to the RFPM and AFPM the magnetic flux and current does not compete for the space in this type of machine. The result is that the current loading and thereby the power density can be much higher. The high current loading has a drawback; high reactance, which again result in a high voltage drop at nominal load, and a need for high induced voltage.

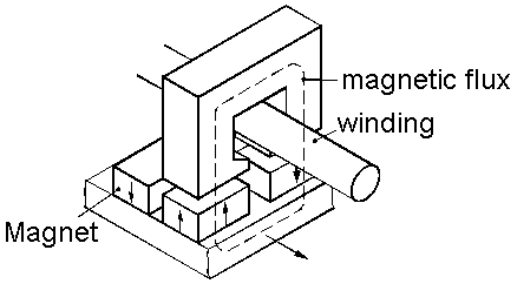

Fig. 11 Example of geometry of TFPM machine with surface mounted magnets from [19]

This makes the converter somewhat more expensive since it has to be rated for the high no load voltage. Reducing the inductance also reduces the power density and the TFPM's performance becomes more like the RFPM's and AFPM's. Another challenge with the TFPM is the large amount of small parts that the machine will consist of. This is both costly and challenging concerning assembly. More information of the machine can be found in e.g.,[18, 20, 21].

1.3 State of the art for the selected applications

As previously stated two applications were chosen to investigate further; direct driven generators for wind turbines and rim driven propellers for ship actuation or propulsion. This chapter will try to give an overview of the present solutions used and the solutions investigated of tomorrow. It also presents other applications and more general literature of interest for this work.

As described earlier the previous chapter, the first machines used permanent magnets made from magnetized soft iron. Due to the low remanent magnetization and general low quality they were soon abandoned for electromagnets. With the introduction of ferrite magnets and later rare earth magnets the use of permanent magnets have become economical viable and have resulted in machines with better performance. It started with small, special machines, and then small mass produced machines, but with increased quality and availability, and reduced price, also larger machines and more general industrial applications have started using permanent magnets.

1.3.1 Rim driven propellers and ship propulsion

Within ship propulsion and actuation there have been much research on PM-machines, driven in the seventies and eighties by naval interests in the larger countries. Though the induction and field wound synchronous machines works well for most of the applications on board, direct drive and special applications might demand PM technology. The PM-machines are also more compact and have higher efficiency, resulting in better utilization of the hull. The PM-machines investigated for ship propulsion includes all types, Rosu [21] gives good presentation of the variety.

Rosu's main focus is to present a RFPM machine suitable for ship propulsion. He focuses especially on magnet configuration and the air gap flux. He finds that a rotor with pole shoes is more resistive to demagnetization, but needs more magnet volume than a rotor without pole shoes. The one without pole shoes has higher magnet loses and somewhat more torque ripple. He also compared the previous mentioned configurations with inset magnets, and found that both surface mounted options gave higher torque than the inset variant.

Millner's (Kaman) [22] AFPM-motor and the Rolls-Royce TFPM motor [23] presented by Husband and Hodge are examples of AFPM and TFPM machines proposed for ship propulsion. Millner presents an AFPM machine of 700Hp that has high energy density and high efficiency. The Rolls-Royce TFPM machine is a 2MW prototype. In general it can be stated that a motor on a ship should be compact and light and the limiting factor is usually the cooling of the machines, as with all larger machines. The Permasyn motor, a RFPM machine, for propulsion of submarines, and other ships, from Siemens should also be mentioned, it is in general the same machine as the generator for the direct driven wind turbine [24]. It has some interesting features such as damper windings.

The concept of rim or tip driven propellers is well known for propulsion and actuation of ROV's and other smaller applications, and also water jets. An example of publications of thrusters for ROV's is Lai's and Abu-Sharkh's integrated PM-motor [25] and Abu-Sharkhs, Turnock and Hughes on testing of a 250mm diameter tip driven thruster [26]. The latter shows that the electric efficiency is high, they points out the problems concerning grit in the air gap and even though the thrust output is lower than reference propeller they conclude that the advantages with the tip driven propeller concept compensates for the disadvantages. The first paper addresses the fact that a rim driven propeller will have an electrical machine with large diameter to length ratio, with the result that the machine gets thin and bendable. Lai et al presents a slotless machine as a solution to get better structural strength, and a simpler machine. But the result shows that the magnet volume increases and the efficiency decreases compared to a slotted stator, and thus might not be as favorable. It can be a good solution if the savings in lamination expenses are larger than the increase in magnet cost, and if high efficiency is not an absolute demand.

Electric Boat Company in USA have been investigating both rim and hub driven propellers [27] using both induction and PM-motors. They have also built and tested scaled models [28]. For the rim driven option the induction machine is not a good option due to the high pole number and the large air gap. Their conclusion is that the PM's is most promising for rim driven applications, both for commercial and military application.

1.3.2 Direct driven generators for wind turbines

Research on direct driven generators for wind turbines have been going on for some years. There have been done some thorough and extensive studies and comparisons of the different generator topologies, and different drive trains, available for wind turbines.

In general comparison of different topologies are somewhat difficult, depending on the parameters chosen, almost any topology can be proven best. Cost, volume, area etc. are often used as parameters for comparison, and being electrical engineers typically the cost or volume of the active material, i.e. the volume carrying either electric current or magnetic flux, are compared. But looking at large machines, it is also important to include the cost and complexity of the structure.

At Risø National Laboratory, Denmark, a conceptual survey of generators and power electronics for wind turbines were performed in 2001 [29]. The survey covers all types of generators and drive trains, with or without gears. They do not conclude on a preferred solutions, but comments the different possibilities. Their comments regarding direct drive generators are concerning the maintenance of slip rings and brushes for wound rotor synchronous machines and the uncertainties regarding high temperatures in the PM synchronous machines.

National Renewable Energy Laboratory (NREL, Poore, R. and Lettenmaier, T.) have also presented an report on different drive trains and generators topologies [30]. Regarding

the PM machine they present a SM RFPM with CC from Kaman Electromagnetic Development Centre. This design was chosen in competition with wound rotors, AFPM, interleaved (distributed) windings, because of cost and efficiency. The chosen generator topology was used for both geared PM drive trains, direct driven PM and a multi-PM drive train with a gear with one input shaft from turbine and several shafts for multiple PM-generators. Comparing the PM-drive trains to the baseline (a double fed induction generator with gear) the cost per kWh of the single PM and the multi-PM solution is lower (13% and 11% for a 1.5MW example), while the direct driven has a higher cost per kWh (6%). The cost for the direct driven PM-drive train is 30% higher than the baseline, but due to the increased energy production (lack of gear box and high efficiency generator) the cost per energy is much closer to the baseline. They also present estimates for the trend for increasing sizes (0.75, 1.5 and 3MW) showing increasing cost for the direct driven PM. This is because they have limited the outer diameter to 4m due to transportation. They claim that the optimal size of the PM-generator is larger than 4m.

Polinder, et al. [31] did a comparison of direct drive and geared generator solution in 2005. Their conclusion is that a doubly fed induction generator with a one stage gear would be the most preferable, concerning energy yield per cost, followed by the cheapest solution namely the doubly fed induction generator with a three stage gear. They claim that the PM-generator might be the best solution because it does not have brushes, and have the advantages of a fully rated converter. The RFPM yields the highest energy yield, are cheaper than the wound field generator, but more expensive than the doubly fed induction type generators.

Dubois et al. wrote a paper with a comparison of different direct driven PM-generator topologies in 2000 [32]. He bases the comparison on results presented in the literature, both theoretical and measured results, and thus his list of references is very interesting. His conclusion is that AFPM and TFPM are the most promising topologies for wind turbines, based on a torque density and cost per torque comparison. In his cost analyses he only includes active material, and does not discuss the complexity or the structural mechanics surrounding the active parts. Dubois later built and tested a TFPM generator showing promising results [19].

Another example of an attempt to compare different PM-generator topologies is done by Chen et al. [33] in 2005. They compare 7 different topologies of RFPM and AFPM generators, including both direct drive and geared solutions, with power ratings up to 200kW. Their conclusion is that a double sided AFPM gives most power per volume and that an outer rotor is better than an inner rotor for RFPM machines. In general the direct driven generators are better than the geared solutions.

Lampola presents in his thesis from 2000 a thorough literature study and comparison of different topologies for wind turbines [34]. He concludes that the RFPM generator is the best for large direct driven generators for wind turbines. The PM's makes it possible to have a short pole pitch, thus reducing the diameter compared to wound rotor. And compared to AFPM and TFPM the simple and balanced design of a RFPM is favorable. In his theses he compares different windings and different magnet shapes. He concludes that a curved surface mounted magnet pole is best, giving the lowest price and highest pull out torque. And the most suitable winding is the classical two layer diamond shaped. He also looks at winding with concentrated coils around every second tooth and finds that the performance cost is slightly higher for this machine. But he says that given the simplicity, and the possibility for even further reduced pole pitch compared to the previous machine, it is a most interesting topology for further investigation.

Spooner is a very interesting man when it comes to generator topologies for wind turbines. In the mid nineties he presented his modular RFPM [40, 41] with buried ferrite magnets and stator with E-core and concentrated coils. It led to a prototype generator installed at the Chalmers, Sweden [35], of 40kW and 75rpm. He has been working on AFPM machines with Chalmers [36] and Bumby [37]. And he has presented an outer rotor direct driven generator with ironless stator [38]. The latter is intended for very large diameters, larger than the hub of the turbine. The use of spokes to connect both rotor to the turbine and stator to the tower ensures a very light construction. Using an ironless stator removes the attractive forces between the stator and the magnets in the rotor, and the only forces are the tangential forces from the current in the winding. It is claimed that mass is only 20-30% of an equivalent design with iron cored stator.

Of other works that have been of importance for this thesis handling of the direct driven generators for wind turbines, should be mentioned Grauers thesis from 1996, describing how to design a RFPM generator[39]. He concluded that the RFPM is smaller than other direct driven generators, and that it has higher efficiency than traditional drive trains with gears. Later he and Kasinathan have a couple of publications on the limitations on force density due to reactance and temperature in 2004 [40] and one on force density limitations due to saturation [41]. Both publications address low speed machines. The first paper concludes, given the limitations presented, that for a machine with q = 1 a force density of 100 kN/m^2 is achievable. It is suggested that the reactance should be kept below one. The suggested machine then has a pole pitch of 110mm, a slot depth of 200mm and depth to width ratio of 16. Adding saturation in the iron, the maximum continuous force density is $70kN/m^2$, and about 130-$190kN/m^2$ transient. Interestingly, adding saturation, the available continuous force density peaks at a slot depth of 200mm, yielding $70kN/m^2$. The first paper also shows how the cost of generator and converter increases depending on reactance. They have compared three different control strategies; Current in phase with induced voltage, induced voltage equal to terminal voltage, and a minimization of generator kVA rating, presented by Hystad [42]. Concluding that for reactance lower than 1.4 the induced voltage should be equal to the terminal voltage, and above Hystad's method should be used.

Hystad [42] optimized a single sided TFPM motor proposed by Hennenberger and Brok, 1997 and a double sided TFPM machine presented by Weh, 1995, including the converter and comparing it with Grauers work. He found that when looking at power densities the double sided TFPM machine was superior, but when also including cost, and in particular the cost of the converter, the double sided TFPM was only slightly better than the RFPM.

Pyrhönen, Kurronen and Pariainen presented the design of Rotateks generator at ICEM 2006 [43]. It is a 16Hz, 16 rpm, 3.35MW PM-generator. They present a generator with 12 individual "linear" machines of 280kW 690V that can be individually connected to a converter. The modular design enables easy on site assembly and repair. One of the most important design targets was the low torque ripple, enabling smooth operation on partial load (30% and lower). This is solved by using magnets with sinusoidal, or curved, sides together with slightly overlapping the rows of magnets (skewing).

Of other topologies can also be mentioned M. Leijons cable wound high voltage generator concepts Windformer [44] and Powerformer [45] which can be directly connected to the grid without gear, converters or transformers. But because of the insulation of the cables, the machine grows very large and heavy. An interesting topology is a generator for small wind turbines with outer rotor, surface mounted magnets and coils wound around iron cores, [46] claiming to have a cheaper, lighter and more cost effective generator than other PM-generators for small turbines. Mueller and McDonald presents a C-core RFPM with air

gap (core) winding, with no iron in stator, which reduces the magnetic forces, and thus reduces the structural cost of the generator [47].

1.3.3 Other relevant publications, in particular CC

Magnusson submitted his thesis in 2004 on synchronous PM-machine with field weakening [48] and later a paper in 2005 together with H. Lendenmann [49] where he compares different machines with concentrated windings. He is in particular discussing parasitic effects of the concentrated coils as harmonics in the MMF, torque ripple and rotating radial forces. He finds that the modular prototype has a very low torque ripple and higher torque capability, but higher losses and more noise than a PM-motor with distributed two layer winding.

F. Meier presented her PhD thesis on a directly driven rotating mixer, a low speed direct drive PM machine with non-overlapping coils, in 2008 [50]. The focus is on the mixer, the design and practical consideration concerning the construction and production, but it features also theory and a thorough bibliography on concentrate coils and their performance. She looks into the winding factor, and compares different methods and source. Calculations of torque ripple and cogging is presented. Of special interest is her overview of sources for analytical tools for PMSM with CC, and of machines with CC presented in literature. Of the results are the measurements on the flux from sub harmonic MMF, the belt leakage and the investigation of the inductance and the large constant power speed range of interest.

A. M. EL-Refaie has presented a most interesting thesis on high speed operation of PM-machines[51]. It is the field weakening capabilities of PM-machines that he is addressing. And unlike many authors ha claims that SM RFPM can be designed to have excellent field weakening capabilities. He has designed, built and tested a 6kW SM RFPM w/CC (@6000rpm, 4kW@600rpm), proving that the machine performs excellent according to the optimum field weakening theory. Due to the low permanence in permanent magnets the PM-machines have lower d-axis inductance than q-axis, opposite of synchronous machines with salient pole wound rotors. This gives an advantage regarding field weakening, torque production and voltage regulations. Chen Lie-Tong and Lai shows an example of how to adapt the d- and q-axis inductances for optimal voltage regulation in [52].

Of other literature that should be mentioned, but not much used in this work are the works of Ishak, Zhu and Howe presenting many interesting publications on the PM-machines, and the modelling of them, an example is [53], they are also referred to in [50].

1.3.4 Applications of large PM-machines, a view at the industry

The applications of large PM-machines can be many. But will of course typically be where either the PM's has better performance than induction and wound rotor synchronous machines, makes a cheaper machine or in applications where using PM's is the enabling technology. The typical applications identified are direct driven converter fed low or medium speed applications such as machines for paper mills, generators for wind and tide turbines, and also some hydro turbines, ship propulsion, traction (e.g. trains) and winches, applications requiring reduced rotor losses such as high speed machines or special application such as short motors for elevators placed in the shaft or motors with large air gap such as rim driven propellers or integrated turbine design.

Direct driven generators for wind turbines and large winches are a typical low speed and high torque application. Gears and high/medium speed machines or, for winches, hydraulic motors are the most common solution. Several companies have developed direct driven generators, ABB [44, 45, 54, 55], Siemens [24] and their SWT-3.0-101 DD [56], Jeumont

Electric (AFPM) [57] and Rotatek (now called The Switch) [43, 58]. Areva Multibrid uses PM with a one stage gear[59], also used by Morphic Dynawind (WinWind) [60]. Compared to Enercon's [61]wound field generator the diameters of the direct driven PM generators are half or less for same power rating. Using PM's the pole pitch get shorter and thus the diameter reduces. And when the diameter is reduced, the price also should go down. Vertical Wind in Sweden has some smaller wind turbines with direct driven PM-generators. [62]. Sway and SmartMotor [63] in Norway has developed a concept for floating wind turbines with direct driven generator [64]

For ship propulsion the compactness and low rotor losses using PM's makes it possible both to replace existing machines and utilize new concepts. ABB's podded propulsion is an example of the latest [55, 65]. The rim driven propellers would not have been possible without the PM's, both because of a large air gap, high pole number and the difficulties with external magnetisation. Small versions of rim driven propellers have been used for propulsion and control of remote operated vehicles for a while. But with the improvements of permanent magnets, the solution of some of the hydrodynamics and some challenges concerning the tribology, several companies are now developing rim driven versions of their propellers, for instance Brunvoll's RDT [66] and Rolls Royce's RDTT [67], Van der Velden's EPS [68] and General Dynamics Electric Boat [27]

Other applications that can be mentioned are conversion of wave energy or tidal current energy [69], utilized with a generator with high pole numbers. Kone's AFPM motor for elevators placed in the shaft is an example of special design enabled by the PM's [65]. Direct driven traction motors for trains are another one [24]. Andritz VA Texh Hydro has the EcoBulb and HydroMatrix for low head hydro power plants [70]. ABB has replaced converter fed induction machines and gears with direct driven converter fed PM-machines for paper mill application, thus saving space, investments and maintenance costs [71].

1.4 Ethical and environmental considerations

It is important to evaluate the consequences of one's actions, the ethical aspect, and be aware of the impact ones work might have on the environment. Though it is easy to claim that one's work is just a small insignificant detail in a bigger system, it might still be useful to think through possible consequences. The ethical and environmental considerations have not been an important part of this work, but it is in this short chapter tried to give some pointers of the challenges concerning PM-machines.

The advances in design of electrical machines are focused on more environmental friendly solutions, higher efficiency and cheaper components. Higher efficiency reduces losses in the drive train and thus reducing emissions and waste. The reduction in cost might, to some extent, be a measure of the reduction of energy needed to produce the machine, though there are many other parameters affecting the cost too. Developing specialized direct driven machines can reduce the need for oil lubricated gears, hydraulic systems etc. reducing the environmental hazard. The reduction of cost might also rise ethical questions, since this is often connected with moving production and assembly from countries with well-developed industry (high cost) to countries with cheaper production cost. The cheaper production cost might thus be a result of an exploitation of the work force. There are some focus on this [72] and some discussion around the consequence of extracting rare earth materials from China, focusing on the environmental and human side of the production of permanent magnets [73].

As for the applications presented in this application the integrated PM-motor for the propeller leads to more efficient propulsion system, better utilization of the hull and in general

more efficient ships. The generator for the wind turbine is in itself probably not too bad; it produces renewable energy and removes gears. But many argue that the wind turbine has environmental effects such as destruction of local area, reduction of wild life and in general a reduction of attractiveness of the area affected by the turbines.

1.5 Outline of thesis

The introduction explains the background, the frames and goals of the thesis, trying to set the scene for the prototypes and applications presented later. It includes a short overview of relevant literature and known industrial projects.

Chapter 2 aims to present adequate theory for the work presented in later chapters. The theory is mainly focused on concentrated windings; it is assumed that distributed windings are known for the reader. It is used a small experimental machine to show examples and comparisons throughout chapter 2. It has a 36 slot stator, with coils around every second tooth. All coil ends are available at a switch board, making different connections available. There were built two rotors for the machine, one with 34 poles, and one with 32. In the theory chapter it is also shown examples with 30 poles. The geometry and technical data of the machine is shown in appendix B.

Chapter 3 includes the work connected with the prototype rim driven azimuth thruster. This is an industry application, where the motor is a safe design, using known design features as surface mounted radial flux design with a distributed fractional slot winding. It is included to show an example of how large permanent magnet machines are used in the industry, it is also included to widen the discussion around concentrated windings showing a large low speed permanent magnet machine where other choices for the winding was made. In the chapter there is also discussed the limitation and compromises made when integrating two different disciplines; propeller and electric machine. It includes the discussion around the large propellers and a description of the 100kW prototype design and performance.

Chapter 4 shows an example of an academic machine, not built for perfection or in any way optimized, but its sole purpose is to study, or do experiments, on phenomena's connected with the design. During the discussing leading to the design, it was chosen to focus on the radial flux machine. The chapter shows the preliminary calculations for a 3MW generator for wind turbine, the discussion around the scaling for a prototype and the chosen parameters for the prototype. It further shows the design, and testing on the prototype, focusing on the phenomena's that both where planned to test, and those unintended.

Chapter 5 presents a summary and conclusions of the results from both the PM-motor for the thruster and the wind generator. Suggestions for further work are added and there are presented a comparison of the two winding layouts. A few words about this works contribution to the knowledge of electric machines are added at the end of this chapter (5.4).

Chapter 2
RFPM machine theory

This chapter's goal is to present relevant and sufficient theory to understand the calculations, measurements, discussions, and conclusions presented in later chapters. For the general theory the text books [74-78] have been used. The chapter presents the magnetic modelling, winding layout, calculations of electric parameters, losses, some considerations concerning forces in the air gap and comments on control strategy.

Finite Element Analysis (FEA) has been widely used throughout the project [79]. Due to the available calculation power in personal computers and availability of FEA-programs rather large and geometrical complex construction can be solved rather fast with a relative high resolution. In this work most of the FEA are performed on the entire 2D cross section of the machines. The analytical tools are important for the understanding of the physical phenomena and problems. In this work the analytical expressions are used to find the main parameters and compare and investigate trends and consequences of change of parameters.

2.1 General concepts: Electric loading, magnetic loading and force density

To define the performance of a machine, and compare it with other similar machines, the electric loading, magnetic loading and force density or magnetic shear stress is often used. The parameters say something about how much performance one get from a volume, and how well the volume is utilized. These parameters are limited mainly by thermal limitation (loss in copper) and magnetic saturation in iron part. The definitions presented by Lipo in [75] are used. The chapter only concerns itself with what's going on in the air gap, and thus neglecting inductances, losses and other parameters in the rotor and stator.

The electric loading is a number for how much current is in the machine. The electric loading is limited by the maximum allowed temperature in the machine; the conductive losses, cooling method and cooling area is the main limiting factors. But also reactance and saturation may limit the electric loading [40, 41]. The electric loading is defined as current (rms) per meter around the stator bore eq. (3).

$$ac = \frac{I_{slot} \cdot N_s}{\pi \cdot D_{is}} \tag{3}$$

The magnetic loading is the amplitude value of the fundamental of the flux density in the air gap. The flux density is limited by saturation in the iron parts (teeth and yokes) and the cost of magnets, and is written as

$$\hat{B}_{g,1} \tag{4}$$

Disregarding the winding factor, or assuming that it is unity, the force density or magnetic shear stress can be expressed by eq. (3) and eq. (4).

$$\sigma_m = ac \cdot \frac{\hat{B}_{g,1}}{\sqrt{2}} \tag{5}$$

Field wound synchronous machines is claimed to have a force density of around 30kN/m^2 (Say [76] claims 28kN/m^2 and Lipo [75] 34kN/m^2) and as previously mentioned in 1.3.1 Grauers et. al. claims that for PM-machines could reach 70-100kN/m^2 [40].

In general the electric and magnetic loading have to share the space in RFPM machines, and increasing one of them results in a decrease in the other. Given a constant volume it will therefore be a limit for the force density. In general both the electric and magnetic loading can be increased by the size of the machine, and thus will also the force density increase by the size. This is discussed in more detail in by others for example [40, 41, 75, 76].

The torque and power of a RFPM machine can be found from eq.(5) and the air gap dimensions:

$$T = \frac{D_{is}}{2} \cdot \sigma_m \cdot A_{gap} = \frac{\pi}{2} \cdot \sigma_m \cdot L \cdot D_{is}^{\ 2} \tag{6}$$

$$P = \omega_{mech} \cdot T \tag{7}$$

2.2 Modelling of the permanent magnet and its surrounding

Depending on the need for accuracy and calculation speed different methods can be used. In general there have been used three levels of calculations for finding the flux during the design and analysis. First the very simple method using magnet and air gap length to find the magnetic flux density in the air gap, together with the electric and magnetic loading to identify the main dimensions, then a lumped circuit model to get the final main dimensions, and finally FEA analysis with linear and nonlinear 2D and 3D time stepping and rotation. These three steps above describe the process of the design from the crude design of the first meetings, to the final analysis of the machine.

2.2.1 Lumped circuit models

A basic lumped circuit model of the magnetic circuit for a PM machine with concentrated coils is presented in Fig. 12. The method can give an accurate picture of the flux paths in the machine, assuming the magnetic path is unsaturated. The result from this model is usually the amplitude value of the magnetic flux through the coil (induced voltage) and the amount of leakage. The same method can of course be used for applications with more than one tooth per pole, just add parallel paths for the tooth reluctance.

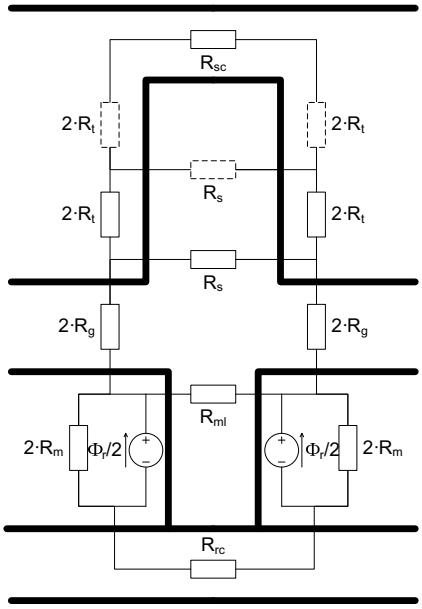

Fig. 12 Principle of lumped circuit model of magnetic circuit, $\Phi_r/2$ is a current source

It is assumed symmetry in centre of tooth and magnets i.e. equal number of magnets and teeth. The reluctances are found from the geometry. The equations for the reluctances are presented in (8) to (14). It is assumed that the diameter, pole number and slot number is so high that slots teeth etc can be assumed parallel. If that is not the case (tapered teeth or slots for example) one can use average values, divide the circuit into more lumped reluctances, etc.

$$\Re_{rc} = \frac{\tau_p}{L_r \cdot w_{rc} \cdot \mu_r \cdot \mu_0} \tag{8}$$

$$\Re_m = \frac{l_m}{L_r \cdot w_m \cdot \mu_{r,Nd} \cdot \mu_0} \tag{9}$$

$$\Re_{g,r} = \frac{g \cdot k_c}{L_r \cdot \tau_p \cdot \mu_0}$$

$$\Re_{g,s} = \frac{g \cdot k_c}{L_s \cdot \tau_s \cdot \mu_0} \tag{10}$$

$$\Re_t = \frac{d_s}{L_s \cdot k_s \cdot w_t \cdot \mu_r \cdot \mu_0} \tag{11}$$

$$\Re_{sc} = \frac{\tau_s}{L_s \cdot k_s \cdot w_{sc} \cdot \mu_r \cdot \mu_0} \tag{12}$$

$$\Re_s = \frac{w_s}{L_s \cdot d_s \cdot \mu_0} \tag{13}$$

$$\Re_{ml} = \frac{\pi}{\mu_0 \cdot L_r \cdot \ln\left(1 + \frac{\pi \cdot g}{\left(\tau_{\mathrm{p}} - w_{\mathrm{m}}\right)}\right)} \tag{14}$$

$$\widehat{\Phi}_r = B_r \cdot w_m \cdot L_r \tag{15}$$

Depending of the degree of simplification the air gap reluctance can be expressed more or less correct using either the pole area or the slot pitch eq. (10). In [75] some consideration around ventilation ducts and their effects on the effective length is presented. There are also different versions of the Carters coefficient (16), in [80] the different coefficient are evaluated. The one used here is:

$$k_c = \frac{1}{1 - \frac{1}{\frac{\tau_s}{w_s} \cdot \left(\frac{5 \cdot g}{w_s} + 1\right)}} \tag{16}$$

The stacking factor in eq. (11) and eq. (12), k_s, is dependent of the lamination type and how it is assembled. It is usually given by the manufacturer, and if properly assembled it should be between 0.95 and 0.97.The magnetic flux in the different parts of the machine can then be found by solving the network. Below are the equations for the flux in the air gap, the tooth and the stator and rotor core given only one slot leakage reluctance.

$$\Re_{eq,1} = \left(\left(4 \cdot \Re_t + \Re_{sc}\right) \| \, \Re_s + 4 \cdot \Re_g\right) \| \, \Re_{ml} \tag{17}$$

$$\Re_{eq,2} = \left(4 \cdot \Re_t + \Re_{sc}\right) \| \, \Re_s \tag{18}$$

$$\widehat{\Phi}_{rc} = \frac{2 \cdot \widehat{\Phi}_r \cdot \Re_m}{4 \cdot \Re_m + \Re_{eq,1} + \Re_{rc}} \tag{19}$$

$$\frac{\widehat{\Phi}_g}{2} = \widehat{\Phi}_{rc} \cdot \left(1 - \frac{\Re_{eq,1}}{\Re_{ml}}\right) \tag{20}$$

$$\frac{\widehat{\Phi}_t}{2} = \frac{\widehat{\Phi}_g}{2} \cdot \left(1 - \frac{\Re_{eq,2}}{\Re_s}\right) = \widehat{\Phi}_{sc} \tag{21}$$

It is assumed that the flux changes as a sine function of time.

$$\Phi\left(t\right) = \widehat{\Phi} \cdot \sin\left(\omega \cdot t\right) \tag{22}$$

The flux densities are found by dividing with the appropriate areas.

Infinite permeability in iron parts

A simplified version of the lumped circuit model is to assume that the iron parts have infinite permeability, and the only reluctance is the one in the air gap and magnets ($\mu_{r,Nd}$=1). There is also assumed no leakage between magnets. In eq. (23) the peak flux density is presented, assuming equal magnet and gap area.

$$\widehat{B}_g = B_r \frac{l_m}{l_m + g} \tag{23}$$

If the magnet area is noticeably smaller than the pole area it would be appropriate to expand eq. (23) into eq. (24), given that the axial length of the pole (rotor) is equal to the machine length.

$$\hat{B}_g = B_r \cdot \frac{l_m}{l_m + g} \cdot k_m \tag{24}$$

The average flux density assuming sine shaped curve:

$$\overline{B}_g = \frac{2}{\pi} \cdot \hat{B}_g \tag{25}$$

This gives the air gap flux per pole:

$$\hat{\Phi}_p = \overline{B}_g \cdot L_r \cdot \tau_p \tag{26}$$

The peak value of the gap flux density will for a machine with q>1/2 give the peak value of the tooth flux density. For a machine with q<1/2 the average value must be used, eq. (27).

$$\begin{aligned} \hat{B}_t &= \hat{B}_g \frac{\tau_s}{w_t} \\ \hat{B}_t &= \overline{B}_g \frac{\tau_s}{w_t} \end{aligned} \tag{27}$$

The core flux density is found from the average air gap flux density.

$$\hat{B}_{sc} = \overline{B}_g \cdot \frac{\tau_p}{2 \cdot w_{sc}} \tag{28}$$

Comparison of simplified and linear lumped circuit model

Using the parameters of the machine from the table model (Appendix A, Fig. 137) some simple calculations of air gap flux density with changing machine parameters is shown (Fig. 13). The motivation for this comparison is to show and point out the differences introduced by simplifying the lumped circuit model. In the figure the horizontal blue line is the plot of eq. (23). The next straight green line is eq.(24), while the red curved line is from the lumped circuit.

From the examples it is evident that assuming infinite permeability and no leakage between poles introduces an error. Including the actual magnet area instead of the pole area assuming infinite permeability coincides fairly well with the lumped circuit. Thus it can be said that for magnets not wider than 0.8 of the pole pitch, with permeability in iron parts higher than 500 and slot width less than 0.5 of the coil pitch, using eq. (24) gives a good impression of the amplitude value of the air gap flux density compared to the linear lumped circuit model.

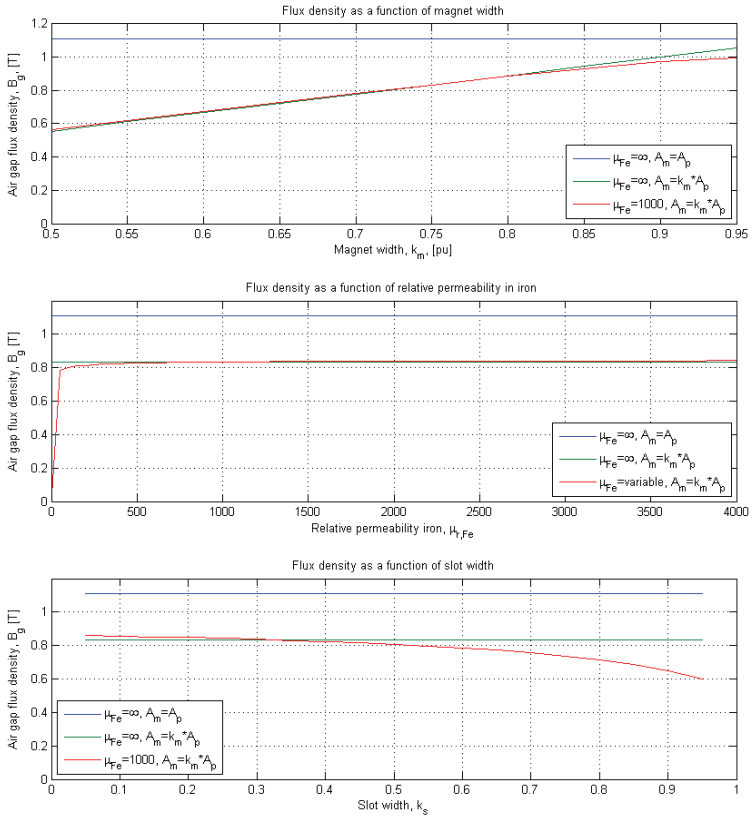

Fig. 13 Result of some evaluation of analytical calculation of magnetic field

2.2.2 Finite Element Analysis (FEA)

Comsol Multiphysics (CM), with the AC/DC module, has been used for FEA [79]. For theory concerning how CM uses the FEM theory consult its manuals. The program features static 2D electromagnetic calculations, nonlinear material properties, rotation, time stepping and 3D calculations.

The calculations of flux density using FEA have been used mainly to investigate and optimize the flux path. However calculation of the magnetic flux is also the basis of the induced voltages, losses in iron parts, eddy currents, forces, torque, inductances etc. It is tried to some extent to explain how the FEA tool is used for the different problems in the later chapters, but in no detail.

Simplifications, symmetry and calculation speed have been, and still is to some extent, a topic when dealing with FEA. With increasing computer capacity, better user interfaces, mesh functions, solvers, visualisations etc. it is easier for the user to calculate larger and more detailed structures, and introduce the FEA on an early stage in the design. In this work most problems have been solved using the entire cross section in 2D.

Having calculated the flux density in 2D the easiest way of finding the flux through an area is to use the vector potential over the cross section. The flux going through a straight line between two points is given by the difference in vector potential between the same two points, eq. (29). Selecting these points correctly one can find the flux through a coil, through the magnet etc. If the number of slots per pole is a fraction, not an integer, the 2D static calculation of the flux density can be used to estimate the flux through a coil as a function of position, hence time. For example a 3 phase machine with 72 slots and 22 poles will for the one static calculation have information of 72 positions of the coils relative to the poles (Fig. 62).

$$\widehat{\Phi} = \left(A_{z,1} - A_{z,2} \right) \cdot L \tag{29}$$

Of course the most correct method would be to integrate the flux density over the cross section, rotate the machine, and find the flux for each step. Regarding this method consult the CM manual.

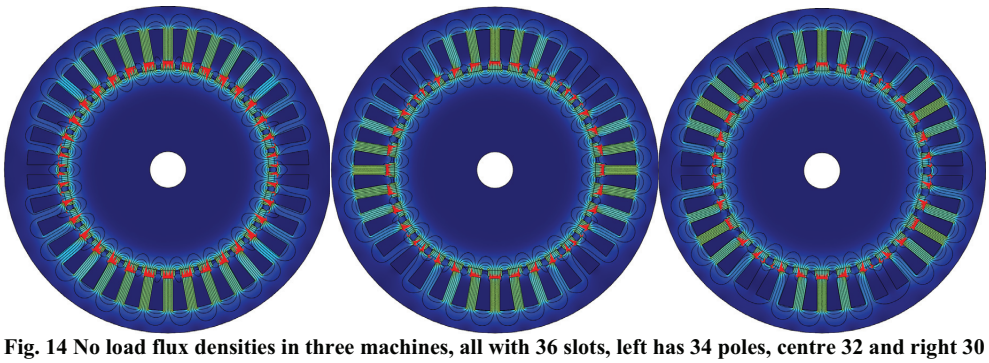

Fig. 14 No load flux densities in three machines, all with 36 slots, left has 34 poles, centre 32 and right 30

2.3 Winding Layout

The theory about how to lay out the winding in electrical machines is well described in several text books, including some of those previously mentioned. Therefore the classical winding layout will only be briefly touched. The focus of this chapter is the concentrated winding, or windings with concentrated coils. It has been claimed in some literature that windings with concentrated coils have poor winding factors, which can be true in smaller machines with few poles and slots. This chapter will show that the winding factor for concentrated coils is high when choosing the appropriate slot and pole combinations, and especially for large low speed application. This chapter is based on [6]. Meier [50], table 3.2, has an overview of different literature regarding winding layout of machines with concentrated coils.

Due to the permanent magnets the effective air gap is large, much larger than in induction and wound field synchronous machines. This reduces the problems induction and wound field synchronous machines have with non-sinusoidal shaped MMF. The harmonics in the MMF travels with different speeds and direction, inducing losses in rotor iron and damper windings. This means that one have fewer restrictions in choosing number of slots and poles, and the winding layout.

Just in case the words used to describe the winding differs from what the reader is used to a clarification is given here.

- A machine has a number of slots (N_s), poles (N_p) and phases (N_{ph}) and a common definition of the relation between them is q, number of slots per pole and phases, eq. (30). If q is an integer the winding is an integer winding, else it is called fractional.

$$q = \frac{N_s}{N_p \cdot N_{ph}} \tag{30}$$

- A machine has several coils per phase (N_c), which all can be in series or in two or more parallel circuits (C). Each coil consists one or more turns (N), and each turn consists of one or more parallel conductors (N_{cond}).
- The name classical windings is used about integer and fractional windings with q>1/2 and overlapping end windings. It is also referred to as distributed winding since several coils is distributed over one pole.
- Windings with concentrated coils or concentrated winding refers to a fractional winding with q<1/2 and none overlapping end windings. It comes in two versions, one with coils around every tooth named two layer or consecutive wound, and one with coils around every second tooth, called one layer or alternating wound. Both windings have the same number of turns per slot, the difference is the size of the end winding and that the consecutive wound machine will have two different phases in the same slot in some of the slots.

2.3.1 The motivation for introducing concentrated windings

The argument for introducing permanent magnets into an electric machine can be many and have been presented numerous times. For low speed high torque application the permanent magnet pole can be narrower for a given flux density than a wound pole. This can be used to increase the frequency or decrease the diameter. For the low speed high torque machine the direct driven generators for wind turbines are good examples. Enercon's generator has an outer diameter of about 14m while the Siemens' PM-generator and Rotatek's (the Switch) generator have outer diameters of around 6m. For general applications with drives the PM-machines introduces higher power density and cheaper solutions.

In high poled electric machines with permanent magnets the diameter of the machine is no longer defined by the field windings need for space. And for very low speed, high torque machines as e.g. direct driven generators for wind turbines the stator winding is now limiting the design parameters. The previous mentioned machines are also examples of machines where the very low speed has resulted in a low frequency (around 16Hz). One of the reasons is because the pole arch cannot be reduced further since it is limited by the slot width. A classical winding demands three or more slots per pole, and having usually half slot half iron in the stator that only leaves one sixth of the pole width for the slot. When decreasing the slot width the fill factor also decreases since it is more difficult to fill in copper and the thickness of slot insulation is constant. The result is that the slot depth increases faster than the slot width decreases. With deeper and narrower slots the reactance grows, there are also some thermal limitations since much of the heat has to be removed trough the long teeth to the stator core [40]. By optimizing the machine with the limitation that there have to be more than 3 slots per pole the result is a trade off by low frequency and choice of diameter.

By introducing concentrated coils, where the number of slots is close to the number of poles the slot width can be increased, the fill factor kept high and the frequency kept at a higher level.

This argumentation is of course simplified, there are many other parameters influencing the dimensions of a machine, reactance is one. But in general a smaller diameter and a higher frequency reduce weight, and thus the cost, of a machine. And for all optimized machines it is

the one with the sufficient performance that cost the least that is the best, not the expensive one with the superior performance.

Other arguments are the simplicity: assembling and repairing a concentrated coil, where there is no overlap in the end windings is much easier than for distributed windings. With one layer windings the coils only needs to be insulated from ground, not different phases, both in the slots and in the end winding. As it can be seen in later chapters the phase shift for each coil in the machine can be used to make multiphase (N_{ph}>3) machines, and by choosing the slot and pole combination right the coupling between coils are small or neglectable, thus having favourable conditions for control. The decoupling also increases the fault tolerance, since a fault in one coil has less influence on the others. Regarding the fault tolerance of concentrated windings (coils) Mitcham et al presents a paper, describing the pros regarding multiphase and non-overlapping coils [81].

2.3.2 Slots, poles and their relative electric positions

Given a machine with N_p poles and N_s slots, the machine will have a total of $N_p \cdot \pi$ electric radians per revolution giving a slot pitch in radians of

$$\gamma_s = \frac{N_p \cdot \pi}{N_s} = \frac{\pi}{q \cdot N_{ph}} \tag{31}$$

Depending of phase spread (σ_e, usually assumed to be 60 degrees), number of phases (N_{ph}, usually assumed to be 3) and disregarding how the coils are connected together each slot can be assigned to a phase. All slots within 0 to 60 degrees will then belong to phase A, between 60 to 120 degrees to phase B, 120 to 180 to phase C, 180 to 240 to phase A and etc. The phase spread and phases is illustrated in Fig. 15.

0-60	60-120	120-180	180-240	240-300	300-360(0)
Phase A	Phase B	Phase C	Phase A	Phase B	Phase C
360-420	420-480	480-540	540-600	600-660	660-720
Phase A	Phase B	Phase C	Phase A	Phase B	Phase C

etc…

Fig. 15 Phase spread and phases

Two examples are shown in Fig. 16 and Fig. 17. The first figure shows a four pole machine with 21 slots, the latter a machine with 34 poles and 36 slots. Both examples assume three phases and a phase spread of 60 degrees.

In Fig. 16 and Fig. 17 the two figures to the left show how each slot (arrows) is placed relative to the magnets (black and white pie-pieces). In Fig. 16 the classical distributed winding is shown where a number of slots are placed over a pole and thus having different electrical angles. The colours of the arrows indicate the phases (given three phases and 60 degrees phase belt). To the right the slots position in electrical angles is given. One rotation of the right pie is then equal to one pole pair (black and white pie piece), and one can see that the different slots falls nicely in under the different phases.

In Fig. 17 is an example of a concentrated winding with approximately one slot per pole. But since the numbers are not equal the phase spread becomes distributed much in the same way as the classical winding, electrically.

This exercise places the different slots in the different phases, but does not consider how to connect the phases. For the two layer distributed winding with q > ½ this solves itself by choosing an appropriate chording, while for one layer distributed and both concentrated

windings some considerations must be done. For how to lay out a classical distributed winding ordinary textbooks should be consulted. The following chapter describes a technique for how to lay out the concentrated winding.

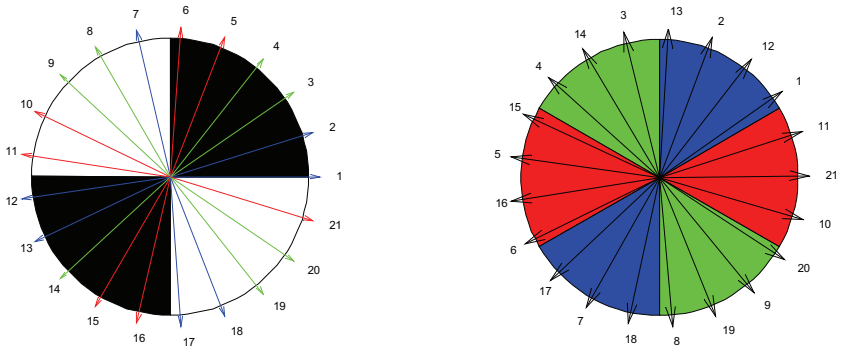

Fig. 16 Mechanical (left) and electrical (right) positions of the slots for a 4 pole 21 slot machine. The numbers denote the slot numbers and colors the phase, the black and white pie pices of the left figure are the poles, and for the figure to the right the phase spread is 60 deg.

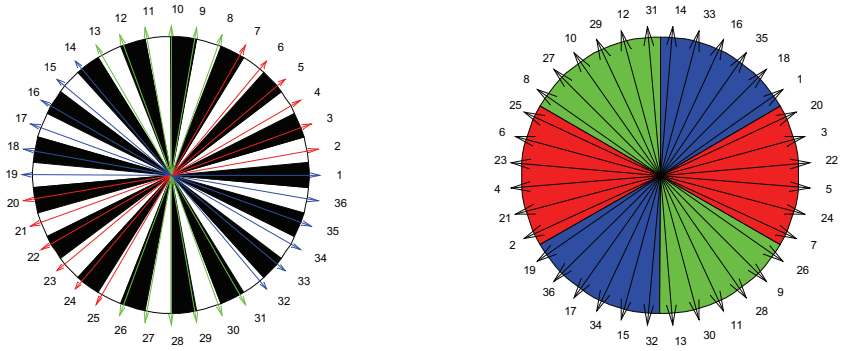

Fig. 17 Mechanical (left) and electrical (right) positions of the slots for a 34 pole 36 slot machine. . The numbers denote the slot numbers and colors the phase, the black and white pie pices of the left figure are the poles, and for the figure to the right the phase spread is 60 deg.

2.3.3 Concentrated windings q<½

As mentioned there are two types of concentrated windings, one with coils around every tooth (consecutive or 2 layer) and one around every second tooth (alternating or one layer). When dealing with concentrated coils it can be easier to relate the coil angles to the teeth instead of the slots. Then each coil can be assigned the electrical angle of the tooth it is wrapped around, instead of the sum of the two slots the coil is occupying. Thus can each coil be assigned the phase it belongs depending on its electrical angle and the chosen phase spread, a set of examples are shown in Table 2. The result is that the coil span for both windings equals the slot pitch, important for the chording factor, while the angle between the coils is equal to the slot pitch for consecutive wound coils (32), and twice the slot pitch for the alternating wound coils (33), which is important for the distribution factor.

$$\gamma_c = \gamma_s \tag{32}$$

$$\gamma_c = 2 \cdot \gamma_s \tag{33}$$

The rules for a concentrated winding are:

- The number of poles must be even
- The number of slots cannot be equal to the pole number
- The number of coils must be a multiple of N_{ph}
- The number of pole pairs, in a section, N_{pp}/F_1, cannot be a multiple of N_{ph}

The number of sections, F_1, describes in how many parts a machine can be divided where each part can operate as a separate machine and fulfil the demands given above. The number of sections is the greatest common divider between total number of slots, N_s, and pole pairs, N_{pp}.

Using the rules above it is evident that for a consecutive wound concentrated winding the allowed slot number is a factor of number of phases, 3, 6, 9, etc. for a three phase machine, while for an alternating wound machine the allowed slot number is a multiple of 2 times the number of phases, 6, 12 18 etc. for a 3 phase machine. In Table 1 some examples of machines with different numbers of poles, slots and sections are presented.

Table 1 Examples of number of poles, slots and sections, N_{ph}=3

N_s	N_p	N_{pp}	F_1	N_{pp}/F_1	F_2	N_p/F_2	q
120	118	59	1	59	2	59	20/59
120	116	58	2	29	4	29	10/29
36	34	17	1	17	2	17	6/17
36	32	16	4	4	4	8	3/8
36	30	15	3	5	6	5	2/5
27	26	13	1	13	1	26	9/26
27	24	12	3	4	3	8	3/8

The number of sections, F_1, is also an indication of how many parallel paths one can have in the machine. That is if number of pole pairs per section is even, the number of parallel paths is two times the number of sections, or if the number of pole pair is odd the number of parallel paths is equal to the number of section. As one can see from Table 1 the number of parallel paths is then equal to the difference between pole and slot numbers.

The difference in slot and pole number will also define how many parallel paths and individual sections a machine might be divided into. To separate F_1 and F_2, F_1 is referred to as sections, while F_2 as parts.

$$F_2 = \left| N_p - N_s \right| \tag{34}$$

If the number of poles dived by number of parts (F_2) is even, the number of sections (F_1) is equal to F_2. If the number of poles dived by F_2 is odd the number of sections (F_1) is equal to $F_2/2$. Dividing the machine into F_2 parts, all coils in the same phase within a part must be connected in series, but the different parts can be connected in parallel.

As an example one can consider the machine in Table 1 with 120 slots and 116 poles. F_2 is equal to 4, dividing the machine into parts with 29 poles and 30 slots each. The number of section, F_1, is two. Hence can the machine be divided into two individual machines, with a total of four parallel paths. In Fig. 18.a) the physical position of the parts and phases together with their electrical angle is shown. In b) the electrical displacement between the parts is shown indicating that even and odd number parts are in opposite directions (electrically). In c)-e) different possibilities for connection between the parts are shown.

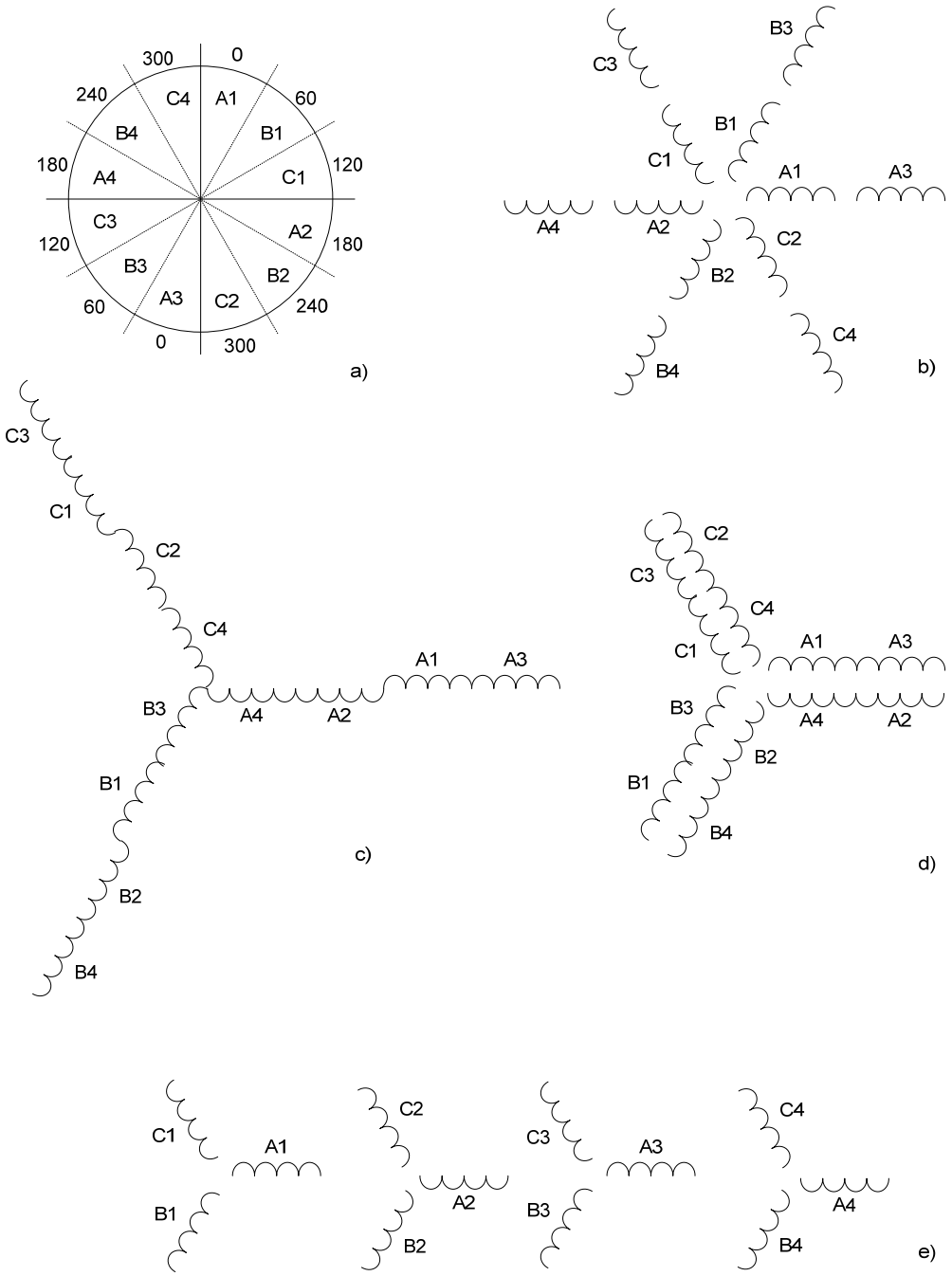

Fig. 18 Example of possible connections of a 120 slot, 116 pole, 3 phase machine with phase spread of 60degrees. a) Phases (A B C) and parts (1 2 3 4). b) Electrical positions. c) All parts in series. d) Two in parallel, common neutral, e) Four in parallel, separate neutral

Table 2 Winding layout for a 36slot stator with 3 different pole numbers

Tooth	30 poles		32 poles		34 poles	
number	1layer	2layer	1layer	2layer	1layer	2layer
1	A	A'	A	A	A	A'
2		A		A'		A
3	C'	C	A	A	A	A'
4		C'		C		A
5	B	B'	C'	C'	A	A'
6		B		C'		A
7	A'	A	B	B	C'	C
8		A'		B'		C'
9	C	C'	B	B	C'	C
10		C		A		C'
11	B'	B	A'	A'	C'	C
12		B'		A		C'
13	A	A'	C	C	B	B'
14		A		C'		B
15	C'	C	C	C'	B	B'
16		C'		B		B
17	B	B'	B'	B'	B	B'
18		B		B		B
19	A'	A	A	A	A'	A
20		A'		A'		A'
21	C	C'	A	A	A'	A
22		C		C		A'
23	B'	B	C'	C'	A'	A
24		B'		C'		A'
25	A	A'	B	B	C	C'
26		A		B'		C
27	C'	C	B	B	C	C'
28		C'		A		C
29	B	B'	A	A'	C	C'
30		B		A		C
31	A'	A	C	C	B'	B
32		A'		C'		B'
33	C	C'	C	C'	B'	B
34		C		B		B'
35	B'	B	B'	B'	B'	B
36		B'		B		B'

2.3.4 Winding factor for concentrated windings

Usually one finds the flux per pole, and uses the winding factor for calculating how well a coil and a winding utilizes the flux. The winding factor is found for the fundamental and for the harmonics, and if properly designed the winding can eliminate or reduce unwanted harmonic contents in the MMF. It has in general three parts: chording, distribution and skewing. Skewing is not presented here since it has not been considered for the example designs. The equations presented her are based on standard literature, rewritten to fit with the concentrated winding.

Chording factor

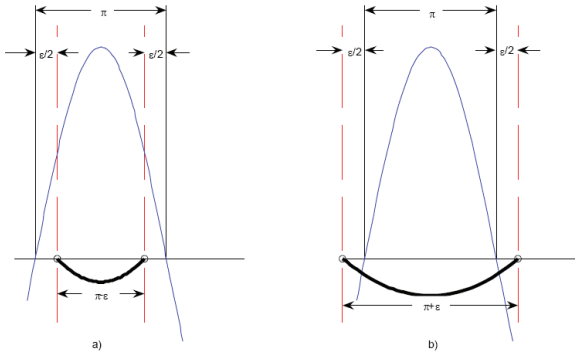

Fig. 19 Chording; Coil span compared to the pole span, a) coil span is shorter than the pole, b) coil span is longer than the pole[6].

The chording describes how much flux each coil entwines. For both types of concentrated winding the coil span is the same, equal to a slot pitch. This is based on the assumption that all flux is in the tooth, and none in the slot. The chording angle, ε, is found from:

$$\varepsilon = \pi - \gamma_s \tag{35}$$

And the chording factor from:

$$k_{en} = \cos\left(\frac{1}{2} \cdot n \cdot \varepsilon\right) \tag{36}$$

where n is the harmonic number and n=1 is the fundamental. With a high number of poles, the slot number can be chosen close to the number of poles, the coil pitch is close to 180degrees and the chording factor close to unity, eq.(37).

$$\begin{aligned} N_p &\approx N_s \Leftrightarrow \\ \gamma_s &\approx 180° \Leftrightarrow \\ k_{e,1} &\approx 1 \end{aligned} \tag{37}$$

Distribution factor

The distribution factor is the relationship between the arithmetic sum and the vector sum of voltages in series connected coils. Based on the equation presented by for example Say [76] for classical fractional slot winding the equation for concentrated winding can be found:

$$k_{dn} = \frac{\sin\left(\frac{n \cdot \sigma}{2}\right)}{z \cdot \sin\left(\frac{n \cdot \sigma}{2 \cdot z}\right)} \tag{38}$$

where σ is the phase spread, and z is numerator between the number of coils and the product of number of phases and poles.

$$q' = \frac{z}{b} = \frac{N_c}{N_p N_{ph}} \tag{39}$$

q′ is equal to q when all teeth are wound, but only half (q′=q/2) when every second tooth is wound.

Winding factor

The winding factor is simply the product of the previous mentioned factors:

$$k_{wn} = k_{dn} \cdot k_{en} \tag{40}$$

In Fig. 20 the chording, distribution and winding factor is plotted as a function of q. Illegal combinations of slots and poles are not removed, so not all combinations might be allowed. Examining the winding factors in Fig. 20, it can be seen that in general the best factor is achieved around q=1/3. q = 1/3 is not an option since it would lead to a one phase machine with serious cogging. The dominating factor is the chording factor; the distribution factor varies between 0.955 and 1. The winding factor for q close to 1/3 is equal to 0.955. For the consecutive wound machine this is the highest achievable winding factor. But for the alternating wound machine some values of q gives a higher winding factor. This can be seen in Fig. 21 which shows a more detailed view of Fig. 20. The blue line is at 0.955. In Table 3 it is presented what kind of q-values are needed to get above winding factors 0.955, 0.95 and 0.9. It is chosen to show the q-values as fraction, rather than decimals since it is then easier to relate the values to eq. (30). The coil span corresponding to the different q-values are also presented.

Looking at the difference between every (top) and alternating (bottom) tooth wound machine in Fig. 20 the only difference is that it is shorter between the high spots of the distribution factor, with the result that the winding factor for the consecutive wound machine is limited to 0.955. This is because the angle between the coils in an alternating wound machine is twice the angle in a consecutive wound machine.

The denominator of q in Table 3 tells something about the minimum pole number that can be chosen and still have a high winding factor. Thus is it easy to see that there are few options for low pole numbers. Machines with concentrated coils must either work on low speeds, or at high frequencies to utilize its advantages towards classic electric machines. The two best choices regarding winding factor for a three phase machine is q equal to 2/7 and 2/5, resulting in a minimum pole number of 14 and 10 (both with 12 slots). As can be seen from Table 4 a higher pole number also increases the variety of pole and slot combinations.

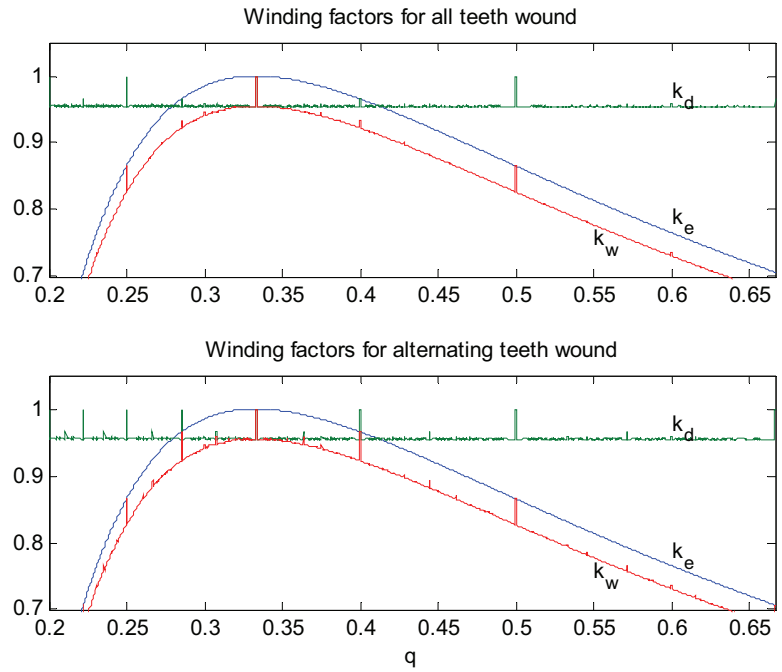

Fig. 20 Fundamental chording, distribution and winding factor as a function of q, top is with all teeth wound, and bottom with alternating tooth wound

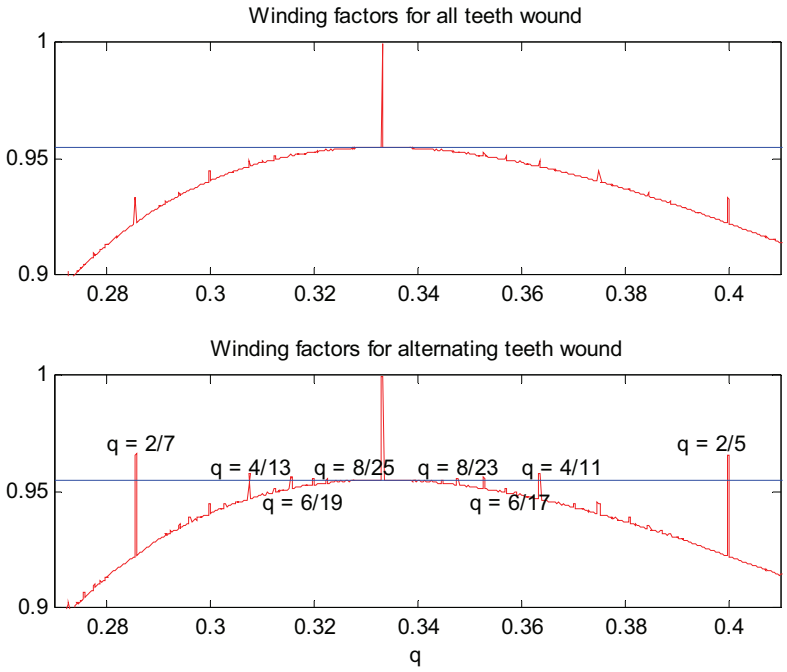

Fig. 21 Fundamental winding factor, zoomed in around q=1/3, same figure as Fig. 22

Table 3 Winding factors, q and slot pitch

	Consecutive		Alternating	
k_w	q	γ_s	q	γ_s
>0.955	-	-	2/7, 4/13, 6/19, 8/25, 8/23, 6/17, 4/11, 2/5	210, 195, 190, 187.5, 172.5, 170, 165, 150
>0.95	[5/16,5/14]	[192,168]	2/7, 4/13, [5/16, 5/14], 2/5	210, 195, [192, 168], 150
>0.90	[3/11, 3/7]	[219,141]	[3/11, 3/7]	[219, 141]

It is usually assumed that a feasible range of q is from ½ to ¼ for a three phase machine. This results in a coil pitch from 240 to 120 degrees. The winding factor for the two extremities is 0.866. The distribution factor is favourable at those points, but the winding factor for the points on the inside is 0.827. For small machines this might be acceptable, but for larger machines the winding factor should be higher. And as shown in Table 3 if a winding factor higher than 0.95 is wanted, q should be between 5/16 and 5/14.

In Table 4 the winding factor for the examples from Table 1 is presented. It shows that an alternating winding, giving the right conditions, can have a higher winding factor than a consecutive wound machine[82].

Table 4 q and winding factors for some slot and pole combinations (same combinations as in Table 1)

N_s	N_p	q (N_{ph}=3)	$\gamma_s[^o]$	Consecutive k_w	Alternating k_w
120	118	20/59	177	0.9452	0.9452
120	116	10/29	174	0.9547	0.9555
36	34	6/17	170	0.9525	0.9562
36	32	3/8	160	0.9452	0.9452
36	30	2/5	150	0.9330	0.9659
27	26	9/26	173	0.9538	-
27	24	3/8	160	0.9452	-

Comparison

It has been published several papers on winding factors for machine with concentrated coils, for example [82-86] and F. Meier has listed several relevant sources regarding the topic in [50]. The somewhat tedious process of finding the winding factor presented in some of the literature was the motivation for the paper [6]. Comparing the result of the winding factor equations all equations usually yields the same results, but not always. The tables presented by [83] coincides well with the factors calculated in [6], [86] and [85] also yields the similar result except for the combinations (N_s/N_p) 12/9, 16/18, 16/21 and 22/21. The difference is minor, but still evident. [84] coincides well for the values within the same range, but alternating and consecutive wound are mixed in the same table. It is also added some values way out of the range (q<1/4) of what is considered feasible for concentrated winding with very high winding factors. These high factors occur when a coil spans 3, 5, 7 poles etc.

2.4 Magneto Motive Force (MMF)

MMF or ampere turns (NI) is the driving force for magnetic flux in the stator and is created by the current in the slots. In induction and wound pole synchronous machines it is a necessity that the MMF is sinusoidal with low harmonic content due to the small air gaps. An example of a nice and sinusoidal MMF curve is presented in Fig. 22. It can be seen that the second spatial harmonic corresponding to the 4 poles (2 pole pairs) is the significant, and that the harmonics are small, with the most significant 5^{th}, 7^{th}, 23^{rd} and 25^{th} .

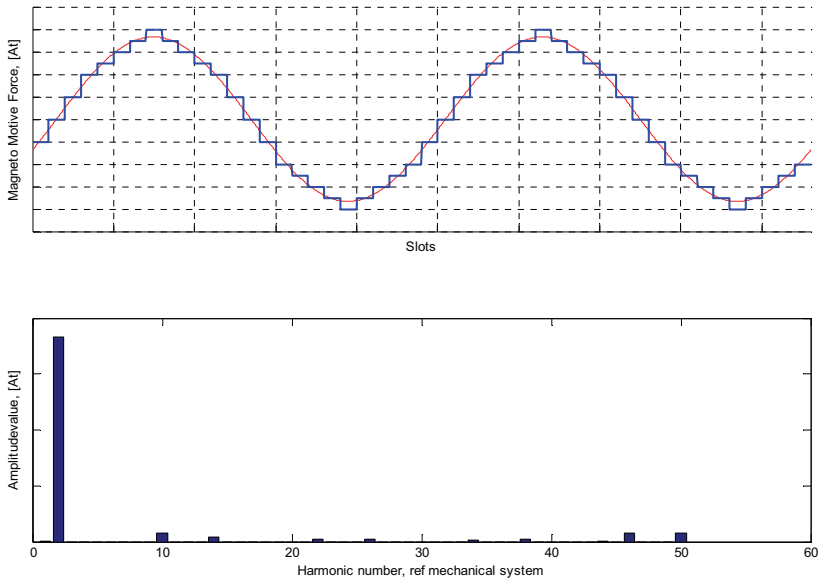

Fig. 22 MMF from a 4 pole machine with 48 slots, two layer winding and a coil span of 12 slots

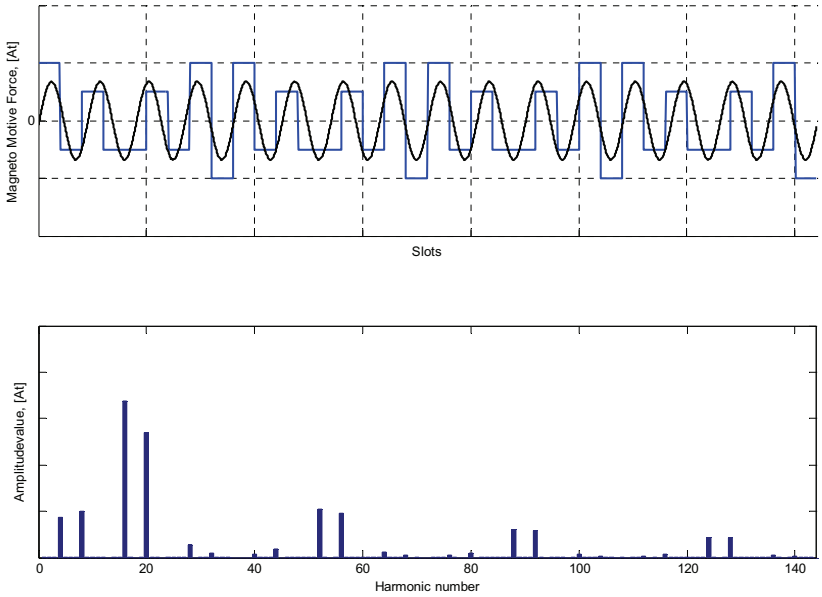

Fig. 23 MMF from a 32 pole machine with 36 slots and two layer concentrated winding, h=Np/2 is the black sinus

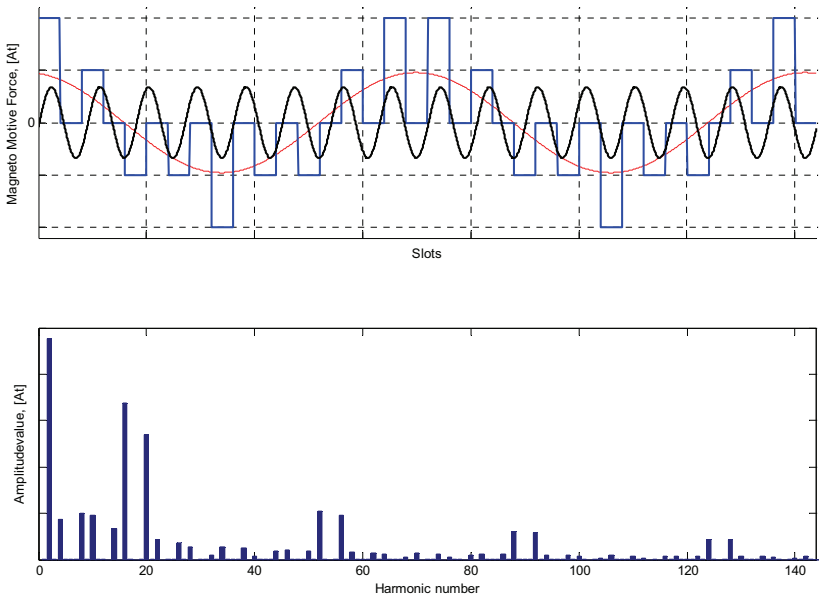

Fig. 24 MMF from a 32 pole machine with 36 slots and one layer concentrated winding, h=Np/2 is the black sinus, while the red is the lowest spatial harmonic (h=2)

MMF from concentrated winding

Examining the curve of the MMF from a machine with concentrated winding it is obvious that the MMF is far from smooth, and that the harmonic content is high. In Fig. 23 and Fig. 24 the MMF for a machine with 32 poles and 36 slots is shown. Fig. 23 is showing the MMF from a two layer winding and Fig. 24 a one layer winding. Both have 16 pole pairs, and thus it is the MMF from the 16^{th} spatial harmonic that will work with rotor and create torque. The main difference is that the one layer machine has a very prominent low (sub) harmonic wave with two periods, and the one layer winding has more components than the two layer. In Fig. 23 and Fig. 24 the 16^{th} harmonic is equal (same number of ampere turns per slot).

The example presented in Fig. 23 and Fig. 24 is not representative for all concentrated windings. With 32 poles and 36 slots the machine has equal number of sections and parts, 4 , with 8 poles, or 4 pole pairs, in each.. For all other machines presented in this work one needs two parts to create a machine ($F_1=F_2/2$). In Fig. 75 and Fig. 76 MMF from such a machine is presented, showing that the higher harmonic ($>N_p/2$) content is equal both in amplitude and harmonics numbers, while the sub harmonics ($<N_p/2$) have the same harmonics, but with much lower amplitude for the two layer winding.

MMF pattern from concentrated winding

There is a pattern for the MMF based on the difference in pole and slot number, and the number F_1 and/or F_2. In Table 5 some examples of patterns are presented and in in Table 6 the harmonic components from Fig. 23 and Fig. 24 are presented as black. Disregarding the amplitude of each harmonic, the harmonics present are equal for one and two layer windings, except for the combination 36/32. It can further be seen that the pattern for MMF can be expressed by N_{ph}, F_1 and F_2. But for this low number of combinations of poles and slots, it cannot be claimed to be conclusive. Regarding the pattern for the 32 pole 36 slot machine in Table 5 this is different from the others, having F_1 equal to F_2, meaning that each part defined as in eq. (34) works as a separate machine with an even pole number, while for the other machines in Table 5 two of these parts are needed to make a complete machine.

Table 5 Overview of harmonic content in MMF for selected machines

				Fundamental space MMF		Pattern of MMF The space harmonics present	
N_s	N_p	F_1	F_2	1 layer	2 layer	$(F_2 \cdot N_{ph} \cdot n \pm F_1)^*$	$(F_1 \cdot N_{ph} \cdot n \pm F_2)^*$
120	118	1	2	1	1	6n±1, n=0,1.2...	3n±2, n=1,3,5...
120	116	2	4	2	2	12n±2, n=0,1.2...	6n±4, n=1,3,5...
36	34	1	2	1	1	6n±1, n=0,1.2...	3n±2, n=1,3,5...
36	32	4	4	2	4	1 layer: 6n±2, n=0,1.2...	3n±1, n=1,3,5...
						2 layer: 12n±4, n=0,1.2...	6n±2, n=1,3,5...
36	30	3	6	3	3	18n±3, n=0,1.2...	9n±6, n=1.3,5...

* Except for the combination of 36/32

Table 6 The harmonics of one and two layer winding for a 32pole 36slot machine

Np	32																			
Ns	36																			
Nph	3																			
h	One	Two	h	One	Two	h	One	Two	h	One	Two	h	One	Two	h	One	Two	h	One	Two
1	-	-	25	-	-	49	-	-	73	-	-	97	-	-	121	-	-	145	-	-
2		-	26		-	50		-	74		-	98		-	122		-	146		-
3	-	-	27	-	-	51	-	-	75	-	-	99	-	-	123	-	-	147	-	-
4			28			52			76			100			124			148		
5	-	-	29	-	-	53	-	-	77	-	-	101	-	-	125	-	-	149	-	-
6	-	-	30	-	-	54	-	-	78	-	-	102	-	-	126	-	-	150	-	-
7	-	-	31	-	-	55	-	-	79	-	-	103	-	-	127	-	-	151	-	-
8			32			56			80			104			128			152		
9	-	-	33	-	-	57	-	-	81	-	-	105	-	-	129	-	-	153	-	-
10		-	34		-	58		-	82		-	106		-	130		-	154		-
11	-	-	35	-	-	59	-	-	83	-	-	107	-	-	131	-	-	155	-	-
12	-	-	36	-	-	60	-	-	84	-	-	108	-	-	132	-	-	156	-	-
13	-	-	37	-	-	61	-	-	85	-	-	109	-	-	133	-	-	157	-	-
14		-	38		-	62		-	86		-	110		-	134		-	158		-
15	-	-	39	-	-	63	-	-	87	-	-	111	-	-	135	-	-	159	-	-
16			40			64			88			112			136			160		
17	-	-	41	-	-	65	-	-	89	-	-	113	-	-	137	-	-			
18	-	-	42	-	-	66	-	-	90	-	-	114	-	-	138	-	-			
19	-	-	43	-	-	67	-	-	91	-	-	115	-	-	139	-	-			
20			44			68			92			116			140					
21	-	-	45	-	-	69	-	-	93	-	-	117	-	-	141	-	-			
22		-	46		-	70		-	94		-	118		-	142		-			
23	-	-	47	-	-	71	-	-	95	-	-	119	-	-	143	-	-			
24	-	-	48	-	-	72	-	-	96	-	-	120	-	-	144	-	-			

Speed and direction of rotation for the harmonics of the MMF

The speed of the different harmonics is given by:

$$\omega_{mech,h} = \frac{N_{pp} \cdot \omega_{mech,N_{pp}}}{h} \tag{41}$$

$$\omega_{mech,h,rotor} = \omega_{mech,h} - \omega_{mech,N_{pp}} \tag{42}$$

$$\omega_{el,h} = h \cdot \omega_{mech,h} \tag{43}$$

where $\omega_{mech,Npp}$ is the mechanical speed in rad/s of the component equal to the pole pair number of the machine, and $\omega_{mech,h}$ the speed of the harmonic h. The electric speed is found by multiplying the mechanical speed with the pole pair number of each harmonic (i.e. harmonic number), thus most convenient to use rad/s. In (42) the speed of the harmonic relative to the rotor is given. Each harmonic component has a clockwise and counter clockwise rotating part. The MMF can be expressed as:

$$\begin{aligned} MMF_h(t,\theta) &= NI_h \cos(h\cdot\theta)\cos(\omega t) \\ &= \frac{NI_h}{2}\left[\cos(\omega t - h\cdot\theta) + \cos(\omega t + h\cdot\theta)\right] \\ MMF_{h,CW}(t,\theta) &= \frac{NI_h}{2}\cos(\omega t - h\cdot\theta) \\ MMF_{h,CCW}(t,\theta) &= \frac{NI_h}{2}\cos(\omega t + h\cdot\theta) \end{aligned} \tag{44}$$

MMF_{CW} rotates clockwise while MMF_{CCW} rotates counter clockwise. The direction of the rotor is usually defined positive in the counter clockwise direction. When adding the fundamental current of three phases some of the CW and CCW cancels out, leaving the components of space harmonics to travel either CW or CCW. Looking at the sign in front of

the latter part of the pattern in Table 5 and comparing it with the sign of the harmonic corresponding to the pole pair number one can determine which direction the harmonics travel. The ones with the sign equal to the pole pair number travels with the rotor, while the others travels against the rotor.

$$h = F_1 \cdot N_{ph} \cdot n \pm F_2 \tag{45}$$

Using (45), the examples from Table 5 and assuming that the rotor rotates CCW, the harmonics corresponding to $F_1 \cdot N_{ph} \cdot n + F_2$ travels CCW while $F_1 \cdot N_{ph} \cdot n - F_2$ travels CW. This sub chapter regarding direction and rotation is based on [87] and [88].

Total Harmonic Distortion (THD) and a method to reduce sub harmonics

Examples of flux lines from the MMF are presented in Fig. 25 and Fig. 26. They show how the sub harmonic content of MMF penetrates the rotor. Especially for the one layer windings this is evident. The two layer winding has a much lower content of sub harmonic flux in rotor.

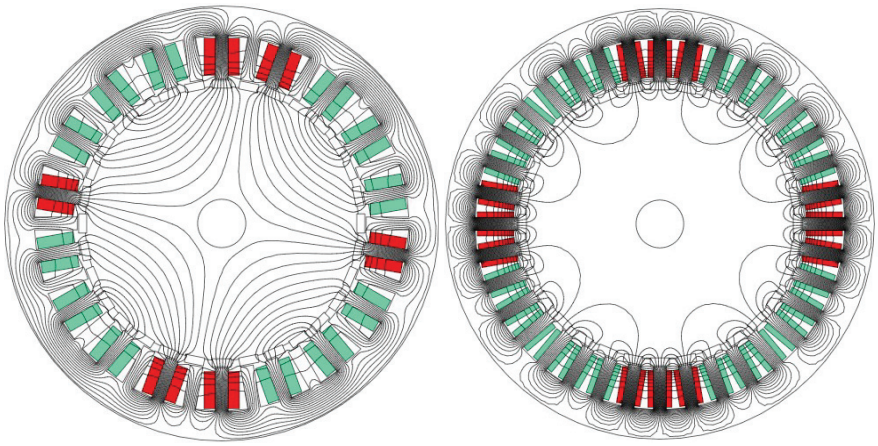

Fig. 25 32 pole 36 slot machine, left one layer, right two layer, red implicates phase A, full current, green half current in the two other phases

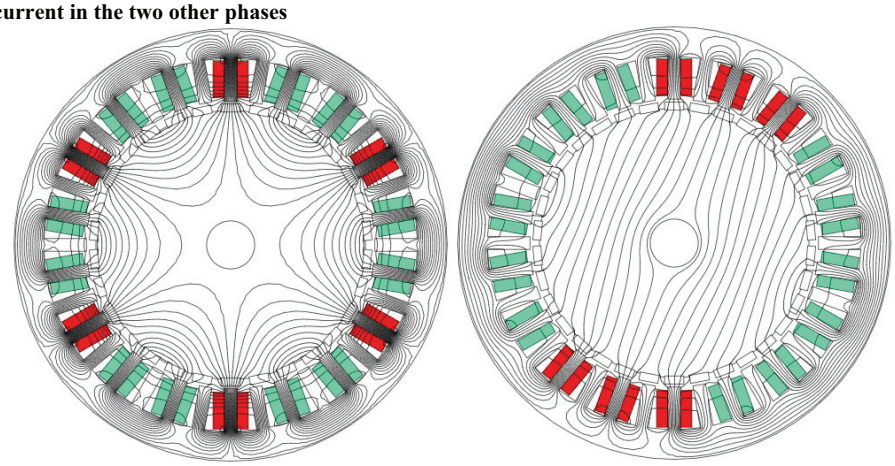

Fig. 26 To the left 30pole 36slot machine, right 34pole 36slot machine

Regarding the sub harmonic components of the MMF it creates a large flux due to the long wave length (area). The reluctance is mainly dependent of the air gap length and the wavelength (width) of the component. By introducing tangential air gaps in the stator and or rotor these sub harmonic components can be reduced. In Fig. 27 results from different segmentations of stator and rotor with tangential air gaps is shown. The MMF in the air gap and its harmonic components are shown in Fig. 28 and Fig. 29. The MMF values are normalized to the amplitude value of the component corresponding to the number of pole pairs in the reference machine. All tangential air gaps in this example are equal and 2mm long.

In Table 7 the value of the fundamental space harmonic for each of the sectioning in this example is shown, together with the space harmonic corresponding to the pole pair number and the total harmonic distortion. The equation for the total harmonic distortion used here is shown in eq. (46). The results shows that regarding the MMF the best way to section the machine is either with method 4), dividing the stator in 6+6sections, or with method 6), having the rotor sectioned in 34 parts, equal to N_p, with a tangential gap below each magnet. Sectioning the rotor gives the lowest fundamental spatial harmonic MMF_1 and highest $MMF_{Np/2}$ (fundamental electric component), while having the gaps in the stator yields the lowest amount of THD. The influence on the flux from the magnets is not considered, but dividing the rotor is probably more favourable for the magnets. Dividing under the centre of each magnet, the path for the flux from the magnet should more or less be undisturbed, not causing cogging unbalance or extra losses. The length of tangential gaps in rotor must be in proportion to the wave length of the harmonic and the air gap.

$$THD_{\%} = 100 \cdot \sqrt{\sum_{h \neq Np/2} \left(\frac{MMF_h}{MMF_{Np/2}} \right)^2} \tag{46}$$

Regarding the other methods presented, dividing the stator in only two sections are no good, Fig. 28.2, reducing the torque producing MMF more than harmonics, ending up increasing the THD. Not as bad is dividing the stator into 6 sections in the teeth, Fig. 28.3, but still decreasing the $MMF_{Np/2}$ and increasing the THD. Probably the simplest, and cheapest, way to decrease the fundamental MMF and THD is to make the rotor yoke thin, Fig. 28.5, increasing the reluctance for the sub harmonic components.

The examples presented is for the rotor in only one position and with current at time 0 (Ib=Ic=-Ia/2), thus are not the effects of the relative position between the tangential air gaps and current fully investigated, neither have the effect on the flux from magnets or with loaded machine. Especially the air gaps in the stator will influence the magnet flux creating causing changes in reluctance depending on position and probably cogging, if not carefully chosen. An example not presented here is separating each coil, air gap in every second tooth, similar to building up the stator with E-cores, with coils around the central core [89].

Table 7 Calculated MMF and harmonic components for examples in Fig. 27, normalized for $MMF_{Np/2}$ in the reference machine

Machine		MMF_1	$MMF_{Np/2}$	THD % of $MMF_{Np/2}$
Reference	1)	1.04	1.00	139
Stator 2sections	2)	0.81	0.72	191
Stator 6 sections	3)	0.67	0.79	158
Stator 6+6section	4)	0.22	0.95	88
Rotor, slim yoke	5)	0.50	1.00	109
Rotor, divided yoke	6)	0.19	0.98	95

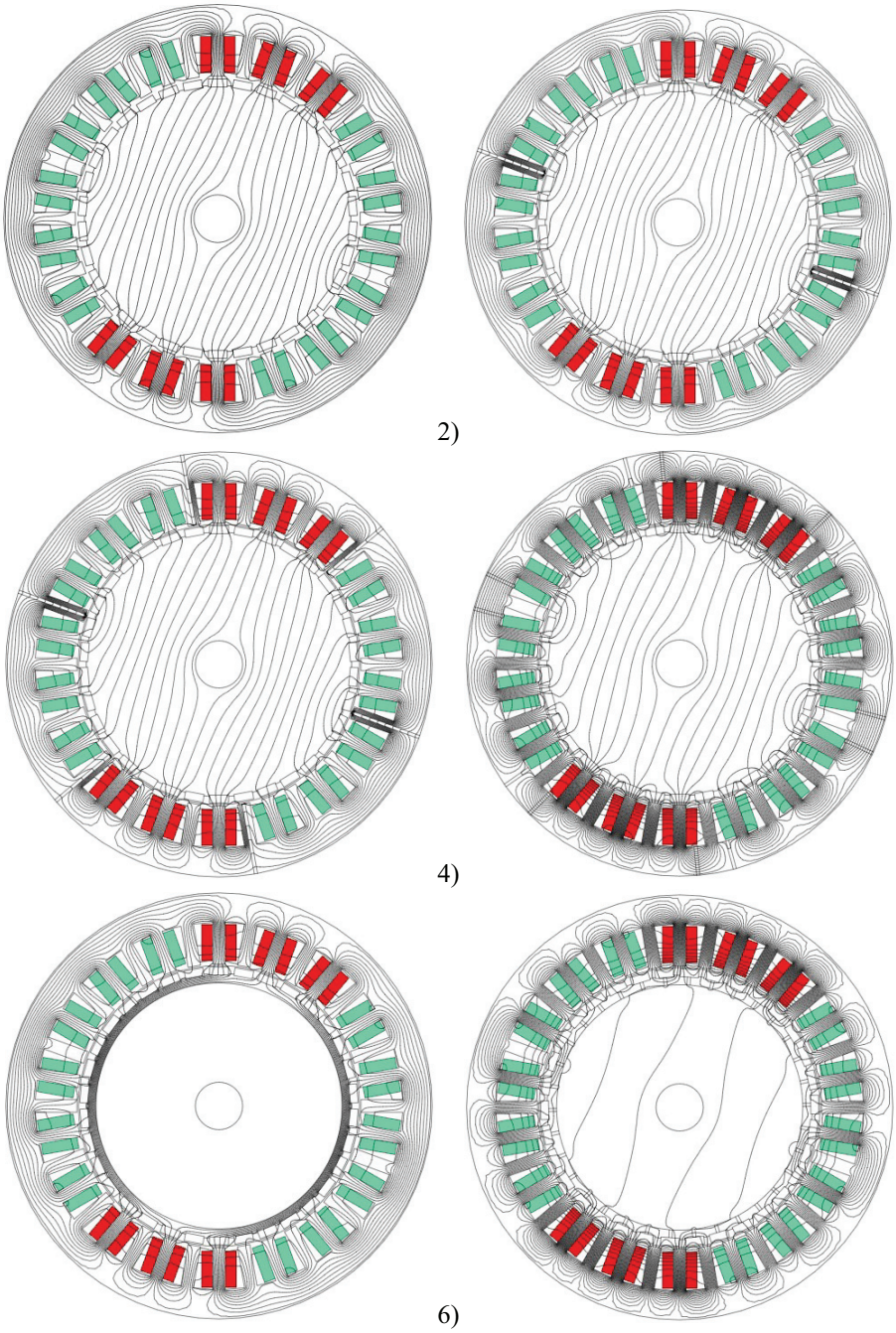

Fig. 27 Flux lines from the MMF for different sectioning of the machine. 1) Reference 34 pole machine 2) Stator in two section divided in teeth. 3) Stator in 6 sections, divided in teeth between phases, 4) Stator divided in 6+6 sections in slots bewteen phases. 5) Thinner rotor yoke 6) rotor yoke divied beneeth each magnet

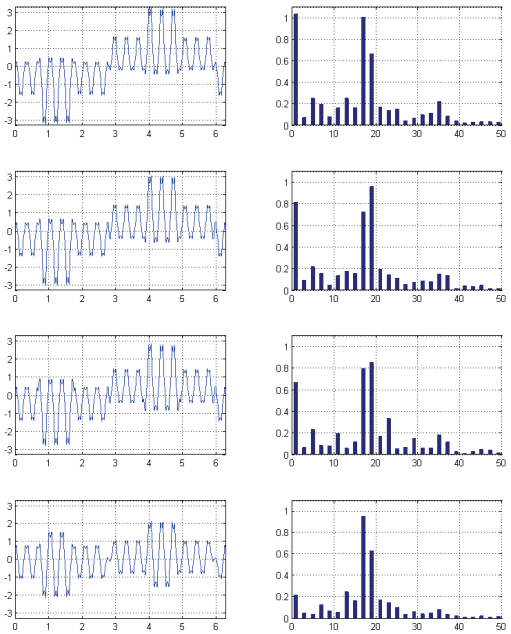

Fig. 28 MMF plots from Fig. 27, 1 to 4, left is the MMF in the air gap, right the harmonic components. Top MMF reference machine, second from the top: stator in two sections, second from the bottom: stator in 6 sections, bottom: stator in 6+6 sections.

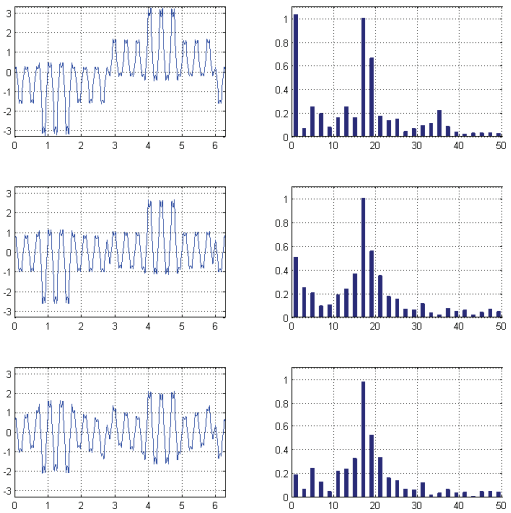

Fig. 29 MMF from Fig. 27 1, 5 and 6. To the left is the MMF in the air gap, right the harmonic components. Top MMF reference machine, centre; slim rotor yoke, bottom: rotor yoke in 34 sections, dived under magnets. .

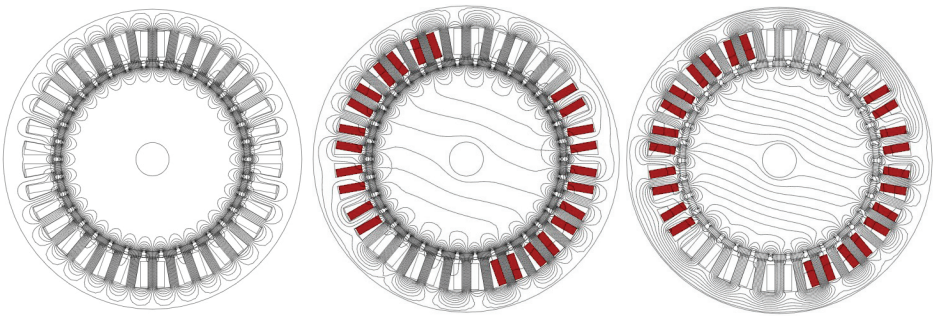

Fig. 30 36slot 34pole one layer winding with I_s=I_q=0, 2 and 8A from left to right

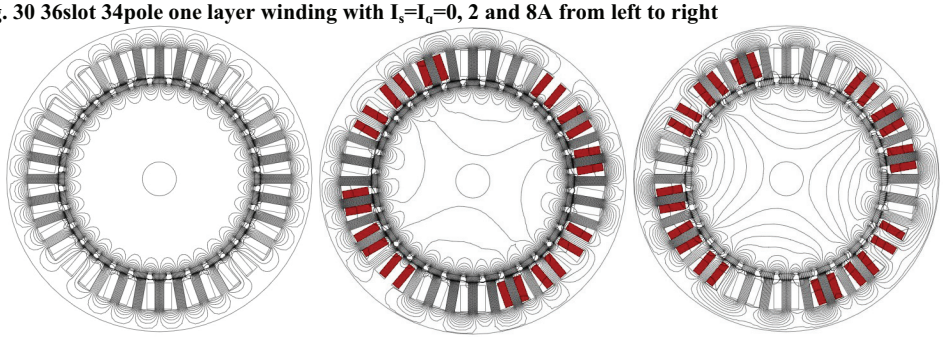

Fig. 31 36slot 32pole one layer winding with I_s=I_q=0, 2 and 8A from left to right

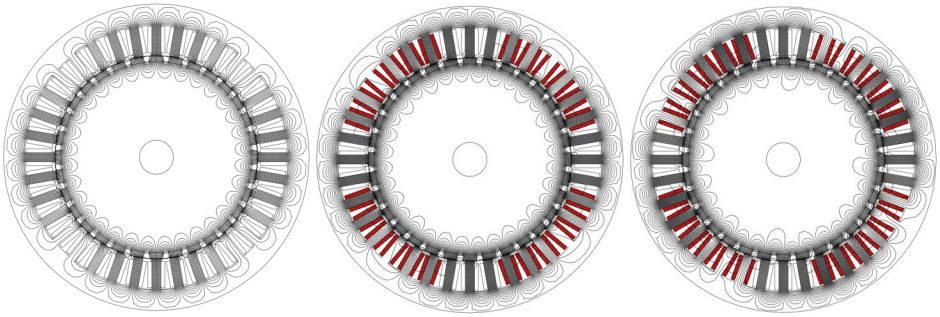

Fig. 32 36slot 32pole two layer winding with I_s=I_q=0, 2 and 8A from left to right

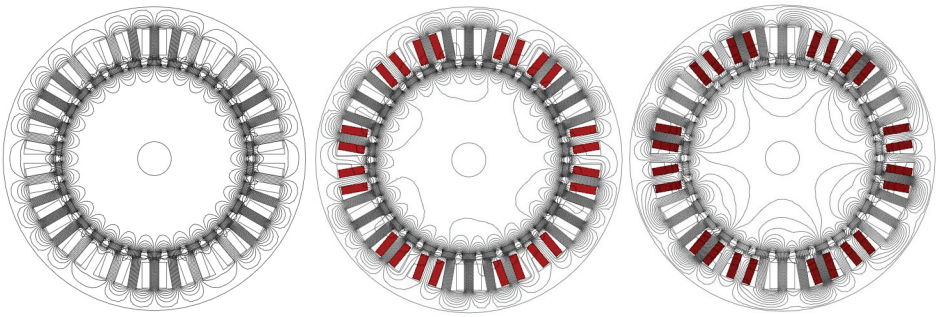

Fig. 33 36slot 30pole one layer winding with I_s=I_q=0, 2 and 8A from left to right

2.5 The total flux from magnets and MMF

An assumption often made for PM machines is that the flux from the magnets is much stronger than the one from the MMF, mostly due to the effective air gap, also neglecting the sub harmonic components, and thus is the flux in the machine mainly dependent of the magnets. This is true as long as the current loading of the machine is low compared to the magnetic loading and with low sub harmonic content. When increasing the current loading the MMF strongly alters the flux compared to the no load flux from the magnets. In Fig. 30 to Fig. 33 plots of the flux lines for no load, 2A (ac=160A/cm=16.0kA/m) and 8A (ac=642A/cm=64.2kA/m) is shown. The FEA calculation assumes losses components. As in Fig. 25 and Fig. 26 it is the lowest sub harmonic component that dominates. It is also evident that the lowest harmonic components (larger wave length) have the largest flux. From Fig. 31 and Fig. 32 it is evident that the MMF from the two layer winding creates much less sub harmonic flux in the rotor than the one layer. This is confirmed by comparing it with the harmonic analysis of MMF (Fig. 23, Fig. 24).

2.6 Electrical Parameters

2.6.1 Induced Voltage

The induced voltage is found by Faradays law of induction or Lenz law:

$$e = \frac{d\Phi}{dt} \tag{47}$$

Given a sinusoidal change in the flux the amplitude value of the voltage per turn is:

$$\hat{e} = 2 \cdot \pi \cdot f_e \cdot \widehat{\Phi} \tag{48}$$

The flux can either be found either be found analytical or numerically (for example eq.(29)). The voltage per coil in rms is found from:

$$E_{coil} = N \frac{\hat{e}}{\sqrt{2}} \tag{49}$$

And the phase voltage:

$$E_{phase} = \frac{N_c}{C} \cdot k_w \cdot E_{coil} \tag{50}$$

FEA can be used to find the voltage directly using transient solver and rotation. Using the transient solver and rotations the electric field strength in the coil area is found, Integrating the electric field strength over an area the voltage can is calculated (51). This can be used to find the voltage per slot, voltage per coil (adding the two sides of the coils), or phase voltage (adding all coils in series).

$$e_{area} = \int \frac{E_z}{A_{area}} dA \cdot L \tag{51}$$

2.6.2 Resistance

The DC resistance in on turn at a given temperature in the winding is found by:

$$R_{DC,turn} = \frac{l_{turn}}{A_{turn} \cdot \sigma_{Cu,T_0}} \tag{52}$$

The DC resistance for a phase is then:

$$R_{DC,phase} = \frac{N_c \cdot N \cdot l_{turn}}{C^2 \cdot A_{turn} \cdot \sigma_{Cu,T_0}} \tag{53}$$

The resistance in the winding is dependent of temperature, frequency and height of the conductor. The AC-resistance for the winding adjusted for temperature can be expressed as in (54) where the k_T compensates for temperature, and the k_{AC} for the frequency and conductor height (diameter).

$$R_{AC} = \frac{k_{AC}}{k_T} R_{DC} \tag{54}$$

The conductivity is dependent of temperature. Depending at which temperature the conductivity is given, T_0, and of the nominal temperature of the winding, T_n, a correction factor can be used [76]:

$$k_T = \frac{234 + T_\sigma}{234 + T_n} \tag{55}$$

Where the coefficient reduces the conductivity with increasing temperature (56).

$$\sigma_T = k_T \cdot \sigma_{T0} \tag{56}$$

The resistance is also dependent of the self induced eddy current effects and proximity effect. Both methods are in fact eddy current effects, but the first is the self induced eddy currents, while the proximity effect is the eddy currents induced in a conductor due currents in nearby conductors. The self induced eddy current effect is dependent of frequency and dimensions of the conductors, and can be dealt with by choosing conductor dimension smaller (or lower) than the skin depth. The proximity effect is dependent of how the conductors are distributed in the slot. and are in smaller machines 50/60Hz adequately handled by the randomness in a fed-in winding, for large machines with rubble bars and in high frequency or special machines with litz wire.

The effects of the eddy currents are discusses and deduced by many sources among them [90] and [91]. In this work a simplification from [75] is used to calculate the self induced eddy currents, eq. (57)

$$k_{AC} = \begin{Bmatrix} 1 + \frac{4}{45} \cdot \left(\frac{h}{\delta}\right)^4 & , \frac{h}{\delta} < 1.5 \\ \frac{h}{\delta} & , \frac{h}{\delta} > 4 \end{Bmatrix} \tag{57}$$

h is the conductor height and δ the skin depth and is shown in eq. (58).

$$\frac{h}{\delta} = h\sqrt{\frac{\omega \cdot \mu_0 \cdot \sigma}{2}} \tag{58}$$

The conductivity in eq. (58) is temperature dependent. A more correct equation would be to include the thermal coefficient from eq. (55) giving:

$$\frac{h}{\delta} = h\sqrt{\frac{\omega \cdot \mu_0 \cdot \sigma_{T0} \cdot k_T}{2}} \tag{59}$$

In [78] a discussion on the effects of transposing of conductors, or neglecting it, is included.

Using FEA tools the current distribution in the slot can be further examined. Fig. 34 is an example of a FEA calculation showing a slot with 19 solid turns carrying the same current (in series). The same current goes in each conductor, but due to the increasing field crossing the slot the eddy currents are increasing and the current density distribution are different.

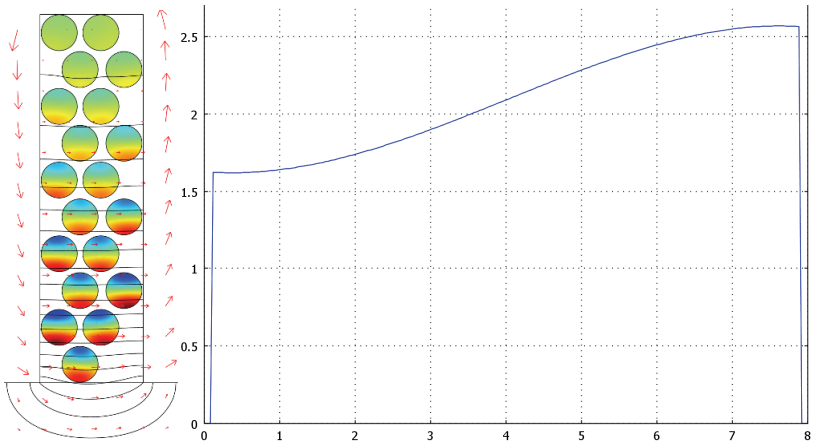

Fig. 34 An example of eddy currents in a slot with 19 solid turns at 50Hz, each turn carrying the same current. To the right a cross sectional plot of the current density of one of the conductors close to the opening

2.6.3 Inductance

The inductance of a winding or a coil describes the amount of magnetic energy that it is able to store. For PM- machines this can be dived into 4 areas: slot, gap, end winding and belt inductance. Zig-zag is not present in surface mounted PM machines since there is no iron in the poles. These are all well described in the literature, and will here only be shortly mentioned. It is presented analytical expressions for the gap, slot and end winding inductance and FEA of the same including a separation into the different parts, including belt inductance.

The gap inductance is depending on the gap geometry, and the square of the number of turns.

$$L_{gap} = N^2 \cdot \frac{\mu_0 \cdot \mu_{r,Nd} \cdot \tau_s \cdot L_s}{2 \cdot \left(l_m + k_c \cdot \mu_{r,Nd} \cdot g \right)} \tag{60}$$

In eq. (60) the magnet is assumed to cover the entire slot pitch, which is fairly correct. If one assume that the magnet only covers 80% of the slot pitch the effective relative permeability of the magnet is reduce with about 2%.

The slot inductance depends on the slot geometry and the distribution of current in the slot. For a slot with parallel sides and conductors equally distributed and a wedge in the slot opening the equation is:

$$L_{slot} = N^2 \cdot \frac{\mu_0 \cdot L_s}{w_s} \cdot \left(\frac{\left(d_s - d_{s,wegde} \right)}{3} + d_{s,wegde} \right) \tag{61}$$

For a machine with straight teeth and tapered slots the fact that the slot width is larger at the bottom than at the air gap has to be taken into account.

There are several approximations for the end winding inductance depending on the book you read. They all have their own assumptions, valid for their cases. But all states that calculating the end winding inductance accurate is tedious. Usually the end winding inductance is small compared to the gap and slot inductance and it can be neglected. But for the application presented here, at least the prototypes, the machines are short with a substantial part of the copper in the end winding, making the end winding count. Hanselman [74] presents his equation assuming no iron and circular end winding:

$$L_{end} = N^2 \cdot \frac{\mu_0 \cdot \tau_c}{4} \cdot \ln\left(\frac{\tau_c}{2} \cdot \sqrt{\frac{\pi}{d_s \cdot w_s}} \right) \tag{62}$$

Eq. (62) is only valid if the radii of the end winding (equal to half the coil pitch, τ_c) is larger than the effective radii of the slot area. Hendershot and Miller [92] uses the geometric mean distance (GMD) to calculate the end winding inductance. The GMD is depending on the geometric shape of the end winding. Assuming that the end winding has a square cross section the equation for GMD is:

$$GMD = 0.447 \cdot \sqrt{A_{end}} \tag{63}$$

Rewritten for one layer concentrated coils the equation for the inductance then is:

$$L_{end} = N^2 \cdot \frac{\mu_0 \cdot \tau_c}{4} \ln\left(\frac{4 \cdot \tau_c}{GMD} - 2 \right) \tag{64}$$

Lipo [75] divides the end winding into several parts, depending on whether the winding is parallel to or perpendicular to the stator. He also uses an effective radius for the area of the end winding.

$$\begin{aligned} L_{e,1} &= \frac{\mu_0 \cdot \tau_c \cdot \left(\pi/2 - 1 \right)}{2 \cdot \pi} \cdot \ln\left(\frac{\tau_c}{\sqrt{\frac{d_s \cdot w_s}{\pi}}} \right) \\ L_{e,3} &= \frac{\mu_0 \cdot \tau_c}{2 \cdot \pi} \cdot \ln\left(\frac{\pi \cdot \tau_c}{2 \cdot \sqrt{\frac{d_s \cdot w_s}{\pi}}} \right) \\ L_{e,4} &= \frac{\mu_0 \cdot \tau_c}{16} \\ L_{end} &= N^2 \cdot \left(L_{e,1} + L_{e,3} + L_{e,4} \right) \end{aligned} \tag{65}$$

All end winding equations are valid for windings where only one coil is in the end winding, and are per end winding. The total inductance per coil and per phase is presented in eq. (66), the mutual inductance and belt harmonics are not included.

$$L_{coil} = 2 \cdot \left(L_{end} + L_{slot} + L_{gap} \right)$$
$$L_{ph} = L_{coil} \frac{N_c}{C^2} \tag{66}$$

This is the DC-part of the inductance, as for the resistance the eddy current effects will add to the inductance, or reactance. But in cases where the conductor diameter is smaller than the skin depth the effect is very small, and will be neglected. The equations for the eddy currents influence on the reactance can be found in for example [75] and [90].

There will also be leakage part connected with the spatial harmonics created by the MMF. Especially for concentrated windings where the MMF from the windings contains a large amount of harmonics, this can be significant. EL-Refaie credits this harmonic leakage for the good field weakening capabilities concentrated windings have [51]. He further compares the MMF from a machine with concentrated windings and one with distributed, both with similar properties, comparing the amount of harmonic content, using that as an evidence that increased inductance is achieved. The belt leakage is discussed in the next chapter.

FEA-calculation of stored energy and inductance

FEA tools can also be used to find the inductance. A 2D calculation of a coil will give the gap and slot part of the inductance and a 2D calculation of the entire cross section will include the sub harmonic components (belt). A 3D calculation of the coil will include also the end winding part of the inductance. Thus using these three methods a calculation of the gap, slot, end winding and belt inductance is presented. The belt leakage for the end winding is not included, that would require a 3D calculation for the entire machine. Neither is the linkage between phases calculated, but discussed. The coupling between phases is dependent of the pole and slot numbers. In Fig. 35 and Fig. 36 examples of a 2D and 3D FEA for one coil and one phase is shown from the table model. The method for finding the inductance from FEA is to apply a current to the winding and calculate the energy stored in the magnetic circuit. The inductance is then given by the energy equation, eq. (67). The calculated inductance for the examples is shown in Table 8.

$$W_m = \frac{1}{2} B \cdot H = \frac{1}{2} L \cdot I^2 \Rightarrow$$
$$L = \frac{2 \cdot W_m}{I^2} \tag{67}$$

The examples in Table 8 show how the different methods for calculating the inductance deviates from each other; the 2D calculation of the coil only including gap and slot inductance, the 3D calculation of the coil add end effects. The 2D calculation of the entire cross sections and all coils in a phase includes the connection between the coils in the same phase.

In Table 9 different parts of the inductance is shown per coil. The example machine is very short, stator 14mm and rotor 10mm, with high and thin coils, coil height 22mm and width 6mm, thus is the end winding inductance a substantial part. The 2D-coil inductance is equal for 30 and 32 poles while the 34pol has 1mm longer air gap, hence the difference in 2D-coil inductance. The difference in 3D coil inductance between the machines is smaller than expected, reducing the importance of the air gap.

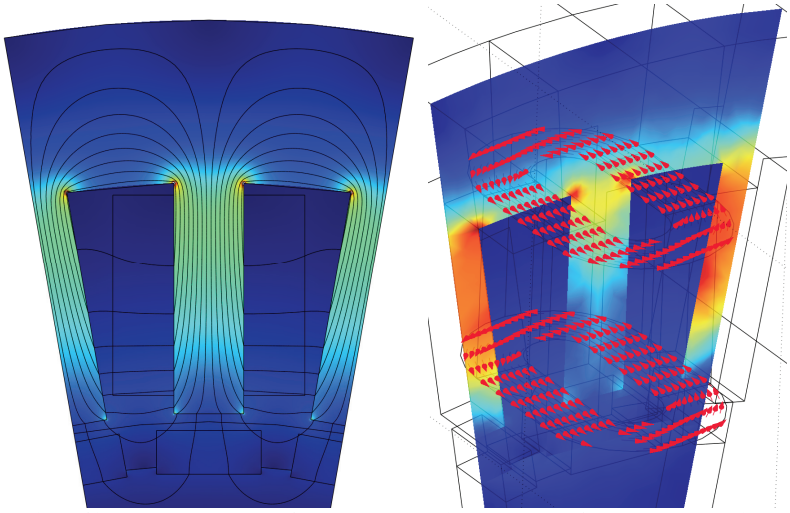

Fig. 35 Calculation of inductance (energy) from only one coil, 2D to the left and 3D to the rigth

Fig. 36 Inductance (energy) for a phase, from upper left to lower right 34pole, 30 pole 32pole one layer and 32pole two layer

For the 30 and 32 pole machine the belt inductance is approximately 0.14mH, while for the 34pole the belt inductance is calculated to 0.51mH. Regarding mutual inductance and connection between phases it can be seen from the flux lines in Fig. 36 that there are none or little connection for the 30 and 34 pole machines, while for the 32 pole machine, and especially the two layer winding the coupling between phases are significant.

Table 8 Inductance calculations using FEA

Winding			Current	Energy Total	Inductance	
Np	Nlayer	Ncs	I	Wm	Lph	Lcoil
#	#	#	[A]	[mJ]	[mH]	[mH]
2D-Phase						
30	1	6	2,8	57,30	14,32	2,39
32	1	6	2,0	28,61	14,31	2,38
32	2	12	2,0	18,99	9,50	0,79
34	1	6	2,0	28,66	14,33	2,39
2D-coil						
32	1	1	3,0	10,12	2,25	2,25
34	1	1	3,0	8,46	1,88	1,88
3D-coil						
32	1	1	2,8	12,08	3,02	3,02
34	1	1	2,0	5,94	2,97	2,97

Table 9 Inductance per part and total inductance, calculated per coil

Pole number		30	32	34	
N_{layer}		1	1	1	
L_{gs}	$L_{2D\text{-}coil}$	2,25	2,25	1,88	
L_{end}	$L_{3D\text{-}coil}$- $L_{2D\text{-}coil}$	0,77	0,77	1,09	+
L_{belt}	$L_{2D\text{-}phase}$-$L_{2D\text{-}coil}$	0,14	0,13	0,51	+
L_{coil}		3,16	3,15	3,48	=

2.6.4 Losses

2.6.4.a Copper loss calculation

The copper loss in the winding is found from eq (68) where R_{AC} is compensated for temperature and eddy currents.

$$P_{Cu} = N_{ph} \cdot R_{AC} \cdot I_{ph}^{\ 2} \tag{68}$$

2.6.4.b Iron loss in stator

The calculation of stator losses are based on data supplied from manufacturer. A matrix of loss density (W/kg) is given based on amplitude value and frequency ($P(\hat{B}, f)$). The harmonic content of the flux density as a function of time (and/or position) is found for each point in a FEA model (69). For each component, having both amplitude value and frequency, a loss density is found of each point in the model. The loss density for each harmonic component can then be integrated over the volume, summed and the loss found.

$$\hat{B}_{amp,i} = \sqrt{\hat{B}_{rad,i}^2 + \hat{B}_{\tan,i}^2} \tag{69}$$

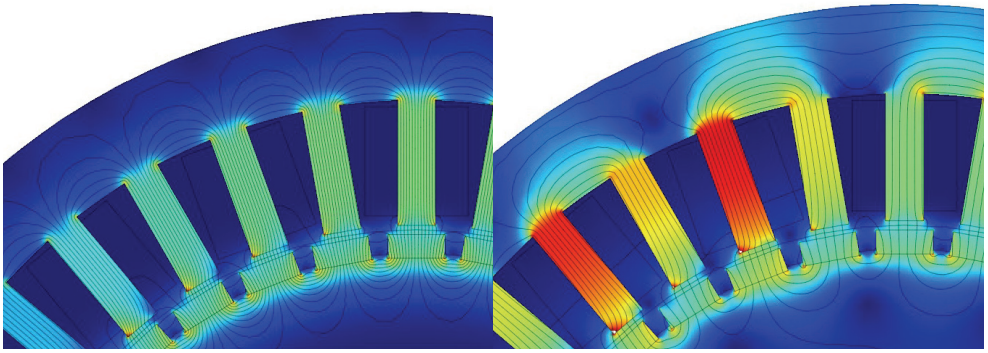

Fig. 37 Flux density in stator at no load(left) and loaded (right)

2.6.4.c Permanent magnet and rotor losses

Ideally there are no flux variations and hence no losses in the rotor. But the change in reluctance due to teeth and slots, the space harmonics in the MMF from the winding and time harmonics in the current will induce losses. The losses for the different parts of the machine can be estimated assuming that the change in flux induces a voltage, and that the cross sectional area have a current path with a resistance given by skin depth and physical properties and dimensions. For the magnets assuming that the skin depth is larger than half the magnet width and a uniform change of flux the losses can be expressed as in (70), it also assumes that the magnet width (w_m) is smaller than the length (L) [75]. It is in this work used a constant value for the conductivity of the magnets. In [93] the dependency of several factors for the resistivity is discussed, among them the temperature, showing a linear increase in resistivity with temperature with the rate $1 \cdot 10^{-9} \Omega \cdot m/K$.

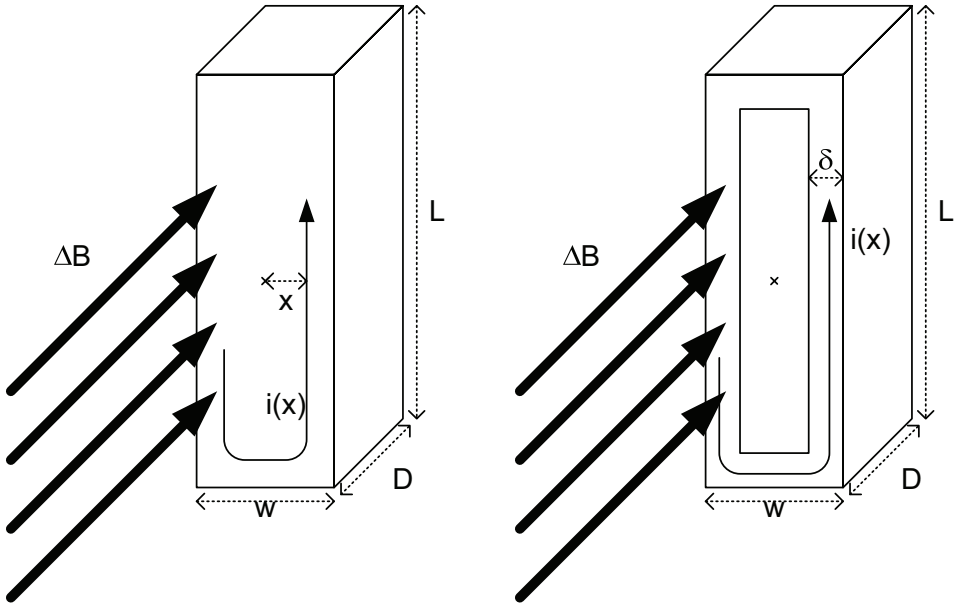

Fig. 38 Simplified calculations for loss in magnets and iron

$$P = \frac{\sigma}{24} \cdot D \cdot L \cdot w^3 \cdot \left(\Delta B\right)^2 \cdot \omega^2 \tag{70}$$

If the skin depth is smaller than the half the width a further simplification can be made (71). The assumption is that the flux density induces a voltage that creates a current that goes through a cross section where the width is defined by the skin depth.

$$\begin{aligned} e &= \omega \cdot \Delta B \cdot w \cdot L \\ R &= \frac{2 \cdot \left(L + w - 2 \cdot \delta\right)}{\delta \cdot D \cdot \sigma} \\ P &= \frac{e^2}{R} = \frac{\left(\omega \cdot \Delta B \cdot w \cdot L\right)^2 \cdot \delta \cdot D \cdot \sigma}{2 \cdot \left(L + w - 2 \cdot \delta\right)} \end{aligned} \tag{71}$$

2.6.5 Efficiency (eta)

The efficiency describes how well a machine converts the energy. Whether it is a generator or a motor is it given by (72). For a generator the input power is the mechanical power at the shaft, and output the electric, and for a motor it is reversed.

$$\eta = \frac{P_{out}}{P_{in}} = \frac{P_{in} - P_{loss}}{P_{in}} = \frac{P_{in} - P_{Cu} - P_{iron,stator} - P_{magnets} - P_{iron,rotor}}{P_{in}} \tag{72}$$

Losses concerning windage and bearings are not treated in this work.

2.7 Forces in the air gap

The goal of the machine is to create a working electromagnetic torque in the air gap either working against the rotor rotation (braking, generator) or together with rotation (accelerating, motor). An expression for that torque is eq. (6).

In the process of generating this working, tangential torque, for rotating machines, other types of torque and forces occurs. Some comes from the geometric of the machine, slot and pole numbers and their shape, other forces comes from harmonics in the current and other from magnetic effects as saturation. The different phenomena's have gotten different names. Reluctance torque is the force that occurs as a result of the difference in reluctance when rotating the machine this can include both the geometric parameters but also the magnetic properties of the material and saturation. Cogging is also a much used word for the variation of torque when rotating the rotor, and is also used for the reluctance torque, but cogging torque often includes harmonics from the currents in the slot. There will also be an attractive force between rotor and stator caused by the flux density distribution in the air gap. Depending on the pole and slot number, and their shape, the attractive force distribution will change according to both the relative position between rotor and stator, and where on the rotor surface one is position (lice on the rotor/stator)

To calculate the forces the flux density in the air gap, and/or on the surface of stator is used. The total force on the rotor can be found using Maxwell's stress tensor.

$$F = \oint_S \frac{1}{\mu_0} \left[\left(B \cdot n\right) B - \frac{1}{2} B^2 n \right] dS \tag{73}$$

Though this method is generally said to only be valid for the total force, it can interpreted so that the force in (73) is found by integrating the force density over an area or along a curve, and thus an expression can be deducted for the force density:

$$\begin{aligned}\sigma_m &= \frac{1}{\mu_0}\left[\left(B\cdot n\right)B - \frac{1}{2}B^2 n\right] \\ &= \frac{1}{\mu_0}\left[B_r B_\phi e_\phi + \frac{B_r^2 - B_\phi^2}{2} e_r\right]\end{aligned} \tag{74}$$

If there are no tangential component Eq. (74) can be further simplified to eq. (75), at Br=1T the force density is approximately 4kg/cm^2:

$$\sigma_m = \frac{1}{2\cdot\mu_0} B_r^2 \tag{75}$$

Regarding the use of eq. (74) it is very sensitive to accuracy and also the parameters of the material or surface integrated on when using FEA tools (CM). In this work Maxwells equation has been used to get an idea of the forces in the air gap of the machine, both radial and tangential.

For concentrated windings there have been pointed out that the differences in slots and pole number rotating create force waves that can cause unsymmetrical forces and excite vibration in the structure (resonance). The fundamental wave form is decided by the pole and slot number. The magnet width, air gap length, slot width etc will decide the amplitude and the harmonic content in the forces wave. In literature where the attractive forces are discussed [48, 80, 87] there are basically two concerns; symmetry of the attractive forces and rotating force waves. Some are satisfied as long as the sum of forces in radial direction is zero (symmetry), but others point out that the wave length and frequency of the rotating force can excite resonances within the machine.

Large PM machines with many poles (large diameter, thin rotor and stator), can be vulnerable for vibration of the lower modes for a circle (Fig. 39). In a machine with concentrated coils the fundamental force wave will have wave length defined by the difference in pole and slot number eq. (76). In Fig. 41 the fundamental force wave for machines with 6 different pole slot combinations are shown (same machines as presented in Table 1, in addition a 27 slot, 22 pole variant is included, no load flux density plots presented in Fig. 40 and Fig. 14). The force is found from the no load flux densities, by integrating the force density on each tooth. Hence the curves have the same number of points as they have teeth. The forces are normalised so they can be compared.

$$\tau_f = \frac{2\cdot\pi}{\left|N_s - N_p\right|} \tag{76}$$

It is evident that with only one in difference between slot and pole a large rotating force is present, while the others more or less are symmetric in radial direction. The fundamental force waves moves with a speed equal to the fundamental MMF of eq. (41), and for the lowest sub harmonic the equation is as in (77), proportional to the mechanical speed, inversely proportional to the difference in pole and slot number and in opposite direction of the rotation.

$$n_{F1} = -\frac{N_p}{\left|N_s - N_p\right|}\cdot n \tag{77}$$

Seen from the stator this fundamental force has a frequency twice that of the electrical frequency.

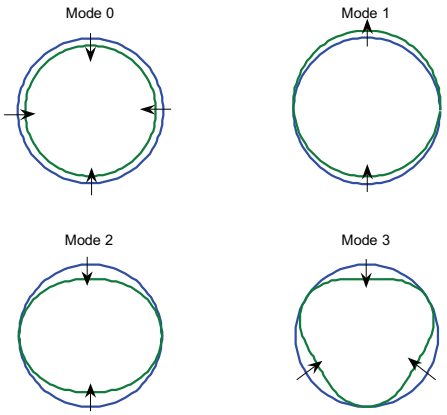

Fig. 39 Some modes of vibration for a circle (cylinder)

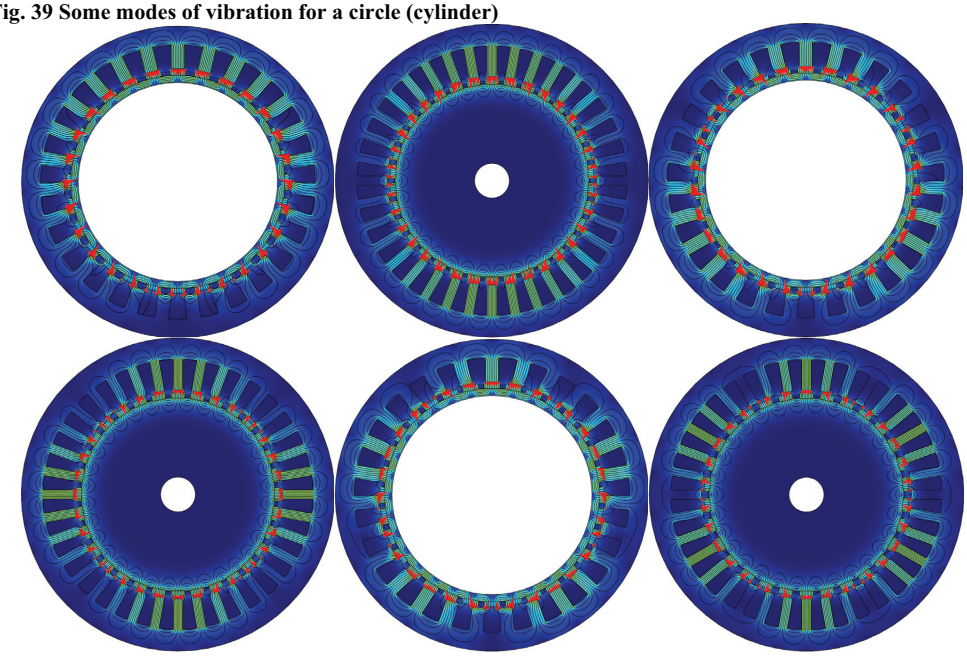

Fig. 40 No load flux density plots of the machines presented in Fig. 41, from upper left to rigth 1 to 6 in in difference between pole ans slot number

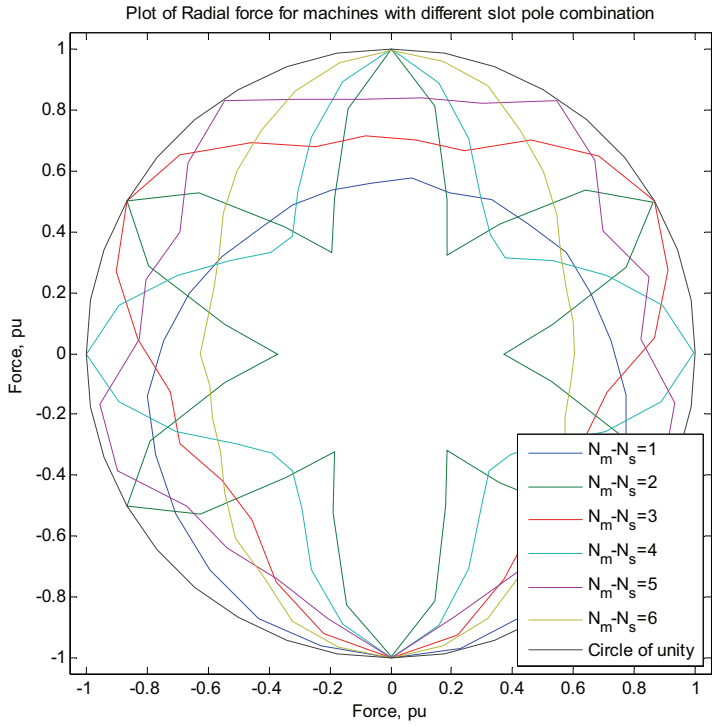

Fig. 41 Fundamental radial forces for different slot pole combination (N_s-N_m [1, ... ,6])

2.8 Control strategies

An electric machine is at its optimum when the current is in the q axis, in phase with the induced voltage, then the minimum current is used to create a given torque. Therefore should the machine be designed with the current in the q-axis. The converter has its optimum with cos(ϕ)=1 and should be designed thereafter. With smaller permanent magnet machines this not been a topic since the synchronous reactance is so small that whether cos(ϕ)=1 or $I_s = I_q$ doesn't make a big difference, induced voltage and terminal voltage have been almost the same anyway.

But when talking about large direct driven motors and generators it becomes an issue because of the increasing reactance. Still the optimum for the machine is to have the current in the q-axis, but for the converter the optimum is to have cos(ϕ)=1 since it makes the smallest VA-rating. Including the converter cost into the equation of optimization one can find a generator design that minimizes the system cost. Grauers [39, 40] and Hystad [42] have discussed the optimum combination of generator design and converter rating based on cost and concluded that if the reactance is below 1.4pu, then the system cost is at a minimum when the induced voltage is equal or close to equal the terminal voltage.

In Fig. 42 and Fig. 43 some vector diagrams for different load cases and reactance are given, and in Table 10 a comparison of the different cases is done. It is assumed a constant induced voltage E, and a constant current I_s. Assuming that converter cost is connected to maximum voltage and nominal current, one get a number for power per volts and amps using

the proposed control mode as a base for the design. It can be seen that the proposed mode of operation with U=E (mode c) gives the most power per volts and amps, and thus can be a good basis for the design of larger converter fed PM-machines.

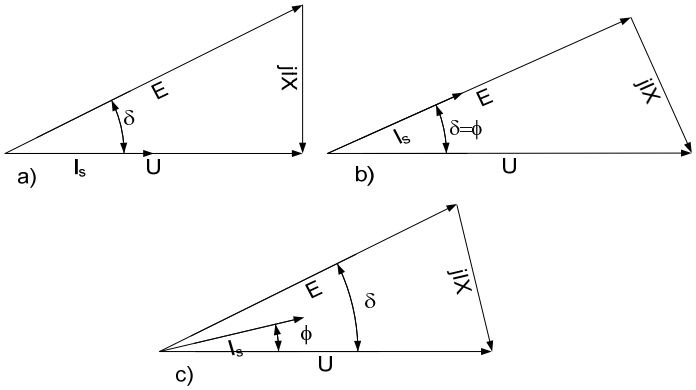

Fig. 42 Vector diagram for different control strategies, for all three the current Is, induced voltage E, and reactive voltage drop jIX is constant, X=0.45pu. a) is for cos(ϕ)=1, b) for Is=Iq and c) for |E|=|U|

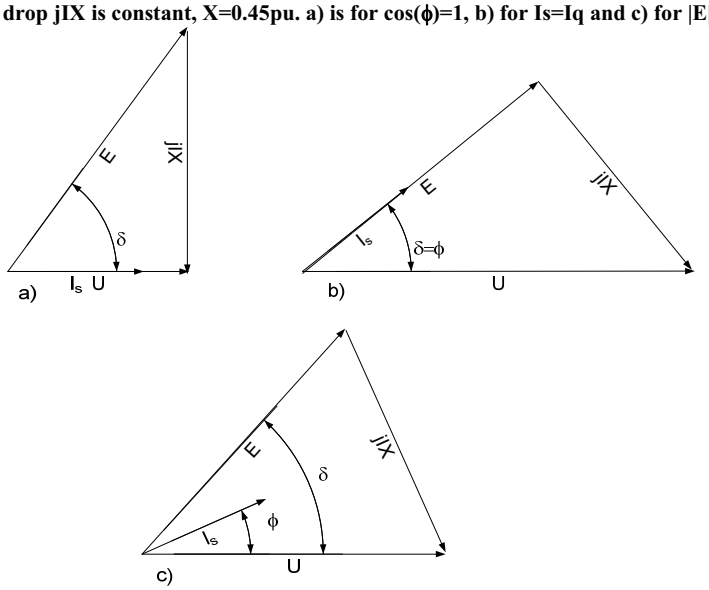

Fig. 43 Vector diagram for different control strategies, for all three the current Is, induced voltage E, and reactive voltage drop jIX is constant, X=0.8pu. a) is for cos(ϕ)=1, b) for Is=Iq and c) for |E|=|U|

Table 10 Comparison of electric parameters and cost of converter for different control strategies

Reactance	Control strategy (Fig. 42 and Fig. 43)	Induced voltage, E	Terminal voltage, U	Current, I_S	Power, P	P/max(U,E)
	a)	1	0.9	1	0.9	0.9
X=0.45	b)	1	1.1	1	1	0.91
	c)	1	1	1	0.97	0.97
	a)	1	0.6	1	0.6	0.6
X=0.8	b)	1	1.3	1	0.99	0.76
	c)	1	1	1	0.91	0.91

To be able to use the different control schemes some kind of active converter or reactive compensation is needed. For the applications in questions, rim driven thrusters for ships and direct driven permanent magnets generators for wind turbines, it is essential to have a variable speed drive to maximize the efficiency at variable loads. Therefore it is likely that a full sized converter will be used, and thus can the machine be design to operate with at one of the modes.

That is for the thruster an inverter must be used to generate the AC voltages that are needed of the rotation. For the direct driven wind generator, which has an opposite power flow than the thruster, a diode rectifier can be used, but that means one can only operate with $\cos(\phi)=1$. Enercon uses a diode rectifier for their system, [94]. But since Enercon uses a synchronous generator with field windings they can regulate the induced voltage and reduce it at low load so the converter does not have to be designed for full voltage.

A method to still use the diode rectifier is to add a reactive load supplying the generator with reactive power, thus raising the voltage [95]. This will, at full load enable the machine to work in mode c) or b) generating more power with the same machine. But for instance raising the terminal voltage to the induced voltage (mode c) at full load, given the case in Fig. 43, the no load voltage will be raised to 1.4pu, making this the dimensioning voltage. The converter doesn't have to carry the reactive current, and thus can the nominal current in the machine be increased and more power drawn. But in the case in Fig. 43 an increase in voltage of 0.4pu only increases the current by 0.06pu, and thus is the power per volts and amps 0.75, close to mode b).

The topic of the thesis is not converter design, but the chapter is included to point out that for larger drives including converters and machine, the design of the system rather than of its components should be optimised, or at least been kept in mind during the design.

Chapter 3
Distributed Classic Winding: The Rim Driven Thruster

This chapter is included to widen the discussion around windings for large low speed PM-machines, showing an application where other choices for the winding were made. It is also discussed the limiting factors and compromises made when integrating two different disciplines; propeller and electric machine. The chapter focuses on the discussion around the large propellers and a description of the 100kW prototype design and performance.

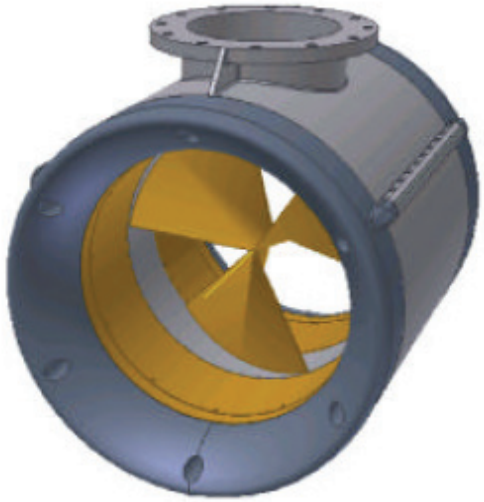

Fig. 44 Conceptual design of the 100kW rim driven thruster

The concept of rim driven thruster is enabled mainly by two technologies; the peripheral bearings and the rare earth permanent magnets. Traditionally tunnel and azimuth thrusters are built with shaft connecting the propeller and the motor. This shaft usually goes from the centre of the propeller, through a knee and up through the hull of the ship. This mechanical construction causes drag and a less effective propeller. Various propeller types are shown in Fig. 45. The rim driven solution is a relatively well known concept for smaller thrusters for ROV up to 200mm, above that the losses in the periphery of the propeller normally gets too high. Due to new bearing designs and methods to reduce the losses in the gap/slit between the rotating at stationary construction the rim driven concept can be taken further up in size and power. The introduction of permanent magnet machines is also necessary to utilize the rim driven propellers. A relatively large distance between rotor and stator (air gap) is necessary to

make room for water flowing between the rotor and stator and protective covering of magnets and stator. Together with the low speed, which gives a high pole number, this excludes the induction machine as a feasible technology. A wound pole synchronous machine will also be less favourable since brushes are out of the question and a brushless magnetization will be complex and demand more space than permanent magnets in the rotor.

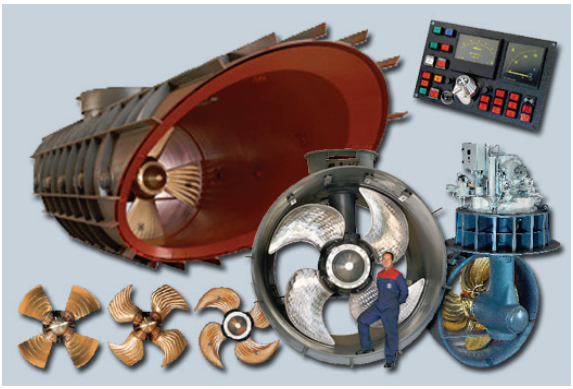

Fig. 45 Some different types of thrusters from Brunvoll AS [96]

The advantages of a rim driven solution are numerous. The hydrodynamic properties are improved both by removing obstacles in the water way, and by reducing the losses connected with water slipping away around the tips of the propellers since the blades are fastened at the rim, not in the centre. The number of moving parts is reduced to one, and there is no need for a water tight sealing around shaft since there is no shaft. There are no rotating seals between gear oil and water, reducing the environmental risk drastically. Since there are no shaft going through the hull, only cables, and the only moving part is surrounded in water most of the vibrations and noise is effectively damped. Moving the motor outside the hull, or to areas where traditional solutions can't fit, more space is available inside the boat for payload. The challenges are mainly the losses connected with the bearings situated around the rim and water in the air gap, the large air gap and sealing of the stator.

3.1 Direct rim driven motor for ship actuation and propulsion; a 2.5 MW motor

Prior to the prototype design a conceptual study of using a PM-motor as a rim drive for the azimuth thruster was conducted in 2001, by prof. R. Nilssen at NTNU [97]. It concluded that a PM-motor would be most suitable for a rim driven propeller. It also presents a preliminary design for a 100kW prototype, and some thoughts about the dimensions of the electrical machine would change with increasing propeller diameter and power.

The conceptual report was followed up by two master theses in 2002, one presenting a 2.5MW Ø3.0m rim driven azimuth propeller by J. Dahle [98], and the other evaluating, and testing, the axial forces with axial displacement of the rotor by Edgar Løvli [99]. The latter will not be further referred too, while the first will be used as a starting point for the discussion around the integration of PM motor with the propeller in this chapter. After Dahle and Løvli finished their work, the prototype thruster was built in 2003. The design and testing of the prototype will be presented in the following chapters.

In this chapter a discussion around the main parameters is presented, The goal is to show the possibilities for variation of parameters and some of the consequences and limitations. Simplified equations are used to show the trends.

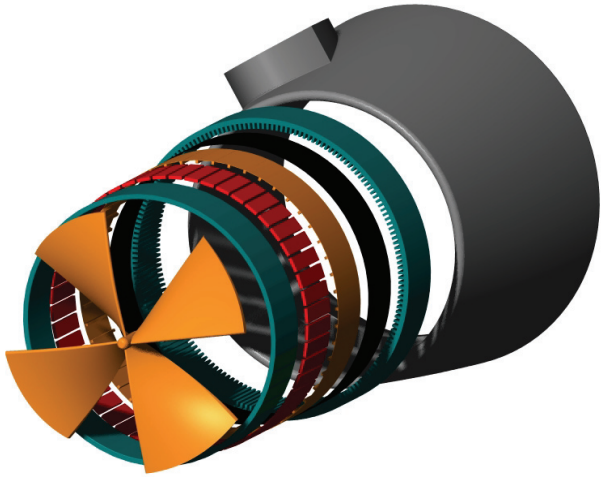

Fig. 46 Conceptual design of the 2.5MW thruster [98]

3.1.1 Presentation of a proposed 2.5MW embedded motor for thruster

The dimensioning factors are given in Table 11 found in [98]. The main parameters are the propeller diameter and the size (length and height) of the nozzle. In addition to containing the motor and bearings, the nozzle also must have sufficient strength and stiffness during manoeuvring. The evaluation presented here are mainly concerned with how dimensions change with parameters such as frequency and pole number and considerations regarding pole pitch and slot number. The parameters evaluated use the dimensions presented by Dahle as a starting point, but other assumptions and simplifications are made, resulting in other discussions and conclusions. The influence of frequency on the inductance and reactance is also considered.

Table 11 Dimensioning factors for the 2.5MW thruster

Description	Quantity	
Power level	2.5	MW
Nominal speed	220	rpm
Propeller diameter	3.0	m
Max length	600	mm
Max thickness	165	mm

Table 12 Starting point for evaluation

Description		Value	
Rotor core thickness	d_{rc}	60	mm
Magnet length	l_m	31	mm
Air gap	g	11	mm
Slot dept	d_s	36	mm
Stator core thickness	d_{sc}	50	mm
Current density	J_{Cu}	4	A/mm^2

There are two important features of the PM-motor in the rim driven propeller. Firstly the design has water in the air gap. This means that the rotor and stator must be sealed off to

prevent short circuits, corrosion or other undesired effects. The other is that the diameter is given by the propeller and is larger than an electric machine usually would have been designed for. This result in a shorter machine and one tend to want to increase the frequency beyond 50Hz to keep the rotor and stator yoke thin. Due to limitations of the nozzle thickness and the demand for mechanical strength in yokes the slots also tend to become relatively shallow.

3.1.1.a Flux density and leakage as a function of pole number

The flux density in the air gap is mostly depending on magnet length, air gap length and material properties. But it also depends on leakage between magnets. In this case the air gap length and diameter is fixed. Increasing the pole number will make the magnets narrower and increase the proportion of leakage flux to the air gap flux increases. In Fig. 47 the simplified lumped circuit that is used for the calculation is shown. The leakage reluctance is from eq. (14). It is assumed fixed air gap length, fixed magnet length and fixed relative magnet width compared to pole pitch (k_m=0.75). The result of the calculations is shown in Fig. 48. The air gap flux density is calculated for a very wide range of frequencies, way out off the relevant frequency range. At 1kHz only 71% of the air gap flux at 50Hz is available. The calculation shows that for the frequency range in question (50Hz-300Hz) the leakage between the poles are relatively low.

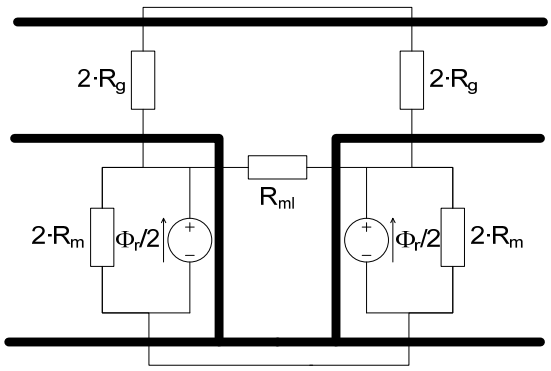

Fig. 47 Simplified lumped circuit, including leakage

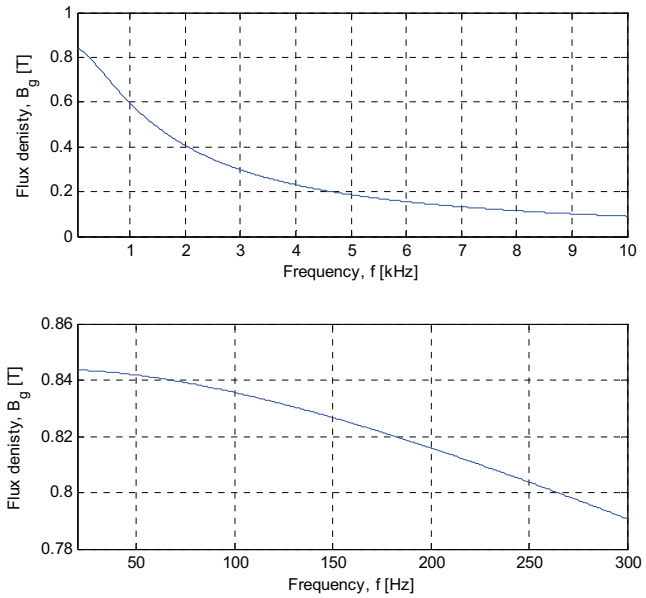

Fig. 48 Air gap flux density as function of frequency. Both curves shows the same, upper a very large frequency range, the lower with a more realistic range

3.1.1.b The influence of pole number and frequency on yoke thickness and outer diameter

The design of the embedded PM-motor starts at the rotor yoke with fixed inner diameter. The thicknesses of the yokes are dependent on the general magnetic loading and pole number. Magnet length, air gap length and slot depth can be held constant, changing pole number and frequency don't affects them much, of course within reasonable limits. In this exercise it is assumed that rotor and stator yoke have equal thickness. The stator yoke can be thinner both due to better material properties and less flux due to leakage between magnets and in slots. The magnet length, air gap and slot depth are kept constant with the values from Table 12. At some point the mechanical strength of the yokes also must be considered. The rotor yoke works as part of the mechanical structure supporting the propellers.

With the speed and inner diameter fixed the change in pole number results in change in pole, and thus magnet, width. The same flux going through the magnet has to cross both the rotor and stator yoke. The thickness of the yokes is thus directly depending of the pole width. That is, one should include the magnet width instead of the pole pitch; the magnet width ratio (k_m) is usually constant and around 0.7 to 0.8. Depending on magnetic loading, basically the remanent flux density for the magnet, magnet width ratio and magnet length ratio, the yoke can be from around one fifth to half the pole pitch ($0.2\tau_p<k_{rc}<0.5\tau_p$). If the magnet ratio is, k_m, lower than 0.7 the yoke can be even thinner, often the case in smaller machines.

In (78) to (83) the equations used to estimate the outer thickness of the stator is presented. The calculated yoke thicknesses are shown in Fig. 49 and the outer diameter in Fig. 50. The increase in frequency reduces the thickness of the yokes and outer diameter. In Fig. 50 the chosen outer diameter (dotted black line) is plotted together with the suggested maximum diameter (solid black line). And in Fig. 49 the dotted line is the stator yoke thickness, while the solid black line is the rotor yoke thickness. From the figures it can be

seen that by increasing the frequency above 100Hz, towards 150 it is possible to keep the design within the original boundaries. At 130Hz with a yoke thickness of $0.3\tau_p$ the outer diameter equals the maximum diameter of 3.33m from Table 11, and with a flux density 0.6T average in the air gap this would give about 1T in the yokes. The evaluation of the yoke thicknesses is also included in the discussion concerning slot dimensions.

$$D_{os} = D_{ir} + 2 \cdot \left(d_{cr} + l_m + g + d_s + d_{cr} \right) \tag{78}$$

$$d_{rc} = d_{sc} = k_{rc} \cdot \tau_p \tag{79}$$

$$\tau_p = \frac{\pi \cdot (D_{ir} + d_{rc})}{N_p} \tag{80}$$

$$N_p = \frac{120 \cdot f}{n} \tag{81}$$

$$d_{rc} = k_{rc} \cdot \frac{\pi \cdot (D_{ir} + d_{rc})}{\frac{120 \cdot f}{n}}$$

$$d_{rc} = D_{ir} \cdot \frac{1}{\frac{120 \cdot f}{k_{rc} \cdot \pi \cdot n} - 1} \tag{82}$$

$$D_{os} = D_{ir} + 2 \cdot \left(D_{ir} \cdot \frac{2}{\frac{120 \cdot f}{k_{rc} \cdot \pi \cdot n} - 1} + l_m + g + d_s \right)$$

$$D_{os} = D_{ir} \cdot \left(1 + \frac{4}{\frac{120 \cdot f}{k_{rc} \cdot \pi \cdot n} - 1} \right) + 2 \cdot \left(l_m + g + d_s \right) \tag{83}$$

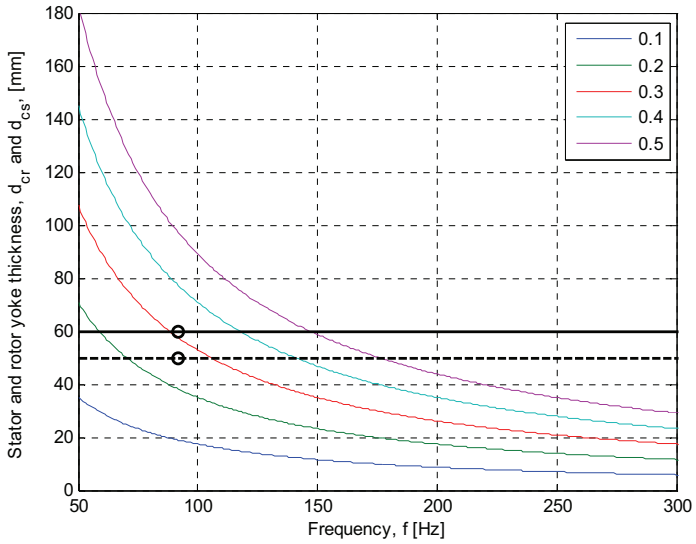

Fig. 49 Stator and rotor yoke thickness as function of frequency for different yoke/pole width relationship k_{rc} (0.1 to 0.5). Black straigth and dotted line are the chosen rotor and stator yoke thickness

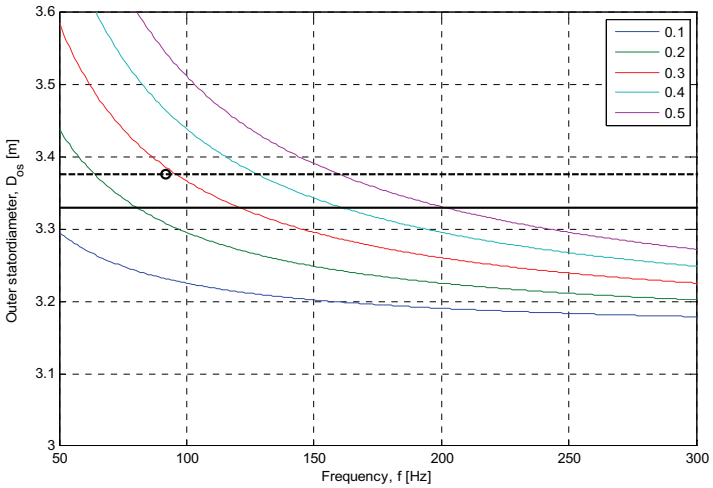

Fig. 50 The outer stator diameter as a function of frequency and the yokes relative thickness compared to pole pitch, k_{rc}: 0.1 to 0.5. Dotted black line is the suggested diameter from [98] while the solid line is the original maximum outer diameter of nozzle

3.1.1.c Current density, current loading and slot dimensions

Using eq (6) a current loading (ac) can be chosen to give the appropriate power within the maximum dimensions, using the values from Table 11 and Table 12. Power factor and efficiency is not included, that is efficiency is not relevant since the power is measured at the terminals, not shaft.

$$P = \omega_m \cdot T = \omega_m \cdot \frac{\pi}{2} \cdot ac \cdot \frac{\hat{B}_{g,1}}{\sqrt{2}} \cdot L \cdot D_{is}^{\,2}$$
$$P = \omega_m \cdot \frac{\pi}{2} \cdot ac \cdot \frac{\hat{B}_g}{\sqrt{2}} \cdot L_{max} \cdot D_{is}^{\,2} \tag{84}$$
$$ac = \frac{P}{\omega_m \cdot \frac{\pi}{2} \cdot \frac{\hat{B}_g}{\sqrt{2}} \cdot L_{max} \cdot D_{is}^{\,2}} = 24\,{}^{kA}\!/_{m}$$

The current loading in (84) is fairly low. As a comparison the power density presented in chapter 2.1 will give a current loading of about 60kA/m. The current loading in this application is limited by the slot depth and current density. The slot depth is limited by the allowed thickness of the motor. In (85) the space left over for slot depth is found based on the chosen yoke thicknesses, air gap and magnet length.

$$\begin{aligned} d_s &= d_{t,max} - l_m - g - d_{rc} - d_{sc} \\ &= 165 - 31 - 11 - 60 - 50 = 13mm \end{aligned} \tag{85}$$

Using the proposed slot number of 180 (q=1.2), and equal slot and tooth width this gives a 28mm wide slot. A slot depth of 13mm (85) and the required current loading this result in a current per slot of about 1290A and a current density in the slot of 3.6A/mm^2 (including insulation etc). A fill factor of 0.4 gives a current density in the copper of about 8.9 A/mm^2 which is very high.

To avoid too high losses due to current density and get a decent efficiency the slot area has to be increased. In [98] it was chosen to increase the slot depth, increasing the motor above the maximum thickness. The slots were increased from 13mm to 36mm, 0.9% of the propeller diameter. With equal slot and tooth width this results in a machine that is 188mm thick, with a current density in copper of 3.2A/mm^2.

Another way to decrease the current density is to increase the frequency, since increasing the pole number reduces the stator and rotor yoke, leaving more space for the slots. The number of slot is increased, keeping q constant. A calculation of the available slot depth given a fixed thickness, as function of frequency is presented in (86). Assuming equal stator and rotor yoke thicknesses (79), and using eq. (82) to find the yoke thickness, the slot depth is plotted as a function of frequency for different k_{rc} in Fig. 51.

$$\begin{aligned} d_s &= d_{t,max} - l_m - g - d_{rc} - d_{sc} \\ &= d_{t,max} - l_m - g - D_{ir} \cdot \frac{2}{\frac{120 \cdot f}{k_{rc} \cdot \pi \cdot n} - 1} \end{aligned} \tag{86}$$

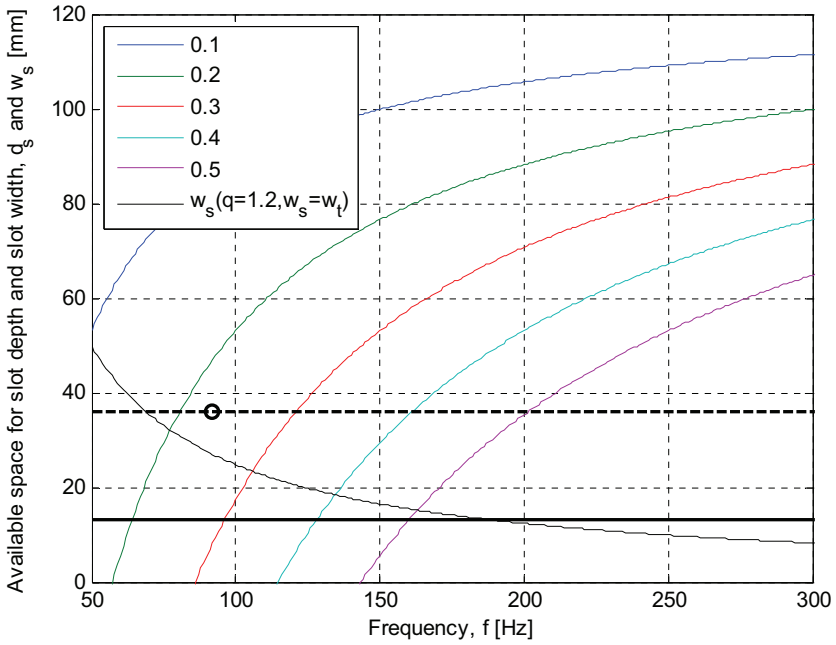

Fig. 51 Available slot depth as a function of frequency with fixed air gap and magnet length

A 25% increase in frequency (f = 115Hz) would give a machine with 40mm deep and 20mm wide slots, with a current per slot of 1000A and a current density in the slot 1.3A/mm^2, 3.2 A/mm^2 in the copper. This could be a feasible solution. Further increase in frequency say up to 150Hz, with a slot depth of 50mm, and a slot width close to 18mm, gives 787A per slot, 1.0A/mm^2 in the slot and 2.5A/mm^2 in the copper. This would also result in a nice looking slot depth/width relationship around 4, (k_c=0.3, 82 poles). The stator and rotor yoke is then around 35mm (Fig. 49).

At 150Hz the current density is fairly low, and taking into account that the machine is surrounded by water, the shallow slots and large diameter, it is expected that the machine could be loaded harder by shortening the length. If one accepts 4A/mm^2 in copper the length can be reduced from 600mm to 375mm, increasing the current loading from 24kA/m to 38kA/m having a force density (magnetic shear stress) in the air gap of 20kN/m^2.

The frequency can be increased further, increasing slot number and slot depth, increasing the available copper area (Fig. 51). However, depending of type of winding, the slot width also decreases and at one point the narrow slots will affect the fill factor and hence the current loading.

3.1.1.d Inductance and Reactance

With changing geometry as the frequency increases the slot and gap inductance will also change as a function of frequency. It is assumed that the total thickness of the machine is limited to 165mm, and that the relationship between core thickness and pole pitch is 0.3. The influence of q on inductance and reactance is also investigated. It is assumed that there is a one layer winding with constant (one) turn per slot (N=1), for all q and frequencies, f. It is further assumed that all coils are connected in series. Only gap and slot inductance are evaluated, neglecting end winding, belt and mutual inductance. Thus will the values presented

be too low, but the trends will be fairly correct. The base value of the impedance (Z_b) for the pu calculation of the reactance is defined in (88).Assuming a fixed amplitude value of the flux density ($B_{g,1}$) the voltage is found from eq. (87).

$$\begin{aligned} E_{ph} &= 2\cdot\sqrt{2}\cdot q\cdot N\cdot f\cdot \hat{B}_{g,1}\cdot\tau_p\cdot N_p\cdot L \\ &= 2\cdot\sqrt{2}\cdot q\cdot N\cdot f\cdot \hat{B}_{g,1}\cdot\pi\cdot\left(D_{ir}+2\cdot\left(d_{cr}+l_m\right)\right)\cdot L \end{aligned} \tag{87}$$

$$Z_b = \frac{3\cdot E_{ph}^{\ 2}}{P_n} \tag{88}$$

The gap and slot inductance is found from eq. (60) and (61). For the slot inductance it is assumed an open slot, completely filled with the coil with parallel sides giving eq. (89). The slot depth increases with frequency, while the width decreases with frequency and q.

$$L_{ph,slot} = N_p\cdot q\cdot N^2\cdot\mu_0\cdot L\cdot\frac{d_s}{3\cdot w_s} \tag{89}$$

For the gap inductance, eq. (90), the pole pitch decreases with frequency, it is assumed that the coil pitch is equal to the pole pitch. Number of turns per slot, or coil side, magnet length and air gap length is constant. The inductance per phase is found from eq. (91).

$$\begin{aligned} L_{ph,gap} &= N_p\cdot q\cdot N^2\cdot\mu_0\cdot L\cdot\frac{\tau_p}{2\cdot\left(l_m+g\right)} \\ &= q\cdot N^2\cdot\mu_0\cdot L\cdot\pi\cdot\frac{D_{ir}+2\cdot\left(d_{cr}+l_m\right)}{2\cdot\left(l_m+g\right)} \end{aligned} \tag{90}$$

$$L_{ph} = L_{ph,gap} + L_{ph,slot} \tag{91}$$

$$X_{pu} = \frac{2\cdot\pi\cdot f\cdot L_{ph}}{Z_b} \tag{92}$$

With the numbers of turns per slot fixed, the inductance, in Henries, will increase proportionally to q and pole number, the dimensions in eq. (89) and (90) will also be changed depending on frequency and q, further altering the inductances. The results are shown in Fig. 52 and Fig. 53. The per unit value of the reactance is, as expected, reduced with the increase in q, mostly due to the reduction of the gap inductance in per unit. The reactance has a minimum at around 150Hz for q=1.2, where the geometric properties are favourable. In Fig. 54 a plot of the reactance shows that there is a linear relationship between q, frequency and minimum reactance.

The carter coefficient is not included in the equations, for open wide slots the effective air gap will be affected. The winding factor is assumed to be unity, which will not be correct. And for many combinations of poles and slots, especially for the lower part of q, the MMF will be much distorted increasing the belt harmonics, including the sub harmonics. For this application with short active length and large diameter the end winding inductance will also add to the total reactance.

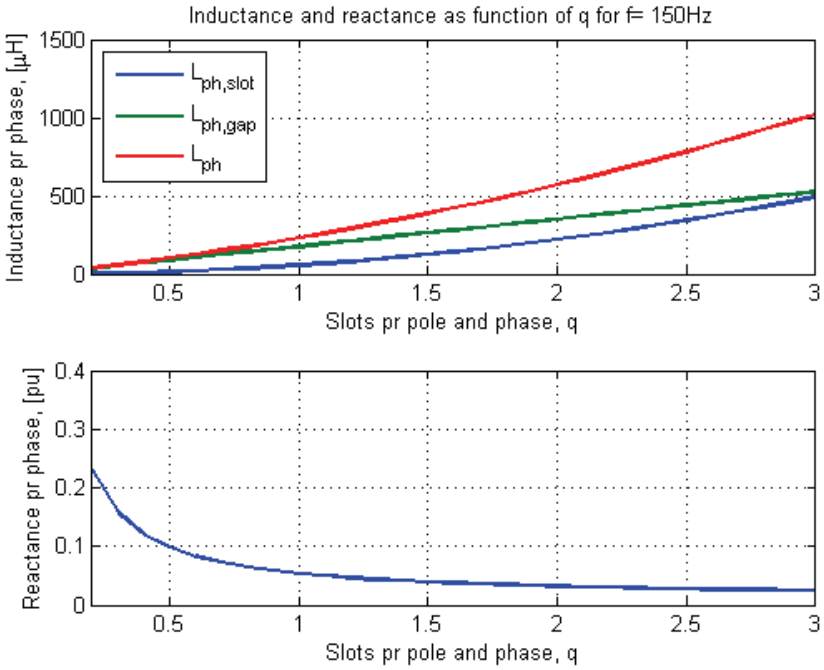

Fig. 52 Slot gap and phase inductance as function of q

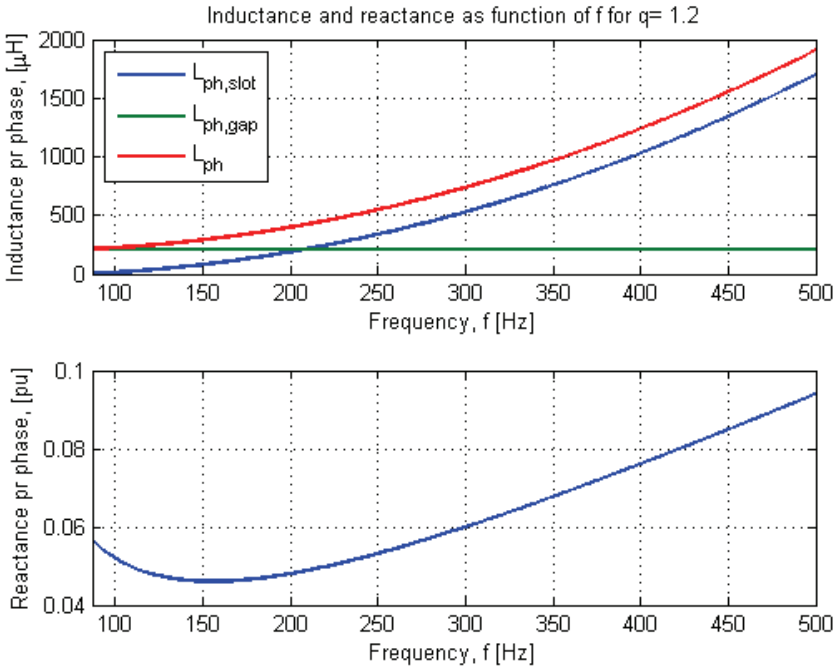

Fig. 53 Slot gap phase inductance as function of f

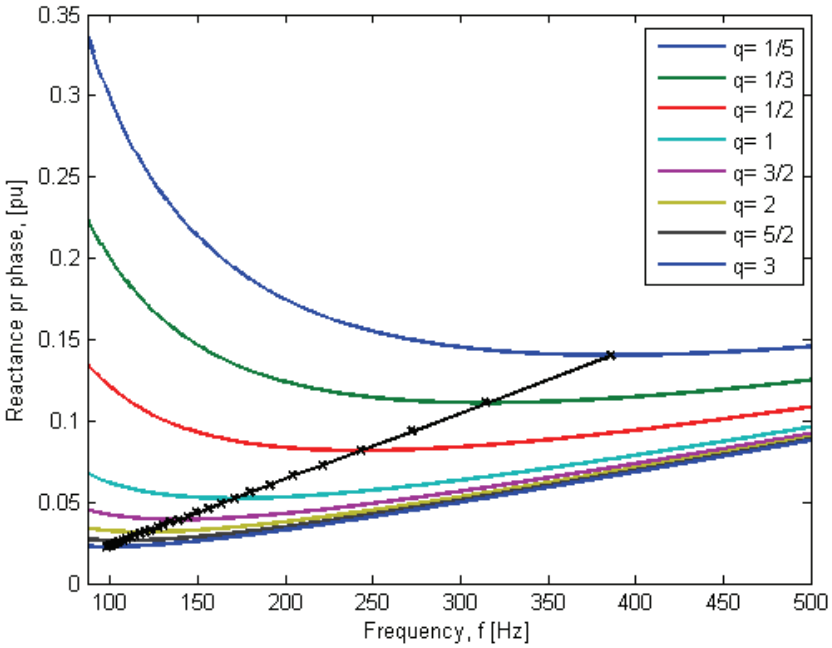

Fig. 54 Minimum reactance (X_{pu}) as function of frequency (x-axis) and q (different curves)

3.1.1.e Type of winding: distributed or concentrated windings

The argumentation for concentrated windings, or coils, in chapter 2.3.1 is mainly focusing on the lack of space for windings when the nominal speed is very low, and a decrease in diameter is desired, such as generators for the wind turbine might be. The example presented in this chapter has a fixed peripheral speed; a propeller has a typical tip speed of somewhat less than 30 m/s, thus is there no argument to reduce the diameter. Increasing frequency to reduce yokes and increase available copper area can be desirable. The slot width for q=1.2 and k_s=0.5 is plotted in Fig. 51. The slot falls below 15mm at 165Hz and 10mm at 250Hz, and. Thus keeping the frequency below 150Hz there is enough space for copper with distributed windings, and the fill factor should be kept fairly high.

Another argument for concentrated coils are simplicity; instead of 3 or more slots per pole, giving the same number of coils for a two layer winding, a stator with concentrated coils will have approximately one slot per pole, and for a one layer winding only half the teeth are wound, giving one sixth of the coils in a machine with q=1. For the example above a 150Hz machine and q=1 would have about 240 slots, and 240 coils, while a one layer concentrated winding would have around 80 slots and 40 coils. The volume of copper is approximately the same, but the work required to assemble the stator is reduced.

In addition to simplicity, both one and two layer, concentrated windings are easier to replace if faults occur, and for the one layer winding the risk for short circuit between phases is strongly reduced since there is no overlap between phases, neither in the slots nor in the end winding. The decoupling of phases in multiphase machine for more accurate position control is not an important feature for a propeller. But if a coil, or a phase, should short circuit, or another fault occurs, it would be favourable if the fault was decoupled, and did not interfere with the other phases.

The simplicity, and crudeness, of the concentrated coils have some drawbacks. It is possible to eliminate all cogging and reluctance torque by carefully choosing the pole slot combination, but it is also dependent of the tolerances during assembly, and also of the roundness and concentricity of the rotor in respect to the stator. Further has the MMF from the winding very high amount of harmonics, and especially the sub harmonic components at high currents can induce quite large losses in the rotor, thus could require a laminated rotor, which not always will be possible, or favourable, for this application.

Both types of windings are feasible for this application. Depending on which parameters one considers the most important, the one or the other might be preferred. Referring to the slot width (Fig. 51) one could argue that if a frequency higher than 150Hz is desired, a concentrated winding should be chosen (yielding a slot width of 50mm). Or that if a frequency below 100Hz a q>1 is the best winding. The consideration made for both the proposed 2.5MW design and the 100kW prototype is that the classical well proven distributed (fractional) slot windings is the preferred choice. This is mostly based on the fact that the slot width is large enough, one wants to avoid the effects of sub harmonics from the MMF and most important, one wants to make a machine with low variation in reluctance torque and noise, relatively independent of mechanical tolerances, roundness and concentricity.

3.1.1.f Summary of the parameters

It has been presented some parameters that are important for the design of a rim driven thrusters using an example with fixed diameter, power level, speed and nozzle thickness. An optimization of the consequence of the changes for the different parameters should of course be done. This could be made based on the cheapest possible machine with or without converter, the most efficient one, maybe the lightest one or a combination of the previous mentioned or other parameters, depending on limits and what's considered important. That has not been within the scope of this work.

The mechanical strength has not been considered, allowing the yokes to grow very slim with increasing frequencies. The force density in the air gap area has been of minor interest since diameter, available length, speed and power level have been fixed. In general the force density in the air gap is low, but as discussed by increasing frequencies the length can be decreased giving an increase in force and power density.

If it is an absolute demand to work within the maximum dimensions given in Table 11 a frequency between 100 and 150Hz should be chosen. Depending on how critical the reactance and converter ratings are, the frequency could be chosen based on minimum reactance. or to a desired level. Though not discussed here, if efficiency is the crucial part, a lower frequency should be chosen, maybe exceeding the thickness demand. If on the other hand weight is of importance a machine with high current density, short length and high frequency should be chosen.

The losses, how they increase with frequency, or current density, and the thermal consequences of increasing frequency have not been discussed. The frequency dependent losses can be countered by using materials with higher quality; Round copper wire can be replaced by litz wire, and thinner low loss electrical lamination can be used in stator. The magnets can be segmented, or even changed from sintered to bonded, but with bonded magnets much of the power density will be lost due to lower remanent flux density. The rotor yoke can also be laminated, and the magnets buried. Increased losses due to increased current density can be compensated by increased cooling (forced or passive). Grauers and Kashanati have to some extent discussed this in [40].

3.1.2 Scaling for the prototype: The 100kW thruster

Since this was meant to be a prototype propeller, and function properly as an azimuth thruster, the propeller performance was the dimensioning and most important factor. The inner tunnel diameter (propeller tip) and speed was decided by the propellers power level. As for the 2.5MW machine the nozzle also has an optimum shape and the electric machine should fit within, both keeping the mechanical strength and preserve the hydro dynamic properties. There were done no other considerations regarding scaling of the model.

3.1.3 Development after the prototype

This work has been related to Brunvoll AS development of their rim driven propeller unit (RDT) [96]. At the time the prototype was built and tested the product (in the range 100kW+) was unavailable in the market. After the prototype testing Brunvoll AS have developed and built a larger (pilot) tunnel thruster of Ø1750mm and 810kW mounted on a bow of an offshore supply vessel. After a series of tests and verifications the pilot RDT is fully integrated into the ships dynamic positioning system. The RDT is now a part of Brunvoll's product range.

Fig. 55 The prototype RDT (Ø600) [100] to the left and the Brunvoll RDT (Ø1750) [96] to the right, approximately right proportioned

Fig. 56 The pilot RDT mounted in the bow (bulb) on the supply vessel togethert with a traditional Brunvoll truster, both with low noise design

3.2 The design of the prototype thruster

In cooperation between Norpropeller AS, Brunvoll AS, dept. Electric Power Eng. at NTNU and SmartMotor AS a prototype rim driven thruster were built and tested. NTNU designed and built the PM-motor together with SmartMotor. The thruster was built and assembled in Molde at Brunvoll's premises. Brunvoll and Norpropeller, the owners of the prototype, made the prototype thruster available for NTNU through AE^3S.

The design and testing of the PM-motor have been presented in [2] and [3]. This chapter presents the design of the prototype. Being an industrial project, other priorities are made regarding choices of concepts and solutions. Instead of focusing on interesting phenomena's, testing the boundaries for the design, safe solutions and conservative choices are made. The discussion leading to design is not a part of this work. It was similar to the one presented in chapter 3.1.1.

The nominal speed for the 100kW thruster was chosen to 700rpm with a tunnel diameter of 600mm. Voltage level was chosen to 400V, giving about 150A as nominal current. The pole number was chosen to 22, as a compromise between frequency and pole pitch. A two layer fractional slot winding was chosen with 72 slots and a coil pitch of 3 slots (γ_s=165 degrees). Special consideration was taken regarding reluctance torque; the slots are semi closed to reduce the difference in reluctance, and there are dummy slots to increase the slot frequency. Concentrated coils were not considered an option at the time, mainly because of the pole pitch is relatively large, and the previous mentioned considerations regarding reluctance and cogging torque. The design is also presented in [2], in this chapter new and updated calculations of the parameters and more test results are presented.

Table 13 Parameters for the design of 100kW thruster

Symbol	Quantity		Value
P	Power	[kW]	100
U	Voltage	[V]	400
n	Speed	[rpm]	700
N_s	Number of slots		72
N_p	Number of poles		22
L	machine length	[mm]	150
R_{ri}	inner rotor yoke radius	[mm]	300
R_{si}	inner stator radius	[mm]	340
d_r	thickness of rotor back iron	[mm]	15
l_m	length of magnet	[mm]	15
g	effective air gap	[mm]	10
d_s	slot depth	[mm]	30
ω_m	magnet width	[mm]	60
B_r	Remanent flux density	[T]	1.2

3.2.1 No load flux density distribution

In Fig. 57 and Fig. 58 plots from the FEA is shown. In Fig. 59 plot of the air gap flux density and its harmonics is shown. From the radial component of the air gap flux density the tooth ripple can be seen as a ripple on top of the main components, neither the 72^{nd} (slot

number) nor the 144th (slots and dummy slots) can be found among the harmonics, but the average of 133 and 155 is 144. The harmonics present are the 3rd, 5th 7th and 9th of the fundamental (number 11).

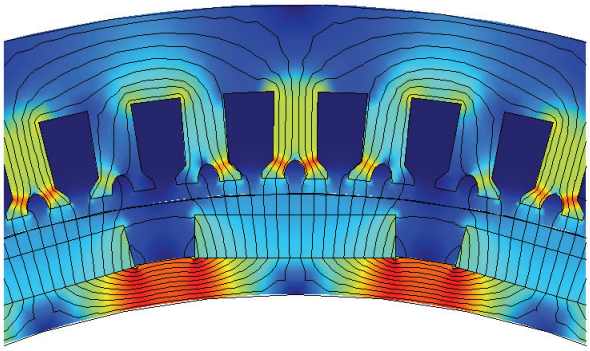

Fig. 57 The no load flux density for a pole

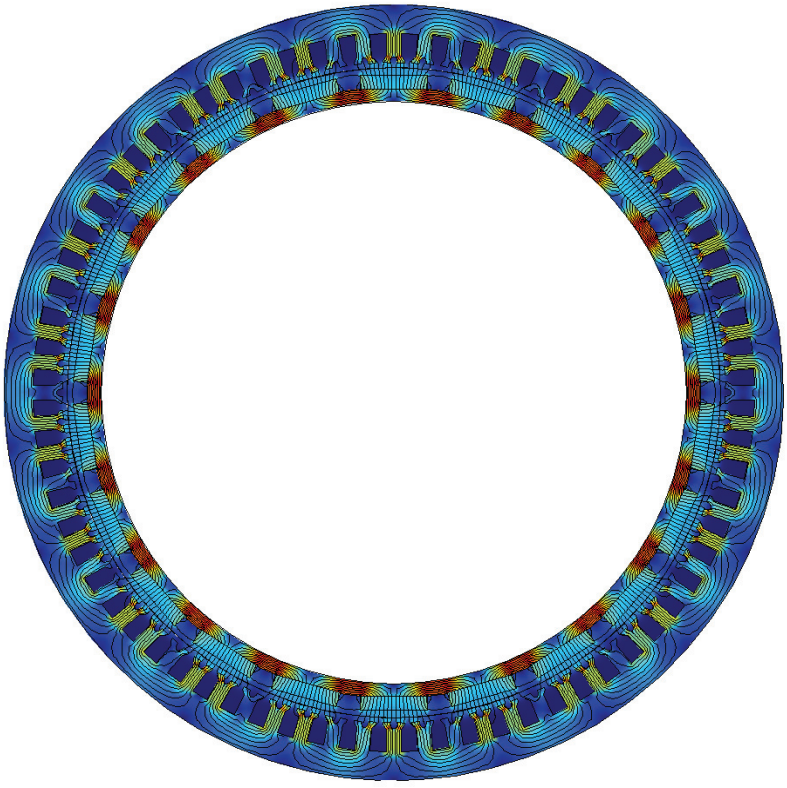

Fig. 58 Flux density in the PM-machine

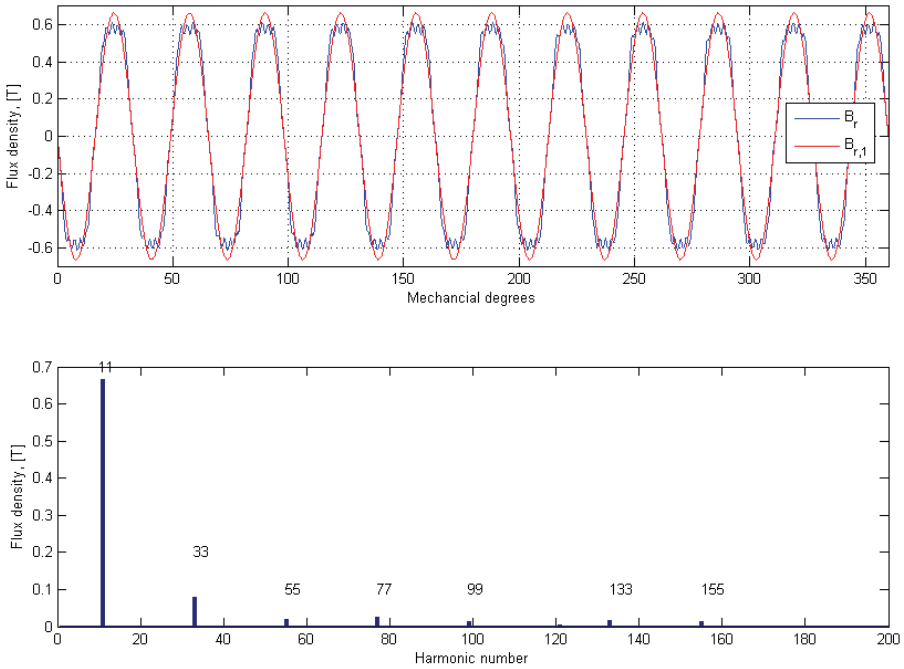

Fig. 59 Radial component of the no load flux density in he air gap and its harmonics

3.2.2 Magneto Motive Force

A plot of the MMF is shown in Fig. 60. The winding layout is shown in Table 14. Due to rather low slot per pole number, and a fractional slot winding, q=12/11, the MMF contains rather high amount of harmonics, both sub and over harmonic components. The sub harmonics present is the 1st, 5th, and 7th. The 11th is the main, corresponding to the pole pair number. The 7th harmonic is about 10% of the 11th. Of the higher harmonics present is the 61st and 83rd the most significant. Due to the large air gap the harmonics will not cause much loss in the rotor. The flux density in the air gap from the FEA is shown in Fig. 61. Due to the teeth, magnet and rotor yoke each harmonic component is smeared out compared to Fig. 60. It can also be seen that the higher harmonics are damped and less visible. But is evident in both figures are the significant two poles having a higher MMF due to the fractional slot combination.

Table 14 Winding layout for the first layer, the second layer is equal, shifted three slots

1	2	3	4	5	6	7	8	9	10	11
AAC'B	A'CB'	AC'B	A'CB'B'	AC'B	A'CB'	AC'B	A'CCB'	AC'B	A'CB'	AC'B
12	13	14	15	16	17	18	19	20	21	22
A'A'CB'	AC'B	A'CB'	AC'BB	A'CB'	AC'B	A'CB'	AC'C'B	A'CB'	AC'B	A'CB'

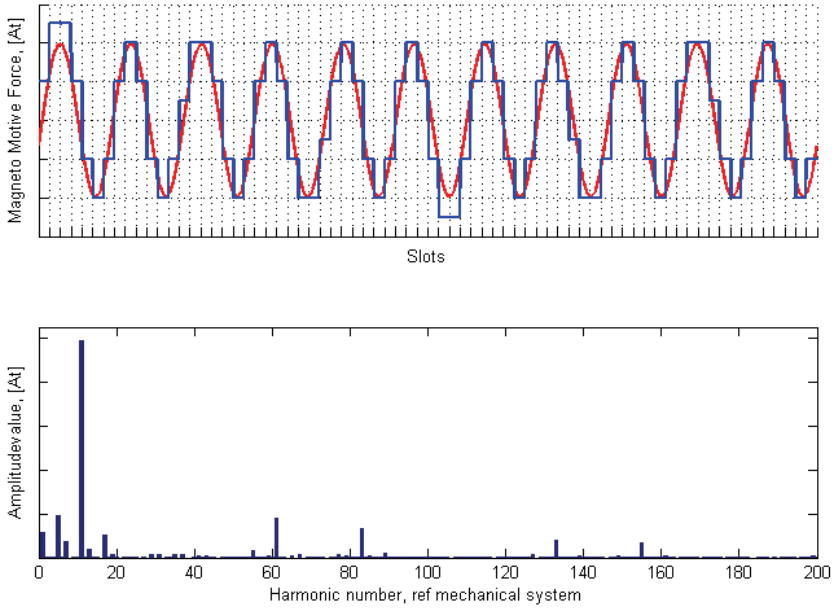

Fig. 60 MMF and its harmonic content

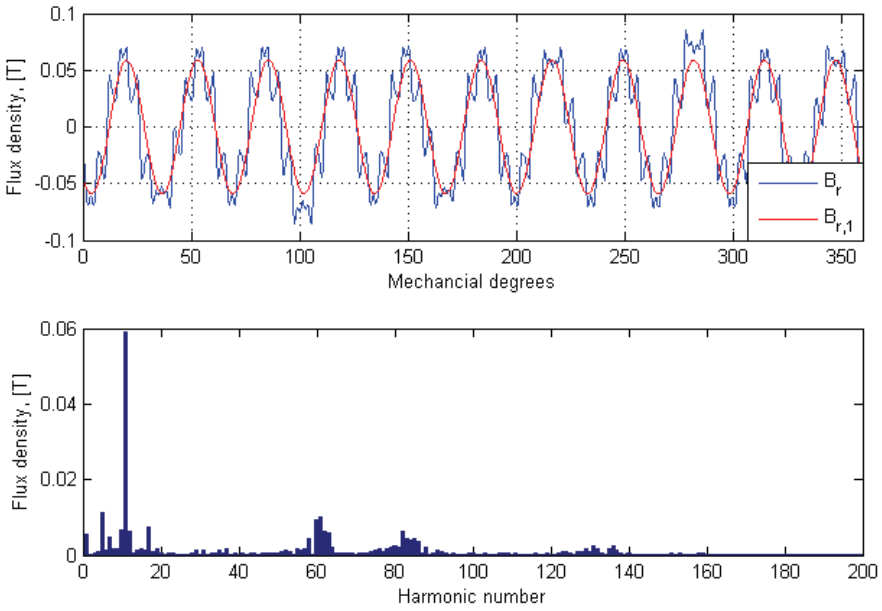

Fig. 61 Flux density in the air gap from MMF (FEA)

3.2.3 Induced voltage

The voltage is calculated from the flux per pole found using FEA. The flux density is found from the difference in Az in the two slots occupied by a coil (29). Since this is a fractional slot winding (q=12/11) where all 22 poles are needed to achieve a balanced machine, a plot of the flux through a coil as a function of electrical position can be made from one stationary calculation getting a plot from 0-360 electrical degrees with 72 (=N_s) points (Fig. 62). The flux density distribution is shown in Fig. 58.The distribution factor is k_d=0.955, eq. (38), in this case the chording will be taken care of by the FEA calculation. The calculated induced voltage is presented in eq. (93).

$$\begin{aligned} E_{line} &= \sqrt{3} \cdot E_{phase} = \sqrt{3} \frac{\hat{E}}{\sqrt{2}} \\ &= \sqrt{3 \cdot 2} \cdot \pi \cdot k_d \cdot N_{sc} \cdot N \cdot \hat{\phi}_1 \cdot f \\ E_{phase} &= 231\text{V} \\ E_{line} &= 400\text{V} \end{aligned} \tag{93}$$

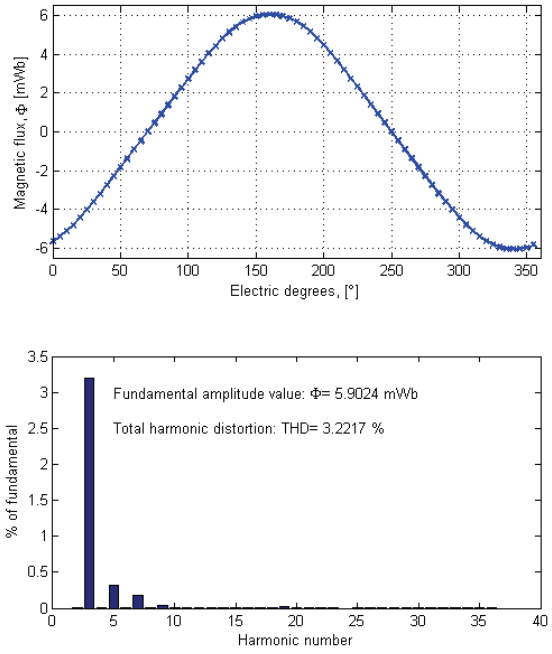

Fig. 62 Flux through one coil as function of electric degrees

3.2.4 Resistance and inductance

In Table 15 the calculated resistance, inductance and reactance is shown. The resistance is found using eq. (53), (54) and (55). The inductance is calculated using 2D FEA to find the energy from the load current, and using eq. (67) to calculate the inductance. A mutual inductance of one third is added.

Table 15 Resistance, inductance and reactance

Resistance			Inductance			Reactance
DC@20C	AC@20C	AC@60C	Self	Mutual	Total	@700rpm
24 mΩ	31.2 mΩ	35 mΩ	0.41 mH	0.14mH	0.55mH	442 mΩ

3.2.5 Summary of electric parameters

To achieve the desired power with the current in the q-axis a current of 140A is needed, giving a terminal phase voltage of 245V. If cos(ϕ)=1 a current of 144A and terminal phase voltage of 232V is needed. This is at nominal frequency (128Hz). The voltage drops for the two cases are about the same.

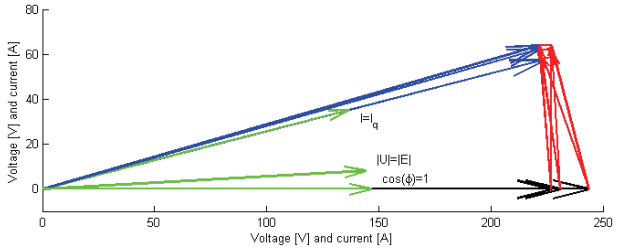

Fig. 63 Vector diagram for three different load cases

Using the induced voltage and the nominal current when $I = I_q$, as base values, the per unit values can be found, they are shown in Table 17. The calculated impedance is 0.27pu, which is fairly low, and around what is expected of smaller PM-machines. Considering the vector diagram in Fig. 63 and the different values for current, voltages and power for different control schemes in Table 16 it is evident that due to the low impedance there are small differences in currents, voltages and losses due to control strategy. Due to the low reactance the dimensioning currents and voltages for the converter is not a big issue.

Table 16 Result of nominal load calculations

	L_{ph}=0.55mH R_{ph}=35mΩ		
	cos(ϕ)=1	|E|=|U|	$I = I_q$
P_{out} [kW]	100	100	100
Q [kVAr]	0	0	20
U_{ph} [V]	227	231	244
I_{ph} [A]	147	145	141
cos(ϕ)	1	1	0.98

Table 17 pu values for the different cases in Fig. 63 and Table 16

	E_{base}= 231 V I_{base}= 141 A Z_{base} = 1.63 Ω		
	cos(ϕ)=0	|E|=|U|	$I = I_q$.
U	1	1	1.06
I	1.04	1.02	1
R	0.021		
X	0.266		
Z	0.267		

3.3 Generator test

The machine was first tested as a generator with resistive load, then as a motor mounted on a boat (Fig. 64). The testing on the boat started with a conventional diesel electric setup with a wound synchronous generator at fixed speed and a convert controlling the propeller. It was followed up with a test where the generator was directly connected to the PM-motor, and later the generator was rebuilt with a PM rotor. With some adjustment to the diesel regulator this system worked pretty much as a mechanical system with shaft and gearbox where the motor followed the generator from zero to maximum speed. The speed of the propeller is controlled by the speed of the diesel engine where the number of poles in the generator and motor sets the exchange ratio. The latter test resulted in a patented propulsion system [101].

Fig. 64 Testing of motor, to the left is the generator test setup and to the right the direct start test setup up with the test boat in the back

There will only be presented results from the generator test here. Some test results regarding temperatures and thrust is presented in [2] and [3].

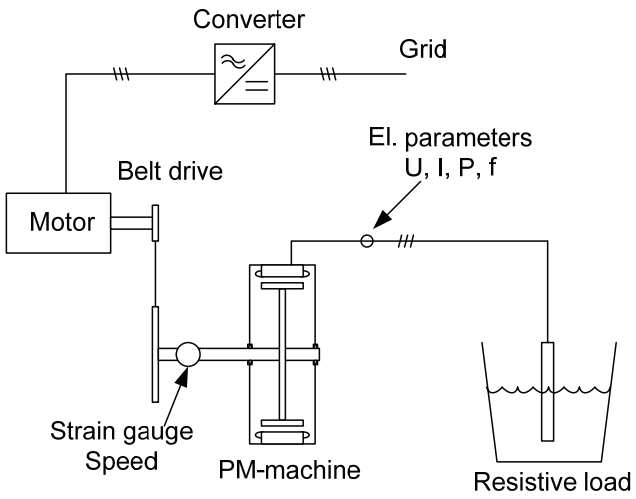

Fig. 65 Setup for generator test

A schematic of the setup for the generator test is shown in Fig. 65 and to the left in Fig. 64 a picture of the machine setup. Electric parameters such as voltage, current, power and frequency is measured at the PM-machine terminal. The input power is measured on the shaft between the belt drive wheel and the PM-machine with strain gauge and speed measurements.

The no load voltage (induced voltage) of the machine is measured to 401V @700 rpm yielding 0.573V/rpm.

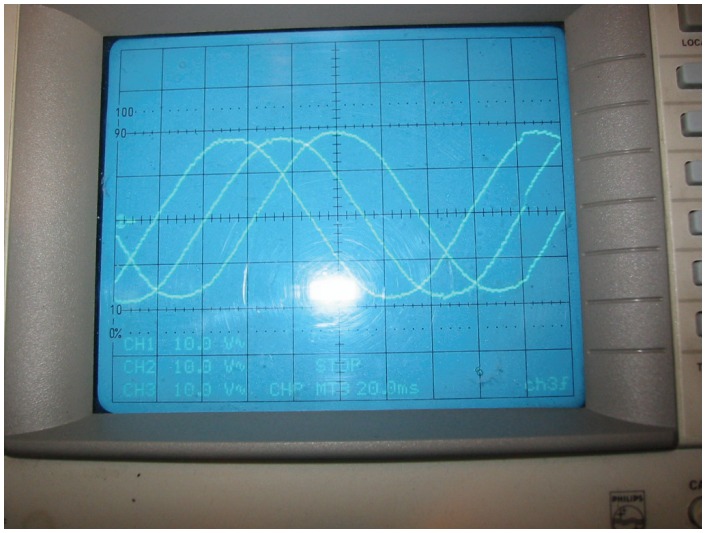

Fig. 66 Picture of an oscilloscope showing the no load voltage with one of the phases inverted for the occasion

3.3.1 Load testing: Voltage drop

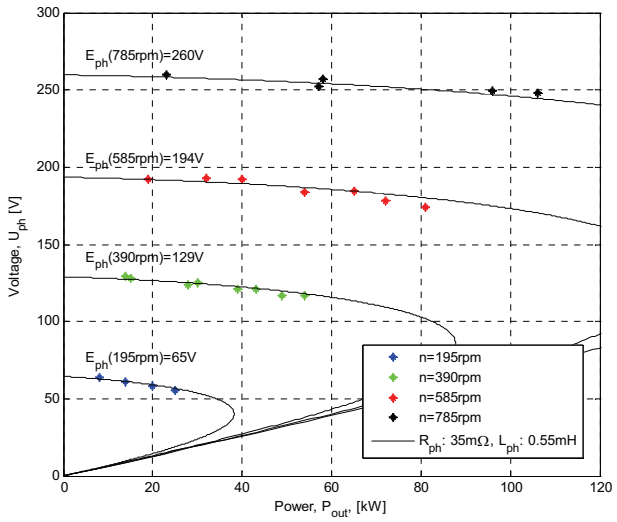

Fig. 67 Voltage drop as a function of load at different speeds with resistive load

The PM-machine was tested at different loads at different speeds to test its performance. The result shows some drop in voltage, up to 20V at full load and full speed (Fig. 67). In Fig. 68 the calculated inductance is shown, assuming R_{ph}=35mΩ. The load is resistive thus is the equation for the inductance as in (94). The nose curve in Fig. 67 is calculated based on the previous mentioned resistance, and calculated inductance (L=0.55mH). The measured values presented in Fig. 67 and Fig. 68 coincides fairly well with the calculated values. There is a spread for the power/voltage measurements around the nose curves, and looking at the estimated inductance values they are somewhat higher than the calculated. The inductance is probably around 0.65mH.

$$L_{ph} = \frac{\sqrt{E_{ph}{}^2 - \left(U_{ph} + R_{ph} \cdot I_{ph}\right)^2}}{2 \cdot \pi \cdot f \cdot I_{ph}} \tag{94}$$

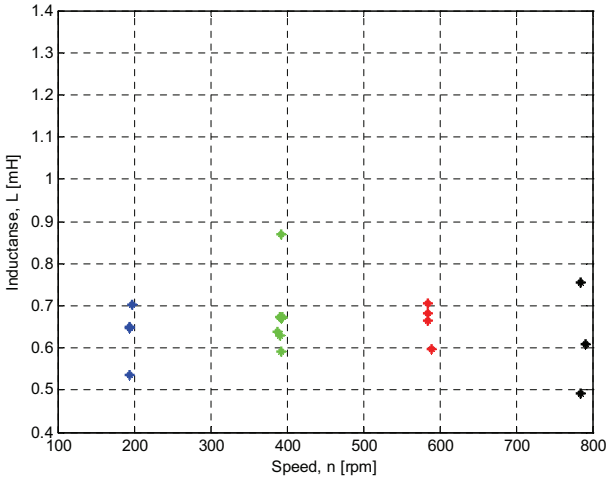

Fig. 68 Calculated inductance assuming cos(ϕ)=1 (resistive load) and R_{ph}=35mΩ

3.3.2 Efficiency

The efficiency was measured using the setup in Fig. 65. There are significant inaccuracy, and large variations in the strain gauge measurements, resulting in an inaccurate efficiency calculation. The result is presented in Fig. 69. The mean efficiency is around 93% and it can be claimed that a best point of 95% for a current around 0.75pu. The measurements include bearing and windage losses.

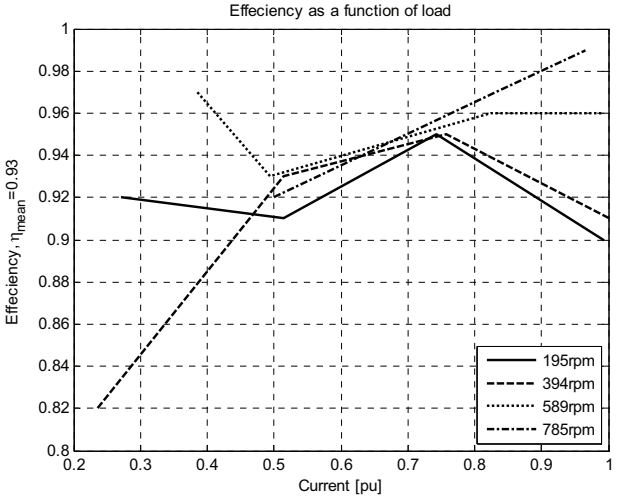

Fig. 69 Measured efficiency

Chapter 4
Low speed machines utilizing concentrated coils

As part of the research on utilization of wind energy at NTNU a laboratory model of a direct driven generator for wind turbines has been built at the dept. of Electric Power Engineering. The argumentation for the chosen design is presented in the first chapter, where a 3MW case is presented and discussed. The discussion on how to scale down to the prototype, and which parameters were important to preserve and control is also included in the first part. Based on the discussion and the decisions made for the 3MW design, and how to test the phenomena, a prototype was proposed and built. The second part presents the design, the third part the build and assembly while the fourth part presents the testing.

4.1 Direct-driven 3MW generator for wind turbine

The direct driven generator for wind turbines has excellent features for using permanent magnetized synchronous generator. A 3MW turbine will typically have a speed of 16-17rpm at nominal conditions, 50Hz result in 350-370 poles. With a pole span of 150mm this result in a diameter around 17m. The generators built for direct driven wind turbines is not this large, that is Enercon's 4MW turbine with wound rotor has an air gap diameter around 12.5m, but "only" 92 poles. Rotatek's 3MW generator is around 6m and yields 16Hz [43], and Siemens generator wind turbine about the same [102]. These generators use stators with more than three slots per pole. Except for Enercon's machine, which has wound poles, the limiting factor for the diameter (downwards) and frequency (upwards) are the slots. The cost of increasing the diameter has thus reduced the frequency. The converter cost of a higher frequency (reactance, reactive power) will also play a vital role in the optimization, together with structural cost and cost of active material.

This project was initiated based on the wish to evaluate the feasibility for using concentrated coils in generators for wind turbines. As mentioned previously the concentrated coils have some pros and cons, where the simplicity, low slot number and large slots are counted as pros, while the wide slots, its crude design and large amount of sub harmonic MMS are cons. In the following chapters the preliminary work leading up to the prototype is presented.

4.1.1 A preliminary study of different generator alternatives

Four generators were designed and compared, two different windings, one with concentrated coils and one with integral distributed winding, and two different frequencies, 30 and 50Hz. The hypothesis is that a more compact and simpler machine can be built using a winding with concentrated coils instead of distributed winding. It was chosen to look at the a 50Hz design since this is a standard frequency and a higher frequency in general means a lighter machine, and 30Hz since this seems to be in the area where optimized very low speed ends up. For this application a full sized converter most likely will be used, and direct connection to the grid unlikely.

The calculations are simplified such that the pole pitch equals the coil pitch, and thus only one pole has to be examined to find voltage, inductance etc. Voltage is found assuming that the peak flux through a coil is found when the pole is directly beneath it (48). The resistance is neglected, but the copper volume is found assuming circular end windings. The inductance is found evaluating the gap and slot inductance. This is a good approximation for the distributed winding, but as can be seen later in the design of the prototype, less accurate for the concentrated winding. The active and apparent power is calculated using the induced voltage and current placed in the q-axis. The diameter is also assumed so large that the machine can be considered linear. With the large number of poles, the error of assuming linear geometry is small. A bigger error is that the sub harmonics MMF are not considered in this preliminary study. The preliminary design focused on power density and volume of active material. The machines were compared based on the weight of active materials, power densities and to some extent their cost (based on material consumption). It was chosen to keep the voltage around 400V.

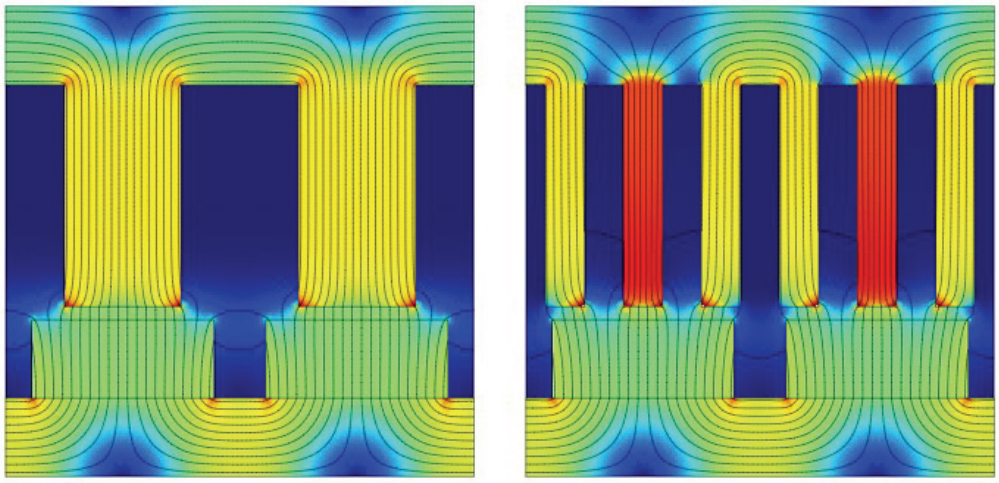

Fig. 70 Examples from the preliminary work, simplified FEA of no load flux density, to the left concentrated coils and the right distributed integer winding

The results from the calculations are presented in Table 18 - Table 20. It is found that a concentrated winding reduces the weight by 1.5 to 2 tons, while increasing the frequency reduces the weight by 0.6-1.1 tons. The largest mass reduction is found in the lamination and rotor yoke, the magnet mass is fairly constant for all four examples, while the copper mass increases slightly with increasing frequency. The reduction in mass going from an integer distributed winding at 30Hz to a concentrated winding with 50Hz is 2.6tons, 15%. Considering the simplicity in the calculation one can't claim that a 50Hz concentrated winding is better than a distributed, especially since the MMF and the effects from it is not

considered. Neither is the structure included, though equal for all machines, further marginalising the effect the weight loss.

The reactive voltage drop, the reactance, deciding the magnet volume and the cost of the converter, is acceptable for all machines. Both machines with concentrated windings have about two times the reactance of the machines with distributed winding.

Regarding the dimensions it can be seen that the slots for the 30Hz concentrated winding is fairly wide, almost 40mm, while for the 50Hz distributed is fairly deep and narrow, 8mm wide and 110mm deep and the tooth is only 5.5mm wide. Thus it can to some extent be claimed that if 30Hz is chosen a distributed winding could be chosen while for the 50Hz solution the wider slots of the concentrated winding is favourable.

Table 18 Results from calculations

	30Hz		50Hz	
	q=1/3	q=1	q=1/3	q=1
S, [MVA]				
P, [MW]	3.14	3.2	3.15	3.02
E, [V]	454	416	408	542
I, [A]	2621	2672	2941	2630
L, [mH]	0.5	0.6	0.4	0.2
Xpu (Zn = 0.145Ω)	0.63	0.27	0.88	0.43

Table 19 Mass of active material

Mass in tons	30Hz		50Hz	
(1000 kgs)	q=1/3	q=1	q=1/3	q=1
Copper	3.4	2.5	3.7	3.9
Lamination	8.2	10.1	7.0	8.8
Magnets	2.3	2.6	2.6	2.6
Rotor yoke	1.4	1.6	0.9	0.9
Total	15.3	16.8	14.2	16.2

Table 20 Dimensions for the different examples

	30Hz		50Hz	
	q=1/3	q=1	q=1/3	q=1
D_g [m]	4.64	4.64	4.64	4.64
L [m]	1.2	1.2	1.2	1.2
g [mm]	5	5	5	5
l_m [mm]	22	22	22	22
w_m [mm]	62	62	37.3	37.3
Dir [m]	4.53	4.52	4.55	4.57
Dis [m]				
ws [mm]	39.5	11.5	24.3	8.3
wt [mm]		9.2		5.5
ds [mm]	70	80	80	110
Dos [m]	4.86	4.84	4.85	4.87

4.1.2 Choice of concept

A final conclusion could not be drawn from the preliminary work. It was decided that a scaled model would be built to test the concept of the chosen design. This model should not

necessary be an optimum PM-generator for a wind turbine, it should be such that one could test the parameters and phenomena of interest

Based on the preliminary work presented in the previous chapter it was decided that the concentrated winding, with its simplicity and coarse slots was the most interesting to evaluate. Thus one could build a machine that can be used to examining among others:

- Consequences of the coarse slots; torque ripple, magnet losses etc
- Sub harmonic MMF, inductance, rotor losses etc

The goal was to try to build and see if such a simple machine could perform as well as other machines with more slots per pole. And a goal in itself; testing a very low speed machine with concentrated coil. Aside for the wind generator application a very low speed high torque machine would also be interesting for other applications such as tidal power generation, electrical steering gear, large actuators, or motors for winches among others.

4.1.3 Scaling from 3MW to 50kW laboratory model

A model is to resemble the original and give answer to questions and present the flaws, and advantages, of the original without too much cost. When scaling it is important to know which parameters one wants to examine, what are the potential challenges one wants to stress and which benefits do you want to show. This model is to test the concept of using concentrated coils and make use of the fact that the reduced number of slots can be used to increase the frequency up to 50Hz. One challenge with the raised frequency is the relative high reactance, another aspect is the relative large slot openings, yet another the effect of the slot pole combination and the MMF.

4.1.3.a Various aspects around the topic of scaling

In this chapter the considerations made regarding scaling are presented. The relationship between speed, frequency, pole number, diameter and peripheral speed is important for the performance. But also magnetic and electrical loading, leakage flux and reactance are important. And finally economical aspects and limitations in the infrastructure are very important parameters and must be taken into account.

Voltage

The voltage is not an important value for the scaling as long as one stays on the low voltage side. The machine concerns itself more about voltage per tooth, or slot, and current per slot. This can be seen when looking at the effect of changes in the numbers of turns in the pu system; none. The voltage available in the laboratory is 400V, and thus the limit. The choice of voltage influence the choice of winding method, number of turns, copper area, etc. this again influences the ac-factor of the winding.

Winding

There was not found a sensible approach to scale the winding adjusting both voltage and the shape of the winding, keeping the same eddy currents and proximity effects. The choices regarding number of turns, parallel strands, number of parallel circuits and type of winding will thus mainly be decided by the properties of the scaled model and its infrastructure. The choices made for the winding in the scaled machine will thus not necessarily be right for the full size machine.

Frequency

The frequency is closely connected to the design of the original machine and should not be changed. The frequency is included in the calculation of reactance, pole number, speed and diameter among others. Reducing the frequency will reduce the speed or pole number and diameter. Keeping the diameter a reduced frequency can increase the available area for slots and copper. For iron losses and other aspects that are dependent on frequency, the frequency should be kept constant in the model or increased to stress the phenomena under investigation. Thus frequency is one factor one would want to keep in the scaled version.

Peripheral Speed

The peripheral speed is decided by the frequency and the pole pitch:

$$\begin{aligned} v_p &= \frac{n}{60} \cdot \pi \cdot D_g = \frac{n}{60} \cdot N_p \cdot \tau_p \\ n &= \frac{120 \cdot f}{N_p} \\ \Rightarrow v_p &= \frac{120 \cdot f}{60 \cdot N_p} \cdot N_p \cdot \tau_p = 2 \cdot f \cdot \tau_p \end{aligned} \tag{95}$$

Considering only one pole one can assume that by keeping the peripheral speed and frequency constant the one pole and the tooth will experience much the same electrically and magnetically loading as in the full machine. This is valid if the diameter is so large that the machine can be assumed linear, or close to, and has the same flux and current density.

This means it is possibility to adjust the number of poles and speed while keeping the pole pitch, to achieve the wanted power rating. The machine length can be changed proportionally to the diameter, Dg/L kept constant, or the parameters can be altered independently.

Rotational speed

For a wind turbine at around 50kW the rotational speed is said to be around 50-80rpm, Entegrity Wind Systems uses 62rpm [103], EMS an 55rpm for their 65kW turbine [104] and the prototype generator built at Chalmers, Sweden 70rpm [105]. Keeping frequency, peripheral and rotational speed it is possible to also choose an optimal rotational speed for the generator, resulting in a given diameter. Then the length has to be adjusted so the wanted output is reached. Choosing a speed that is suitable for a wind turbine the model can be tested on a real wind turbine.

It can also be chosen to keep the very low speed of the original machine of 16 rpm. Keeping the frequency this will result in the same pole number. To scale the model the length, diameter and hence pole and slot pitch be adjusted. It should be possible to build a model in the scale 1/60 (power) by changing the all dimensions proportionally (linear). But this would give an electromagnetic different machine with other values for electric and magnetic loading. Mechanically this would be a difficult task, and one would not learn much from. It is generally difficult to scale the mechanical behaviour.

Number of poles per slots and phases, q

The number of poles and or slots may also be chosen as a starting point for the scaling. That is, two out of three might be chosen of frequency, number of poles and speed. The third parameter is given by the other two. The relationship between poles and slots are important

regarding reluctance torque, MMF, losses and vibrations. Looking at the reference machine it has 12 equal parts where each part has 29 poles and 30 slots. Two parts are thus needed to make a machine (section), and an approach can be to keep q in the laboratory model.

Equal electric and magnetic loading

Given that slot pitch, slot depth and current density is kept equal to the original machine, the electric loading is equal too. Having the magnetic loading defined as the flux density in the air gap this is also a parameter that should be possible to preserve by keeping the air gap and magnet length equal. The synchronous reactance is also a reflection the electric loading of the machine. and keeping the geometry in the model equal to the original then the reactance in per unit is equal or close to equal, end winding effects may not be proportional to the active area.

Other parameters to consider

To get a correct scaling mechanically to examine the forces effect on the structure the strength should resemble the forces in the machine. If not the smaller laboratory model gets stronger and stiffer than the original. This can, electromagnetically, be an advantage since it removes some possible problems from the model. The structural strength of the construction is beyond and outside the scope of the thesis. The forces created by the electromagnetic effects are to be calculated and evaluated, but not more than that.

There are also other parameters that influences the decisions of the prototype machine; economy, production capacity, limits in the infrastructure, size of the door, crane capacity etc.

4.1.3.b Evaluation of different methods of scaling

Six different design examples were chosen for evaluation to examine the effect the method of scaling has on the machines parameters. The results from the different designs are presented in Appendix A. In Table 21 a short comparison is made. It should be mentioned that the designs presented are not the finalized design they represent simplified theoretical approaches to the design. The different scaling approaches evaluated are:

A. Choosing a speed suitable for a 50kW wind turbine. A speed of 70rpm was chosen (equal to [105]) and the frequency, pole and slot width together with the slot depth was kept constant. The pole number is thus given and the length reduced to the required power level. The electric and magnetic loading is the same, so is the slot and gap inductance. It is a stiffer machine mechanically. This generator has a different pole and slot combination than the proposed 3MW machine.

B. Keeping the speed constant at 17rpm, reducing all dimensions proportionally until wanted power is reached. Frequency is kept constant. This is the most special and unique machine, keeping the relation between the dimension constant and the high number of poles. Mechanically this might be the most correct one, but electromagnetically it does not give much information. Flux density, current loading and reactance are all parameters that are changed. It would also be the most challenging machine to assembly with all its small parts.

C. Using two parts of the original machine. The peripheral speed and frequency is constant. Length is reduced till the power is reached. The relative low diameter results in some differences due to the curvature, but in general looking at one pole it is the

same machine. It has the same pole and slot combination as the original which should result in much the same torque patterns.

D. Using four parts of the original machine. The peripheral speed and frequency is constant. Length is reduced till the power is reached. The diameter is twice of that in C, and the speed and length is half. Since it is more of the equal parts the torque pattern should magnify itself and effects of mechanical tolerances might become more visible. And due to the larger diameter this machine is more like the original linear 3MW machine. The machine is very short and the end winding will therefore be a large part of the winding.

E. Using two parts reducing all dimensions proportionally, keeping the Dg/L relation constant. Reduces the dimensions some, keeps the pole slot combination, little bit less current loading and reactance. This is a hybrid of C. and F. both keeping the slot pole combination and keeping the D_g/L relationship.

F. Keeping the pole pitch and D_g/L constant, reducing number of poles. Makes the smallest machine. Keeps the current loading and slot and gap inductance, but changes the slot pole combination and thus sub harmonic MMF, reluctance torque etc.

Table 21 Comparisons of the different design examples towards the proposed 3MW wind generator

	B): 17rpm	A) 70rpm F) 136rpm	C) 2 parts (103rpm) D) 4 parts (51)	E) 2 parts (103rpm) proportional
D_g [mm]	1660	A) 1158 F) 587	C) 733 D) 1547	661
L [mm]	430	A) 76 F) 152	C) 115 D) 55	171
M_{tot} [kg]	612	A) 268 F) 237	C) 252 D) 268	262
ac (X_{pu})	lower (X_{pu}=0.3)	equal (X_{pu}=0.8)	equal (X_{pu}=0.8)	lower (X_{pu}=0.7)
D_g/L	equal	larger	larger(C) much larger(D)	equal
ω_s/d_s	equal	equal	equal	equal
ν_p	lower	equal	equal	somewhat lower
Teeth	thin and short	A) equal F) wide tapered	equal	somewhat thinner and shorter
Mechanically	thin ring	same thickness smaller diameter	same thickness smaller diameter	somewhat thinner smaller diameter
q	equal	different	equal	equal

4.1.3.c The chosen method of scaling

The electromagnetically parameters are the most important to evaluate, that's not saying that the structural aspects are less important, they might be more important for such machines, but this thesis concerns itself with the electromagnetic aspect. Therefore is the mechanical consequences not emphasized. It has already been pointed out that the most important feature of the direct driven generator is the concentrated coils combined with the high frequency in the generator.

Alternative D. was chosen, it has the same peripheral speed, large enough diameter to preserve the idea that it is a linear machine, and the same pole slot combination as the proposed 3MW design. The electrical parameters in per unit are close and the electric and magnetic loading the same. This is an alternative that is feasible to build and still keeps the image that the generators for direct driven wind turbines are large, the prototype having a

much higher D_g/L than the 3MW design. In addition, but not an important argument the nominal speed is a little lower, but not too far from the natural speed of a 50kW wind turbine.

To only analyze the effects of the concentrated coils, the large slot openings alternative F. would give the cheapest and smallest machine, but it would have been a significant smaller machine with fewer pole/slots and a different q. Some of the interesting parameters are the large diameter and the pole slot combination. Alternative B. would make a too large and complicated design, losing too much of the electromagnetic similarities. The D_g/L relationship is not an important factor to keep constant (B. E. and F.), and since it is not supposed to test the generator in an actual turbine the speed is not important (A.).

4.2 The design of the 50kW prototype

Based on the suggested 3MW design, the discussion around scaling and which parameters to test, a design was made. The calculation of the chosen design is presented in this chapter. In Table 22 the design parameters are shown, while in Table 23 the machine dimensions are presented. In Fig. 71 drawings of the generator is shown. The design is a surface mounted radial flux permanent magnet machine with one layer concentrated coils (SM RFPM CC) machine. The slots are open and with parallel sides. Every other tooth is straight, the others are tapered. There is one magnet per pole and the magnets are rectangular. This is a patented construction from SmartMotor AS [106].

Table 22 Design parameters for the prototype generator

Nomenclature		Symbol		Comments
Power level	P_g	kW	50	Laboratory limitations
Voltage level	E	V	300	Limited by overspeed and converter rating
Nominal speed	n	rpm	51.7	Scaled speed
Nominal frequency	f_n	Hz	50	
Current	I	A	120	
Ampere-turn	NI	kA	2.3	
Electric loading	ac	kA/m	56	
Remanent flux density	B_r	T	1.2	

Table 23 Dimensions of the generator

Stator			Rotor		
D_{os}	1777	mm	D_{or}	1547	mm
D_{is}	1557	mm	D_{mr}	1507	mm
			D_{ir}	1450	mm
L_s	100	mm	L_r	100	mm
d_s	80	mm	l_m	20	mm
w_s	22.3	mm	w_m	33	mm
w_{ti}	18.5	mm	g	5	mm
N_s	120		N_p	116	
Coil					
D_{cond}	1.2	mm	N	19	
N_{coil}	60		N_{cond}	36	
$N_{turn,ph}$	380		$N_{turn,sec}$	95	

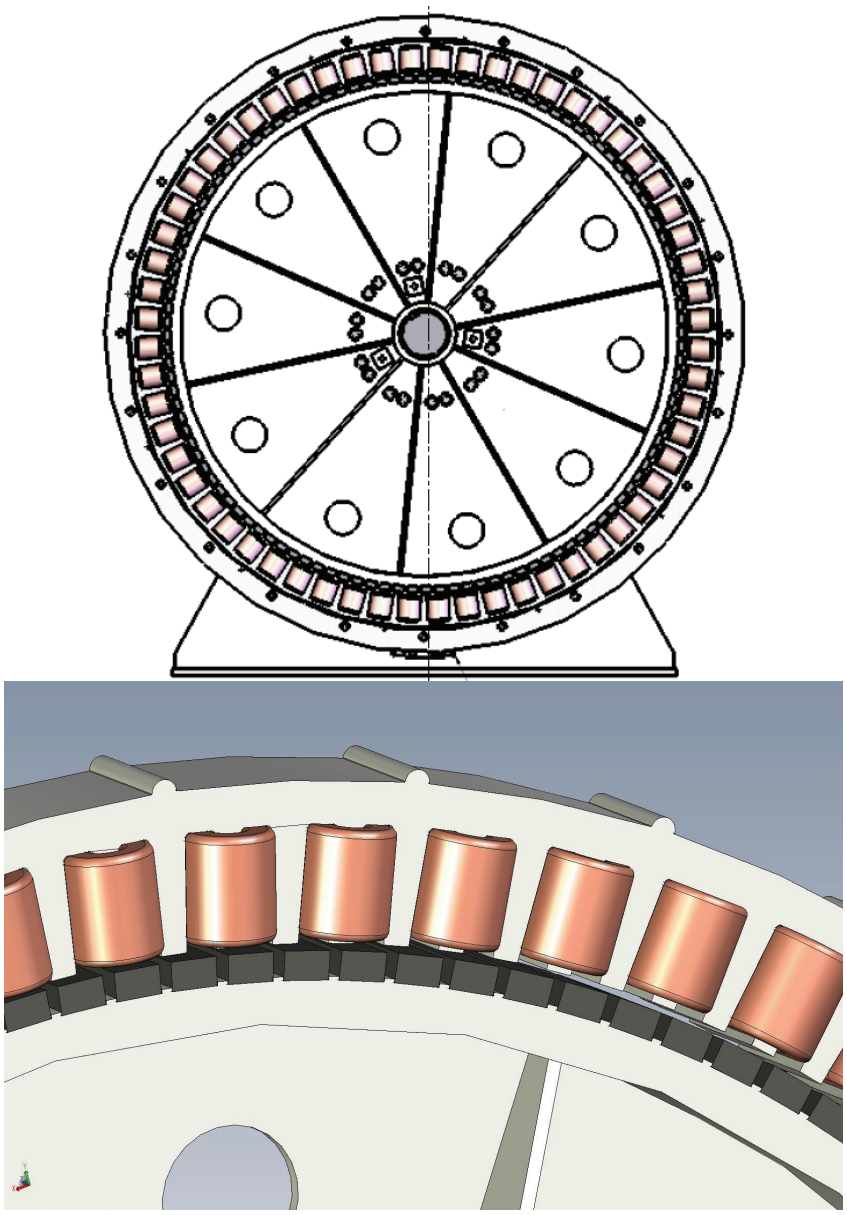

Fig. 71 Drawings of the generator showing the rectangular magnets, the concentrated coils around the straight teeth, and the tapered teeth between the coils

4.2.1 No load flux densities

The distribution of the no load flux density in the machine is found using FEA. The no load flux density is used for calculating the induced voltage, iron losses, no load forces in the air gap and no load torque. In Fig. 72 the flux density is shown. In the straight tooth the flux density is around 1.2T while one third up in the tapered tooth the flux density is around 1.0T. In the rotor yoke the flux density between the magnets are around 0.8T. The highest values are found in the corners of the magnets and in rotor yoke around the corners of the tooth tips, up to 2.0T.

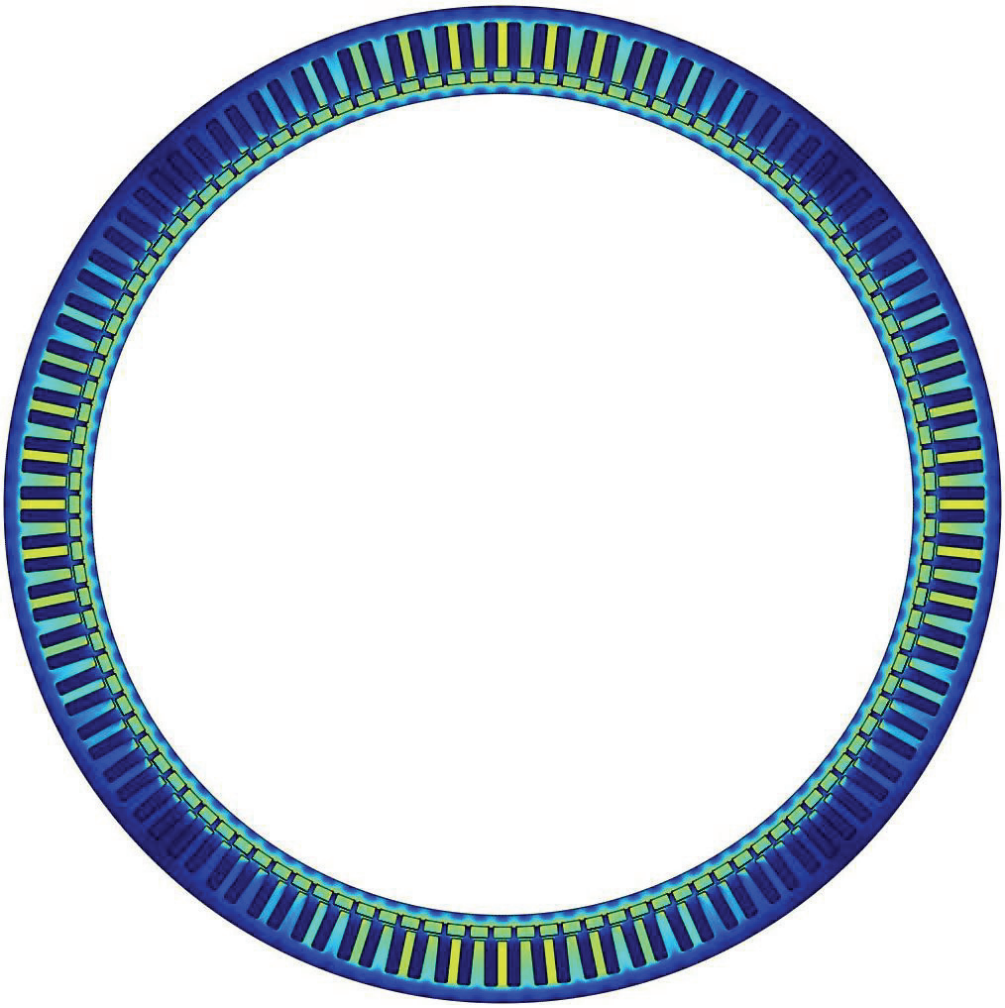

Fig. 72 No load flux density distribution

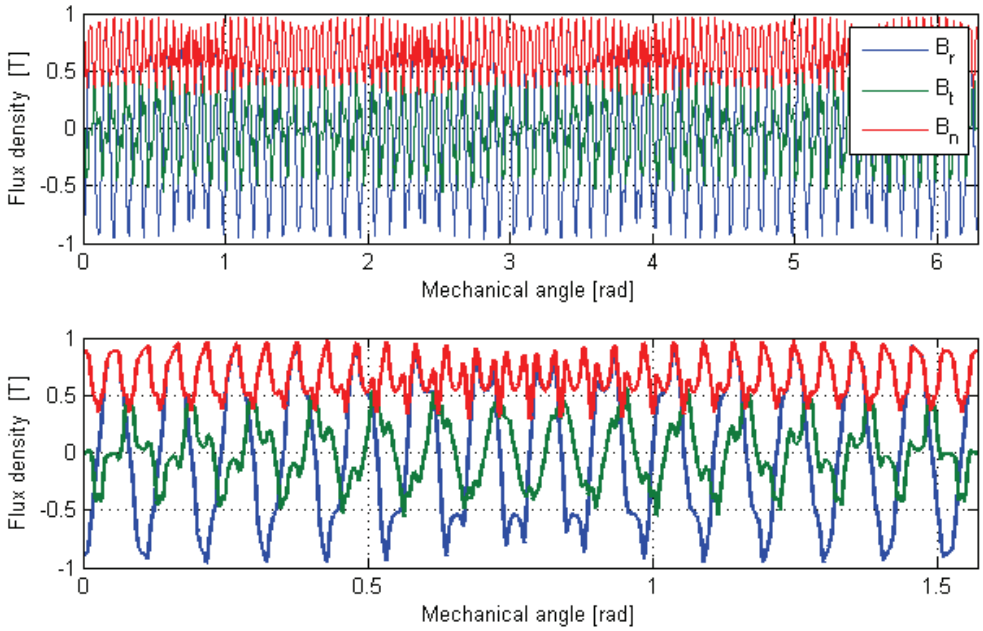

Fig. 73 Air gap flux density for the entire air gap (top) and one quarter of the machine (bottom)

The no load air gap flux density is far from sinusoidal, depending of the relative position of tooth and magnet, the flux twist and turns to get from the magnet to the tooth. In the figure above (Fig. 73) the flux density in the air gap is plotted. The top figure shows the entire circumference, while the lower shows one fourth (N_p/F_2). The harmonic content of the different components is shown in Fig. 74. The tallest radial and tangential component is the 58^{th}, while for the absolute value it is the 116^{th}.

The average flux density (DC-component of the absolute value) is 0.64T, while the fundamental radial component, 58^{th}, has an amplitude value of 0.85T. Though the harmonic content of the air gap flux is high, is the flux as a function of position very smooth. This is shown in the calculated induced voltage shown in Fig. 85.

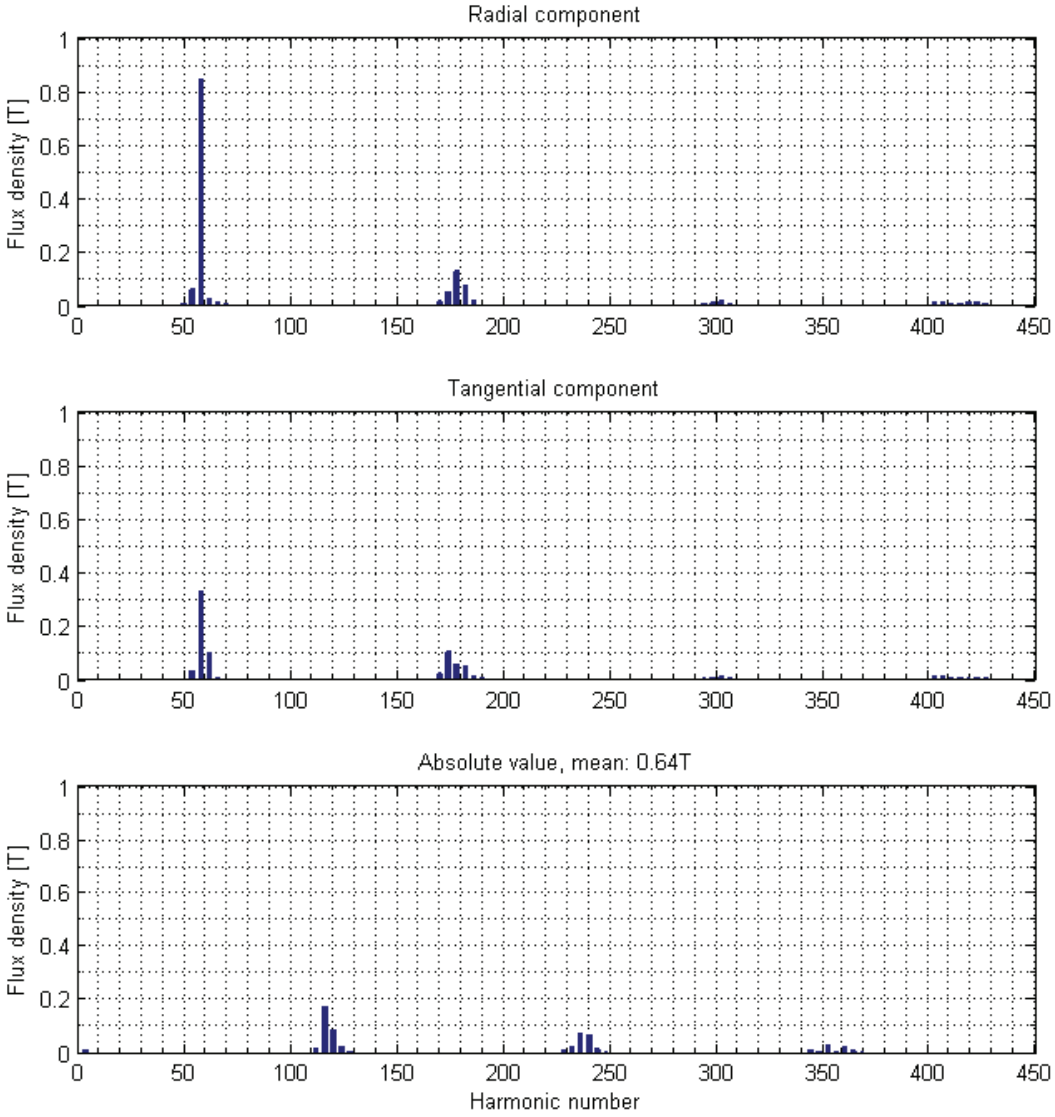

Fig. 74 Harmonic content in the air gap flux density, rms

4.2.2 Magneto Motive Force, MMF

A curve of the MMF from the winding is presented in Fig. 75. It is a simplified calculation placing the slot current in a point at the stator bore. The blue square wave is the MMF, the black is the one corresponding to the number of pole pairs (58). The single layer winding produces a substantial amount of sub harmonics ($h<N_p/2=58$), where the second is the largest, even larger than the fundamental. Of the higher harmonics it can be seen that they are gathered around 180, 300, 420, which corresponds to the 3rd, 5th and 7th multiple of the number of coils. A presentation of the MMF calculated using FEA, and the corresponding flux densities is shown later in this chapter.

4.2.2.a Comparison of the MMF in one and two layer winding

In Fig. 76 a plot of the MMF from a two layer winding with the same pole slot combination is shown. The sub harmonic content is much lower with a two layer winding. The harmonic content of higher harmonics is also reduced i.e. fewer components, those present are of same amplitude. The same groups corresponding to the 3rd, 5th etc. of the coil number are present. The amplitude of the 58th harmonic is identical for the one and two layer winding. The y-axis in both Fig. 75 and Fig. 76 are equal. Comparing the harmonic content of the MMF for the two windings, summing up all components except the 58th, the two layer winding has 70% of the harmonic content compared to the one layer winding. The difference is largest for the sub harmonic, the two layer winding has only 34% of the sub harmonics compared to the one layer, while for the higher harmonics the number is 90%.

A comparison of the losses in the rotor from the MMF with a one and two layer winding is presented in Fig. 77. It shows the contribution of the different harmonics to the losses for each winding. The losses are found using a simplified calculation based on the flux density calculated from (96) and (98), neglecting how the eddy currents influences the flux density. The losses are calculated from (70) or (71) depending on the skin depth. The losses in the two layer winding adds up to 70% of the one layer winding, corresponding to the difference in harmonics in the MMF. The difference is made up by the sub harmonics, and mainly the second spatial harmonic for the one layer winding, corresponding to over 25% of the total MMF loss for the one layer winding. From 62nd and up the loss components are close to equal. In this comparison the 500 first harmonics are evaluated. The higher harmonics can be neglected since their wavelength is smaller than the effective air gap, l_m+g. This loss calculation is only meant as a comparison of the two different concentrated windings, showing the impact of the sub harmonic content. Further analysis of the losses is presented in chapter 4.2.9. In Table 24 the comparison of both harmonics and losses are presented.

$$B_{g,i} = \mu_0 \cdot \frac{MMF_i}{l_m + g} \tag{96}$$

$$\Phi_i = \frac{2}{\pi} \cdot B_{g,i} \cdot \frac{L \cdot \pi \cdot D_g}{2 \cdot i} \tag{97}$$

$$B_{m,i} = B_{g,i}$$

$$B_{y,i} = \frac{\Phi_i}{2 \cdot L \cdot d_{ry}} \tag{98}$$

Table 24 Comparison of loss from one and two layer winding

	One layer		**Two layer**	
Harmonic content				
Total	100	%	70	%
Sub	100	%	34	%
Higher	100	%	90	%
Losses				
Total	100	%	70	%
2nd	25	%		

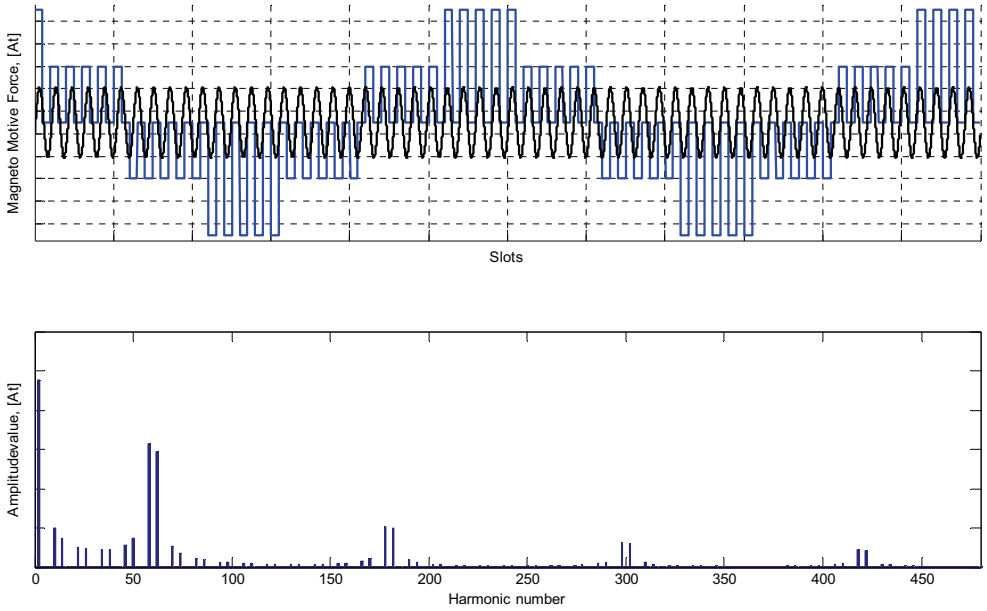

Fig. 75 MMF from the 116 pole 120 slot generator with one layer winding

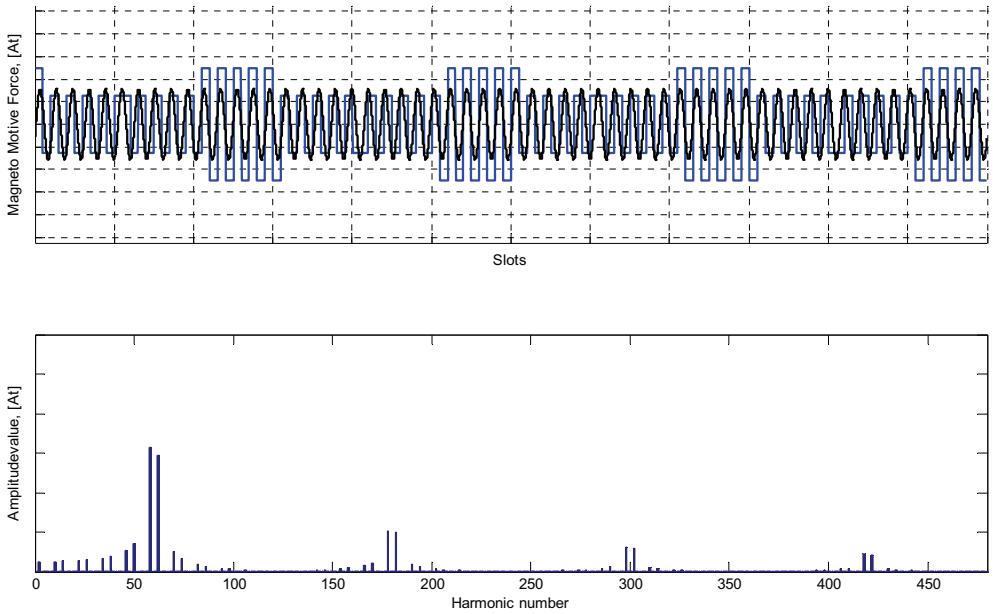

Fig. 76 MMF from the 116 pole 120 slot generator with two layer winding

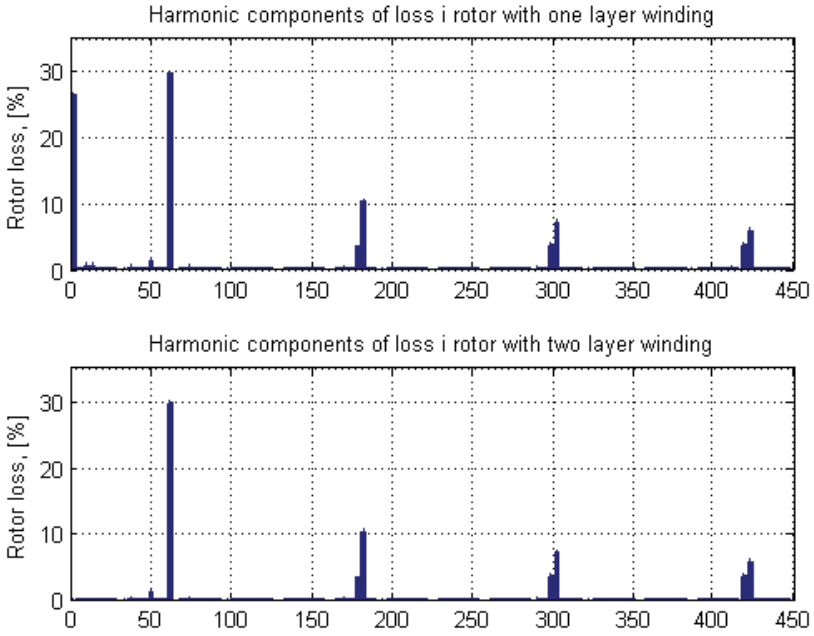

Fig. 77 Comparison of losses from MMF in one and two layer winding. presented as percent of total loss in the one layer winding

4.2.2.b MMF and air gap flux density from FEA

In Fig. 79 and Fig. 80 the radial component of the MMF and the resulting flux density from the non linear FEA is presented. Plot of the flux lines and flux densities is presented in Fig. 78. The harmonic spectre of the two parameters is also shown. It can be seen that due to the saturation in the iron and the long iron path for the second harmonic, it is smaller in the FEA than in Fig. 75, and that the higher harmonics is faster damped due to effect of slot openings (trapezoidal MMF).

The MMF causes high flux densities in the machine, presented in Fig. 78, in the teeth the average at the base of straight teeth the average of 1.2T, while it in the yoke (shifted 45degrees mechanically) is 0.9T. The applied current for the FEA calculation is amplitude value of the nominal rms current, 170A.

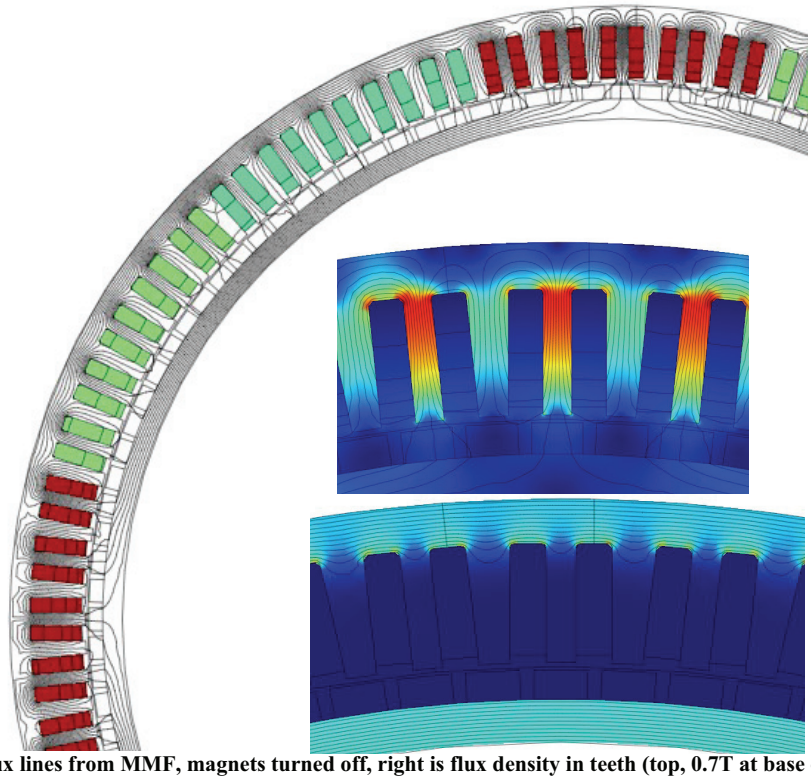

Fig. 78 Flux lines from MMF, magnets turned off, right is flux density in teeth (top, 0.7T at base of straight tooth) and yoke (bottom, 0.5T in both rotor and statoryke)

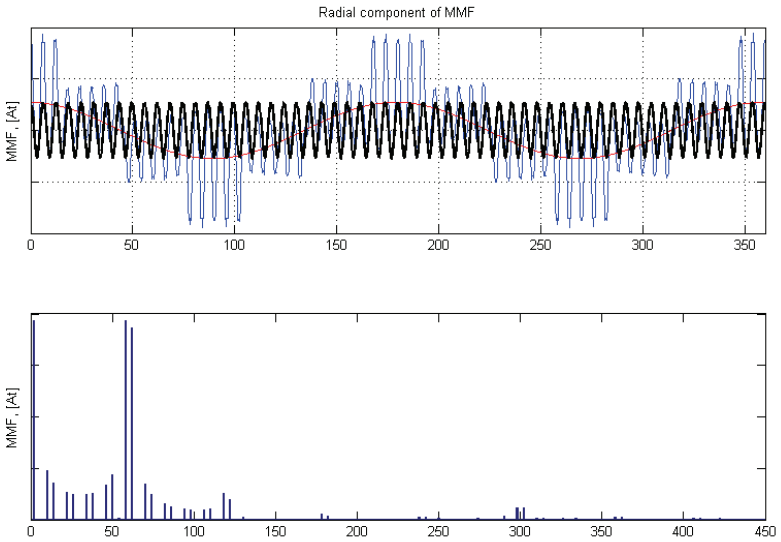

Fig. 79 MMF from FEA of the generator with one layer winding

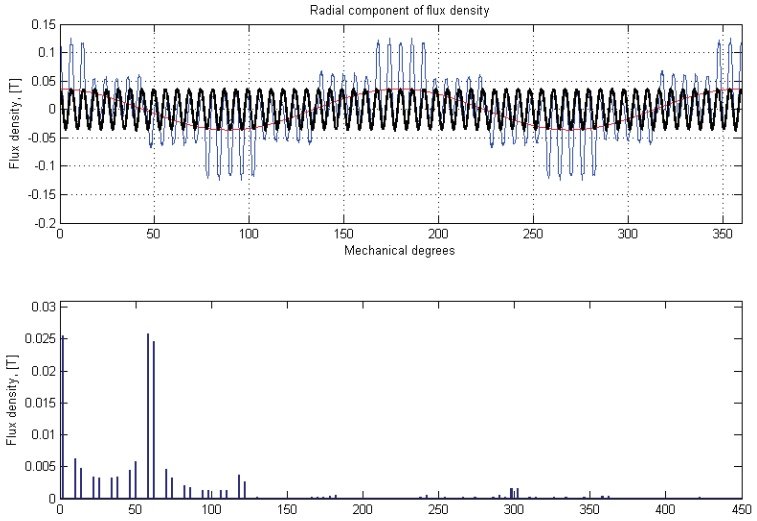

Fig. 80 Flux density from the MMF in the air gap from the FEA of one layer winding

4.2.3 Flux density with loaded machine

A calculation of the flux density in the air gap of the generator at full load is shown, it is shown an example where the current is in the q-axis (Fig. 81 and Fig. 82). The harmonic content of the flux density is also shown. In Fig. 81 it can be seen how the MMF directs the flux lines in the rotor yoke, the flux does not split half going right or left from a magnet, it is now turning either right or left. This can also been seen in the smaller machines in Fig. 30-Fig. 33. It should also be noticed the flux lines caused by the MMF enclosing several coils. Some comments on the induced losses due to these fluxes are presented in chapter 4.2.9. The most stressed tooth has a flux density of around 1.8T, while the highest values in the rotor yoke are 1.3T.

The harmonic content of the radial component of air gap flux is much lower than the no load flux and flux from the MMF, except for the 58^{th} harmonic its only the 62^{nd}, 22^{nd} and some around the 180^{th} that are visible, Fig. 82.

A calculation of the amplitude values for some of the harmonic components of the air gap flux density as function of load angle is shown in Fig. 83. It can be seen that the 58^{th} (corresponding to the pole pair number and fundamental electric frequency) changes in amplitude value from 0.77T to 0.91T.

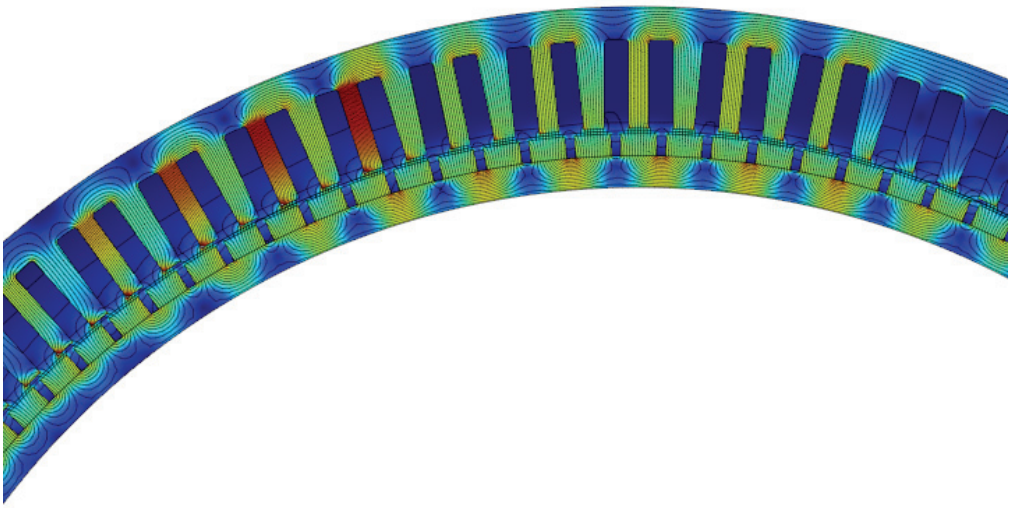

Fig. 81 Flux density and flux lines with current in q-axis

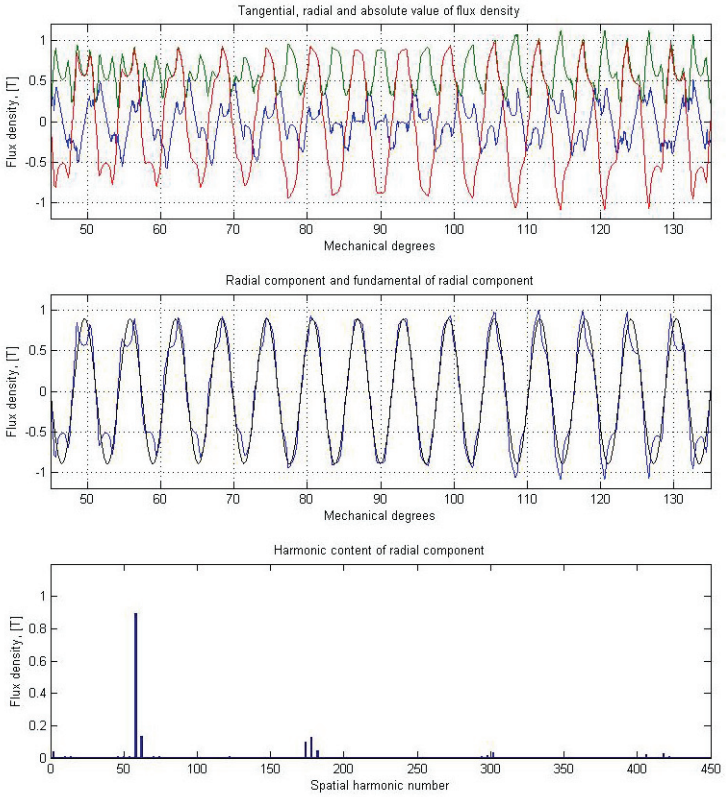

Fig. 82 Flux densities in the air gap; top: radial component red, tangential blue and absolute value green, centre: radial component and its fundametnal, bottom; Harmonic content of radial component

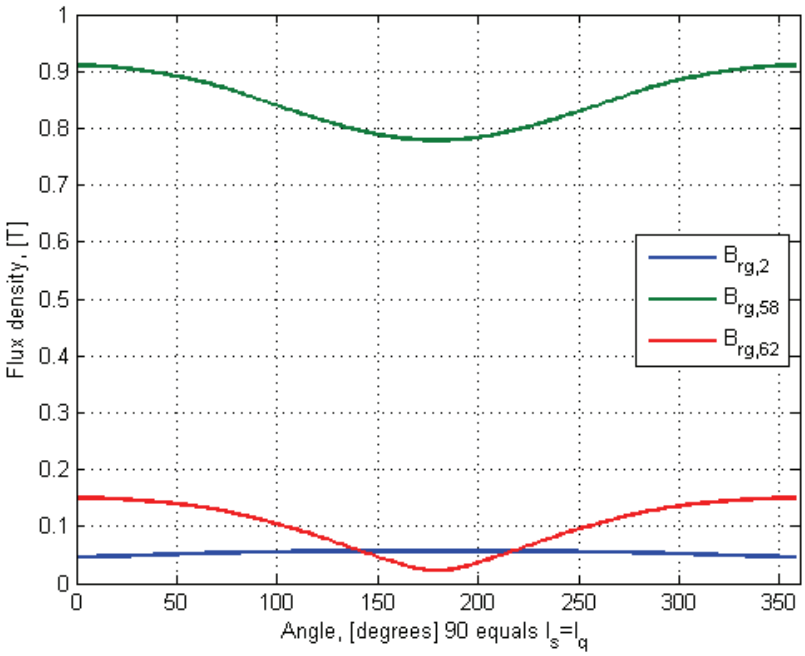

Fig. 83 RMS value of air gap flux densities for the 2nd (blue), 58th (green) and 62nd (red) spatial harmonic for different angles between current and magnets

4.2.4 Induced Voltage

The voltage is calculated using the nonlinear FEA, calculating the voltage to 300V. For comparison there are presented results from the different methods for calculating the voltage; four static methods where two are analytical and are two from FEA, and two methods based on rotating FEA calculation. The results are shown in Table 25. The winding factors are found from equation (36), (38) and (40), and in eq. (99) the fundamental factors are presented.

$$k_{d,1} = \frac{\sin\left(\frac{\pi}{6}\right)}{5 \cdot \sin\left(\frac{\pi}{5 \cdot 6}\right)} = 0.957 \quad k_{e,1} = \cos\left(\pi \cdot \left(1 - \frac{N_p}{N_s}\right)\right) = 0.999 \quad k_{w,1} = 0.955 \tag{99}$$

For the simple lumped circuit with infinity permeability in iron voltage is calculated both using the air gap and magnet area. As it is shown in (2.1) the magnet area reduces the flux significantly, and compared to the other results it is most correct to use the magnet area, not the total air gap.

The lumped circuit calculation assumes linear behaviour of the iron. The relative permeability is set to 740, which is given for the M250-50A lamination for flux densities around 1.5T. The numbers in the table below the lumped circuit calculations denotes numbers of parallel leakage resistances in the slot. This method yields a voltage closer to the goal of 300V. It is important to include one path across the slot, but increasing the numbers further has little effect.

The 2D linear FEA uses the same relative permeability as the lumped circuit. The non linear FEA uses an approximation of the saturation curve for M250-50A, appendix C-4, and an arbitrary curve for soft iron for the rotor yoke, appendix C-1. Both the static 2D FEA calculations are using the same model. The difference is how the flux and voltage is calculated. The one coil solution uses the flux in a coil where the magnet is directly beneath, and assumes this to be the amplitude value of the flux. While Az(slot) slot finds the flux through several coils (the 30 coil having different electric angle in the static calculation, as in chapter 3.2.3), and uses the fundamental of the curve. A plot of the flux is shown in Fig. 84.

The rotating model makes use of two different methods, one where the change in electric field (Ez) is integrated over the coil area, and one where the vector potential (Az) at the bottom of the slot is used. The voltage for both calculations is fairly similar. Plots of the time dependent calculation using the Ez value is shown in Fig. 85, showing the no load voltage for a coil and for a phase. Both show very low harmonics, and for the voltage per phase only the third harmonic is significant. Comparing the calculated coil and phase voltage (Ez) it can be seen that the distribution factor is 0.9568, which is identical to the calculated distribution factor, eq. (99).

Table 25 Voltage calculations

Simple lumped $\mu_{r,fe}=\infty$ [V]		Lumped [V], $\mu_{r,fe}=740$				
A_g	A_m	0	1	2	3	4
357	281	336	307	306	306	306

	2D static FEA one coil [V]	2D static FEA Az(slot) [V]	2D rotating FEA Ez(t) [V]	2D rotating FEA Az(t) [V]
linear	281		292	
nonlinear	297	300	299	296

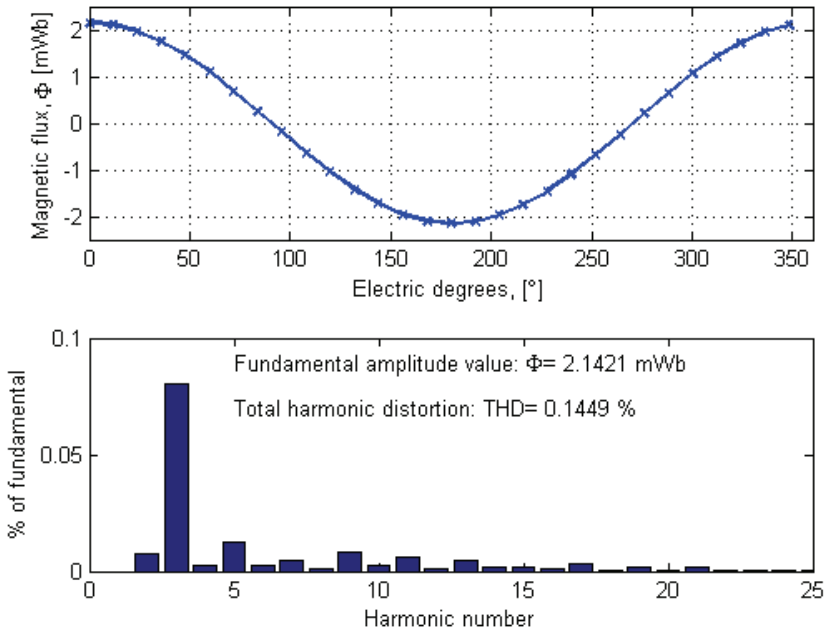

Fig. 84 Plot of the flux in 30 coils with their relative position and the harmonics from the curve

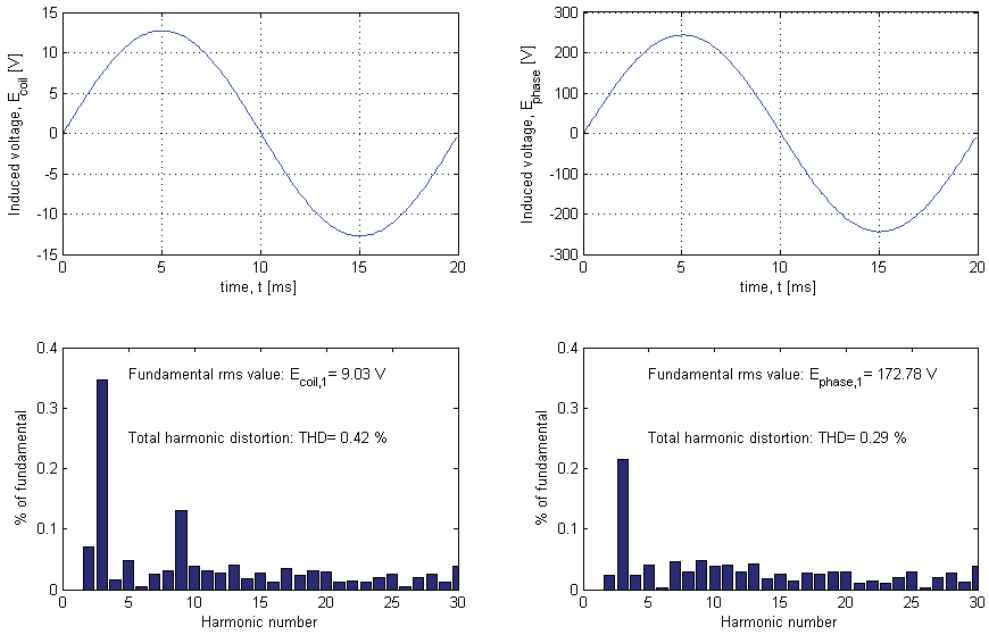

Fig. 85 Induced voltage (from Ez) per coil to the left and per phase to the right

4.2.5 Resistance

Based on theory presented in 2.6.2, the resistance is found. The result is presented in Table 26. There are presented two different temperature coefficients and two different AC-coefficients. The lowest AC factor assumes that there are $N*N_{cond}$ in the slot carrying equal amount of current, while the highest is a FEA calculation assuming solid round conductors. The latter is added because testing of the machine indicates that the dividing of each turn in parallel conductors only partly works. It is assumed copper in all conducting parts, with conductivity, σ_{Cu}, of 58e6 S/m @ 20C. R_{con} is the resistance in cables from coils to terminals.

In Fig. 86 a FEA calculation of an assumed rectangular turns of solid copper. There coil are three turns wide and 6 1/3 turns high. The curves to the right show the current density and for the turns closest to the slot opening the circulating currents are large. This simplified calculation indicates an AC-factor of around 4.

Table 26 Calculated resistance

		$R_{ph,coil}$ [mΩ]	R_{con} [mΩ]	R_{ph} [mΩ]
DC@ 20°C	-	54.9	1.2	64.4
AC@ 80°C	k_T=1.24, k_{AC}=1.04	70.7	1.5	82.7
AC@115°C	k_T=1.37, k_{AC}=1.04	81.9	1.8	96.2
Solid AC@ 80°C	k_T=1.24, k_{AC}=2.10	142.9	1.8	157.3
Solid AC@115°C	k_T=1.37, k_{AC}=2.10	155.6	1.8	169.9

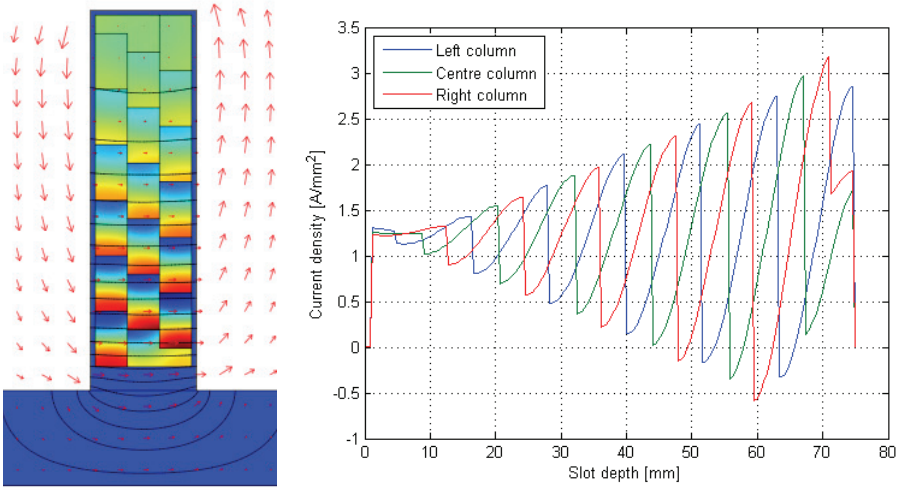

Fig. 86 A FEA calculation of AC resistance using rectangular wires

4.2.6 Inductance

The calculated inductance is presented in Table 27. Plots of the geometries with flux lines from the FEA are presented in Fig. 87. There are presented different calculations of the inductance trying to isolate the different parts of the inductances. Due to the size of the machine and limitation in the FEA tool, a 3D FEA of the entire machine is not made. Comparing the 2D and 3D FEA of the coil the contribution from the end winding can be found. Comparing the 2D FEA of the coil and the entire machine, the contribution from the sub harmonics can be found. This comparison is made in Table 27. The calculations show that the analytic calculation and FEA have comparable results for the gap and slot inductance, 3.4mH. The contribution from the end winding (per coil) is found to 0.57mH, while the sub harmonics adds another 0.6mH. The sub harmonic contribution is also called belt harmonics [75]. The belt harmonics from the end winding is not included, but expected to be very small. From 2D FEA of the entire cross section it can be seen that only a few, two of twenty, flux lines are going through the coils of the other phases and thus can the mutual inductance, the connection between phases, be expected to be low, and thus neglected.

Table 27 Calculated inductances

		W_m/m [N]	W_m [J]	L_{part} [uH]	L_{ph} [mH]
Analytical	Slot and gap			84	3.36
2D FEA	Entire cross section	287.9	28.8	3998	4.00
	Coil	12.2	1.2	169	3.40
3D FEA	Coil		1.4	198	3,96

	Slot and gap inductance	L_{gs}	[mH]		3.40
	End winding component	L_{end}	[mH]	+	0.57
	Sub harmonic component	L_{belt}	[mH]	+	0.60
	Sum	L_{ph}	[mH]	=	4.57

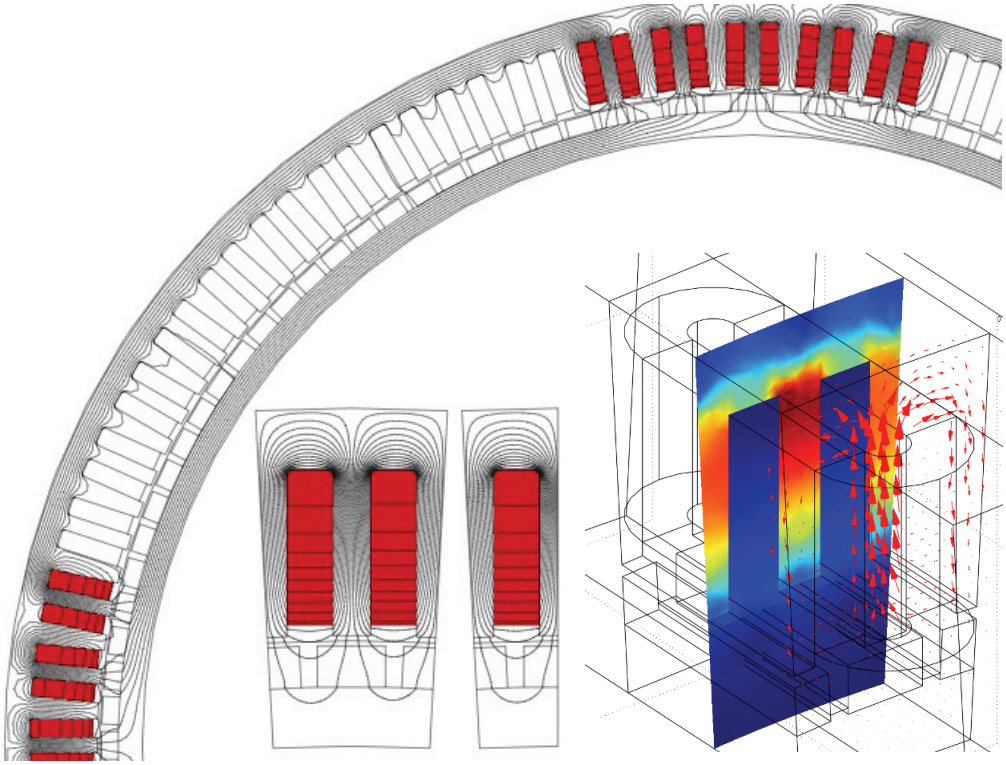

Fig. 87 FEA inductance calculation, top: 2D entire machine, left: 2D slot and coil, right: 3D coil

4.2.7 Summary of electric parameters

Having calculated the induced voltage, resistance and inductance, the current during different load conditions can be found. The calculated resistance at 115C and stranded wire from Table 26 is used.

Table 28 Summary of electrical parameters

Induced voltage	Resistance	Inductance	Reactance @50Hz
E_{ph} [V]	R_{ph} [mΩ]	L_{ph} [mH]	Xph [Ω]
173	96.2	4.57	1.44

In chapter 2.8 some different drive philosophies have been discussed. Based on the parameters calculated previously in this chapter, the different load cases are investigated: cos(ϕ)=1, |E|=|U| and I=I_q. The result is shown in Fig. 88 and Table 29. These examples shows that it is not possible to reach 50kW with a resistive load (cos(ϕ)=1), it further shows that when |E|=|U| a reactive power of 32kVAr is needed to compensate for the armature reaction, or increase the flux, while at I=I_q the as much as 45kVAr are needed. A calculation of the parameters for R_{ph}=170mΩ is also included in Table 29 showing the effect of increased resistance. The machine has been designed to operate at nominal load with induced voltage equal to terminal voltage (|E|=|U|).

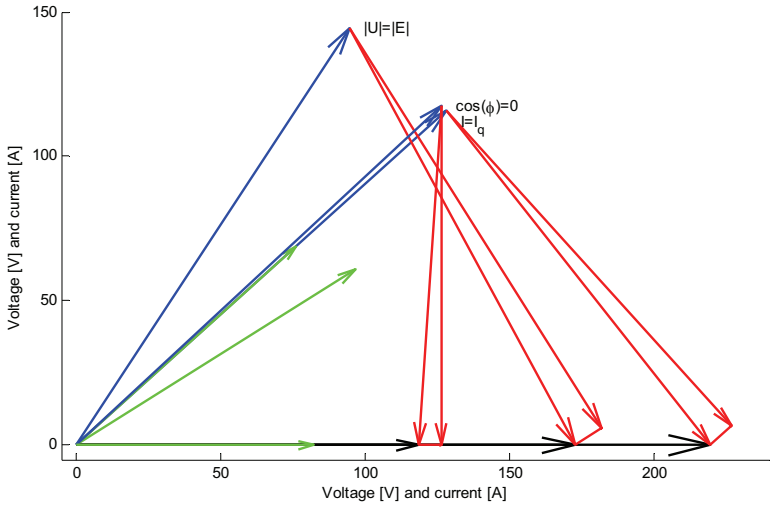

Fig. 88 The vector diagram for three different load cases, with L_{ph}=4.1mH and R_{ph}=96.2 mΩ

Table 29 Result of nominal load calculations

	L_{ph}=4.57mH R_{ph}=96.2mΩ			L_{ph}=4.57mH R_{ph}=170mΩ		
	cos(ϕ)=0	|E|=|U|	I = I_q	cos(ϕ)=0	|E|=|U|	I = I_q.
P_{out} [kW]	29	50	50	28	50	50
Q [kVAr]	0	-32	-45	0	-38	-50
U_{ph} [V]	118	173	219	115	173	219
I_{ph} [A]	82	114	102	80	121	108
cos(ϕ)	1	0.85	0.74	1	0.80	0.71

Using the induced voltage and the nominal current when I=I_q, as base values the per unit values are found, Table 30. The calculated impedance is 0.84-0.90, which is fairly high for a PM machine. Traditionally it is said that it is close to 0.2 in smaller machines due to the effective air gap, and thus has a very low impact on control strategies etc. But as pole numbers increases, the contribution from the sub harmonic MMF and few large slots, the inductance increases too.

Table 30 Per unit values for the different cases in Table 29 and Fig. 88

	E_{base}= 173 V I_{base}= 102 A Z_{base}= 1.70 Ω			E_{base}= 173 V I_{base}= 108 A Z_{base} = 1.60 Ω		
	cos(ϕ)=0	|E|=|U|	I = I_q	cos(ϕ)=0	|E|=|U|	I = I_q.
U	0.68	1	1.27	0.66	1	1.27
I	0.80	1.12	1	0.74	1.12	1
R	0.056			0.106		
X	0.844			0.897		
Z	0.846			0.904		

4.2.8 Air gap forces

Using the flux density in the air gap the forces between the rotor and stator can be evaluated. It is presented an evaluation of the torque as function of position, both with locked rotor and rotating rotor with constant current. It is also presented an evaluation of the no load

flux density in the air gap to get an impression on radial and tangential forces with an unloaded machine.

The force and torque are found using Maxwell's stress tensors with a FEA tool. The result is dependent of the resolution (mesh) of the model. The number of nodes per pole must be high enough. It is also an issue that in each node the values are in the order of 10^5-10^6 while the result of the integration is in the order of 10^2. The FEA model used has been of the entire cross section, hence have there been some limitation on the mesh. For this calculation there are about 9000 nodes around the air gap, giving a resolution of 78 nodes per pole or 0.57mm per node. The result must therefore be treated with some caution being aware of the chance for numerical errors.

4.2.8.a No load air gap forces

The no load flux density in the air gap is plotted in Fig. 73. Using Maxwell's stress tensor to calculate the force density on each point around the air gap, eq. (74), a plot of the force density in the air gap can be obtained, Fig. 89. The harmonic content of the force is shown in Fig. 90. Summing up the radial force around the air gap the result is zero.

From the harmonic content of the forces densities calculated at t=0 (magnet directly beneath centre slot of phase A) it can be seen that the most prominent harmonic of the radial force equals the pole number (116). There is a significant sub harmonic (No. 4) that corresponds to the difference in poles and slots. This force rotates fairly fast, 1500rpm, corresponding to a 4 pole machine, eq. (77), and might induce vibrations in the stator of mode 4 (Fig. 39)

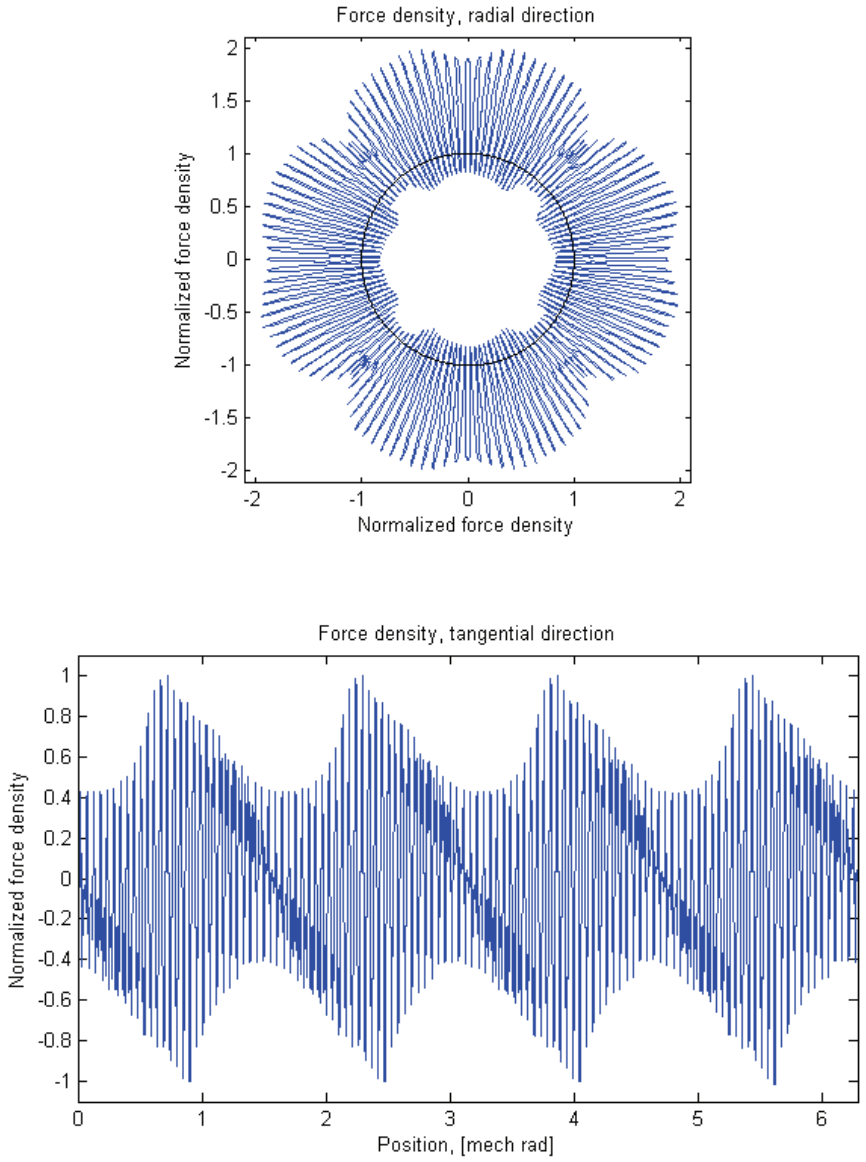

Fig. 89 Plot of the calculated air gap force density (t=0) at no load; Top the force density in radial direction plotted around the unity circle, bottom the tangential force density plottet as a function of posistion.

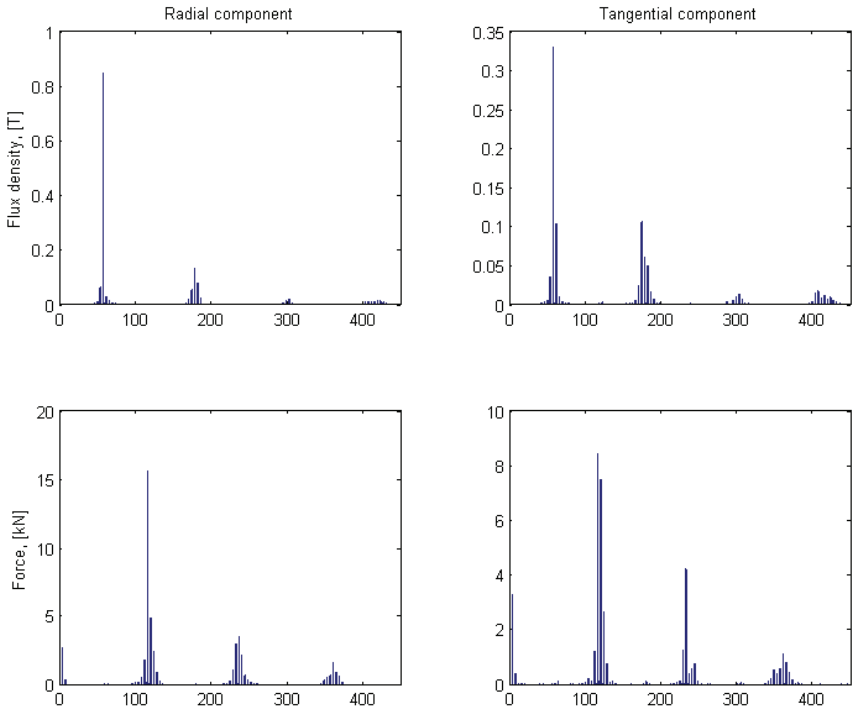

Fig. 90 Harmonic content for the flux density (top) and force (bottom), the radial component to the left, the tangential to the right, t=0

Integrating the force density in tangential direction over the air gap for different position of the rotor a plot of the torque as function of position can be obtained. The tangential torque is presented in Fig. 91, assuming lossless components. The result shows a ripple with amplitude of 109Nm, around 1.2% of the nominal torque (9.2kN). The frequency equals the tooth number, 51.7Hz. There is also an offset in the calculations of 23Nm.

Integrating the force density in radial direction a curve of the radial pull (mode 0 in Fig. 39) between stator and rotor can be made, Fig. 92. It shows that the stator and rotor pulls on each other with a force of 122kN/m^2, corresponding to pressure of 122kPa or 1.2bar. It also shows that there is a variation of this pressure of 95Pa with a frequency of 104Hz.

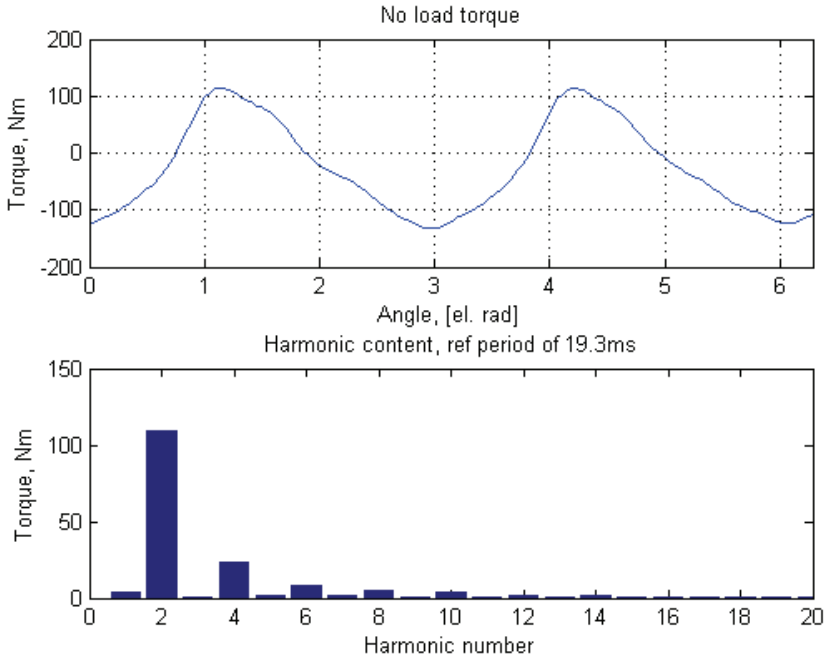

Fig. 91 Torque (tangential) as function of position and its harmonics

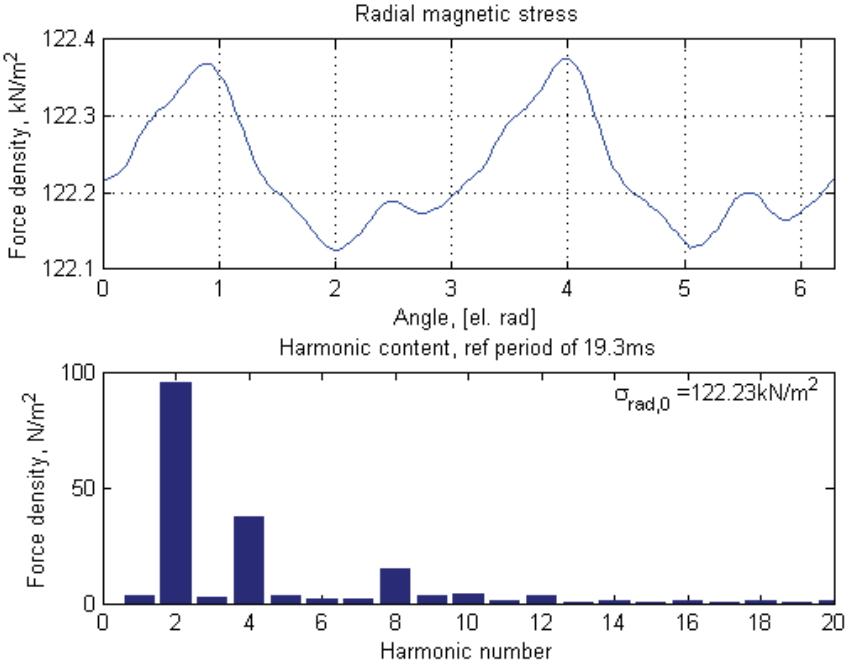

Fig. 92 Force density in radial direction, magnetic stress or magnetic pressure

4.2.8.b Torque as function of I_q

A calculation of the torque in the air gap as function of I_q is presented in Fig. 93. It is shown a much wider current span than is appropriate for the machine to show how the torque develops when saturation occurs. The torque is calculated using Maxwell's equation (73) on a boundary in the centre of the air gap. The FEA calculation shows that a current of 96A is sufficient to reach the required torque, assuming no losses. Including the resistive losses from Table 28, corresponding to 590Nm at 51.7rpm a total of 9.82kNm in the air gap is needed to get the nominal torque at the terminals. This corresponds to an rms current of 102A which is the same as the calculated operating point in Table 29 (96,2mΩ, $I=I_q$).

Regarding the shape of the torque curve it is fairly linear up to I_{amp}=200A with a gradient of 68.2Nm/A. This shows that the torque/current relationship is linear within the nominal conditions and that the magnetic saturation is not a problem. At around I_{amp}=200A the saturation effects starts to get noticeable, changing the torque production of the machine. At 3-400A a new gradient of 53.1Nm/A can be found. At the end of the curve the gradient increases again to 58.4Nm/A, in this area the machine is far into saturation, close to 4T in the highest loaded teeth, and the parameters for the FEA model of the magnetic circuit might not be well defined.

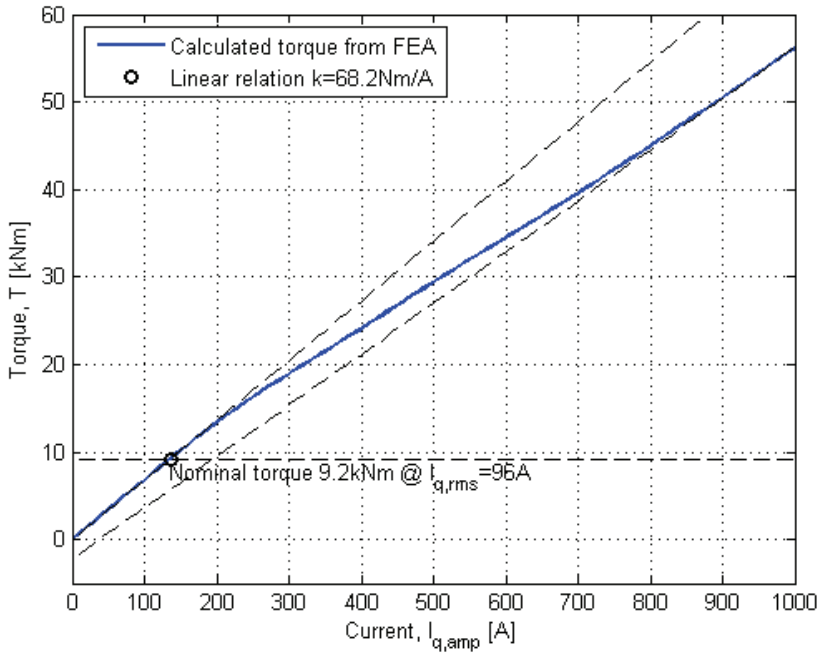

Fig. 93 Calculated torque as a function of $I_{q,amp}$, 100A corresponds to a current loading ac=33kA/m

4.2.9 Loss calculations

The losses evaluated here are the copper losses, iron losses in stator iron and magnet losses in the rotor. The losses are found for the no load flux, the flux from the MMF (magnets turned off) and loaded losses (current and magnets on). The losses are summed up in Table 32. The calculation with load assumes a current of 102A in the q-axis.

To calculate the stator losses, data of the specific loss at different flux densities and frequencies from the manufacturer of the lamination is used (appendix C-4,[107]). The stator lamination is assumed loss less during the FEA calculation, the harmonic content of radial and tangential component are then found for each points in the FEA, using a lookup table with amplitude and frequency as input the losses for each point is found (loss density). Integrating the loss density over the volume the total stator loss can calculated.

The rotor losses are calculated using transient 2D FEA. The calculation assumes an infinite long machine, not including end effects. The method needs some time steps to converge, and since the entire cross section is used for the calculation, a crude mesh is used to keep the size of the model within the PC's limits. The material parameters used are presented in appendix C.

4.2.9.a Copper loss

The copper losses are dependent of the load current and given by eq. (68). The result is shown in Table 29. It is assumed a current of 102A, a winding temperature of 115C and a resistance per phase of 96.2mΩ (Table 29), giving a copper loss of 3.0kW, 170mOhm yields 5.3kW.

4.2.9.b No load losses

Stator losses

Based on data from the supplier of stator lamination the core losses can be estimated. The flux density in two teeth, one straight one tapered, is evaluated, and the amplitude and frequency of the change in flux density are used to calculate losses. In Fig. 94 the calculated loss distribution is presented. It is found by using the flux density and frequency for the different harmonics (up to the 15^{th}) and a look up table from the supplier of the electric lamination. It can be seen that at the corners and tooth tip the loss is fairly high, but small areas. The loss in the straight tooth is close to 1.7W/kg, while the tapered tooth has an average of almost 1W/kg. When summing up the losses it is found that the two teeth have an average loss per kg of 0.94W/kg giving a total of 264W for the stator.

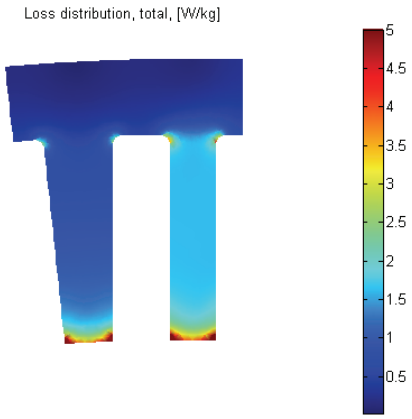

Fig. 94 Loss distribution in a part of the stator, peak in tooth tip about 10W/kg

Rotor losses

In Fig. 95 a plot of the change in magnet at three different places is shown; upper left corner, centre of the surface and in the middle of the magnet. All three points shows relative large change in flux, especially at the surface. The conductivity of the magnet is set to $6.25 \cdot 10^6$S/m. The iron yoke has a conductivity of $6.7 \cdot 10^6 \Omega$m. With a μ_r of around 1000 the skin depth of the iron yoke is much smaller than the shortest dimension in the cross section.

The no load losses in the rotor is found by integrating resistive losses in the rotor. The relative permeability of magnet is 1.05 and the curve from C-1 is used for the iron yoke. The losses in the magnets are found to be 377W, while the rotor loss is 66W. The losses are the mean of the last part of the calculated time, where the curve has converged. The lower plot in Fig. 96 shows variation in calculated losses, corresponding to the slot number. In Fig. 97 the induced current is shown, where one can see that the largest currents are induced directly under the magnets.

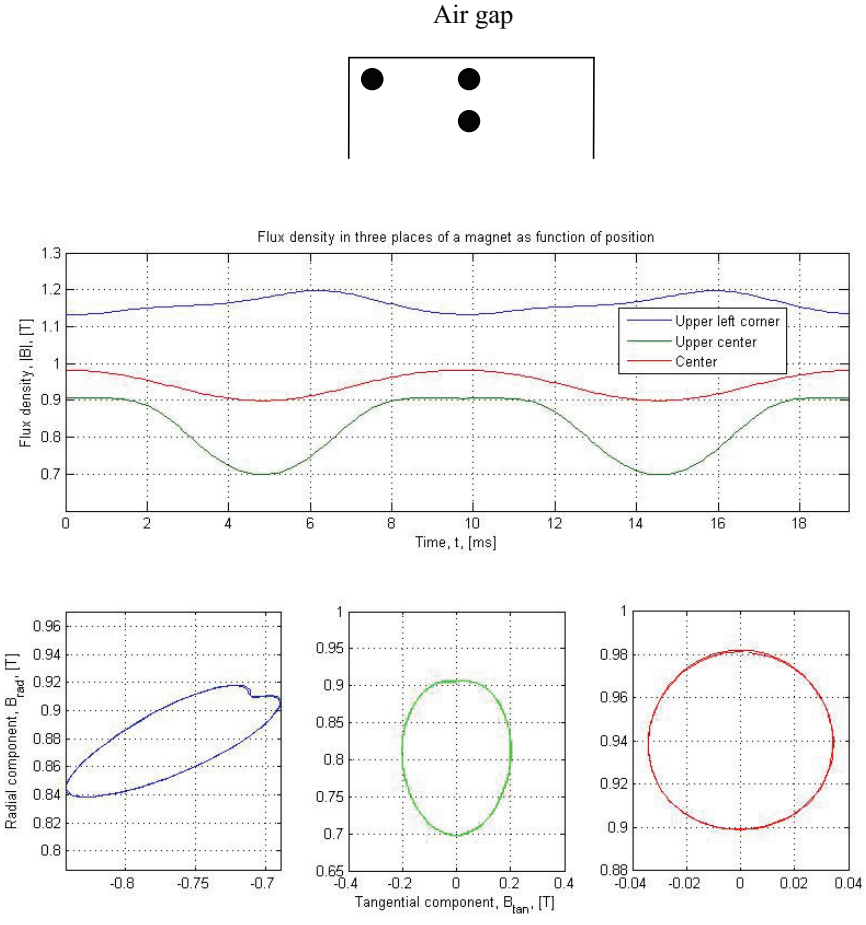

Fig. 95 Flux density in a magnet at three different positions

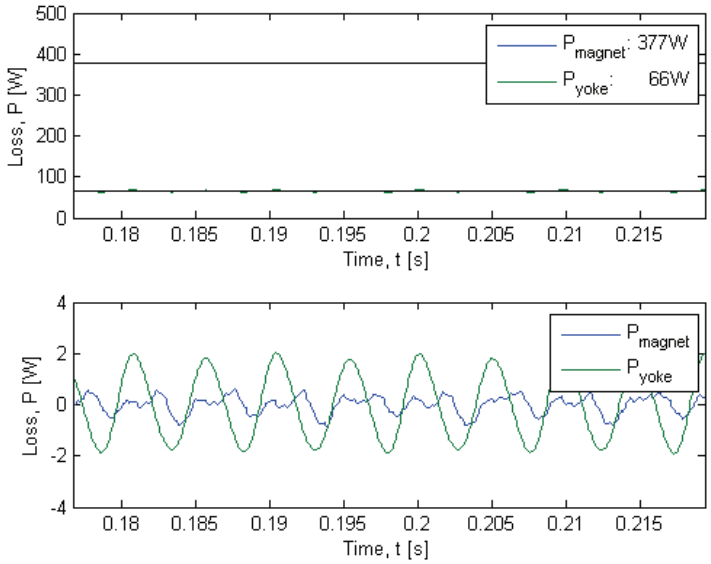

Fig. 96 Induced losses in rotor yoke and magnets, top the mean value, bottom, the time variation

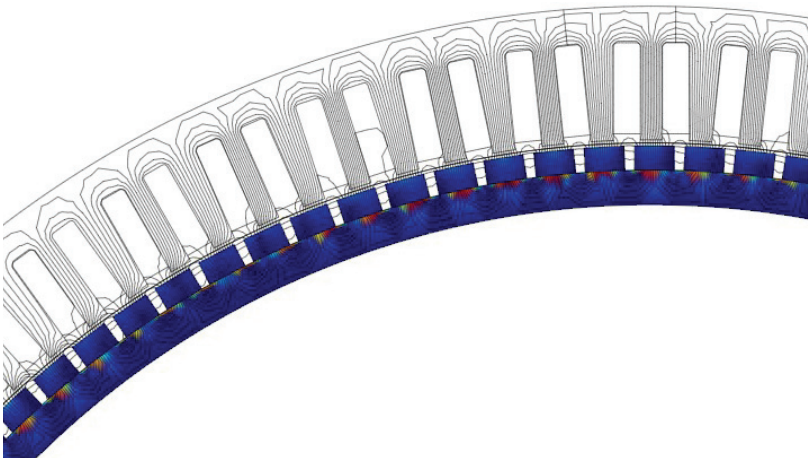

Fig. 97 Induced currents in rotor, 1.5A/mm2 in rotor yoke beneath magnets

4.2.9.c Losses from MMF

A calculation without magnetization in magnets and with currents in rotor is performed to investigate the effect from the load current.

Stator losses

The loss in stator from the MMF is found from FEA using 102A sinusoidal current. The losses are evaluated using similar method as for the no load losses in stator. The result is presented in Fig. 98. It is found that the significant losses are caused by the first harmonic while the third harmonic contributes some and the higher only cause loss in the corners of the slot. The losses density is highest in the corners and at the base of the straight tooth, where the flux density is the highest. The stator losses from the MMF add up to 150W.

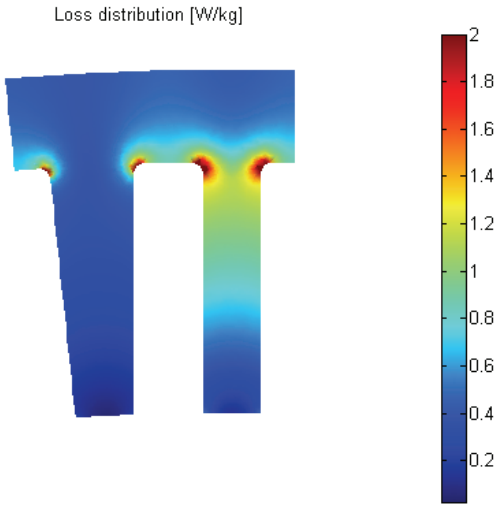

Fig. 98 Loss distribution in stator from MMF

Rotor losses from MMF

With reference to the comparison of loss from MMF for the one and two layer winding in Fig. 77 it is of interest to compare the estimate using the air gap flux density and an analytic approach with the built in loss calculation in the FEA tool. The calculated losses are presented in Table 31.

Using the radial component of the air gap flux density from the FEA model (Fig. 80) the harmonic components of the flux in the rotor can be calculated using the equations in chapter 2.6.4.c. There are leakage fluxes, especially for the higher harmonics, that don't enter the rotor, but are included in the loss calculation due to the method. But as the results show, it is the lower harmonics that dominates the losses, and the higher harmonics are insignificant. The speed and direction of each harmonic component relative to the rotor is found using eq. (41) and eq. (45). The calculated speeds are presented in Fig. 99.

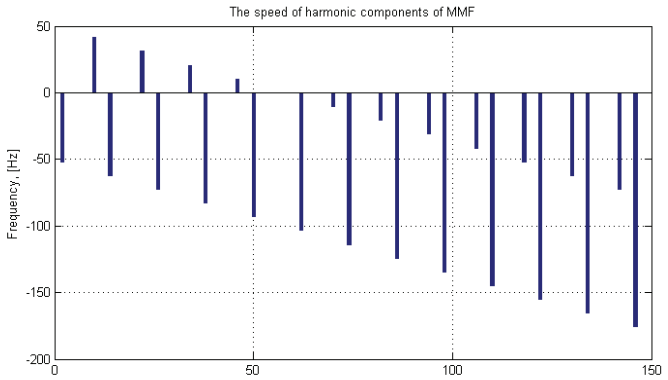

Fig. 99 The speed of the different harmonic components of the MMF relative to the rotor

The flux and flux density in the magnets are the same as in the air gap, eq. (101). The flux in the rotor yoke is calculated from the average value of the flux density over an area of the air gap depending on the harmonic number, (100), resulting in a flux density in the yoke given by the yoke thickness (102).

$$\Phi_i = \frac{2}{\pi} \cdot B_{rg,i} \cdot \frac{L \cdot \pi \cdot D_g}{2 \cdot i} \tag{100}$$

$$B_{m,i} = B_{rg,i} \tag{101}$$

$$B_{y,i} = \frac{\Phi_i}{2 \cdot L \cdot d_{ry}} \tag{102}$$

The skin depth for the magnet is for all relevant harmonics larger than half the pole width, eq. (70). In the upper left part of Fig. 100 the harmonic components of the flux density in radial direction is presented (same as Fig. 80), below is the losses connected with each harmonic component. Of the higher harmonics not shown in the figure, only harmonics around the 300th contributes to the losses. The loss in the magnets adds up to about 175W.

For the rotor yoke the skin dept is smaller than the yoke thickness, eq. (71) is therefore used. A permeability of 1000 is used for the iron. The result is presented in the right part of Fig. 100. Due to wide pole and high frequency (51.7Hz) the 2nd harmonic creates significant losses. The 62nd harmonic also contributes, rotating against the rotor at twice its frequency (relative to the rotor), with an amplitude of the flux density close to the N_{pp}. It can of course be discussed whether the component will penetrated the yoke. The losses in the rotor yoke add up to about 466W.

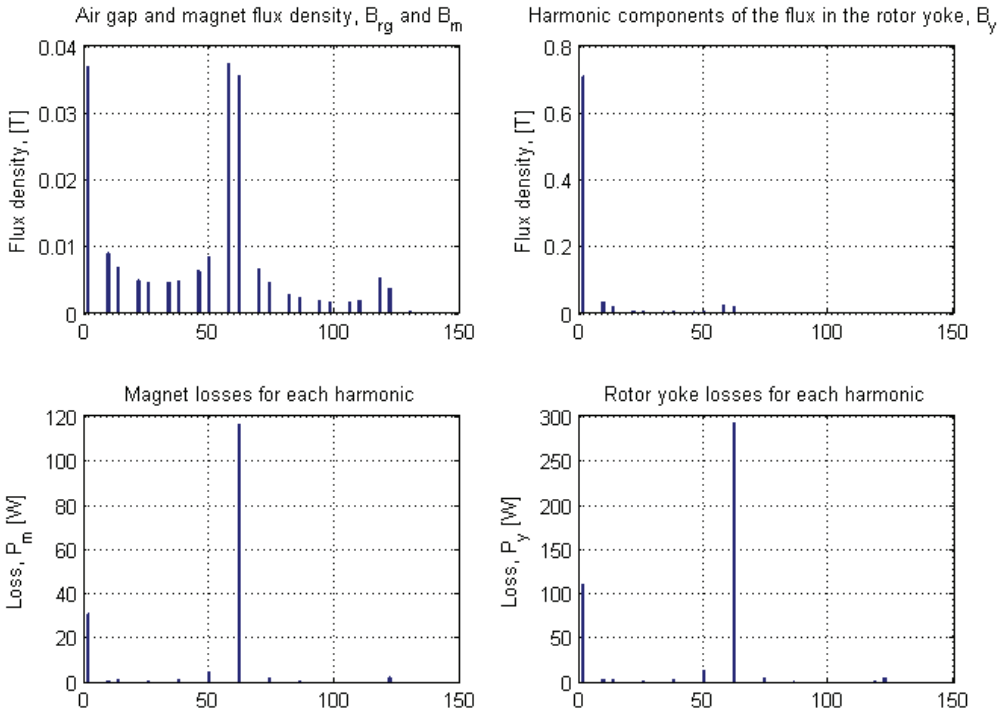

Fig. 100 Harmonic components of flux densities and loss in magnets and rotor yoke

Using FEA the losses are found to be 431W in the magnets and 115W in the yoke, Fig. 101. The upper shows the total loss, while the lower shows the variation depending on position. In difference to Fig. 96 the variation corresponds to the electric period of 20ms. In the FEA model the rotor is rotating at nominal speed. A figure from the FEA showing the current densities is presented in Fig. 102.

Comparing the analytic estimate with the FEA the sums are in the same area. The analytic estimate does not take into account the effect of the eddy currents on the flux, and assumes that all magnetic flux passing the centre of the air gap also enters the rotor and is thus larger. The analytical estimate calculates too low magnet losses, too high yoke losses. The result is shown in Table 31. The same conductivity is used for both calculations, while for the FEA a nonlinear permeability is used.

Table 31 Comparison of the two different MMF loss calculations

	Magnet loss [W]	Rotor yoke loss [W]	Sum [W]
Air gap flux	175	467	642
FEA	431	115	546

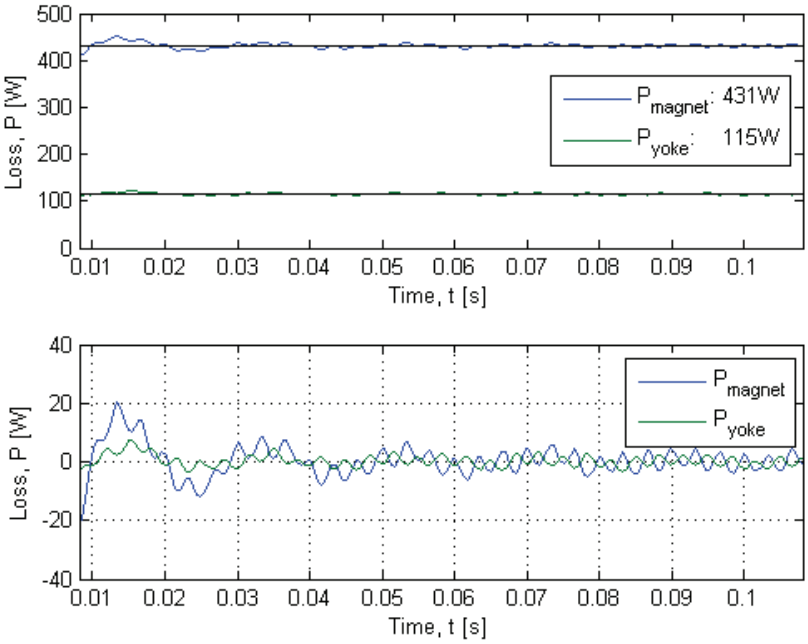

Fig. 101 Rotor losses from MMF, FEA calculation

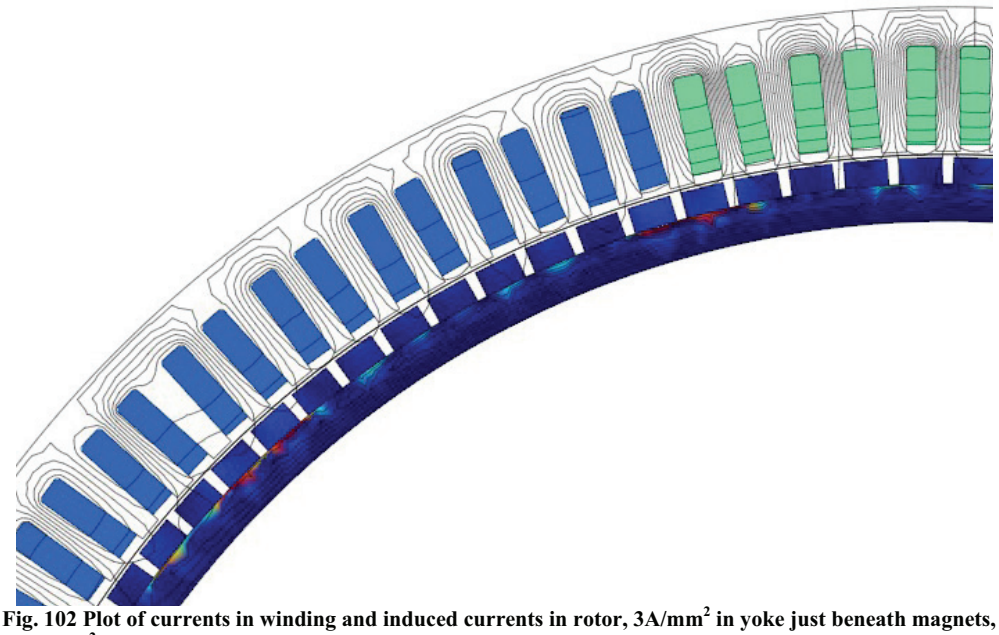

Fig. 102 Plot of currents in winding and induced currents in rotor, 3A/mm^2 in yoke just beneath magnets, 1.4A/mm^2 in green slots

4.2.9.d Losses with loaded machine

The losses with loaded machine are calculated with a current of 102A in the q-axis. The rotor losses are calculated using FEA directly, while the stator losses are found from the flux density and a look up table (Table 47). The calculated rotor losses are depending of position and vary over time and it is the mean value over a several periods that are presented. A plot of the current densities in the rotor is shown in Fig. 104, while the loss distribution in the stator is shown in Fig. 103. The loss in the stator adds up to 340W. The loss in the magnets is 700W and for the yoke 167W, a plot of the loss calculation from the FEA is shown in Fig. 105.

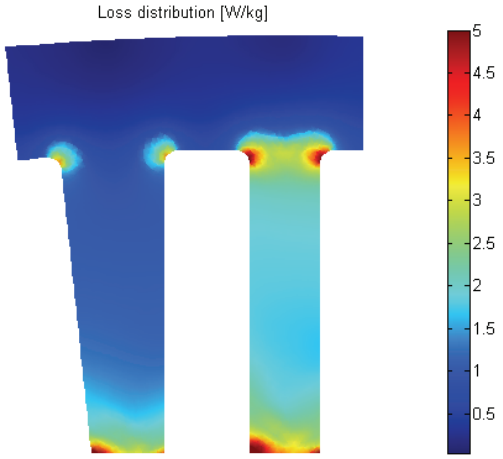

Fig. 103 Loss distribution in stator, peak in corner is 15 W/kg

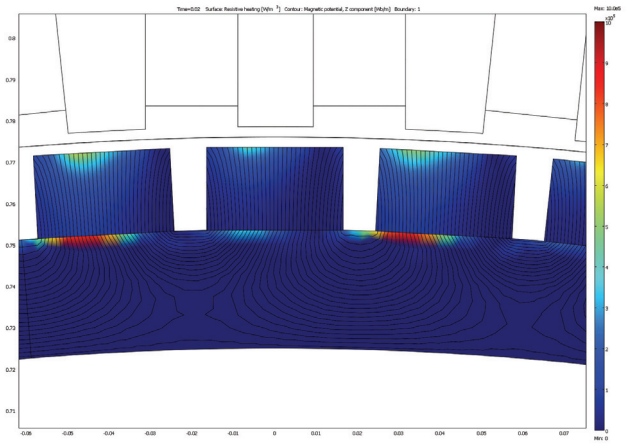

Fig. 104 Plot of flux lines and resistive losses in rotor at full load at one instant (not average)

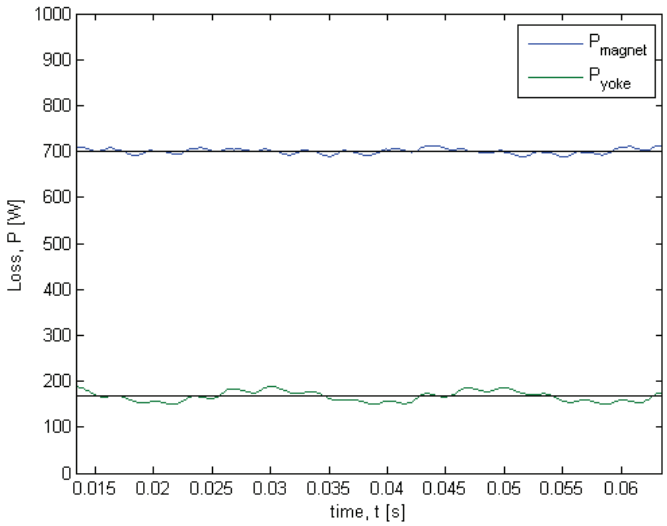

Fig. 105 Magnet and rotor yoke loss as function of time

4.2.9.e Summary of loss calculation

The calculated losses are presented in Table 32. The no load losses are calculated to be around 700W, 1.4% of the dimensioning power. The losses from the MMF are calculated with the rotor at nominal speed and Br=0. The dominating losses are the copper losses, while the losses caused by the magnetic field from the MMF are much lower, they are in the same area as the no load magnetic losses; around 700W. Due to the size of the model a relatively crude mesh (2mm) have been used for the eddy currents in the rotor, reducing the accuracy. Recommendation for the mesh is that it should not be larger than half or one third of the skin depth in question. This is mainly an issue for the rotor yoke with its relatively high permeability.

The calculation of the loaded condition is not the sum of the MMF and no load case. The difference can of course be a result of the different methods of calculating the losses (and

flux densities). But it is also a result of the flux picture is changing when loading, both regarding amplitude and harmonic content, saturation effects, and that the losses proportional to the square of the flux density.

In the last column the efficiency is presented, not including losses such as bearings, windage and stray losses, eq. (72). For a PM-machine this is fairly low efficiency, but it is in the same range as the induction machine in the test set up of 89%. The main contribution is the copper losses. The machine is originally designed to be stressed regarding copper losses (92.3% efficiency), but with the issues presented later with the parallel conductors working as a solid bar the efficiency is reduced further.

Table 32 Summary of losses

	Current	Magnetic field				Efficiency
	$P_{Winding}$ [W]	P_{magnet} [W]	$P_{rotor\ yoke}$ [W]	$P_{stator\ core}$ [W]	P_{total} [kW]	P_n = 50kW [%]
MMF	3000 5300	431	115	150	3.7 6.0	- -
No load	-	376	66	264	0.7	-
Loaded	3000 5300	700	167	340	4.2 6.5	92.3 88.5
% of Pn	6.0 10.6	1.4	0.3	0.7	8.4 13.0	

4.3 Building of the PM-generator and test jig

The machine was built according to the design presented in the previous chapter. In addition to the PM-machine a large jig had to be constructed to place induction machine, gear PM-machine, instrumentation, connections and cabling. The production drawings were made by Inventas AS, the production of the different mechanical parts by Delprodukter AS. SmartMotor AS took part in the initial phase of the generator design. The stator was manufactured by Coates Heimdal AS. The assembly of the jig and mounting of the magnets was done at the university by the workshop at the department of Electric Power Engineering.

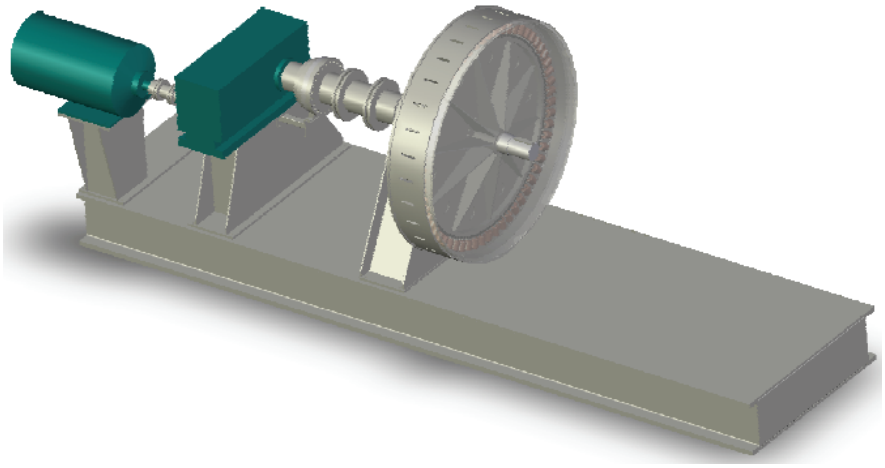

Fig. 106 3D model of the test jig from Inventas

In Fig. 108 to Fig. 113 some pictures from the building process is presented. Building this machine was very informative regarding the process of designing and construction an electric machines. The starting point for the test jig is the design of the active part of the generator, which is only a ring 100mm long, outer diameter of 1777mm and a thickness of 165mm. During the design of the mechanical structure this grew to a jig 6,5m long, 2m wide (outer stator house) and over 2,5m high, weighing 8 tons.

In addition to the test jig the infrastructure in the laboratory were updated to supply the machines both with power and also measurement and control. New converters were designed with a power level of about 130kVA. A test setup including a 50kW induction machines for system testing of induction generators was included. A solar wall, fuel cell and other renewable sources are connected to the laboratory. From the start this was an initiative taken to strengthen the research on low speed high torque machines, but as more people found it interesting more components and functionality were put in and the project is now fronted as a laboratory for new renewable energy [108].

4.3.1 The fundament

The fundament is designed to ensure mechanical stability and strength for the rotating machinery. The fundament is designed both for the existing machine, but also to make place for a second machine directly connected with the first, thus the slightly over dimensioned length. The mechanical construction included an analysis of the structure for vibrations, Fig. 107. Important lessons of strength, machining, tolerances, size and costs were learned. The parts were assembled and the surfaces painted at the workshop.

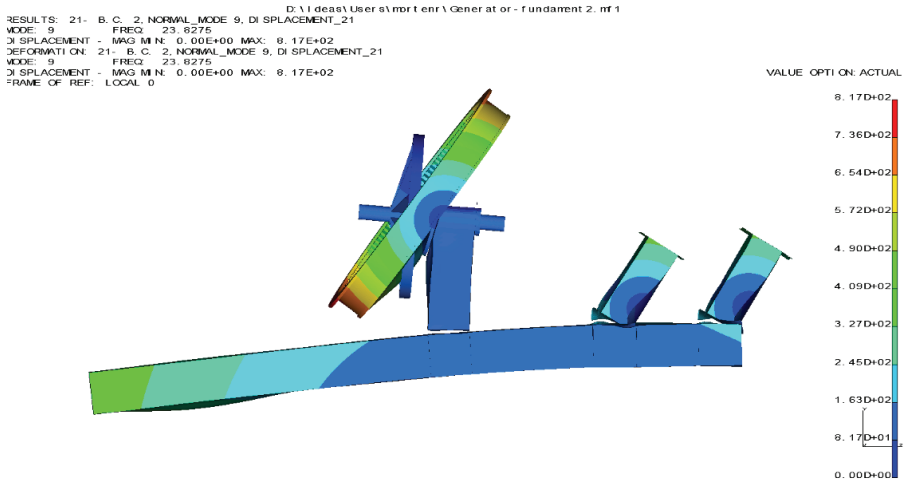

Fig. 107 Example from the structural analysis performed by Inventas AS

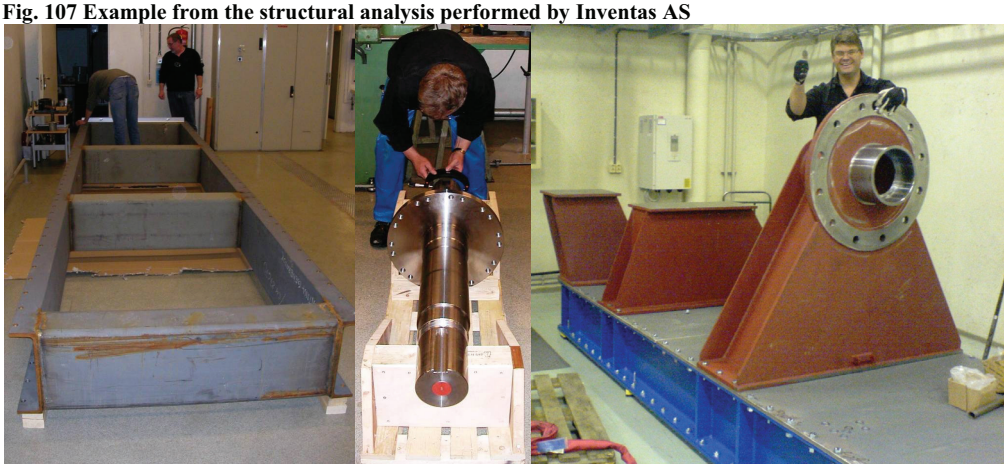

Fig. 108 From left: The frame of the jig, the shaft and fundament with brackets for induction machine, gear and PM-machine

4.3.2 Stator and windings

The stator lamination is laser cut in sections of 60 degrees; they are stacked and welded before the stator lamination was placed in the house. The sheets at both ends of the stator are thicker, 1mm, than the rest to make sure the lamination stack don't spread out at the teeth more than necessary. The coils are wound on moulds in sections of 5, corresponding to number of coils pr phase pr part (F_2), they each have 19 turns, and consists of 36 parallel round conductors of Ø1.2mm. It is used 2 layers of slot insulation (0.5mm thick), due to the possibility of rectifying (active/passive). The stator is lacquered after the coils are mounted. All the conductors from the winding are lead to a terminal box where the sections are connected together. This is done to make sure the maximum flexibility and to keep all different options regarding connections open (parallel, serial, delta, star etc. Fig. 18).

Fig. 109 The coils are wound five and five in series, making up one section

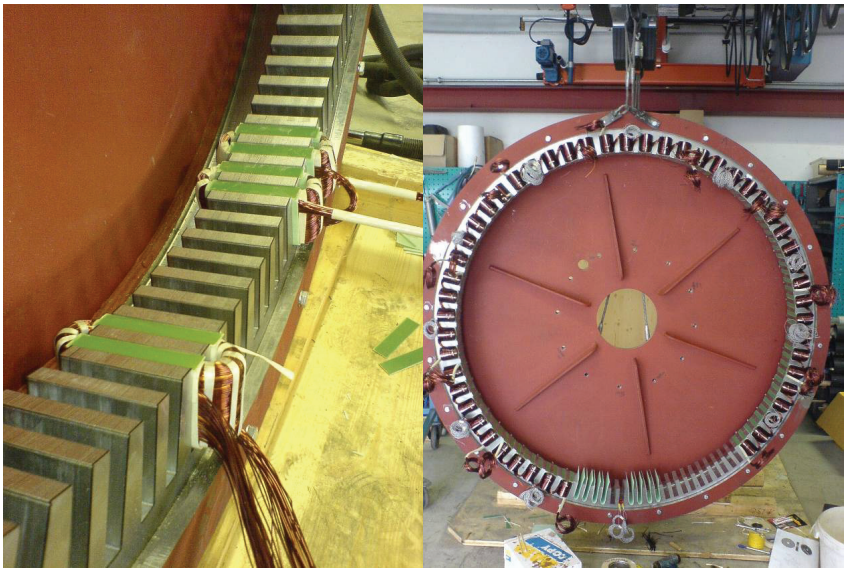

Fig. 110 The stator lamination and coils. To the left is some test coils, and to the right is the almost finished wound stator

4.3.3 Rotor and magnets

A challenge with the rotor was the tolerances regarding the positioning of the magnets, both radial and tangential. The rotor has a diameter of 1507mm, and the accuracy demanded is 0.05mm, while the tangential accuracy is 0.1mm. This is relatively small tolerances for such a diameter, but well within what is possible. Each pole consist of one magnet 100mm long, 33mm wide and 20mm high (L, w_m, l_m). The magnets are all equal. The magnets are glued, manually, to the rotor. The rotor, including the magnets, was painted.

Fig. 111 The mounting of the magnets and painted rotor

4.3.4 Final assembly

The shaft was intentionally made long to make sure that the rotor was centred before the magnets started pulling on the stator when mounting. A set of bolts (tierce) was used both to pull the rotor towards the flange on the shaft, and to prevent the rotor to move too fast. The rotor is secured with 20 bolts to the shaft. An eccentric bolt is used to move the centre of stator relative to the centre of the rotor (concentric).

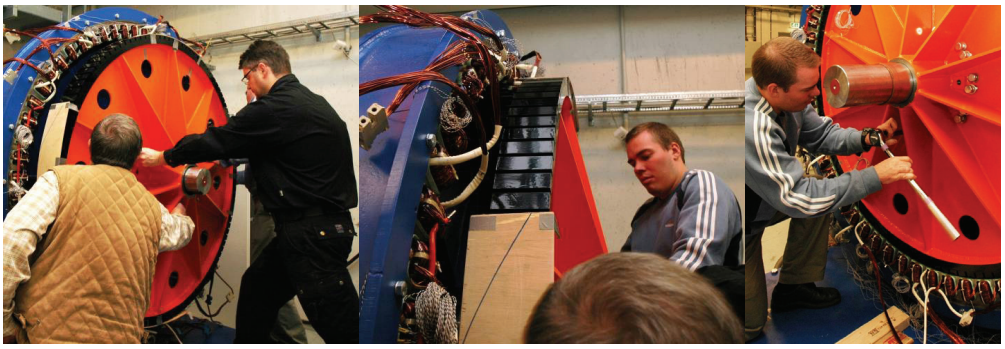

Fig. 112 Mounting of the rotor

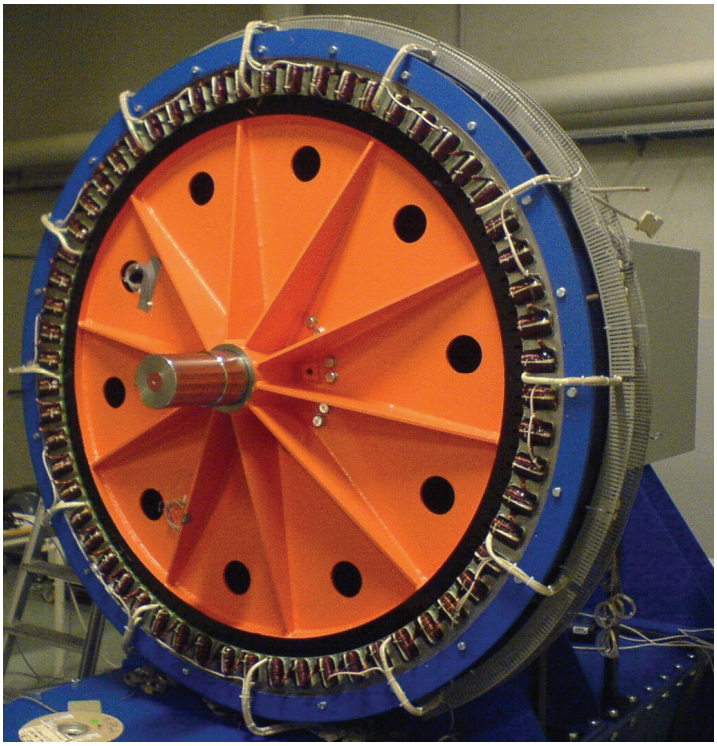

Fig. 113 The (almost) finished PM-generator

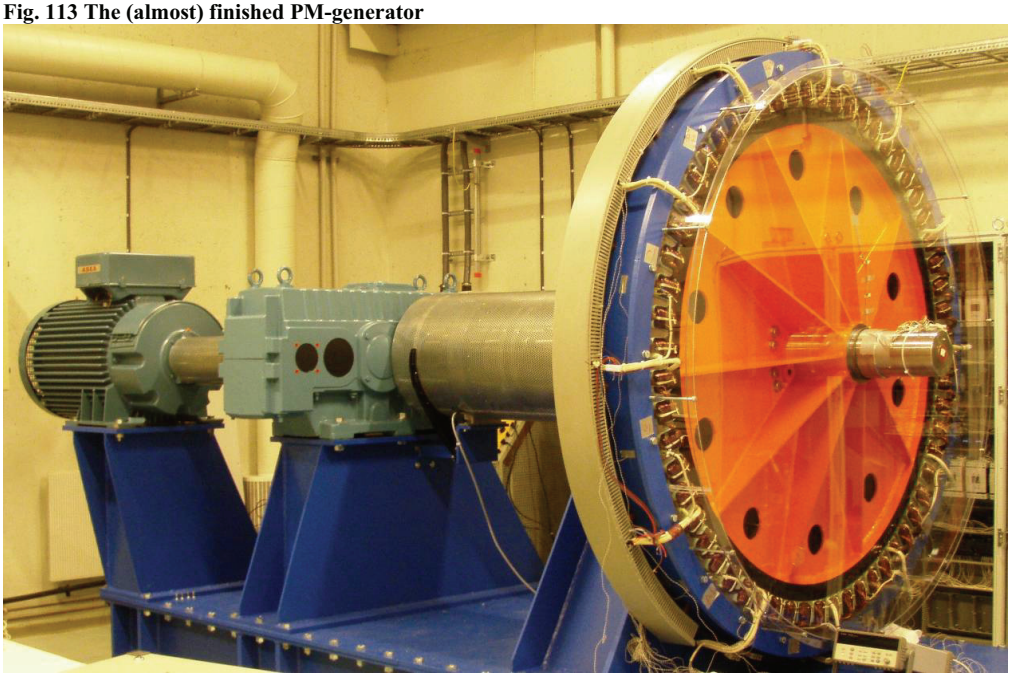

Fig. 114 The test setup

4.4 Testing of the PM-generator

The generator is tested to find the induced voltage, resistance, inductance and losses. Special care during testing is given the proximity effect and eddy currents in the winding since initial tests revealed a high AC-factor. A schematic of the setup for the no load and load testing is shown in Fig. 115. The measurements of the resistance and inductance of the winding was done without the rotor inserted, Fig. 123, thus not including the effect of the sub harmonic MMF. This is taken into account when fitting the parameters to the measured load curve.

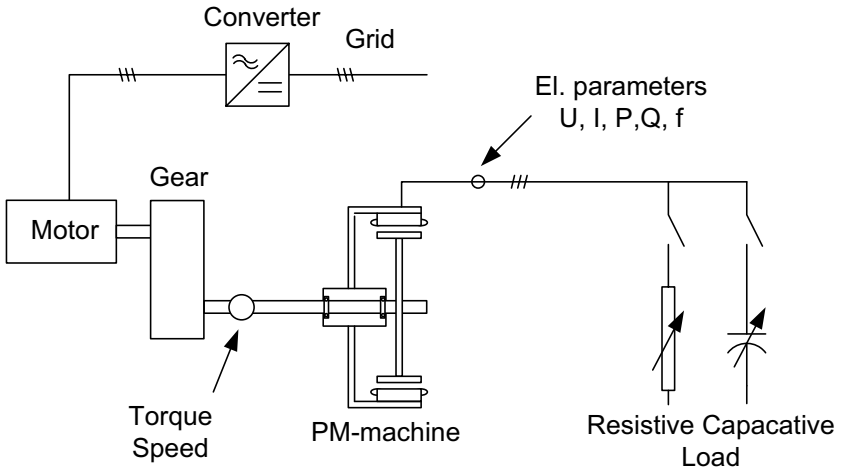

Fig. 115 Schematic of test setup for no load and load tests of PM-generator

4.4.1 Induced Voltage

The induced voltage is measured while rotating the rotor at nominal speed, 51.7rpm. The voltage was measured per tooth, per section with 5 coils in series, phase and line voltage with all four sections in series. The result yields a good overview of the voltage, the winding factor and consequence of the concentricity of rotor relative to the stator.

4.4.1.a Induced voltage per tooth

The induced voltage in the tooth tip, the tooth bottom and in the core were measured to verify that the voltage per turn has a low harmonic content and to find how much flux is leaking from the tip to the bottom of the tooth.

From Fig. 117 it can be seen that the induced voltage per tooth has low harmonic content. It can also be seen that there is a slight difference in voltage from top to bottom of (1.2mV=0.25%). The core voltage should be half the voltage at the bottom of the slot, and be in phase with the tooth voltage. But it is slightly lower (1%) and lagging 5degrees behind the other two. This can be a measuring inaccuracy; it can also indicate that the flux lines goes from one pole to the next but skipping some poles enclosing several poles. This effect is not examined further.

The tooth voltage is also measured over a full revolution to check if the rotor is circular and that the magnets are distributed equally around the rotor, Fig. 118. It is found that there is a variation of the frequency of 1%. The variation of induced voltage is only 5.4mV. The frequency variation corresponds to 0.33mm variation in magnet position (tangentially), but it can probably be explained also by the fact that there are some oscillations, or vibration, in the

drive system, excited by cogging in the PM-generator, teeth in the gear and/or harmonics in the induction machine. The variation of voltage can also be caused by varying magnet properties. The measurement of tooth voltage can be used the control how the parameter changes with time to see if there are any reduction or changes in performance.

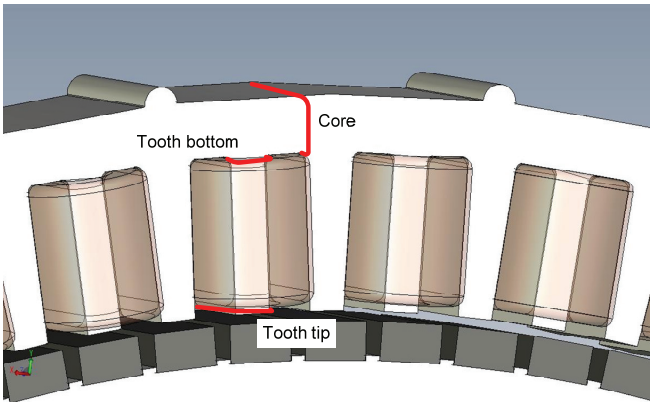

Fig. 116 Posistion of coils for measuring tooth and core voltages

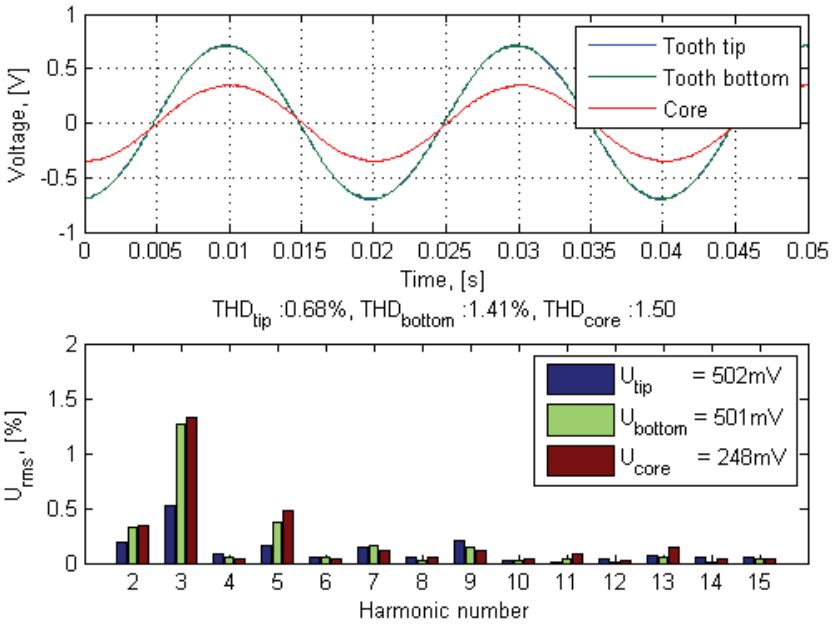

Fig. 117 Voltage shape for the induced voltage in tooth and core and the 15 first harmonics

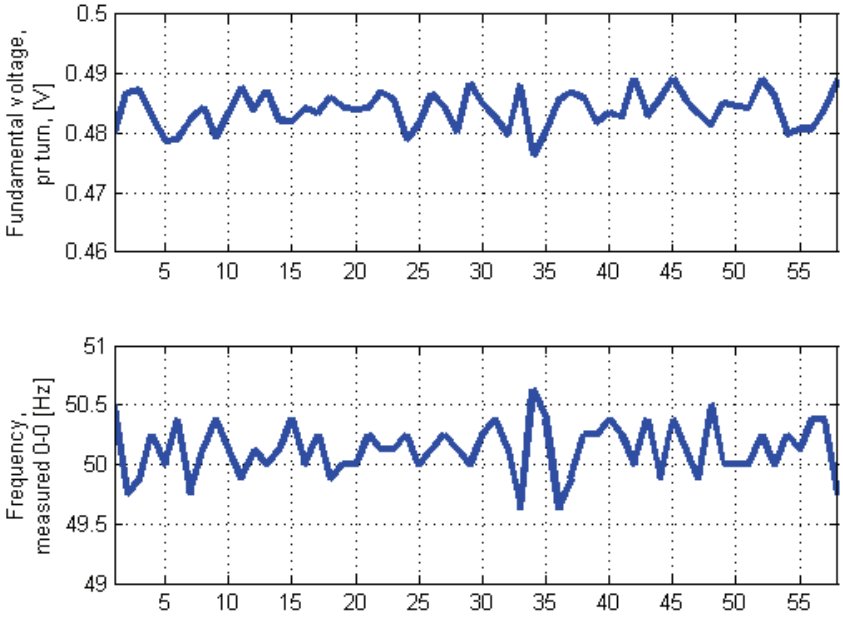

Fig. 118 Amplitude of fundamental and frequency for one revolution with an average speed of 50.15Hz

4.4.1.b Induced voltage per part

The no load voltage for each part are measured and the fundamental and harmonic content found. In Fig. 119 the fundamental and harmonic content is shown. The THD is low. It can be seen that there is difference between parts in the induced voltage. In Fig. 120, left, the distribution is shown relative to the mechanical position of the machine. The average induced voltage at 50Hz is 44.9V and the maximum deviation from the average is 3.3% (U_{C2}). The machine is not entirely centred; the rotor is a little closer to C2.

Adjusting the rotor 0.5mm towards B4/C4 an indication of the sensitivity of eccentricity can be found (Fig. 120, right). The deviation from the mean value then increases to 7.3%. The rotor is now closest to B4. Since the phases are equally distributed around the machine, and all are connected in series, the phase voltages (A, B, C), are fairy equal even though each part differs in value. But if connected in parallel this would result in circulating currents between the parts, increasing the losses. The consequence of differences in induced current in parallel paths is not further examined. In [109] some views on how to use the difference in parallel paths to reduce the magnetic pull in the air gap is presented.

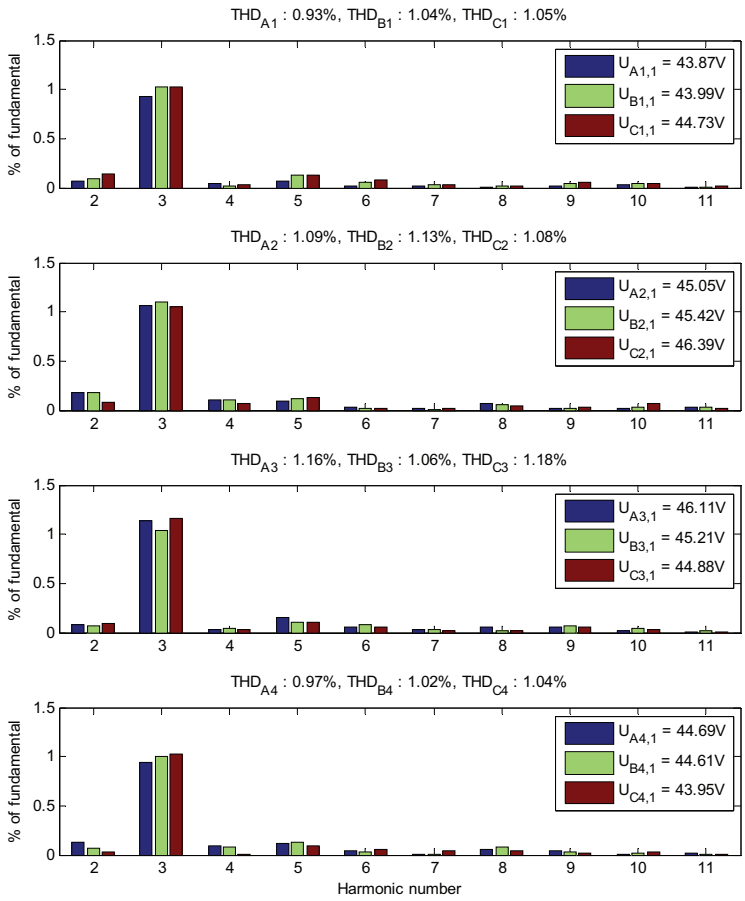

Fig. 119 The fundamental value and harmonic content of the no load voltage for each part

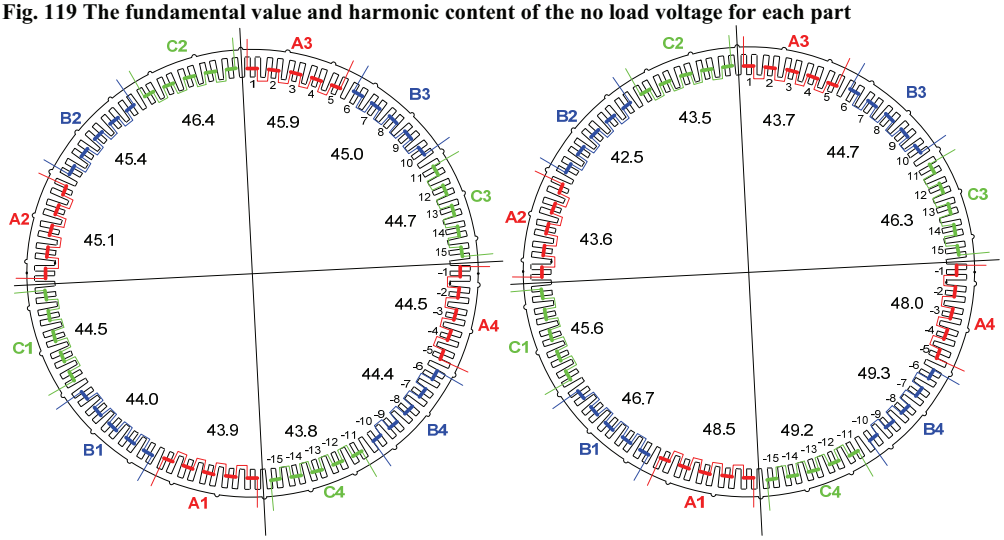

Fig. 120 Fundamental voltage distribution in the machine, measured over each part, left posistion 1, right moved 0.5mm towards B4

4.4.1.c Induced phase and line voltage

All parts in each phase are connected in series and the voltage between phase and neutral measured. In Fig. 121 the fundamental and harmonic content of the phase (top) and line (bottom) voltage is shown. There is still some difference between the fundamental phase voltages, but only 0.5% for the phase voltage 0.3% for the line voltage from the average. The THD is down to about 0.65% for the phase voltage, and that is mainly 3rd harmonics. And as expected the THD for the line voltage is lower, and down to 0.25%.

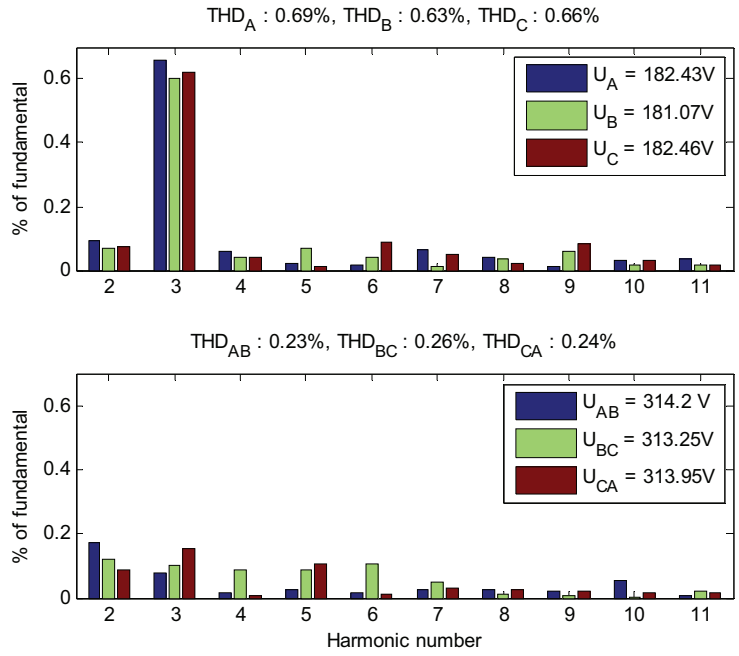

Fig. 121 Harmonic content of the phase voltage (top) and line voltage (bottom)

4.4.1.d Comparison of measured no load voltages, winding factor

A comparison of the measured induced voltages showing the fundamental values at 50Hz are presented in Table 33. Using the measured values and comparing it with the tooth voltage multiplied with the appropriate number of series connected turns the distribution factor can be found and compared with the theoretical value of 0.956. The chording factor is already included in the tooth voltage. It can be seen that the distribution factor for the section is a bit lower than the theoretical, while the phase voltage coincides fairly well. The difference in measured and theoretical distribution factor is caused by the eccentricity and the difference in induced voltage per part. Due to the eccentricity the phase angles between coils and part are also influenced. The measurements for the different induced voltages are taken at different times, causing a slight deviation in frequency between measurements. This is compensated for, but there is a possibility that this compensation is not accurate enough.

Table 33 Comparison of measured induced voltages

Comments	Calculated Parameter	[V]	Measured Parameter	[V]	Distribution factor
Distribution factor, k_d	Theoretical				0.956
Induced voltage per tooth	$E_{C1,1}$		$E_{C1,1}$	0.50	
Induced voltage per part	$5 \cdot N \cdot E_{C1,1}$	47.6	E_{C1}	44.7	0.939
			$E_{Sec,mean}$	44.9	0.943
Induced voltage per phase	$4 \cdot 5 \cdot N \cdot E_{C1,1}$	190.3	E_C	182.5	0.958
			$E_{Ph,mean}$	182.0	0.956
Induced voltage per line	$\sqrt{3} \cdot 4 \cdot 5 \cdot N \cdot E_{C1,1}$	329.6	E_{CA}	314.0	0.953
			$E_{Ph,mean}$	313.8	0.952

4.4.2 Resistance and inductance

Based on the initial results showing a high and uneven AC-factor in the winding, there are put some work into mapping the AC resistance. The reason for the high AC-factor is that the parallel conductors are not working as intended reducing the eddy and proximity effect. The rotation, or transposition, of the conductors is incomplete and they keep their relative position throughout each series connected part, thus acting more or less like a solid conductor, 12mm high and 7mm wide. The winding has 19 turns per coil and 36 strands per turn. A schematic of how the coils are wound is shown in Fig. 122.

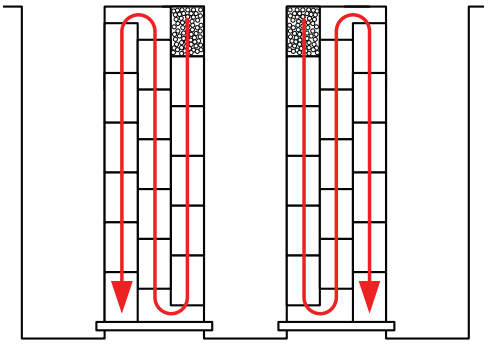

Fig. 122 A schematic of the cros section of a coil

All measurements presented in this chapter is made without rotor, except the one with induced rotating currents at no load, excluding the rotor losses from the resistance and sub harmonic MMF from the inductance. The error is small but not neglectable; rotor loss from MMF adds 700W at 102A, Table 32, corresponding to a resistance of 22mΩ, 23% of the conductive losses. The increase in inductance due to sub harmonic MMF is significant; calculated to 0.6mH, 13% of the inductance, Table 27. This part is included when adapting the parameters to the load curve in chapter 4.4.2.e.

The testing includes measurements of resistance and inductance from active and reactive power, comparing temperature rise for AC and DC currents estimating the AC-factor and a frequency scan of the winding. The investigation of the AC factor includes measurement of resistance and inductance in each parallel conductor for a part, circulating current at no load and current sharing when loaded.

4.4.2.a Resistance and inductance calculated from active and reactive power

The resistance in the generator was measured by applying a voltage and measuring the current both for DC and for 50Hz AC. For the DC test a 30V 100A DC supply was used, while for the AC measurement a three phase variac with 0-400V 150A. The results are presented in Table 34. The DC measurement is performed by applying current through all sections (4x3) in series, measuring the current and voltage drop over each section. The AC measurement is performed with all coils connected in series with the winding connected in a star measuring voltage, current, active and reactive power over each section. The measurements are taken at approximately same temperature, at 80C +/- 3C for both DC and AC resistance. The test setup for the resistance and inductance measurements is shown in Fig. 123.

From Table 34 it can be seen that the DC-resistance for all parts are close to equal, while the AC resistance varies some from part to part. These variations are not equally distributed between the phases, resulting in a lower AC-resistance in phase A than the two other. Since it is used relative thin conductors in the winding the self induced eddy currents is low, therefore it can be assumed that it is the proximity effect that causes the high AC-factor. The measured resistance corresponds well with the calculated values the solid conductor at 80C in Table 26 for phase B and C. The measured resistance for phase A is a little lower. The inductance of the winding and its different parts are fairly equally distributed with equal values.

Table 34 Measured inductance and resistance for DC and for 50Hz AC current both @80C

Part /Phase	$R_{DC,20}$ [mΩ]	$R_{AC,50Hz}$ [mΩ]	k_{AC}	L [mH]
A1	15.05	32.2	2.14	1.09
A2	15.05	30.5	2.03	1.09
A3	14.97	29.6	1.98	1.08
A4	15.02	29.9	1.99	1.09
A	**60.09**	**122.1**	**2.03**	**4.35**
B1	15.20	35.9	2.36	1.09
B2	15.15	33.1	2.18	1.09
B3	15.05	35.0	2.33	1.08
B4	15.24	38.7	2.54	1.10
B	**60.64**	**142.7**	**2.35**	**4.35**
C1	15.26	37.5	2.46	1.09
C2	15.32	37.5	2.45	1.09
C3	15.04	34.7	2.31	1.10
C4	15.24	33.9	2.22	1.10
C	**60.86**	**143.6**	**2.36**	**4.37**

This method, measuring the voltage, currents, active and reactive power, has an issue on the accuracy when measuring on highly inductive loads due to the large angle between current and voltage. A small inaccuracy in percentage of the angle results in relatively large error in calculated resistance. Power is in the area of 700W, while the apparent power is around 7700VA, giving a phase angle of 85 degrees. The ±3C difference is not compensated for, leaving a possible thermal coefficient error in the order of 0.99 to 1.01, +/-1%.

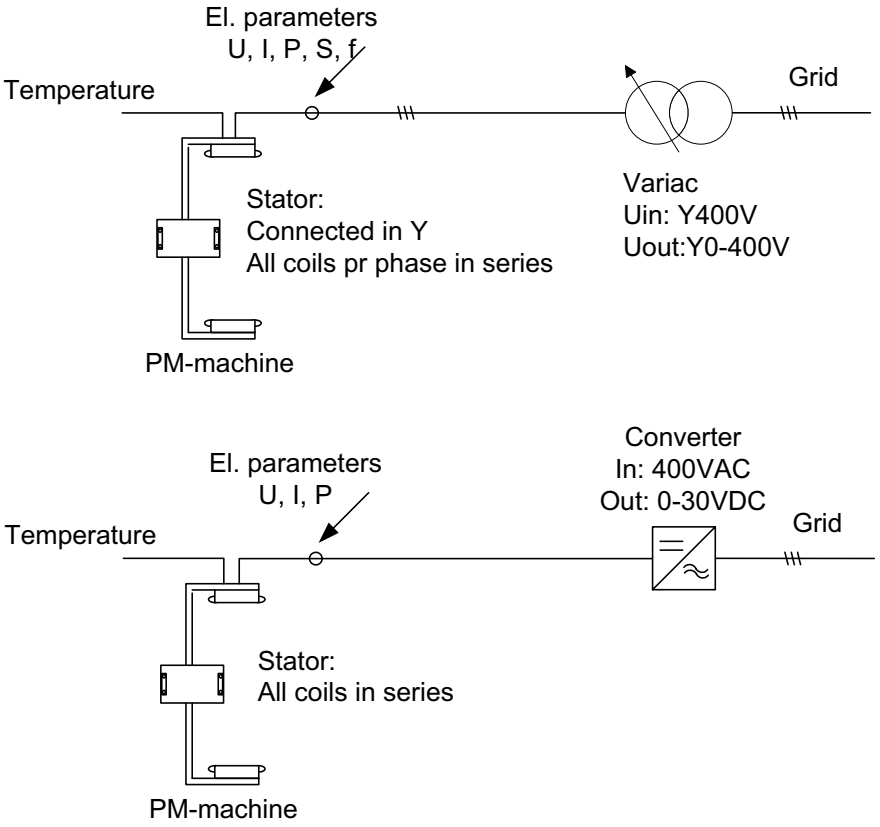

Fig. 123 Schematics of test setup for AC (top) and DC (bottom) test of winding

4.4.2.b Estimating copper losses using temperature measurements

Another method of estimating the AC factor is from the temperature difference between applying DC and AC current to the stator. When only applying DC current to the stator only DC copper losses are present, leaving the winding as the only heat source. The thermal model can be simplified to a heat source, a thermal resistance and an ambient temperature. The ambient temperature, copper temperature and losses are measured leaving only the thermal resistance unknown, eq. (103). Assuming that the equivalent thermal resistance is equal for both AC and DC current, eq. (104), placing all AC-losses in the winding, neglecting the iron losses induced by the AC current, the difference in temperature rise can be used to estimate the AC resistance, eq. (105).

$$\Re_{eq,DC} = \frac{P_{Cu,DC}}{\Delta T} \tag{103}$$

$$\Re_{eq,DC} = \Re_{eq,AC} = \frac{I_{DC}^2 R_{DC}}{\Delta T_{DC}} = \frac{I_{AC}^2 R_{AC}}{\Delta T_{AC}} \tag{104}$$

$$R_{AC} = \frac{I_{DC}^2 \cdot R_{DC} \cdot \Delta T_{AC}}{I_{AC}^2 \cdot \Delta T_{DC}} \tag{105}$$

In Table 35 the measured values and calculated AC coefficient is presented. It is assumed that each part can be separated from each other and has its own thermal resistance.

Comparing it with the result in Table 34 it shows a lower AC factor than from the power measurements. The measurements are done when the temperature has reached steady state, and the temperature rises in both cases are comparable. The factor $k_{AC,0}$ is compensated for the difference in temperature rise for the DC and AC measurement. eq. (55).

This method assumes all losses in the winding, no losses in the iron, which is close to true. There are inaccuracies connected with offsets in the measurements, the temperature sensors accuracy, their position and immediate surroundings, but most would be equal for both DC and AC measurements. The temperatures are measured in the centre of the coils. This method should be advantageous since it measures the losses more or less directly.

Table 35 Estimation of AC factor based on temperature measurement

	U [mV]	ΔT_{DC} [K]	R_{DC} [mΩ]	ΔT_{AC} [K]	I_{AC} [A]	R_{AC} [mΩ]	k_{AC}	$k_{AC,0}$
A1	1579	60,4	15,05	55,0	75,2	26,7	1,77	1,81
A2	1579	60,0	15,05	54,0	75,2	26,3	1,75	1,80
A3	1570	59,2	14,97	51,7	75,2	25,4	1,70	1,76
A4	1576	60,8	15,02	52,2	75,2	25,1	1,67	1,73
A			**60,10**			**103,5**	**1,72**	**1,77**
B1	1594	59,9	15,20	58,2	75,2	28,7	1,89	1,90
B2	1589	62,0	15,15	57,8	75,2	27,5	1,81	1,85
B3	1579	57,6	15,05	54,8	75,2	27,9	1,85	1,87
B4	1599	61,9	15,24	63,9	75,2	30,6	2,01	1,99
B			**60,64**			**114,6**	**1,89**	**1,90**
C1	1601	NA	15,26	NA	76,0	NA	NA	NA
C2	1607	63,6	15,32	64,2	76,0	29,5	1,92	1,92
C3	1578	59,7	15,04	55,6	76,0	26,7	1,78	1,81
C4	1594	61,6	15,20	56,3	76,0	26,5	1,74	1,78
C			**60,82**			**110,3**	**1,81**	**1,84**

4.4.2.c Frequency scan of the winding

To further examine the resistance and inductance a frequency converter was used to apply voltage at different frequencies. The result is shown in Fig. 124. The reactance curve is close to linear yielding an inductance of 4.3mH. The resistance is increasing slightly more than linear (106). The resistance and inductance is found measuring active and reactive power, the measurement is done on phase C.

$$R_{AC} = 0.069 + 0.062 \cdot f + 0.020 \cdot f^2 \tag{106}$$

At 50Hz the resistance per phase is about 150mΩ, yielding an AC-factor of 2.2. The resistance found using the inverter is a little higher than the one found using the 50Hz source. This may be a combination of measuring error (switching frequency disturbs the measuring device) and that the high switching frequency of the converter increases the AC factor (losses) some.

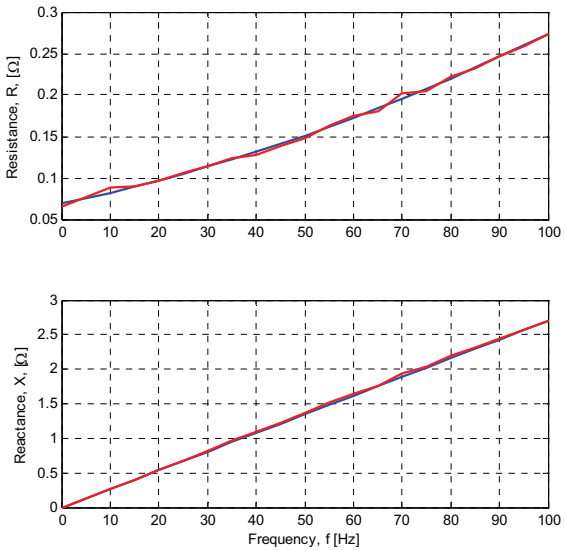

Fig. 124 Resistance and reactance as a function of frequency

4.4.2.d Examination of AC-factor

The winding is wound with 36 parallel conductors, or strands, with about six turns in radial direction and three in the tangential direction, there are 19 turns per coil, resulting in relative high turns (12mm). The turns were not deliberately rotated to counter the eddy current effect from the field in the slot, it was assumed that with so many parallel conductors, turns and coils in series all the handling during the winding operation would cause all conductors to be at all positions. But since the coils are wound on bobbins, and the fact that the operator took pride in preventing rotation of the conductors, it didn't happen. It is evident that the conductors more or less keeps their relative position throughout the entire part, and when shorted at each end, effectively creating a solid bar of copper with circulating currents.

The phenomena examined are the conductor's individual resistance and inductance, the current sharing between the conductors when loaded, the induced voltage in each conductor and the no load circulating currents in the part.

Measurement of each conductor

Measurements of inductance and resistance of each parallel conductor was performed using 50Hz AC source of 2.1V, and measuring current (around 4A) with cold machine (20°C). It shows that the resistance of each conductor is around 0.5Ω+/-0.02, corresponding to 14mΩ per part and 55mΩ per phase. This is equal to the calculated DC resistance in Table 26, and shows that the self induced eddy currents are low. Compared to the measured values in Table 34 and Table 35 where the DC resistance is found to 61mOhm @80C the AC coefficient per conductor is 1.12 (55x1.24/61=1.12). The inductance is found to be around 0.8mH per conductor. Since only one conductor is activated at the time, the current in this test is much too low to magnetize the iron, and thus is the measured inductance very low.

Load sharing, proximity effect

The load sharing between the conductors are examined by applying voltage to a part and measuring the current in each parallel conductor relative to each other. The test is done without rotor. The result from one part (A_1) is shown in Fig. 125. The blue curve and arrow is the applied voltage, the red is the vector sum of all the currents and the green is the current in the different strands. The current in the parallel strands spreads out over a wide area, it can be seen that the component parallel to the sum of the currents are fairly equal (1.92A +/- 0.23A); it is the component normal to the sum of currents that varies the most. This shows that the mutual induced eddy currents between conductors are substantial. In Table 36 a comparison of vector and arithmetic sum of the currents in the parallel pats is shown. It is only the fundamental of the currents that is used for the calculation, the harmonics are neglected (THD below 1.5%).

Table 36 Comparison of vector and arithmetic sum of the first harmonic of the currents

Parameter	Value
Vector sum (I_{A1})	69.1 A
Arithmetic sum ($I_{A1,1}$+ $I_{A1,2}$+…+ $I_{A1,22}$)	87.5 A
Current factor	1.27
Loss factor (k_{AC})	1.60

The loss factor is the AC-factor. It is only measured for one of the parts (A_1) and comparing the AC factor with A_1 in Table 34 and Table 35 (k_{AC} equals 2.14 and 1.81) this measurement yields a lower AC factor. Regarding accuracy the measured sum and calculated sum of currents are not equal, both angle and amplitude are a couple of percent of.

A full examination of all the parallel conductors in each part (36 conductors, 4 parts in series per phase and 3 phases, 864 ends) could lead to connection diagram for how to reduce the effect of the mutual induced eddy currents.

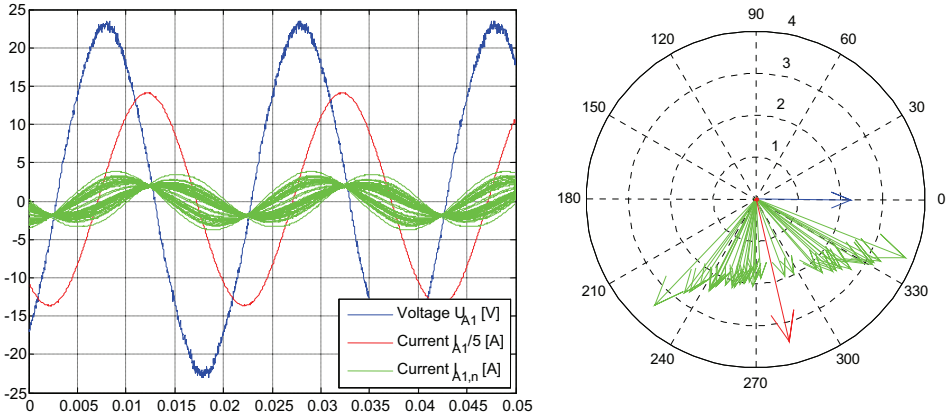

Fig. 125 To the left a plot of the currents in the parallel conductors (green), blue is voltage and red is the sum of currents divided by 5 in the time domain. To the right a vector plot of the same situation, here the voltage is scaled by a factor of 10 and the sum of the current by a factor of 20.

No load circulating currents

The induced currents circulating in a part at no load was also measured. The motivation was to exclude the possibility for significant difference in induced voltage due to the relative positions of the conductors. The currents are measured at nominal speed, over one period and for arbitrary rotor position. The sum of currents should be equal to zero, but since there is some inaccuracy in the measurements, the measurement could not be made at the same instance and the currents vary depending on rotor position, the sum deviates from zero. The result is shown in Fig. 126. The sum of the currents at no load is shown in Table 37. The losses connected to these currents are negligible. Thus can it be concluded that the induce voltage in each conductor is close to equal.

Table 37 Sum of no load circulating currents

Sum	1st	3rd	5th
Arithmetic [A]	2.9	0.8	0.1
Vector [A]	0.022	0.014	0.003
Loss [W] @ 120mΩ	1.1	-	-

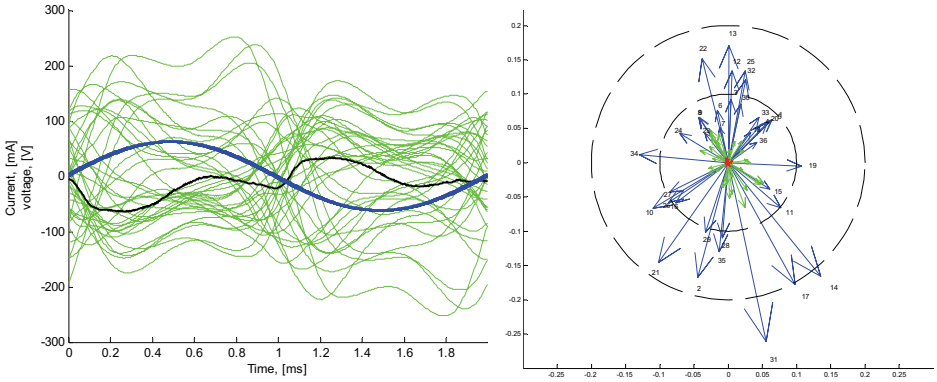

Fig. 126 Left plot of circulating currents in time domain (green), blue is the no load voltage and black the sum of currents (should be zero). To the right a vector plot of the circulating currents. Blue is the fundamental (largest), green the third harmonic and the red dot in the centre is the fifth. Number indicates conductor number

4.4.2.e Summary of measured resistance and inductance

Based on the previous calculated AC coefficients a summary is presented in Table 38. It shows a spread in the measured coefficient from 1.6 to 2.4. It is attached uncertainties to all measurements, but they all show a high AC factor. Based on the instrumentation and measurements technique it is the result from active and reactive power measurements and frequency scan that are used further. They will at least not give too optimistic results regarding losses, efficiency and voltage drops.

Table 38 Comparison of calculated AC coefficient

Phase	$R_{DC,80C}$	AC coefficient, k_{AC}				Inductance
	[mΩ]	4.4.2.a	4.4.2.b	4.4.2.c	4.4.2.d	[mH]
A	60.1	2.03	1.77	-	1.60	4.35
B	60.4	2.35	1.90	-	-	4.35
C	60.8	2.37	1,84	2.17	-	4.37

4.4.3 Load curve; testing with capacitive load

The generator was loaded with resistive and increasing capacitive load to investigate the load capabilities. The result is presented in Fig. 127. The results shows that using only the resistive load available (cos(ϕ)=1) it is not possible to reach 50kW, a maximum output of 28.5kW was reached. Adding capacitive load the output power increased, and with a capacitance around 850μF an output power just below 50kW (48.3kW, red line) can be reached. At that point that point 35kVAr is supplied to the generator, somewhat less than presented in Table 42. The black stippled lines are the required resistance for the different loads and voltages.

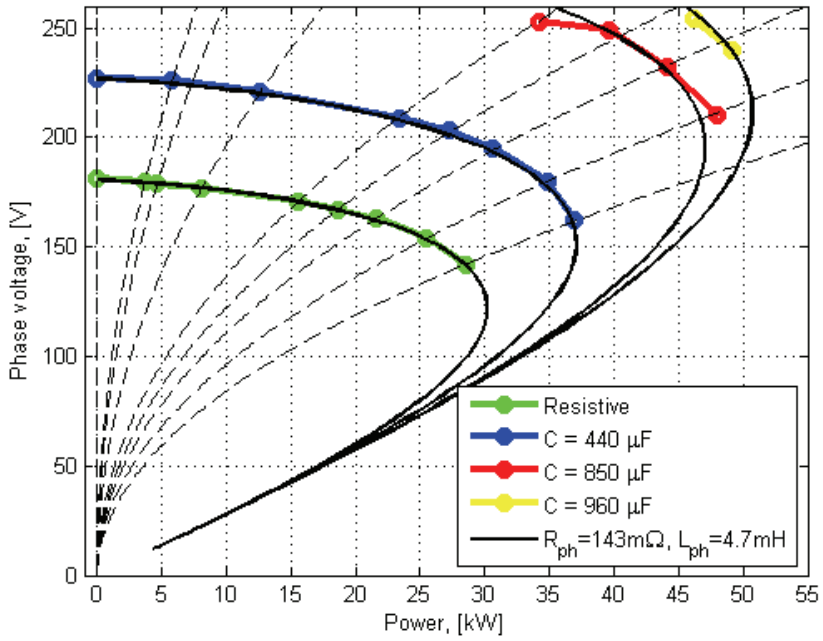

Fig. 127 Load testing of the PM-generator

The black solid lines are the calculated load curves where the generators parameters have been adapted to fit the measured parameters. It can be seen that the inductance must be increased somewhat, to 4.7mH, adding 0.4mH from the measurements without stator, while the resistance is kept constant at 143mOhm.The adapted load curve is mostly dependent of the reactance and less of the resistance. It is difficult to get an accurate match for the higher capacitive loads. The curve fitting is made based on a best guess. The curves from the adapted parameters show that a maximum of 30kW is possible with resistive load, but to reach 50kW a capacitive load of almost 1mF, or 40kVAr is needed. This is in the same range as the calculated reactive loads from Table 29.

4.4.4 Losses and efficiency

The dominant loss in this machine is the copper losses, while iron and magnet losses are much lower, but shouldn't be neglected. The windage and bearing losses should be small, the peripheral speed is only 4.6m/s and the rotational speed is only 51.7rpm. Iron losses and losses in the magnets are mostly frequency dependent, but are as the calculations shows also

load dependent. The copper losses are mostly load dependent but due to the high AC-coefficient it is also affected by the speed of the machine.

The losses are found measuring the input and output power of the machine, without load, with load and at different speeds. A summary of the measured losses are presented in Table 40.

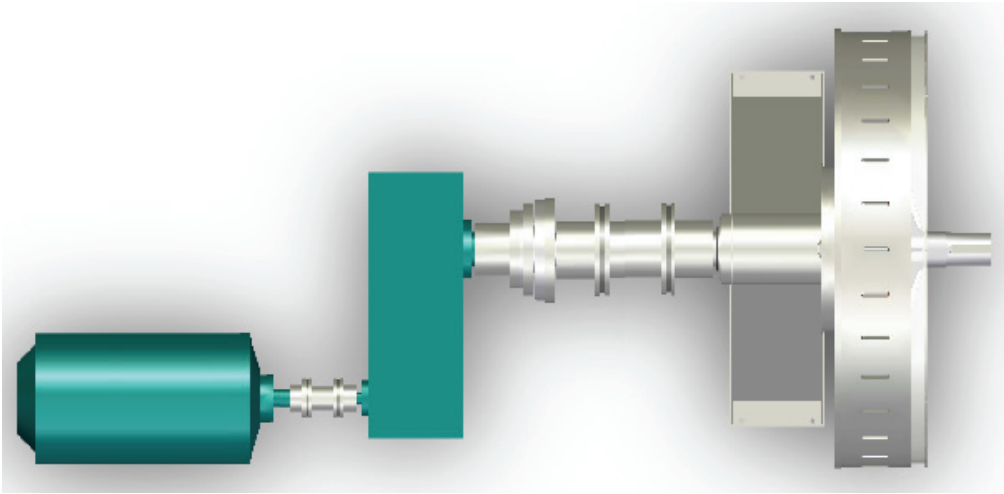

Fig. 128 Machine setup; induction motor, gear, torque meter and PM-generator

4.4.4.a No load losses

The no load losses were measured at different speeds using a torque meter on the shaft between gear and generator (Fig. 128). The temperature was also measured to get an indication of where the losses at no load were generated. Due to cogging at low speed (less than 10rpm) it was not possible to get good measurements around zero rpm.

No load losses as a function of speed

In Fig. 129 the speed dependency of torque and power is plotted. The generator was run both clock and counter clock wise to check for offsets in the torque meter. Blue curve is the measured no load torque. The red curve is an extrapolation towards zero assuming that the derivative close to zero is constant thus resulting in a constant component in the no load torque. The torque was measured with a warm machine. This measurement indicates that the no load losses for the machine is 695W. These losses include windage and bearing losses, no load losses in stator and rotor.

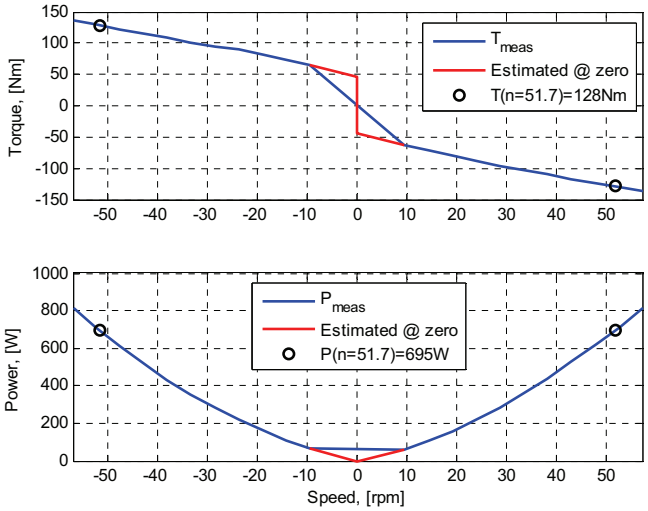

Fig. 129 No load curves of Torque and Power as function of speed

No load temperature rice

The temperature rise in stator and rotor was measured to get an impression of the loss distribution at no load in the generator. The stator temperature was measured continuously, while generator had to be stopped to measure the rotor temperature. The measured temperature rise in the generator is shown in Fig. 130. It can be observed that after about 15 hours of continuous operation the temperature in the stator is stable. After 28 hours the generator was stopped and rotor temperature measured.

The highest temperature in the generator is the magnet surface, with a temperature rise of 17.5K, The tooth tip of the stator is the highest in the stator with 15.8K. There is little or no loss in the winding, having a lower temperature rise than the surrounding lamination.

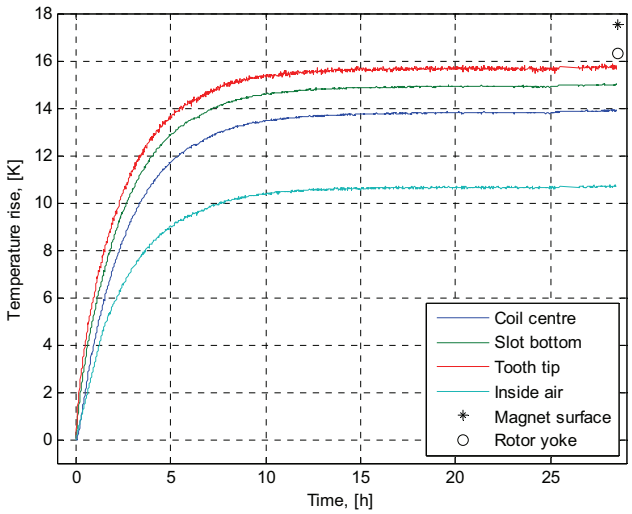

Fig. 130 Measured temperature rise in stator around part A1 at no load

A picture was taken with a thermal camera after about an hour with running at no load, Fig. 131. It shows that the temperature rise is highest in the magnets and iron yoke (6C) and that there is some rise in temperature in the coils. Due to the shiny surface of the lamination no temperature is measured there.

Based on the temperature measurements and thermal image, it is safe to assume that the electromagnetic losses at no load are generated in the rotor and stator lamination. Based on the temperature rise it can further be assumed that most of the losses are in the rotor, but both volume and thermal paths influence the temperature rise together with the loss. This corresponds well with the calculated losses in Table 32.

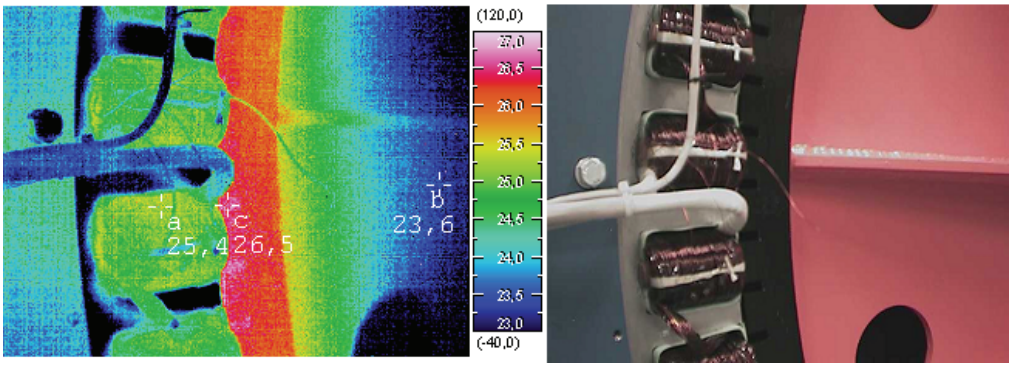

Fig. 131 Thermal image of stator and rotor after one hour at about 50Hz

No load torque ripple at low speed

The torque ripple at no load and low speed (9.5rpm) is measured and presented Fig. 132 showing the ripple for half a revolution. It is found that the most prominent ripple harmonic is the one coinciding with the tooth number and the next in line the one coinciding with the pole number. It is reasonable to believe that the gear and induction drive also is the source for some of the ripples, but no information of this is present. Of other harmonics present and not shown in Fig. 132 are a group of harmonics spread around the area of 2200Hz, which is in the same area as the switching frequency of the converter and one single harmonic at 12605, which has the factors 5 and 2521.

Comparing the measured torque ripple with calculated presented in Fig. 91 the amplitude is about half. The measurements of the torque ripple and the general experience during the testing concludes that the ripple is too high at low speed increasing wear and tear on the equipment. Above speeds of 10 rpm the vibration is within acceptable limits. 50Nm is only 0.5% of the nominal torque.

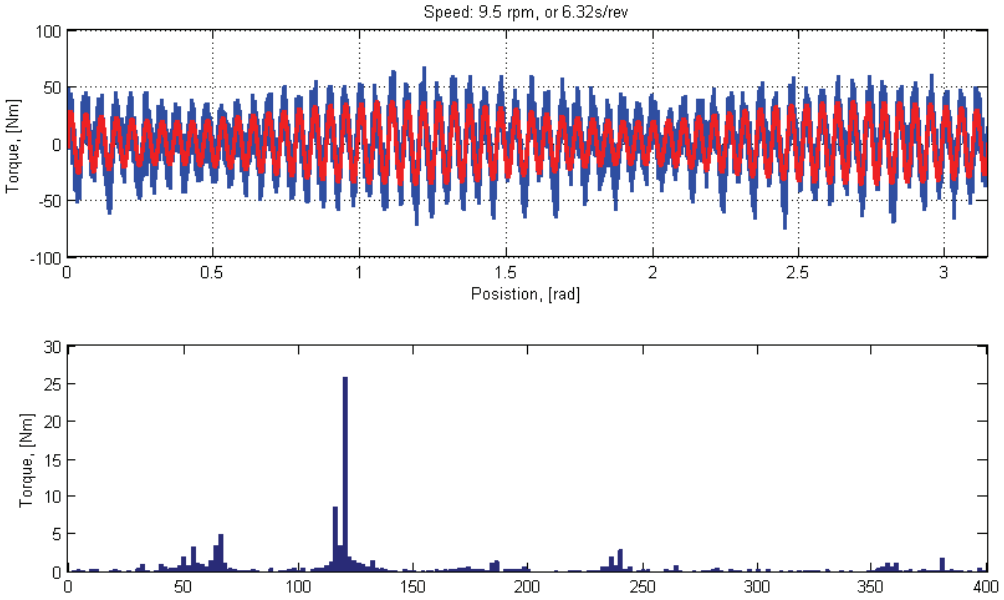

Fig. 132 Measured no load torque (blue top) and calculated harmonic content (bottom) red curve top is the sum of the 116th and 120th hamronics.

4.4.4.b Losses at partial load

The result from a test at partial load, 32kW, is shown in Fig. 133 and Table 39. The load is passive, with a fixed resistance and capacitance, resulting in a load (in kW) dependent of the induced voltage and voltage drop in the generator. With increasing temperature the winding resistance increases and induced voltage decreases slightly, resulting in lower load. The load resistance per phase is 2.1Ω and the capacitance is 495μF per phase, both constant through the test.

The power is measured on the shaft (input) and on the terminals (output), and is presented in Table 39. The efficiency is calculated, and found to be around 89.1%, decreasing a little with increasing temperature. Subtracting the copper losses from the total losses, using the measured resistance from Table 42 and load current, the other losses can be found. There are some variations in the measurements, but after the bearings have warmed up the other losses can be summed up to 1.6kW. These losses (named "other") include bearings, windage, stator iron losses and rotor losses. Further subtracting the measured no load losses that should include no load losses in rotor and stator, bearing and windings, a loss of 0.9kW is left. These 0.9kW must then be caused by the load, and most likely from the MMF. The losses are summed up and compared to the calculated values in Table 40. Using the results from the no load and testing at loaded conditions a summary and separation of losses are presented in Table 40. The losses are compared with the calculated losses.

Examining the measured losses at no load and with load and comparing them to the calculated losses, it is evident that the calculated copper losses are too low, which have been discussed earlier. Comparing the no load losses there is no difference in calculated and measured losses. The measured losses include both windage and bearing, and it would be expected that the measured losses would be higher than the calculated. For the other losses the calculated loss is the difference between loaded and no load losses in Table 32. The difference

in 420W between the calculated and measured losses is probably caused by accuracy, deviation in the calculations, stray losses and other load effects not accounted for. The measurements and calculations are in the same area, confirming each other. But neither measurements nor calculations are complete and accurate enough to make a definite verification of the models used for calculations.

Table 39 Efficiency at partial load @ 50Hz (32kW warm)

Temperature rise		Shaft			Generator			Losses			
Coil (meas) [K]	Magnet (est.) [K]	Speed [rpm]	Torque [kNm]	Power [kW]	Power [kW]	Reactive [kVAr]	cos(ϕ)	Total [kW]	Copper [kW]	Other [kW]	Efficiency [%]
0	0	51.7	7.6	41.1	36.8	12.2	0.95	4.4	2.1	2.2	89.4
45	21	51.7	7.1	38.4	34.6	11.4	0.95	3.8	2.3	1.5	90.0
58	41	51.6	6.9	37.3	33.2	11.1	0.95	4.1	2.3	1.7	89.0
65	50	51.7	6.7	36.3	32.4	10.8	0.95	3.9	2.3	1.5	89.3
67	54	51.7	6.7	36.3	32.1	10.6	0.95	4.2	2.3	1.8	88.5
69	55	51.7	6.6	35.7	31.9	10.5	0.95	3.8	2.3	1.5	89.3
69	59	51.7	6.6	35.7	31.7	10.5	0.95	4.0	2.3	1.7	88.8

Table 40 Summary of measured losses

	Copper [kW]	No load losses [kW]			Other losses [kW]			Total [kW]	Efficiency [%]
		Magnet	Rotor yoke	Stator	Magnet	Rotor yoke	stator		
32 kW	**90C**								
Measured	2.3		0.7			0.9		3.9	89
Calculated	*1.4	0.38	0.07	0.26	0.32	0.10	0.08	2.6	93
Difference	0.9		0.0			0.42		1.3	

* Using 75A at 90C with the calculated $R_{ph@90C}$=83mΩ from 4.2.5

4.4.4.c Load dependent losses: thermal consideration

The temperature rise and input and output power is plotted in Fig. 133. It can be seen how the load falls with increasing temperature in the generator. The decrease in power is both because of increased copper resistivity and decrease in the magnets remanent flux density resulting in lower induced voltage.

The highest temperature rise is as expected in the coil (70K), followed by the tooth tip (58K). The temperature rise on the magnet surface is about 56K. The air temperature inside the machine has risen with 40K. Ambient temperature is around 20C.

In Fig. 133 it is also showed an estimate of the magnet temperature. This is calculated using the measured current and voltage, and the induced voltage, inductance and resistances from Table 34. The resistance is compensated for the measured temperature in Table 39. The equation for the temperature dependency of the magnet is shown in eq. (107). It is assumed that the percentage reduction in voltage equals percentage reduction in remanent flux density in magnet, eq.(108). The temperature coefficient for the magnet is 0.1%/K, hence can the temperature be estimated from eq. (109). Since the measurements are per phase while the magnets rotate and affect all phases, it is the mean value of the phases that is representative. The temperature found will be an average of all magnets. As can be seen from Fig. 133, the estimated magnet temperature corresponds with the measured temperature after the stop.

$$E(T) = U + I \cdot Z = U + I \cdot \left(R(T) + jX \right) \tag{107}$$

$$\Delta E_T = \Delta B_{r,T} = \frac{E(T)}{E(T_0)} \tag{108}$$

$$\Delta T_m = \frac{\Delta B_{r,T}}{k_{Br,T}} \tag{109}$$

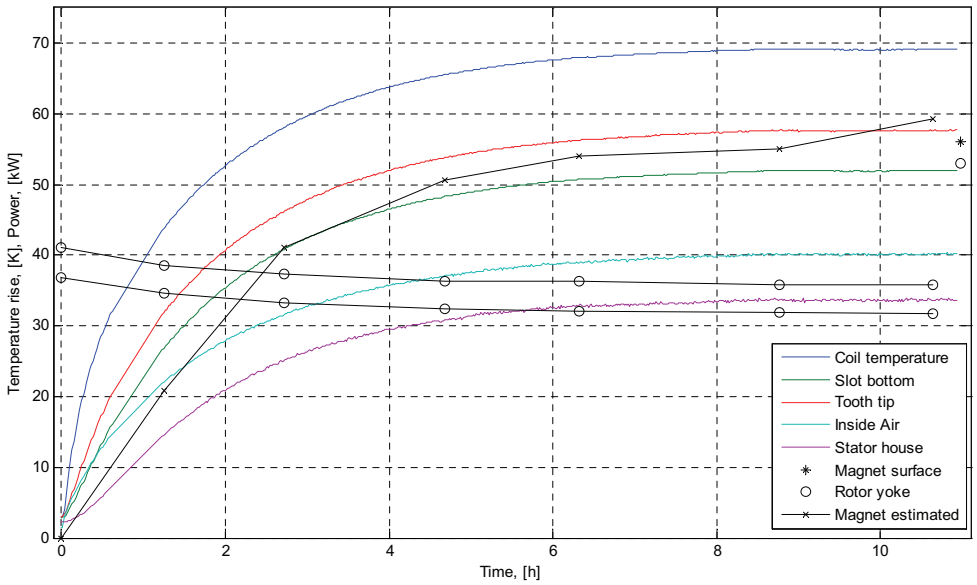

Fig. 133 Temperature rise in generator at about 32 kW, measured input and output power and an estimate of magnet temperature is shown

4.4.4.d Estimation of efficiency curve

In Fig. 134 two curves of the efficiency as a function of load at constant speed is shown. One (blue) assumes constant temperature of 90C. The equation for the loss estimation is shown in eq. (110) to eq.(113). For the other (green) there is made an estimation of the temperature rise in the copper yielding increased resistance depending on the load. It is assumed the same magnet temperature for both cases. The no load and other losses is the same for both, eq. (111) and eq. (112). While the copper loss is calculated using a loop where the temperature rise is estimated from (115) and the loss in eq. (114). This method needs a few iterations (temperature vs. loss) to converge. Both methods makes an assumption that the input power is given by (110). The efficiency is calculated with eq. (116).

$$P_{in} = 3 \cdot E_{\Delta T=56} \cdot I \tag{110}$$

$$P_{noload} = P_{noload,32kW} \tag{111}$$

$$P_{other} = P_{other32,kW} \cdot \frac{I}{I_{32kW}} \tag{112}$$

$$P_{Cu} = P_{Cu,32kW} \left(\frac{I}{I_{32kW}} \right)^2 \tag{113}$$

$$P_{Cu,T_2} = P_{Cu,32kW} \cdot \frac{k_{T_2}}{k_{T_1}} \cdot \left(\frac{I}{I_{32kW}} \right)^2 \tag{114}$$

$$\Delta T_2 = \Delta T_1 \cdot \frac{P_{noload} + P_{other} + P_{Cu,T_2}}{P_{loss,32kW}} \tag{115}$$

$$\eta_{50kW} = \frac{P_{in} - P_{Cu,50kW} - P_{other,50kW} - P_{noload}}{P_{in}} \tag{116}$$

Assuming constant temperature the losses at 50kW is estimated to be 7.8 kW, with the copper loss dominating, resulting in an efficiency of 86%. The method compensating for the increased temperature reaches 50kW output power with 10.8kW loss and 82% efficiency. But the calculated temperature rise is 190K. These estimated values are presented to get an impression of the load and temperature dependency of the machine.

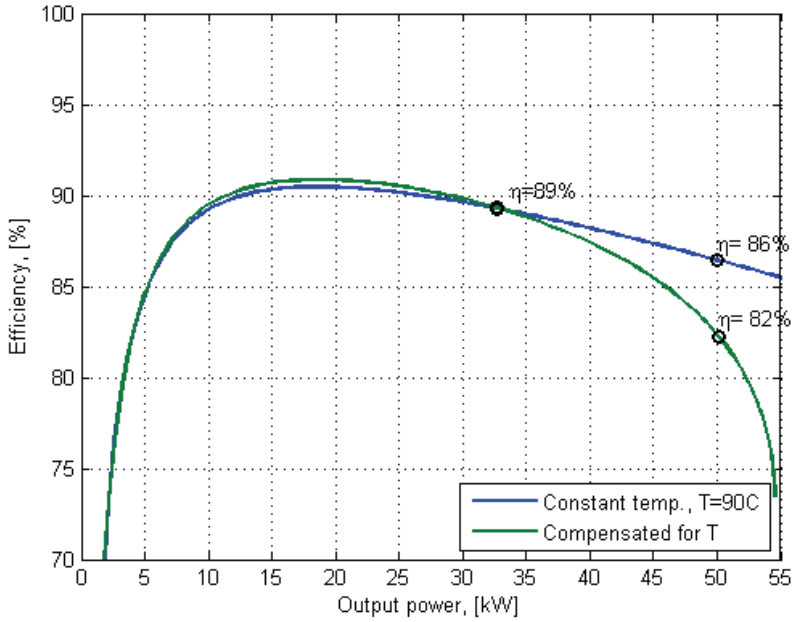

Fig. 134 Estimated efficiency curves

Table 41 Estimated loss and efficiency at 50kW

50 kW	Copper [kW]	No load losses [kW]	Other losses [kW]	Total [kW]	Efficiency [%]
Constant temperature	**90C**				
Estimated	5.6	0.7	1.6	7.8	86
Compensated temperature	**210C**				
Estimated	8.5	0.7	1.6	10.8	82

4.4.5 Summary of the electric parameters

A summary of the measured parameters are given in Table 42. The voltage, DC-resistance and inductance are equal for all phases. The AC-resistance varies between the parts and phases.

Table 42 Summary of the measured parameters for the 50kW PM-generator

Parameters	Value	
E_{ph}	181	V
$R_{DC,\Delta T=60K}$	61	mΩ
$R_{AC,\Delta T=60K}$	143	mΩ
$R_{AC,\Delta T=80K}$	152	mΩ
L	4.7	mH

Regarding the rating the nominal power initially was set to 50kW. But because of the high losses in the winding and passive cooling this is not achievable in steady state. In addition it would be preferable to lower the rating due to the reactance. Having a temperature rise at 32kW/33kVA of 70K, a rating of 33kW/35kVA could be appropriate. Using the parameters from Table 42 a new operating point is found, presented Table 43 and Fig. 135.

The high reactance together with the losses in the winding and temperature rise in the rotor, results in a proposed new rating of the generator to about 35kVA for continuous duty. Since this is a laboratory model intermittent duty is the most common and the machine volume is relatively large so for short period of time (minutes) 50kVA should be feasible. The reduction of rating decreases the current loading, ac, from around 50kA/m to 30kA/m. The force density in the air gap is reduced from about 24kN/m^2 to 17kN/m^2.

Table 43 Result of nominal load calculations

	L_{ph}=4.7mH R_{ph}=152mΩ		
	cos(ϕ)=1	|E|=|U|	I = I_q.
P_{out} [kW]	30	33	33
Q [kVAr]	0	13	18
U_{ph} [V]	122	181	195
I_{ph} [A]	82	65	64
cos(ϕ)	1	0.93	0.87
NI [At]	1558	1235	1216
ac [kA/m]	38	30	30

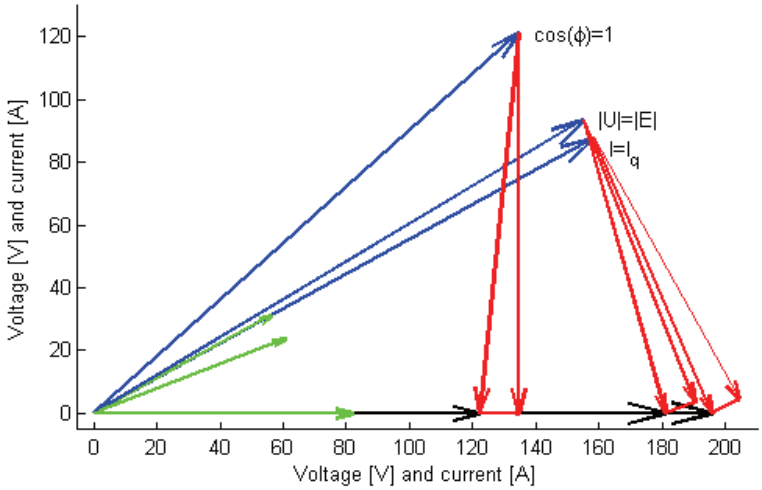

Fig. 135 The vector diagram for three different load cases around 33kW, with L_{ph}=4.7mH and R_{ph}=152 mΩ

Using the induced voltage and the nominal current when I = I_q, as base values the per unit values can be found, they are shown in Table 44. With the de-rating the per. unit resistance and reactance is lower. The resistance is still high; it would have been around 0.02 if the AC-factor had been at a reasonable level. The reactance is 0.53 which seen from the converter is a more sensible level, and reduces the need for reactive power.

Table 44 Per unit values for the de-rated machine

	E_{base}= 181 V I_{base}= 64 A Z_{base} = 2.83 Ω		
	cos(ϕ)=1	|E|=|U|	I = I_q.
U	0.67	1	1.08
I	1.28	1.02	1
R	0.054		
X	0.523		
Z	0.525		

Chapter 5
Summary of design and testing of PM machines for 100kW thruster and 50kW wind turbine

It has been presented two different applications for surface mounted radial flux permanent magnet machines. In one, the thruster, the permanent magnet rotor is one of the enabling technologies, while for the second, the direct driven generator for the wind turbine, the permanent magnets together with the winding design feature a simpler and more compact design. Both applications are large PM-machines and both are low speed machines (lower than 300rpm), at least for the higher power levels.

Due to the different characteristics of the applications different choices are made for the design. Electromagnetically the most obvious difference is the peripheral speeds, high for the thruster, very low for the wind generator, resulting in different choices for pole span and frequency. Regarding the prototypes the two different machines had to fulfil two different roles. The PM-motor for the thruster had to be a safe, conservative design where the main purpose was to prove the concept of the rim driven propeller, not to investigate the PM-machine. The generator for the wind laboratory is an experimental machine built to examine the phenomena occurring in low speed high pole PM-machines using concentrated coils.

In this chapter it is tried to sum up the results of the work presented regarding two different applications in question. It is also attempted to compare and make some conclusions regarding choice of winding layout using the two applications as examples.

5.1 The rim driven thruster

5.1.1 Summary of the presented work

It has been shown that the PM-motor successfully enables the concept of the rim driven propeller, or thruster. The application features a PM-motor with the rotor surrounded by water, large air gap, large diameter and relatively high peripheral speed. It has been presented a discussion around choice of parameters for a 2.5MW version. No conclusions are made, but depending of demand for efficiency, size and material cost a frequency between 100-150Hz could be chosen. The optimum choice of pole number, slot number and geometrical design will be an issue for the product optimization. Parameters such as material quality, volume, weight, losses, efficiency, duty cycle, cooling and running cost must be taken into account.

With the large air gap and possibility for a classical winding q larger than one the MMF, magnetic flux and torque is smooth and sinusoidal. However if other parameters, such as electric insulation, magnetic coupling and simplicity are considered more important, a

concentrated winding can be chosen. The thermal properties of the prototype azimuth thruster are very good and indicate that the machine can be built compact with high efficiency.

5.1.2 Conclusion

During the project with the 100kW prototype thruster it was shown that it is possible to integrate the PM-motor inside the nozzle of an azimuth thruster. The concept features advantages compared with traditional thruster solutions such as no boss, no gear, no shaft through the hull, no electric motor or shaft connection inside the hull strongly reducing noise, only one rotating part, possibility for improved hydrodynamic performance and increased hull utilization. The discussion around the parameters of the electric motor shows that PM-motor can be made very compact, to fit in the nozzle, and in little or no degree have effect on the optimum hydrodynamic performance.

5.1.3 Future work

The design of the PM-motor for the prototype thruster was a success; it worked and performed as requested. The future or ongoing work on the PM motor is an industrial optimization on production cost and performance. The optimization includes hydrodynamics, mechanics and thermodynamics in addition to the electromagnetic. Standardization or a product range regarding diameter, rotation speed and power must be made.

As for the academic interest further examination of the pros and cons regarding classical distributed winding and concentrated coils would be most interesting. It has in this work been chosen a distributed winding based on arguments as reluctance torque and peripheral speed. A more general study should be performed to investigate how the propeller parameter such as power level, speed and diameter influence the geometry of the PM-motor. The type of thruster, azimuth or tunnel, will also strongly influence the available space for the PM-motor.

Of other topics that would need further attention is study of redundancy, including multiphase and sectioning, the benefit from simplicity regarding cost and assembly and insulation between phase and earth. The operation and control of the machine could also be further investigated especially regarding coupling between phases, parallel converters and multiphase solutions increasing redundancy and fault tolerance.

5.2 The direct driven generator for wind turbine

5.2.1 Summary of the presented work

A study was performed to evaluate different technologies for a 3MW generator for direct driven wind turbines. The conclusion was that the SM RFPM with CC is a promising technology that could be a good solution for the direct driven wind turbine. It was also important for the choice of concept that the technology in question successfully had been used in other smaller applications in the surrounding research community in Trondheim and there was an interest locally to further investigate the technology for larger applications. A preliminary 3MW design is presented, followed by a discussion around how to scale and build the prototype was performed. It was attempted to preserve as much as possible of the proposed 3MW design with focus on the magnetic field and the pole slot combination, reducing the diameter but keeping the peripheral speed.

The purpose of the wind generator is to examine phenomena connected with the concentrated winding in a low speed high pole number machine. The important part of the concept is the premade coils with parallel rectangular coil sides and straight open slots, for

easy production and assembly. During the design where elaborate elegant solutions were discussed and compared with simple production friendly alternatives, the latter were usually chosen. Right or wrong, the decisions were made to investigate how a simple and production friendly machine would perform. These choices are most noticeable for the winding and magnets. For this prototype it was chosen to use rectangular magnets without skewing and a winding with round strands without any deliberate transposing.

The 50kW wind generator is successful as a prototype. It proves that the fractional concentrated winding with the rectangular magnets and open slots can produce a sinusoidal voltage with low harmonic level. The prototype also successfully pinpoints the challenges with the open slots and rectangular magnets that cause torque ripple, and the losses in the rotor from the sub harmonic MMF causing temperature rise in the rotor.

The testing revealed a high AC factor as a result of the choice of winding method. The parallel strands work more or less like a solid conductor. With proper handling of the winding the AC factor should be reduced to an acceptable level. For the prototype one could have transposed the winding in the end turns or changed from round wire to litz wire. A consequence of the high AC factor is high losses in the stator with subsequent high temperatures in the winding. By introducing forced cooling with air through the machine or water jacket cooling, the symptoms of the flaw can be treated.

At no load and low speed there are considerable amount of vibration and noise in the gearbox. From the harmonic content of the measurements it can be seen that it is the pole and slot number that are the most prominent. To avoid these components different choices regarding magnet geometry, skewing, or semi closed slots should have been made. Concentricity and roundness of the rotor and stator may also influence the vibrations.

The choice of frequency has resulted in a relative high reactance causing a high voltage drop and a consumption of reactive power at the intended nominal load. The power factor at full load (50kW) with the current in the q-axis is calculated to 0.7, and 0.85 at E=U. Due to the fixed induced voltage and the reactance a unity power factor can only be achieved at partial load. The measurement of the load curve in Fig. 127 coincides well with the calculated values in chapter 4.2.7.

There are presented calculations of the losses in rotor caused by the sub harmonics showing that they are significant. Though the effective air gap is large the long wave length of the sub harmonics yields a high flux in the rotor yoke with a high frequency (just above 50Hz). At partial load (32kW), the rotor (magnet) temperature rise was measured to 55C, thus getting close to the temperature limit of the N35grade magnets.

5.2.2 Conclusion

The prototype wind generator presents a very good opportunity to study phenomena connected with the concentrated windings in high poled machines. The results from the testing of the generator shows a very smooth voltage, crude MMF causing losses in the rotor and challenges with reluctance torque at no load and low speeds. The prototype has shown some challenges concerning the chosen winding and AC factor, and improvements are needed to achieve the intended power level.

The prototype has it challenges, but treated right, the concept could have some advantages compared to other types of windings, though more research and development are needed. Using the results from the prototype some conclusions can be made for the full size wind generator.

- The winding with its number of turns and parallel conductors is one parameter that was not possible to scale. Thus it has been evident that the winding chosen for the prototype is not an option for the 3MW generator. Probably a solution using premade roeble bars would be preferable. Depending of the system integration and converter technology medium or high voltage could also be favourable.
- The choice of open slots and rectangular magnets gave unwanted vibrations at no load and low speed. To avoid vibrations and possible resonance measures should be taken to lower the reluctance torque; the magnet fraction can probably be optimized, the magnet shape altered and of course introducing skewing would be advantageous. Also magnetic wedges could reduce the reluctance torque, but that would also increase the inductance.
- The magnet grade was chosen due to price and availability. The temperature rise in the rotor is relatively high and with increased loading the temperature is likely to increase above the allowed 80C of the N35grade magnets. The magnet grade must be increased to allowed higher temperatures. In additions measures should be taken to reduce the losses, for example sectioning the rotor.
- The choice of concentrated coils results in a relatively high inductance, and the high frequency results in a high reactance. For the larger generator a lower frequency would probably be advantageous when including the cost of reactive power for the converter.
- The MMF has high sub harmonic components due to the chosen one layer winding, resulting in large rotating flux in the rotor. If one layer winding is to be used measures must be taken to reduce the rotor losses
- A sectioning of the generator into several individual machines can also be sensible both regarding dimensioning, redundancy and control. Into this discussion multiple phases and coupling between coils and phases can be included.

5.2.3 Future work

The prototype generator enables the university to do experiments and further research on low speed high poled PM machines utilizing one layer concentrated windings. The scope of this work includes the design and testing of the prototype. The future work should include further analysis of the design and result and improvements of the prototype.

The two most obvious tasks regarding further work, except for the winding, are the reluctance torque and losses from the MMF in the rotor. There is literature on both topics. Regarding the reluctance torque the work should include examination of the pole slot combination, magnetic wedges in the stator, the magnet fraction, magnet shape and different methods of skewing. The open slots are a part of the concept but the semi-closed or closed slots could be used as a reference.

The MMF from the one layer winding creates high rotor losses. Finding measures to reduce these losses is an important task if the one layer winding is to be used. Pole slot combinations should be evaluated, different materials for magnets and rotor yoke can be considered and the mechanical design of rotor (tangential air gaps) should be evaluated. Other types of winding layouts are of course an option, but then the concept is abandoned.

Of other interesting subjects that have occurred during the work, but not pursued are testing of multiphase ($N_{ph}>3$), and control of multiphase machines with focus on coupling between the different phases. It could be interesting to investigate how the parallel circuit and

rotating currents affect the performance of the generator. And look into how the different possibilities for connecting the individual sets of windings (Fig. 18).

Due to the distribution of the coils over several poles the coil in one of a section end will increase the flux while the other end will decrease the flux when the current is in the q-axis. This condition will be fixed depending on the stator geometry. It will also occur in classical windings but here the distributed windings are within a pole. The effect of this internal difference in angle can be of interest to study further, regarding flux density in teeth and core, losses and thermal imbalance.

5.3 The winding layout; Concentrated or Distributed winding

In this work different choice for the two prototype machines were made. There were leading arguments. For the thruster the main argument was reliability and a conservative design with a focus on minimum reluctance torque. While the focus for the generator for the wind turbine was the wish to examine the phenomena regarding high poled concentrated windings. Both machines had some preliminary work discussing the different choice, but neither was optimized.

The main difference between the two applications presented in this work is the peripheral speed of the rotor, presented in Table 45. The peripheral speed of the thrusters is almost a decade higher than for the wind turbine. As presented in eq. (95) and repeated in eq. (117) the peripheral speed, frequency and pole pitch are closely connected. Hence with a high peripheral speed either the frequency or pole pitch must be large, or with a very low speed the frequency or pole pitch must be equivalent smaller.

$$v_p = 2 \cdot f \cdot \tau_p \tag{117}$$

For both applications the arguments regarding simplicity, insulation between phases, less coupling between coils and phases and could be used as valid arguments. As earlier stated neither of the machines are optimized, it is tried to make sensible choices, but there are no systematic evaluation of the consequences of the choices. Regarding the frequency, and optimization of machines, it can be seen from the discussion of the two machines that the choice of frequency for the thruster probably would be around 100-150Hz, while for the wind generator the frequency tend to go towards 30Hz.

$$f_{truster} > 50Hz > f_{wind} \tag{118}$$

Table 45 Summary of peripheral speeds for the applications in question

		Full size	Prototype		Comment
Thruster	n D_{or} v_{Dor}	220 3181 37	700 660 24	rpm mm m/s	Relatively high peripheral speed
Wind turbine	n D_{or} v_{Dor}	17 4640 4.1	51.7 1557 4.2	rpm mm m/s	Very low peripheral speed

5.4 Contributions

The main theoretical effort of this work has been focused on the study of concentrated windings, and that is also the area where the contributions to the knowledge of electric machines have come. During the discussion of the presented applications using existing theory, some light has been cast on the performance of the concentrated winding, its pitfalls and advantages. It has been shown that with enough poles the winding factors will be as high as the classical windings. For some different pole slot combinations the MMF and sub harmonic content have been evaluated and discussed, showing how the sub harmonic MMF creates losses and contributes to inductance. The consequences for flux density distribution, counter rotating fields with high speeds, sub harmonic magnetic flux and losses have been shown and pointed out. During the design and testing of the wind generator some phenomena have been identified and measured. The wind generator has also been an important contribution in the development of core technology used by local industry in Norway, and the university have gotten a unique possibility to examine the phenomena of one layer concentrated windings

This work is also a part of the development of the PM-motor for the rim driven thruster, one of the enabling technologies for the concept. This is an internationally new product developed by national industry, with their main market internationally. This work has contributed to the discussion around the main dimension, integration between hydrodynamics and electromagnetics and type of winding.

Bibliography

[1] Ø. Krøvel, R. K. Nilssen, and A. Nysveen, "A Study of the Research Activity in the Nordic Countries on Large Permanent Magnet Synchronous Machines," in *NORPIE* Trondheim, Norway: NTNU/EPE, 2004.

[2] Ø. Krøvel, R. K. Nilssen, S. E. Skaar, E. Løvli, and N. Sandøy, "Design of an Integrated 100kW Permanent Magnet Synchronous Machine in a Prototype Thruster for Ship Propulsion," in *ICEM* Cracow, 2004.

[3] Ø. Krøvel, K. Andresen, and N. Sandøy, "Thermal Properties of a Prototype Permanent Magnetized Electrical Motor Embedded in a Rim Driven Thruster," in *NORPIE* Lund, Sweden: EPE, 2006.

[4] Ø. Krøvel and R. K. Nilssen, "Design and Measurements on a Small Radial Flux Permanent Magnet Generator with Concentrated Coils," in *Comsol Conference*, Copenhagen, 2006.

[5] S. E. Skaar, Ø. Krøvel, R. K. Nilssen, and H. Erstad, "Slotless, Toroidal Wound, Axially-Magnetized Permanent Magnet Generator for Small Wind Turbine Systems," in *The 2003 Australasian Universities Power Engineering Conference - AUPEC 2003*, Christchurch, New Zealand, 2003.

[6] S. E. Skaar, Ø. Krøvel, and R. K. Nilssen, "Distribution, coil-span and winding factors for PM machines with concentrated windings," in *ICEM* Crete, Greece: ICEM, 2006.

[7] "Energy Efficient - All Electric Ship," http://www.ivt.ntnu.no/imt/electricship, Accessed: 2010, March

[8] "Norges forskningsråd," www.forskningsradet.no, Accessed: 2010, March

[9] P. Dunsheath, *A History of Electrical Engineering*, First ed. London: Faber and Faber, 1962.

[10] K. J. Overshott, "Magnetism: it is permanent," *IEE Proceedings A Science, Measurement and Technology,* vol. 138, pp. 22-30, Jnuary 1991 1991.

[11] N. Tesla, "Electric Motor", USA Patent: 416194, 1889

[12] Wikipedia. "Wikipedia - Electric Motor," http://en.wikipedia.org/wiki/Electric_motor, Accessed: 2007, 6. January

[13] D. De Cogan, "S7 (history of technology) meeting report - Tesla and the AC motor," *Engineering Science and Education Journal,* vol. 8, pp. 147-147, August 1999 1999.

[14] J. Jenkins. "Sparkmuseum," http://www.sparkmuseum.com/MOTORS.HTM, Accessed: 2007, 5. January

[15] Neorem Magnets. "Neorem Magnets," www.neorem.fi, Accessed: 2007, September

[16] S. R. Trout, "Rare Earth Magnet Industry in the USA: Current Status and Future Trends," in *Rare Earth Magnet Workshop* Newark, DE, USA, 2002.

[17] F. Idland, "Optimization of an Axial Flux Permanent Magnet Generator using Genetic Algorithm," Siv.Ing, Department of Eletrical Power Engineering, Norwegian University of Science and Technology, Trondheim, 2004, p. 23.

[18] T. Nilsen, "Axial Flux Permanent Magnet Machines with emphases on Winding Design and Stator Arrangement," Pre project Siv.Ing, Dept. Electrical Power Engineering, Norwegian University of Science and Technology, Trondheim, 2004, p. 9.

[19] M. R. J. Dubois, "Optimized Permanent Magnet Generator Topologies for Direct-Drive Wind Turbines," Doctor, Technishe Universisteit Delft, 2004, p. 270.

[20] H. Weh and J. Jiang, *Berechnungsgrundlagen für Transversalflussmaschinen*: Springer-Verlag, 1988.

[21] M. Rosu, "Large Output-Power, Low-Speed Permanent MAgnet Synchronous Motor Designs for Ship Propulsion Drive," Licentiate, Department of Electrical and Communications Engineering, Helsinki University of Technology, Espoo, Finland, 2001, p. 77.

[22] A. R. Millner, "Multi-hundred horsepower permanent magnet brushless disc motors," in *Applied Power Electronics Conference and Exposition, 1994. APEC '94.* , Orlando, FL, USA, 1994.

[23] S. M. Husband and C. G. Hodge, "The Rolls-Royce transverse flux motor development," in *IEEE International Electric Machines and Drives Conference, IEMDC'03.* : IEEE, 2003.

[24] G. Dorr, "Trends and Developments of Electrical Machines in the 21st Century," in *ICEM* Bruges, Belgium: ICEM, 2002.

[25] S. Lai and S. Abu-Sharkh, "Structurally Integrated Slotless PM Brushless Motor with Spiral Wound Laminations for Marine Thrusters," in *The 3rd IET International Conference on Power Electronics, Machines and Drives (PEMD)* Dublin, Irland: IET, 2006.

[26] S. Abu-Sharkh, S. R. Turnock, and A. W. Hughes, "Design and performance of an electric tip-driven thruster," *Proceedings of the Institution of Mechanical Engineers, Part M: Journal of Engineering for the Maritime Environment,* vol. 217, pp. 133-147, 21 May 2003 2003.

[27] D. M. Kane and M. R. Warburton, "Integration of permanent magnet technology," in *IEEE Power Engineering Society Summer Meeting*: IEEE, 2002.

[28] M. Lea, D. Thompson, B. Van Blarcom, J. Eaton, J. Friesch, and J. Richards, "Scale Model Testing of a Commercial Rim Driven Propulsor Pod," *Journal of Ship Production,* vol. 19, pp. 121-130, 1 May 2003 2003.

[29] L. H. Hansen, L. Helle, F. Blaabjerg, E. Ritchie, S. Munk-Nielsen, H. Bindner, P. Sørensen, and B. Bak-Jensen, "Conceptual survey of Generators and Power Electronics for Wind Turbines," Risø National Laboratory, Roskilde, Denmark ISBN 87-550-2743-1, ISBN 87-550-2745-8 (internet), ISSN 0106-2840, December 2001 2001.

[30] R. Poore and T. Lettenmaier, "Alternative Design Study Report: WindPACT Advanced Wind Turbine Drive Train Designs Study," NREL: National Renewable Energy Laboratory, Golden, Colerado NREL/SR-500-33196, August 2003.

[31] H. Polinder, F. F. A. van der Pijl, G.-J. de Vilder, and P. Tavner, "Comparison of direct-drive and geared generator concepts for wind turbines," in *IEEE International Conference on Electric Machines and Drives*: IEEE, 2005.

[32] M. R. J. Dubois, H. Polinder, and J. A. Ferreira, "Comparison of generator topologies for direct-drive wind turbines," in *NORPIE* Aalborg, Denmark, 2000.

[33] Y. Chen, P. Pillay, and A. Khan, "PM wind generator topologies," *IEEE Transactions on Industry Applications,* vol. 41, pp. 1619-1626, November-December 2005 2005.

[34] P. Lampola, "Directly Driven, Low-Speed Permanent-Magnet Generators for Wind Power Applications," PhD, Departmen of Electrial Engineering, Helsinki University of Technology, Espoo, Finland, 2000, p. 62.

[35] M. Ellsén, I. Mathiasson, and O. Carlson, Dr., "Series and Parallel Compensation for the Permanent Magnet Synchronous Generator at the Chalmers Test Wind Turbine," in *Nordic Wind Power conference* Espoo, Finland, 2006.

[36] B. J. Chalmers and E. Spooner, "An axial-flux permanent-magnet generator for a gearless wind energysystem," *IEEE Transactions on Energy Conversion,* vol. 14, pp. 251-257, Jun 1999 1999.

[37] J. R. Bumby, R. Martin, M. A. Mueller, E. Spooner, N. L. Brown, and B. J. Chalmers, "Electromagnetic design of axial-flux permanent magnet machines," *IEE Proceedings Electrical Power Applications,* vol. 151, pp. 151-160, March 2004 2004.

[38] E. Spooner, P. Gordon, J. R. Bumby, and C. D. French, "Lightweight ironless-stator PM generators for direct-drive wind turbines," *IEE Proceedings Electric Power Applications,* vol. 152, pp. 17-26, 7 January 2005 2005.

[39] A. Grauers, "Design of Direct-driven Permanent-magnet Generators for Wind Turbines," Doctor of Philosophy, School of Electrical and Computer Engineering, Chalmers Universityr of Technology, Gothenburg, 1996, p. 133.

[40] A. Grauers and P. Kasinathan, "Force Density Limits in Low speed PM Machines due to Temperature and Reactance," *IEEE Transactions on Energy Conversion,* vol. 19, 3. September 2004.

[41] P. Kasinathan, A. Grauers, and E. S. Hamdi, "Force density limits in low-speed permanent-magnet machines due to saturation," *IEEE Transactions on Energy Conversion,* vol. 20, pp. 37-44, March 2005 2005.

[42] J. Hystad, "Transverse Flux Generators in Direct-driven Wind Energy Conversion," Dr.Ing, Department of Electrical Power Engineering, Norwegian University of Science and Technology, Trondheim, 2000, p. 116.

[43] J. Pyrhönen, P. Kurronen, and A. Pariainen, "Permanent Magnet 3 MW Low-Speed Generator Development," in *ICEM 2006* Chania, Crete, Grece: ICEM, 2006.

[44] M. Dahlgren, Dr., H. Frank, M. Leijon, Dr., F. Owman, Dr., and L. Walfridson, "Windformer - Wind Power goes large-scale," *ABB Review,* vol. 3, pp. 31-37, 2000.

[45] M. Leijon, "Powerformer - A radically new rotating machine," *ABB Review,* vol. 2, pp. 21-26, 1998.

[46] A. Chertok and D. Hablanian, "Development of a Direct Drive Permanent Magnet Generator for Small Wind Turbines," TIAX LLC, Cambridge, MA, USA January 7 2005.

[47] M. A. Mueller and A. S. McDonald, "A lightweight low speed permanent magnet electrical generator for direct-drive wind turbines," in *European Wind Energy Conference, EWEC* Brussel: EWEC/EWEA, 2008.

[48] F. Magnussen, "On Design and Analysis of Synchronous Permanent Magnet Machines for Field-weakening Operation in Hybrid Electric Vehicles," Doctor of Philosophy, Electrical Machines and Power Electronics, Department of Electrical Engineering, Royal Institute of Technology, Stockholm, 2004, p. 251.

[49] F. Magnussen and H. Lendenmann, "Parasitic Effects in PM Machines with Concentrated Windings," in *IAS*: IEEE, 2005.

[50] F. Meier, "Permanent-Magnet Synchronous Machines with Non-Overlapping Concentrated Windings for Low-Speed Direct-Drive Applications," PhD, Electric Machines and Power Electronics, Royal Institute of Technology, Stockholm, 2008, p. 177.

[51] A. M. EL-Refaie, "High Speed Operation of Permanent Magnet Machines," PhD, WEMPEC, University of Wisconsin, Madison, 2005, p. 596.

[52] T. F. Chen, Y. Lie-Tong, and L. L. Lai, "Performance of a three-phase AC generator with inset NdFeBpermanent-magnet rotor," in *Electric Machines and Drives Conference, IEEE Int.* Cambridge, MA, USA: IEEE, 2001.

[53] D. Ishak, Z. Q. Zhu, and D. Howe, "Comparison of PM Brushless Motors, Having Either All Teeth or Alternate Teeth Wound," *IEEE Transactions on Energy Conversion,* November 2004.

[54] C. J. A. Versteegh, "Design of the Zephyros Z72 wind turbine with emphasis on the direct drive PM generator.," in *Norpie* Trondheim, Norway: NTNU, 2004.

[55] I. Waltzer, "Technology Trends in Large Permanent Magnet Motor Applications," in *ICEM* Bruges, Belgium: ICEM, 2002.

[56] Siemens. "Press Release: SWT-3.0-101 DD," http://w1.siemens.com/press/en/pressrelease/?press=/en/pressrelease/2009/renewable_energy/ere200912023.htm, Accessed: 2010, January 7th

[57] "Jeumont Electric," http://www.jeumontelectric.com/pages/uk/page.aspx?c=1&p=5, Accessed: 2010, Januray 7th

[58] "The Switch," http://www.theswitch.com/, Accessed: 2010, Januray 7th

[59] "Areva Multibrid," http://www.multibrid.com/, Accessed: 2010, January 7th

[60] "Dynawind - Morphic," http://www.morphic.se/sv/DynaWind/, Accessed: 2010, January 7th

[61] "Enercon GmbH - Energy for the world," http://www.enercon.de, Accessed: 2010, April

[62] "Vertikal Wind AB," http://www.verticalwind.se, Accessed: 2010, January 8th

[63] "SmartMotor AS," www.smartmotor.no, Accessed: 2010, February 14th

[64] "Sway AS," www.sway.no, Accessed: 2010, March

[65] T. Jokinen, "Large Permanent Magnet Machines," in *International Agean Conference on Electrical MAchines and Power Electronics* Istanbul, Turkey, 2004.

[66] Brunvoll. "Flyer for Rim Driven Thruster," http://www.brunvoll.no/public/cmsmm.nsf/lupgraphics/RDT%20leaflet%2012-2009.pdf/$file/RDT%20leaflet%2012-2009.pdf, Accessed: 2010, January 8th

[67] D. Tinsley, "Design for harsh environments," *Shipping World & Shipbuilding,* pp. 10-13, April 2006 2006.

[68] V. d. Velden. "Van der Velden Maritime Systems," http://www.vdvelden.nl/, Accessed:

[69] E. Segergren, "Simulation of Direct Drive Generator for Underwater Power Conversion," Licetiate, Division for Electricity and Lightning Research, Department of Engineering Physics, University in Uppsala, , Uppsala, Sweden, 2003, p. 33 (ex. appendices).

[70] E. Sclemmer and F. Müller, "Electromagnetic Finite Element Calculations of Permanent Magnet Generators for ECOBulb and HYDROMATRIX Applications," in *INTERNATIONAL CONFERENCE ON RENEWABLE ENERGY AND POWER QUALITY* Vigo, Spain: ICREPQ, 2003.

[71] T. Heikkilä, "Permanent Magnet Synchronous Motor for Industrial Inverter Applications - Analysis and Design," Doctor of Science, Laboratory of Electrical Engineering, Lappeenranta University of Technology, Lappeenranta, Finland, 2002, p. 109.

[72] L. Hilsum, "Chinese pay toxic price for a green world," in *The Sunday Times*, 2009.

[73] G. Hatch. "Chinese Rare Earth Production: A Darker Shade Of Green?," http://treo.typepad.com/raremetalblog/, Accessed: 2009, Dec. 12

[74] D. C. Hanselmann, Dr., *Brushless Permanent Magnet Motor Design*, Second ed.: The Writers' Collective, Cranston, Rhode Island, 2003.

[75] T. A. Lipo, *Introduction to AC Machine Design*, Second ed. Madison, WI: WISPERC, UW, Madison WI, 2004.

[76] M. G. Say, *The Performance and Design of Alternating Current Machines*, Third ed. London: Sir Isaac Pitman & Sons Ltd., 1948.

[77] D. C. Hanselmann, Dr., *Brushless Permanent-Magnet Motor Design*, First ed. New York: McGraw-Hill, Inc., 1994.

[78] J. Pyrhönen, T. Jokinen, and V. Hrabovcová, *Desing of Rotating Electrical Machines*, First ed.: John Wiley & Sons, 2008.

[79] Comsol Multiphysics, ver: 3.3.0.405, Comsol AB, Stockholm, Sweden, 2006, www.comsol.no

[80] D. C. Hanselman, Dr., *Brushless Permanent Magnet Motor Design*, Second ed.: The Writers' Collective, Cranston, Rhode Island, 2003.

[81] A. J. Mitcham, G. Antonopoulos, and J. J. A. Cullen, "Favourable slot and pole number combinations for fault-tolerant PM machines," *IEE Proceedings Electric Power Applications,* vol. 151, September 2004.

[82] D. Ishak, Z. Q. Zhu, and D. Howe, "Comparison of PM brushless motors, having either all teeth or alternate teeth wound," *IEEE Transactions on Energy Conversion,* vol. 21, pp. 95-103, March 2006.

[83] F. Libert and J. Soulard, Dr., "Investigation of Pole-Slot Combinations for Permanent-Magnet Machines with Concentrated Windings," in *International Conference on Electrical Machines (ICEM'04)* Cracow, Poland: ICEM, 2004.

[84] J. Cros and P. Viarouge, "Synthesis of high performance PM motors with concentrated windings," *IEEE Transactions on Energy Conversion,* vol. 17, pp. 248-253, June 2002.

[85] F. Magnussen and C. Sadarangani, "Winding factors and Joule losses of permanent magnet machines with concentrated windings," in *IEEE International Electric Machines and Drives Conference, 2003. IEMDC'03.*: IEEE, 2003.

[86] P. Salminen, M. Niemelä, J. Pyrhönen, and J. Mantere, "Performance analysis of fractional slot wound PM-motors for low speed applications," in *IEEE Industry Applications Conference, 2004. 39th IAS Annual Meeting*: IEEE, 2004.

[87] B. Taraldsen, "Stator Swingungen in Synchronmaschinen mit Bruchlochwicklungen," Dr.ing, dept. of Electric Power Engineering, NTNU, Trondheim, 1985, p. 132 + VIII.

[88] R. D. Begamundre, *Electromechanical Energy Conversion With Dynamics Of Machines*, 2nd ed. New Dehli: New Age International, 2003.

[89] E. Spooner, A. C. Williamson, and G. Catto, "Modular design of permanent-magnet generators for wind turbines," *IEE Proceedings Electric Power Applications,* vol. 143, pp. 388-395, September 1996 1996.

[90] J. Lammerander and M. Stafl, *Eddy Currents*. Prague: Iliffe Books Ltd., 1964.

[91] A. B. Field, "Eddy Currents in Large, Slot-wound Conductors," in *Annual Convention of AIEE*, Ashville, N.C. USA, 1905.

[92] J. R. Hendershot, Jr. and T. J. E. Miller, *Design of Brushless Permanent-Magnet Motors*, First ed. Oxford: Magna Physics Publishing and Clarendon Press, 1994.

[93] S. Rouho, M. Haavisto, E. Takala, T. Santa-Nokki, and M. Paju, "Temperature Dependence of Resisitivty of Sintere Rare-Earth Permanent-Magnet Materials," *IEEE Transactions on Magnetics,* vol. 46, January 2010.

[94] G. Enercon. "Enercon GmbH - Energy for the world," Accessed: 2006, December

[95] T. I. Reigstad, "Direct Driven Permanent Magnet Synchronous Generators with Diode Rectifiers for Use in Offshore Wind Turbines," M.Sc, Dept. Electric Power Engineering, NTNU, Trondheim, 2007, p. 120.

[96] "Brunvoll AS," www.brunvoll.no, Accessed: 2010, February 13th

[97] R. Nilssen, J. Lode, and S. E. Skaar, "Integrert propell og motor for elektrisk fremdrift av skip," Trondheim: inst. for Elkraftteknikk, NTNU, 2001, p. 19.

[98] J. Dahle, "Design of a permanent magnet synchronous machine for integration in an azimuth thruster," Master, dept. Electric Power Engineering, NTNU, Trondheim, Norway, 2002, p. 94.

[99] E. Løvli, "Bygging av PM-motor for bruk i truster for fremdrift av skip," Siv.Ing. (M.Sc), Dept. Electrical Power Engingeering, Norwegian University of Science and Technology, Trondheim, 2002, p. 105.

[100] "Norpropeller AS," www.norpropeller.no, Accessed: 2010, February 14th

[101] R. Vårdal and N. Sandøy, "Drivsystem for skip", Norway Patent: 318223, 2003

[102] E. de Vries, "REW Exclusive: Siemens New 3.6 MW Direct-drive "Concept" Wind Turbine," in *Renewable Energy World.com*, 2008.

[103] I. Entegrity Wind Systems. "Entegrity Wind Systems Inc.," http://www.entegritywind.com/, Accessed: 2007, July

[104] Energy Maintainance Service. "Energy Maintainance Service, LLC," http://www.energyms.com, Accessed: 2007, July

[105] M. Ellsén and O. Carlson, Dr., "Drift av Hönö provstation - HÖNÖ, Teknisk slutrapport i prosjektet," Institutionen för energi och miljö, Avdelningen för elteknik, Chalmers tekniska högskola, Göteborg October 2006.

[106] S. Øvrebø, E. Løvli, and F. Idland, "Annordning ved elektrisk maskin", Norway Patent: 324241, 2006

[107] "Cogent," www.cogent-power.com, Accessed: 2010,

[108] "Wind Power Laboratory at NTNU," http://www.elkraft.ntnu.no/Vindkraftlab/, Accessed: 2010, January 22

[109] O. W. Andersen, Prof. Tekn.Dr., "Compensation of Unbalanced Magnetic Forces by Distributed Parallel Circuits," in *International Conference on Electric Machines, ICEM* Cracow, Poland, 2004.

Appendices

A. Nomenclature

Symbol	Denomination	Description
In general		
A	m^2	Area
A		Magnetic vector potential
B	T	Flux density
d	m	Depth usually in radial direction
D	m	Diameter
e/E	V	Induced voltage
f	Hz	Frequency
I	A	Current
J	A/mm	Current density
k		Constants
l/L	m	Length, usually into plane
L	H	Inductance
N		Numbers
P	W	Active power
Q	VAr	Reactive power
R	Ω	Electric resistance
R	K/W	Thermal resistance
$\Re$	At/Wb	Reluctance
S	VA	Apparent power
T	K	Temperature
U	V	Voltage
w	m	Width, usually tangential
Φ	Wb	Flux
λ	W/(K·m)	Thermal conductivity
σ	1/(Ω·m)	Electric conductivity
^		Peak or amplitude value
–		Average value
Special		
A_g	m^2	Area of air gap
A_m	m^2	Area of magnets
A_{turn}	m^2	Copper area of one turn
A_{end}	m^2	Area of end winding/turn
b		Denominator of q´
B_g	T	Air gap flux density
B_r	T	Remanent flux density

d_s	m	Depth of slot
$d_{s,wedge}$	m	Depth of slot wedge
D_{cond}	m	Conductor diameter
D_{os}	m	Outer diameter of stator lamination
D_g	m	Air gap diameter (either centre, inner stator or outer rotor)
D_{is}	m	Inner diameter
D_{or}	m	Outer rotor diameter
D_{mr}	m	Diameter of surface where magnets are glued
e	V	Induced voltage per turn or tooth
E_{coil}	V	Induced voltage per coil
E_{phase}	V	Induced voltage per phase
f_n	Hz	Nominal electric frequency
F_1		# of basic windings
F_2		Sifference in pole and slot number
g	m	Air gap length
GMD	m	Geometric Mean Distance
I_{ph}	A	Phase current, rms?
I_{slot}	At	Total current in slot, rms? Ampere turns in a slot
k		An arbitrary constant
k_c		Carter coefficient
k_{dn}		Distribution factor for th n'th harmonic
k_{en}		Chording factor for the n'th harmonic
k_{AC}		AC-coefficient for resistance calculations
k_s		Lamination stacking factor
k_T		Temperature compensation for resistance
k_w		Winding factor
l_m	m	Length of magnet in magnetizing direction
L	m	Length of machine, active area
L_r	m	Length of rotor
L_s	m	Length of stator
l_{turn}	m	Length of one turn
L_{gap}	H	Inductance of air gap
L_{slot}	H	Inductance of slot leakage
L_{end}	H	Inductance of end winding/turn
L_{coil}	H	Inductance per coil
L_{ph}	H	Inductance per phase
m		# of turns/conductors in the height of a slot
N		# of turns in one coil
n		# of turns/conductors in the width of a slot
n	rpm	rotational speed
n		harmonic number
N_c		# of coils per phase
N_{cond}		# of parallel conductors per turn
N_m		# of magnets
N_p		# of poles
N_{pp}		# of pole pairs
N_{par}		# of parallel circuits
C		# of parallel circuits
N_{ph}		# of phases
N_s		# of slots

P_{Cu}	W	Copper losses
P_e	W	Eddy current losses, iron
P_h	W	Hysteresis losses, iron
q		Slots per pole and phase
q´		Coils per pole and phase
R_λ	W/K	Thermal resistance, conductivity
R_α	W/K	Thermal resistance, convection (and radiation?)
R_{AC}	Ω	AC-resistance
R_{DC}	Ω	DC-resistance
$\Re_{eq}$	At/Wb	Equivalent reluctance
$\Re_g$	At/Wb	Air gap reluctance
$\Re_m$	At/Wb	Magnet reluctance
$\Re_{ml}$	At/Wb	Leakage reluctance between magnets
$\Re_{rc}$	At/Wb	Rotor core reluctance
$\Re_s$	At/Wb	Slot reluctance (leakage)
$\Re_{sc}$	At/Wb	Stator core reluctance
$\Re_s$	At/Wb	Slot reluctance (leakage)
$\Re_t$	At/Wb	Tooth reluctance
T_n	K	Nominal temperature of winding
T_σ	K	Temperature at which the conductivity is given
w_m	m	Width of magnet
w_t	m	Width of tooth
w_{ti}	m	Width of tooth at air gap
w_{rc}/d_{rc}	m	Width/depth of rotor core
w_s	m	Width of slot
$w_s´$	m	Width of conductor
w_{sc}/d_{sc}	m	Width/depth of stator core
z		numerator of q´
α		Thermal heat transfer coefficient
Φ_g	Wb	Flux in air gap
Φ_p	Wb	Flux per pole (Pole flux)
Φ_r	Wb	Remanent flux per magnet
Φ_{rc}	Wb	Flux in rotor core
Φ_{sc}	Wb	Flux in stator core
Φ_t	Wb	Flux in tooth
δ_{skin}	m	Skin depth
λ	W/(Km)	Thermal conductivity
μ_r		Relative permeance of a material
$\mu_{r,fe}$		Relative permeance of iron
$\mu_{r,Nd}$		Relative permeance of magnet
μ_0	H/m, N/A^2	Permeability of vacuum
$\sigma_{Cu,20}$	1/Ωm	Electric conductivity of copper @ 20C
τ_p	m, rad, deg, %	Pole pitch

τ_s	m, rad, deg, %	Slot pitch
ω	rad/s	Rotational speed
ξ		Relative height of conductor? (h/δ)
γ_s	rad, deg	Slot pitch
γ_c	rad,deg	Coil pitch
σ	rad, deg	Phase spread (usually 60 deg)
ε	rad, deg	Chording angle

B. Table model with concentrated coils

This machine is a result of the desire to test different winding configurations. That is, given a fixed stator and different rotors with different pole number, parameters as voltage, winding factors, cogging etc can be measured and compared with calculations. The starting point for this machine design was an old, used induction machine stator with 36 slots which gave the main the dimensions of the machine. Fig. 136 shows two pictures of the setup. The test machine is the one with black stator, shiny rotor and copper windings. The other components are an induction machine and a frequency converter used to drive the model.

Fig. 137 shows the dimensions of the machine and in Table 46 they are also listed (diameters). The coil dimensions are shown in Fig. 137. It was built two different rotors, one with 34 magnets (or poles) and one with 34.

Table 46 Dimensions of the table model

Stator [mm]		Rotor [mm]	
D_{os}	270	D_{or}	168
D_{is}	180	D_{mr}	166
L_s	14	L_r	10
d_s	26.5	l_m	5
w_t	8	w_m	12
Ns	36		
Coil (Fig. 137)			
D_{cond}	0.85mm	N	178
		N_{coil}	18

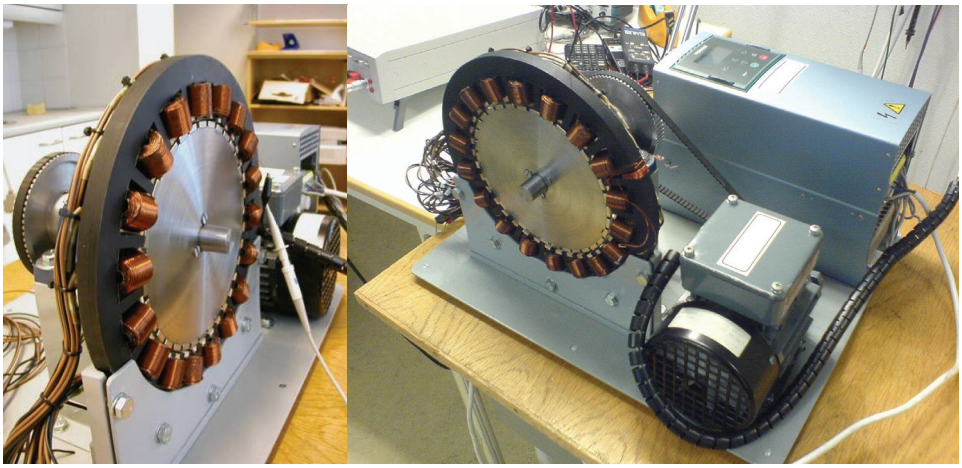

Fig. 136 Picture of the laboratory setup.

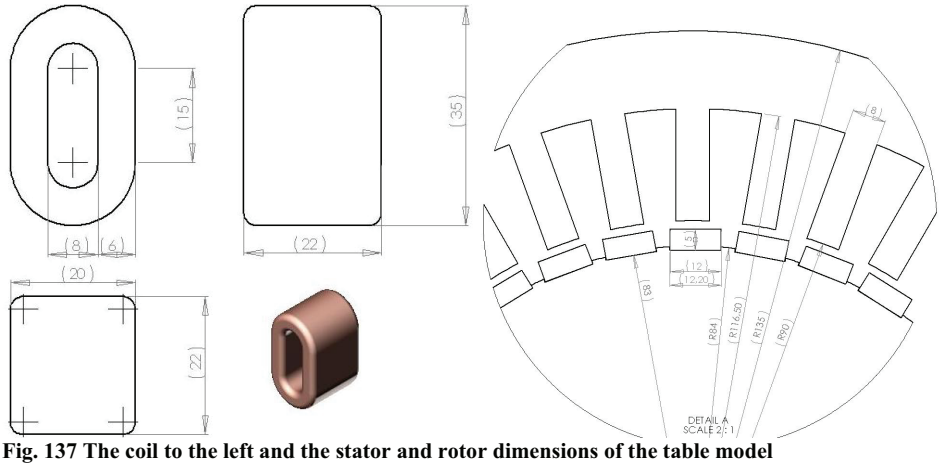

Fig. 137 The coil to the left and the stator and rotor dimensions of the table model

C. Material properties

A presentation of the different materials properties used for calculation of the design.

C-1. Copper

Conductivity@20C:	$58 \cdot 10^6$S/m
Temperature dependency:	$(234+T)/(234+T_0)$

C-2. Permanent magnets

Grade:	N35
Conductivity:	$6.25 \cdot 10^5$S/m,
Resistivity	$1.6 \cdot 10^{-6}$Ωm
Relative permeability:	1.05
Remanent Flux density:	1.2T
Temperature dependency (B_r):	0.1%/C
Temperature maximum:	80C

C-3. Soft Iron

Conductivity:	$6.7 \cdot 10^6$S/m
Relative permeability:	Fig. 138

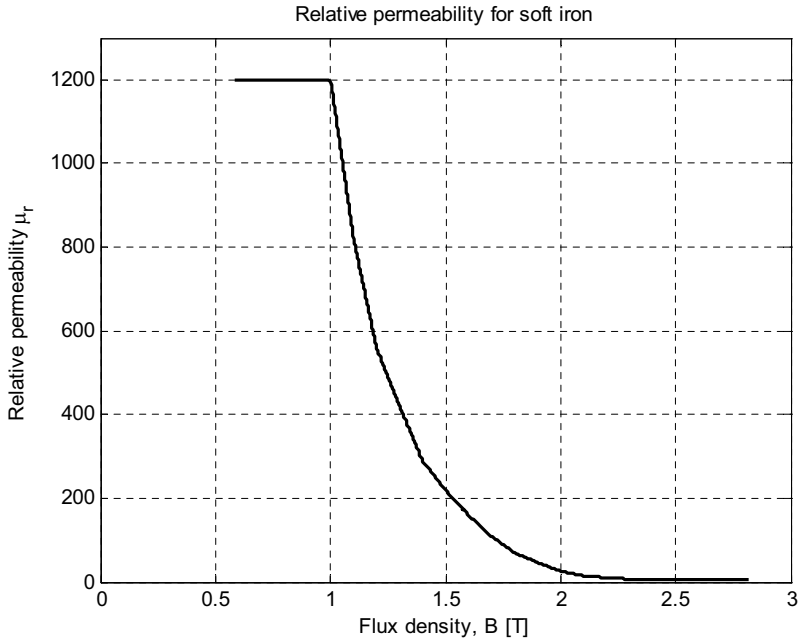

Fig. 138 Relative permeability for soft iron

C-4. Lamination M250-50A

Conductivity:	0 S/m
Relative permeability:	Fig. 139 (Adapted for numerical convenience)
Losses:	Table 47, the row with 2T is added to expand the range, when implemented rows of 0W/kg are added for both 0T and 0Hz, linear interpolation is used.

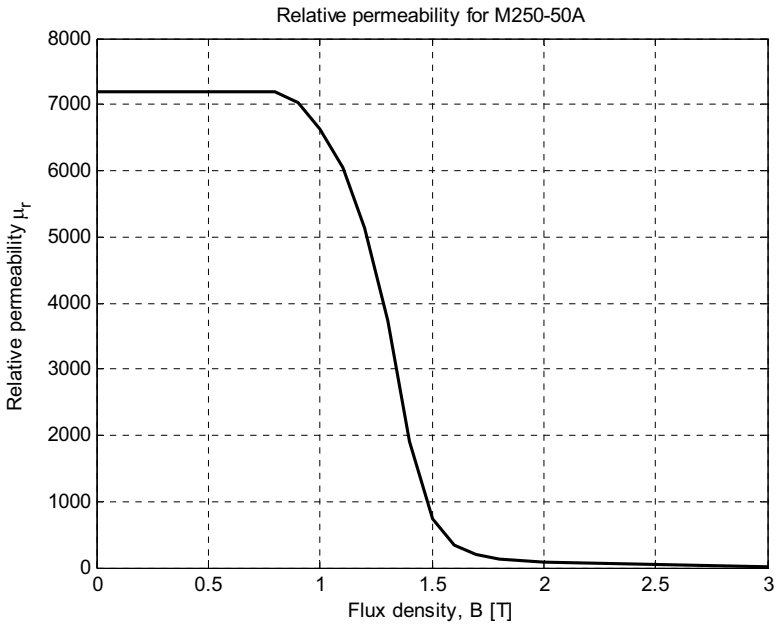

Fig. 139 Relative permeability for electric sheet M250-50A, adapted

Table 47 Loss matrix for SuraCogent M250-50A [107]

Loss [W/kg]		Frequency [Hz			
		50	100	200	400
Flux density [T]	0.5	0.31	0.78	2.11	6.0
	0.6	0.42	1.08	2.99	8.5
	0.7	0.54	1.40	3.86	11.3
	0.8	0.68	1.77	4.91	14.7
	0.9	0.83	2.18	6.12	18.7
	1.0	0.99	2.63	7.50	23.4
	1.1	1.18	3.13	9.02	28.8
	1.2	1.39	3.70	10.77	35.2
	1.3	1.64	4.28	12.75	42.4
	1.4	1.96	5.22	15.42	50.9
	1.5	2.34	6.24	18.31	60.7
	2*	4.68	13.28	36.62	121.4

D. The calculations of the different design examples for the 50kW prototype direct driven wind turbine generator

On the following pages a summary of the preliminary example designs for 50kW prototype wind turbine based on the different methods of scaling of the 3MW generator is presented. A comparison of them is presented in Table 21 on page 87.

D-1. A: 70rpm, constant frequency and peripheral speed

TABLE I
AN AERODYNAMICALLY CORRECT 50KVA GENERATOR (70RPM)

Symbol	Name	Value	
f_n	frequency	50.17	Hz
n	speed	70	rpm
N_p	# poles	86	
N_{sec}	# sections	2	
Ns	# slots	84	
N_{cph}	# coils per phase	14	
Dimensions			
D_g	air gap diameter	1158	mm
L	machine length	76	mm
τ_s	slot pitch	43.7	mm
τ_p	pole pitch	42.3	mm
k_{slot}	slot fraction of slot pitch	0.55	
k_{magnet}	magnet fraction of pole pitch	0.80	
d_s	slot depth	80.0	mm
l_m	magnet length	22.0	mm
g	air gap	5.0	mm
d_c	Conductor diameter	5.2	mm
Electrical parameters			
J	Current density	4	A/mm^2
N	# turns	44	
I_{slot}	Slot Current	3682	At
E	Induced voltage	232.6	V
Φ_{tooth}	Mean flux in tooth	1.2	T
I	nominal current	83.7	A
P	power	52.0	kW
S	Apparent power	57.7	kVA
Tn	Nominal torque	7.09	kNm
η	efficiency	93.5	%
L_{phase}	Inductance per phase	78	mH
R_{phase}	Resistance per phase	147	mΩ
pu-values			
U_{base}	base voltage	230	V
S_{base}	base apparent power	50	kVA
I_{base}	base current	72.5	A
Z_{base}	base impedance	3.2	Ω
X_{pu}	reactance pu	0.77	
R_{pu}	resistance pu	0.046	
Masses			
M_{Cu}	Copper	100	kg
$M_{lamination}$	Stator lamination	121	kg
M_{magnet}	Magnets	36	kg
$M_{rotoryoke}$	Rotor yoke	11	kg
M_{total}	Total	268	kg

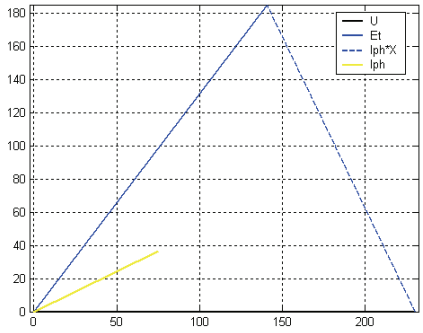

Fig. 140 Vector diagram with voltages and current

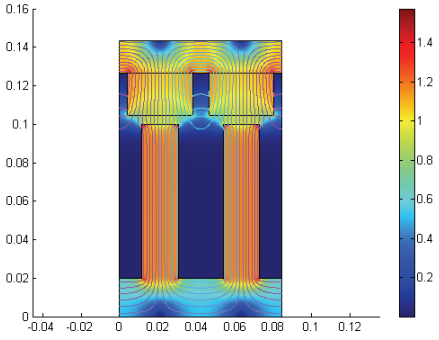

Fig. 141 Flux lines and density from magnets

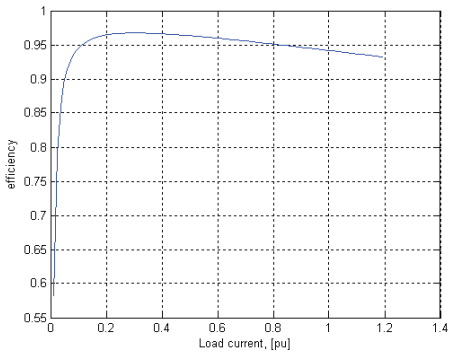

Fig. 142 Estimated efficiency

D-2. B: 17rpm, all dimensions scaled proportionally

TABLE II
348 POLES, 50HZ, 17RPM

Symbol	Name	Value	
f_n	frequency	49.3	Hz
n	speed	17	rpm
N_p	# poles	348	
N_{sec}	# sections	12	
Ns	# slots	360	
N_{cph}	# coils per phase	60	
Dimensions			
D_g	air gap diameter	1660	mm
L	machine length	429.3	mm
τ_s	slot pitch	14.5	mm
τ_p	pole pitch	15.0	mm
k_{slot}	slot fraction of slot pitch	0.55	
k_{magnet}	magnet fraction of pole pitch	0.8	
d_s	slot depth	29.5	mm
l_m	magnet length	7.8	mm
g	air gap	1.8	mm
d_c	Conductor diameter	4.9	mm
Electrical parameters			
J	Current density	4	A/mm^2
N	# turns	6	
I_{slot}	Slot Current	456	At
E	Induced voltage	256	V
Φ_{tooth}	Mean flux in tooth	1.25	T
I	nominal current	76.1	A
P	power	51.8	kW
S	Apparent power	52.5	kVA
Tn	Nominal torque	29.1	kNm
η	efficiency	88.7	%
L_{phase}	Inductance per phase	3.4	mH
R_{phase}	Resistance per phase	295	mΩ
pu-values			
U_{base}	base voltage	230	V
S_{base}	base apparent power	50	kVA
I_{base}	base current	72.5	A
Z_{basc}	base impedance	3.2	Ω
X_{pu}	reactance pu	0.33	
R_{pu}	resistance pu	0.093	
Masses			
M_{Cu}	Copper	166	Kg
$M_{lamination}$	Stator lamination	302	Kg
M_{magnet}	Magnets	105	Kg
$M_{rotoryoke}$	Rotor yoke	39	kg
M_{total}	Total	612	kg

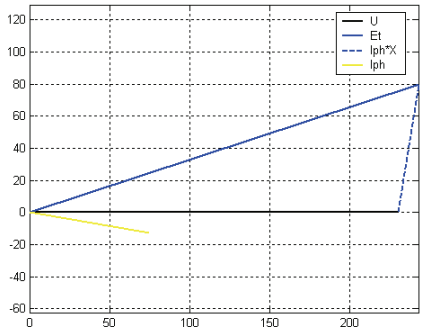

Fig. 143 Vector diagram with voltages and current

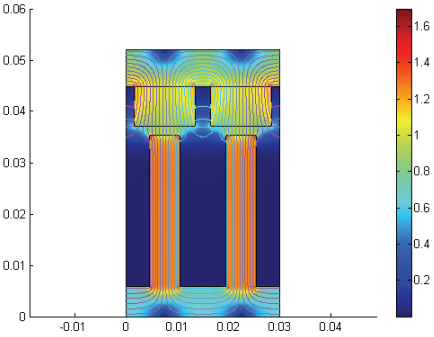

Fig. 144 Flux lines and density from magnets

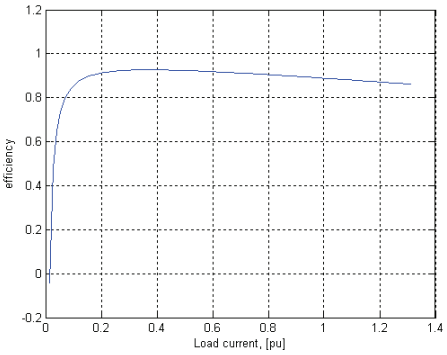

Fig. 145 Estimated efficiency

D-3. C: Two parts of the reference design; equal pole pitch,

TABLE III
TWO PARTS, EQUAL POLE PITCH

Symbol	Name	Value	
f_n	frequency	50	Hz
n	speed	103	rpm
N_p	# poles	58	
N_{sec}	# sections	2	
Ns	# slots	60	
N_{cph}	# coils per phase	10	
Dimensions			
D_g	air gap diameter	733	mm
L	machine length	115	mm
τ_s	slot pitch	41.0	mm
τ_p	pole pitch	41.9	mm
k_{slot}	slot fraction of slot pitch	0.55	
k_{magnet}	magnet fraction of pole pitch	0.80	
d_s	slot depth	80.0	mm
l_m	magnet length	22.0	mm
g	air gap	5.0	mm
d_c	Conductor diameter	5.2	mm
Electrical parameters			
J	Current density	4	A/mm^2
N	# turns	41	
I_{slot}	Slot Current	3452	At
E	Induced voltage	230.4	V
Φ_{tooth}	Mean flux in tooth	1.2	T
I	nominal current	84.2	A
P	power	52.3	kW
S	Apparent power	58.1	kVA
Tn	Nominal torque	4.83	kNm
η	efficiency	94.6	%
L_{phase}	Inductance per phase	7.5	mH
R_{phase}	Resistance per phase	121	mΩ
pu-values			
U_{base}	base voltage	230	V
S_{base}	base apparent power	50	kVA
I_{base}	base current	72.5	A
Z_{basc}	base impedance	3.2	Ω
X_{pu}	reactance pu	0.75	
R_{pu}	resistance pu	0.038	
Masses			
M_{Cu}	Copper	83	kg
$M_{lamination}$	Stator lamination	121	kg
M_{magnet}	Magnets	37	kg
$M_{rotoryoke}$	Rotor yoke	11	kg
M_{total}	Total	252	kg

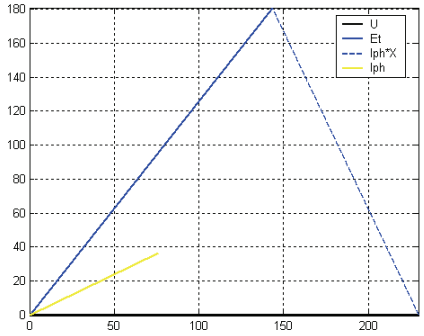

Fig. 146 Vector diagram with voltages and current

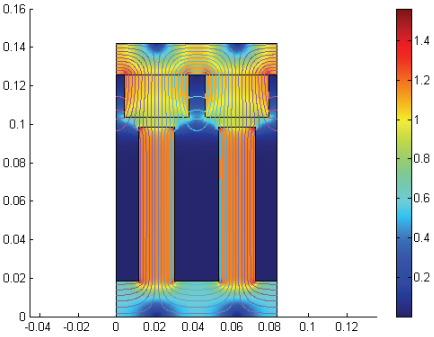

Fig. 147 Flux lines and density from magnets

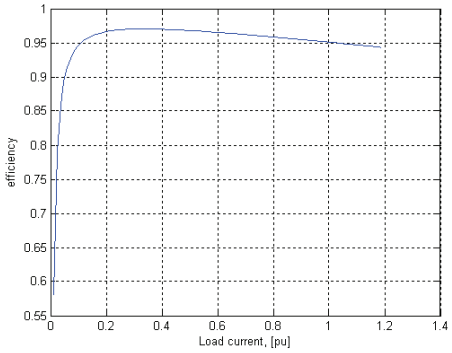

Fig. 148 Estimated efficiency

D-4. D: Four parts of the reference design; equal pole pitch

TABLE IV
FOUR PARTS, EQUAL POLE PITCH

Symbol	Name	Value	
f_n	frequency	50	Hz
n	speed	51.7	rpm
N_p	# poles	116	
N_{sec}	# sections	4	
Ns	# slots	120	
N_{cph}	# coils per phase	20	
Dimensions			
D_g	air gap diameter	1547	mm
L	machine length	55	mm
τ_s	slot pitch	41.0	mm
τ_p	pole pitch	41.9	mm
k_{slot}	slot fraction of slot pitch	0.55	
k_{magnet}	magnet fraction of pole pitch	0.80	
d_s	slot depth	80.0	mm
l_m	magnet length	22.0	mm
g	air gap	5.0	mm
d_c	Conductor diameter	5.2	mm
Electrical parameters			
J	Current density	4	A/mm^2
N	# turns	42	
I_{slot}	Slot Current	3429	At
E	Induced voltage	225.8	V
Φ_{tooth}	Mean flux in tooth	1.2	T
I	nominal current	841.6	A
P	power	50.4	kW
S	Apparent power	56.3	kVA
Tn	Nominal torque	9.31	kNm
η	efficiency	92.7	%
L_{phase}	Inductance per phase	7.6	mH
R_{phase}	Resistance per phase	169	mΩ
pu-values			
U_{base}	base voltage	230	V
S_{base}	base apparent power	50	kVA
I_{base}	base current	72.5	A
Z_{basc}	base impedance	3.2	Ω
X_{pu}	reactance pu	0.755	
R_{pu}	resistance pu	0.053	
Masses			
M_{Cu}	Copper	109	kg
$M_{lamination}$	Stator lamination	113	kg
M_{magnet}	Magnets	35	kg
$M_{rotoryoke}$	Rotor yoke	11	kg
M_{total}	Total	268	kg

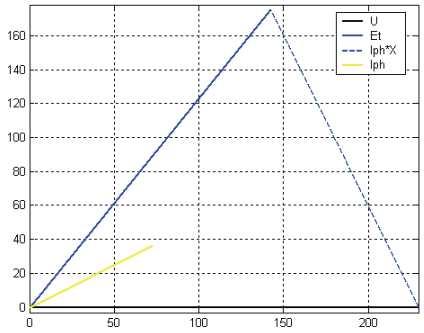

Fig. 149 Vector diagram with voltages and current

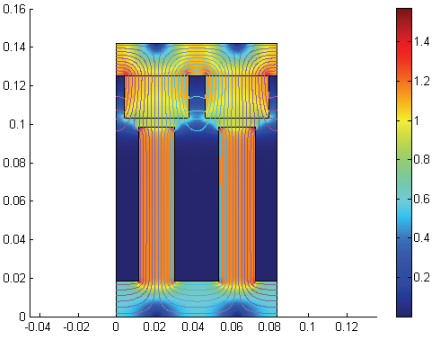

Fig. 150 Flux lines and density from magnets

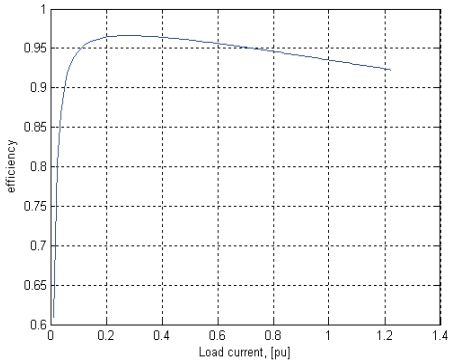

Fig. 151 Estimated efficiency

D-5. E: Two parts from the reference design, D_g/L constant

TABLE V
TWO PARTS, EQUAL D_G/L

Symbol	Name	Value	
f_n	frequency	50	Hz
n	speed	103	rpm
N_p	# poles	58	
N_{sec}	# sections	2	
Ns	# slots	60	
N_{cph}	# coils per phase	10	
Dimensions			
D_g	air gap diameter	661	mm
L	machine length	171	mm
τ_s	slot pitch	35.1	mm
τ_p	pole pitch	35.8	mm
k_{slot}	slot fraction of slot pitch	0.55	
k_{magnet}	magnet fraction of pole pitch	0.80	
d_s	slot depth	69.1	mm
l_m	magnet length	18.8	mm
g	air gap	4.3	mm
d_c	Conductor diameter	5.0	mm
Electrical parameters			
J	Current density	4	A/mm^2
N	# turns	41	
I_{slot}	Slot Current	2532	At
E	Induced voltage	228.6	V
Φ_{tooth}	Mean flux in tooth	1.2	T
I	nominal current	79.1	A
P	power	50.5	kW
S	Apparent power	54.6	kVA
Tn	Nominal torque	4.66	kNm
η	efficiency	94.7	%
L_{phase}	Inductance per phase	6.9	mH
R_{phase}	Resistance per phase	126	mΩ
pu-values			
U_{base}	base voltage	230	V
S_{base}	base apparent power	50	kVA
I_{base}	base current	72.5	A
Z_{basc}	base impedance	3.2	Ω
X_{pu}	reactance pu	0.68	
R_{pu}	resistance pu	0.040	
Masses			
M_{Cu}	Copper	77	kg
$M_{lamination}$	Stator lamination	133	kg
M_{magnet}	Magnets	40	kg
$M_{rotoryoke}$	Rotor yoke	12	kg
M_{total}	Total	262	kg

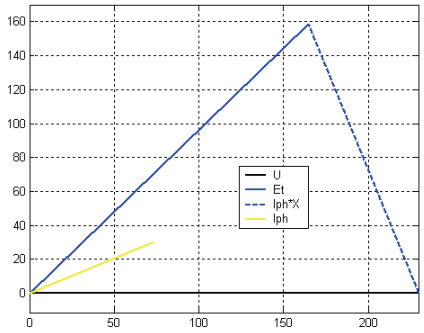

Fig. 152 Vector diagram with voltages and current

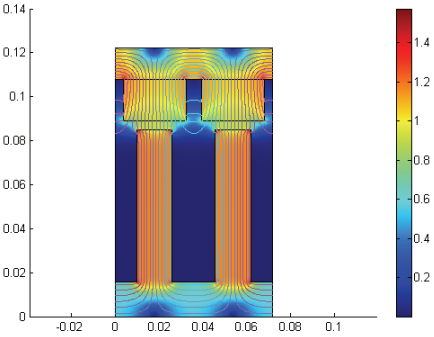

Fig. 153 Flux lines and density from magnets

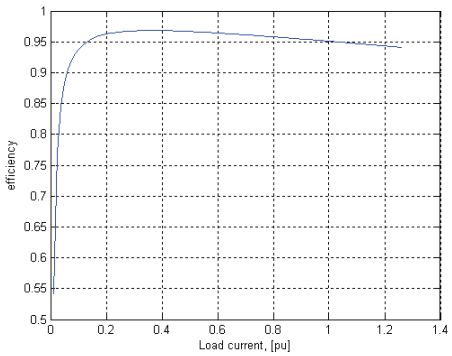

Fig. 154 Estimated efficiency

D-6. F: Equal pole pitch (τ_p), D_g/L constant

TABLE VI
50 HZ MACHINE

Symbol	Name	Value	
f_n	Frequency	50	Hz
n	Speed	136	rpm
N_p	# poles	44	
N_{sec}	# sections	4	
Ns	# slots	48	
N_{cph}	# coils per phase	8	
Dimensions			
D_g	air gap diameter	587	mm
L	machine length	152	mm
τ_s	slot pitch	39.1	mm
τ_p	pole pitch	41.9	mm
k_{slot}	slot fraction of slot pitch	0.55	
k_{magnet}	magnet fraction of pole pitch	0.80	
d_s	slot depth	80.0	mm
l_m	magnet length	22.0	mm
G	air gap	5.0	mm
d_c	Conductor diameter	5.2	mm
Electrical parameters			
J	Current density	4	A/mm^2
N	# turns	43	
I_{slot}	Slot Current	3589	At
E	Induced voltage	245	V
Φ_{tooth}	Mean flux in tooth	1.25	T
I	nominal current	83.5	A
P	power	52.7	kW
S	Apparent power	57.6	kVA
Tn	Nominal torque	3.7	kNm
η	efficiency	94.7	%
L_{phase}	Inductance per phase	8.3	mH
R_{phase}	Resistance per phase	121	mΩ
pu-values			
U_{base}	base voltage	230	V
S_{base}	base apparent power	50	kVA
I_{base}	base current	72.5	A
Z_{base}	base impedance	3.2	Ω
X_{pu}	reactance pu	0.823	
R_{pu}	resistance pu	0.038	
Masses			
M_{Cu}	Copper	82	kg
$M_{lamination}$	Stator lamination	108	kg
M_{magnet}	Magnets	37	kg
$M_{rotoryoke}$	Rotor yoke	11	kg
M_{total}	Total	237	kg

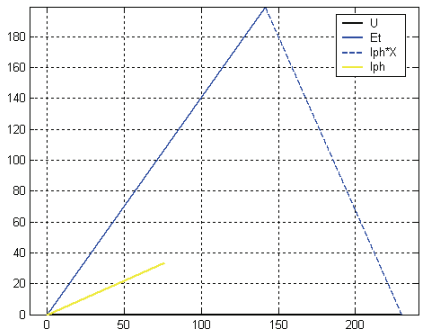

Fig. 155 Vector diagram with voltages and current

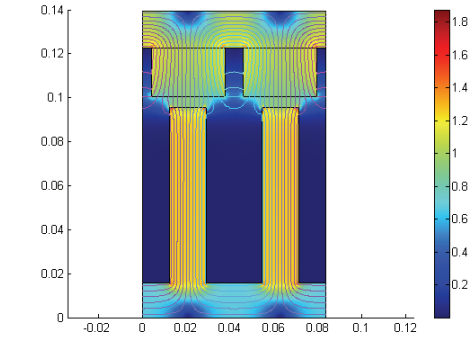

Fig. 156 Flux lines and density from magnets

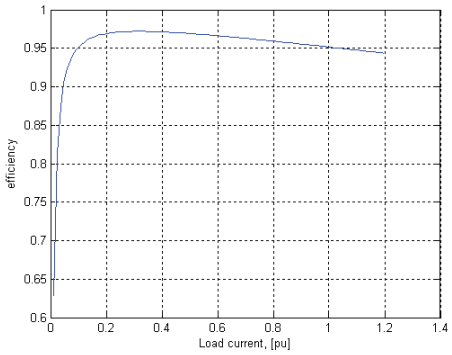

Fig. 157 Estimated efficiency